Synthesis and characterization of group 12 dithiolate complexes as single source precursors for the preparation of hexadecylamine capped metal sulfide nanoparticles and polymer nanocomposites

OSUNTOKUN JEJENIJA

Department of Chemistry

Faculty of Science and Agriculture

University of Fort Hare

Together in Excellence

January 2016

Synthesis and characterization of group 12 dithiolate complexes as single source precursors for the preparation of hexadecylamine capped metal sulfide nanoparticles and polymer nanocomposites

By

OSUNTOKUN JEJENIJA (200907706)
B.Sc Chemistry (Ibadan), B.Sc (Hons) Chemistry (UFH) MSc Chemistry (UFH)

Being a thesis submitted to the Faculty of Science and Agriculture in fulfilment of the requirements for the award of the degree of

Doctor of Philosophy in Chemistry

of the

University of Fort Hare,

Supervisor: Professor P. A. Ajibade

January 2016

Declaration by Candidate on Plagiarism

I, Jejenija Osuntokun, declare that:

1. The research in this thesis, except where otherwise indicated, is my original research.
2. This thesis has not been submitted for any degree or examination at other university.
3. This thesis does not contain any other person's data unless specifically acknowledged as being sourced from them.
4. This thesis does not contain any other person's writing, unless specifically acknowledged as being sourced from other researchers. Where other written sources have been quoted, then:
    a. Their words have been re-written but the general information attributed to them has been properly referenced.
    b. In all instances where the exact words of other authors have been used, then their writing has been placed in italics and inside quotation marks, and referenced.
5. This thesis does not contain text or graphics from the internet copied and pasted, unless specifically acknowledged, and the source being detailed in the dissertation/thesis and in the references section.

Sign

_____ _____

Date Jejenija Osuntokun

Certification

This is to certify that this research is a record of original work carried out by Jejenija Osuntokun under my supervision in the Inorganic Materials Research laboratory of the Department of Chemistry, University of Fort Hare in fulfilments of the requirements for the award of Doctor of Philosopy in Chemistry.

_____ _____

Date

Supervisor

P. A. Ajibade
Professor of Inorganic Materials Chemistry
B. Sc (Hons), MSc (Ibadan);
PhD (UniZul); MRSC (London)

Dedication

To the memory of my late, father, Tomo Osuntokun

Acknowledgement

I wish to acknowledge the omnipotent God that sees the thought, the depth of the mind of every man and his dreams. God has been my ultimate provider and my defender. I wish to acknowledge Professor Peter Ajibade, my supervisor for his guidance, criticism and encouragement. I pray God will bless him and his family beyond his imaginations. My gratitude also goes to Dr O. Oyedeji for his words of support and encouragement. He has been a real father for the orphan.

I was not created alone and I am sincerely indebted to my mum for her prayers, my siblings; Tomilola, Tomide, Tayo, Temidola, Tolu and Tanwa for their moral supports. My appreciation goes to mum, Mrs Bimpe Osuntokun, for her prayers and frequent phone calls through out the course of my studies. I remember my late dad, Tomo Osuntokun, for his words of encouragements even when I had no idea of pursing a PhD programme. He has been a source of inspiration and even at death I have had reasons to remember his words and apply them as a source of motivation in time of over bearing challenges. To my friends that are many to mention, to my colleagues in the inorganic laboratory I want to say thank you all.

Last but not the least to my dear wife, Dr Adejoke Bamigboye, I want to say a special thank you. She has been a great support and for taking care of the kids, (Timileyin Osuntokun and Nimioluwa Osuntokun) in my absence.

Contents

List of Figures

List of Tables

Abreviations and Symbols

Chemical reagents

1, 10 phen	1, 10 phenanthroline
2, 2’ bpy	2, 2 bipyridine
Py	Pyridine
mtu	methylthiourea
dmtu	dimethylthiourea
detu	diethylthiourea
diptu	diisopropylthiourea
Me	methyl
CED	1-cyano-1-carboethoxy-2,2-ethylene dithiolate
Me_4tds	tetramethylthiuram disulfide
PMMA	polymethyl metharcrylate
PVA	poly(vinyl alcohol)
PVP	poly(vinyl pyrrolidone)
HDA	hexadecylamine
TOPO	tri-n-octylphosphine oxide
TOP	tri-n-octylphosphine

Intrumentation

UV/Vis	ultra-violet/visible
IR	infrared spectroscopy
NMR	nuclear magnetic resonance spectroscopy
SEM	scanning electron microscopy

TEM	transmission electron microscopy
EDX	energy dispersive X-ray spectroscopy
TGA	thermogravimetry analyser
XRD	X-ray diffraction
XPS	X-Ray photoelectron spectroscopy
PL	photoluminescence
SAD	selected-area diffraction
UHV	ultra high vacuum
LEDs	light emitting diodes
OD	zero dimensional
1D	one dimensional
2D	two dimensional
3D	three dimensional
LAPW	linear augmented plane wave
NMTO	new generation muffin–orbital
COHP	crystal orbit hamilotonia population
TB	tight binding
ESCA	electron spectroscopy for chemical analysis
Eg	the bang gap of the material
Mmol	millimole
α	absorption coefficient
n	depends on the type of trasition
A	constant
h^{ν}	photon energy
E_k	photo electron

$\phi\phi$	work function
mm	Electron mass
qq	Electron charge
v	Potential difference
$h\,h$	Planks constant
λ	Effective electron wavelength
ppm	parts per million
JCPDS	Joint committee of Powder diffraction standards

Research Outputs

1. Ajibade P. A.; Osuntokun, J. Synthesis and Characterization of Hexadecylamine Capped ZnS, CdS, and HgS Nanoparticles Using Heteroleptic Single Molecular Precursors *J. Nanomater*. **2014**, 782526, 1-7.
2. Osuntokun, J.; Ajibade, P. A. Synthesis and structural characterisation of CdS nanoparticles using nitrogen adducts of mixed diisopropylthioure and dithiolate derivatives of Cd (II) complexes. *Superlattices*. *Microstruct*. **2015**, 83, 89-100.
3. Osuntokun, J.; Ajibade P. Synthesis and characterization of Zn(II), Cd(II) and Hg(II) complexes of diethyl thiourea and 1-ethoxylcarbonyl-1-ethylenecarbonyl-2,2-dithiolate and their use to prepare metal sulfides nanoparticles. *Asian J. Chem*. **2015**, 27, 4563-4567.
4. Osuntokun, J.; Ajibade, P. A Structural and thermal studies of ZnS and CdS nanoparticles in polymer matrices. *J. Nanomater*. **2016**, 3296071, 1-14.
5. Osuntokun, J.; Ajibade, P. A. A study of morphological and thermal behaviour of polyvinyl achohol (PVA) encapsulated ZnS and CdS nanoparticles. Submitted.
6. Osuntokun, J.; Ajibade, P. A. Effect of pyridine on structural properties of ZnS, nanoparticles from (1-cyano-1-carboethoxy-2, 2-ethylenedithiolato–κ*S*,*S*')–bis(*N*,*N*'-diisopropylthiourea–κ*S*)Zn(II) and its nitrogen donors as single source precursors. Manuscript in preparation.

Abstract

A series of heteroleptic mixed ligand complexes of some alkyl substituted thiourea, tetramethyl thiuram disulfide and 1-cyano-1-carboethoxy-2,2 ditholate of Zn(II) Cd(II) and Hg(II) have been synthesized by stoichiometry reactions of the ligands with respective metal salts. They have been characterized with analytical and spectroscopic techniques. Seven out of the 19 complexes synthesized are pyridine 2, 2 bipyridine and 1, 10 phenanthroline adducts of dissopropyl parent adducts of Zn(II) and Cd(II) complexes. All the complexes are proposed as four coordinate except the pyridine adducts, 2, 2' bipyridine and 1, 10 phenanhroline adducts that are proposed as five and six coordinate respectively. All the complexes are solid, air stable and moisture stable for a many months. They are not soluble in common organic solvents but partially soluble in coordinating solvents like DMF and DMSO and due to their insolubility problems all attempts to grow single crystal of the complexes proved abortive.

The complexes gave respective metal sulfide on thermal decomposition in TGA and this makes them to be potentially useful single source precursor for the synthesis of metal sulfide. All the complexes were invariably thermolysed in HDA to synthesis a series of HDA-capped ZnS, CdS and HgS nanoparticles. The optical properties of the nanoparticles reveal that they are all blue-shifted from the absorbance edge and this confirms quantum confinement of the nanoparticles. The transmittance electron microscope showed that the nanoparticles are in nanodimension. ZnS nanoparticles from the pyridine adducts gave HDA-capped ZnS nanoparticles with a mixture of hexagonal and cubic phases while the HDA capped CdS from the 2, 2 bipyridine and 1,10 phenanthroline gave anisotropic nanoparticles. The sizes of the CdS from the 1,10 phenanthroline adducts were also found to be biggest while CdS

nanoparticles from 2,2 bipyridine adduct were also revealed to be bigger than the particle sizes obtained from the parent complex, (1-cyano-1-carboethoxyethylene-2,2-dithiolato-κ,*S*'S)-bis(N, N'-diisopropylthiourea -κ*S*)cadmium(II).

ZnS and CdS polymer encapsulated nanocomposites were also synthesized using a solution casting method. The polymers employed were; Polymethyl metharcrylate (PMMA), Poly(vinly alcohol) (PVA), and poly vinyl pyrrolidone (PVP). The structural and thermal properties of the pure polymers and the respective nanocomposites were investigated. It was observed that the ZnS/PVA and CdS/PVA were the most thermally stable composites when the thermal stability of the pure polymers were compared relative to the nanocomposites using data obtained from thermal decomposition results of the TGA.

CHAPTER 1

1.1 Classification of solid materials

The classification of matter can be based on various properties but according to the electronic potential, they can be categorised as follows;

1.1.1 Conductor - Materials that are partly filled with mobile electrons belong to this category of solid mateterials and electron move freely in these materials when a potential difference is applied. A typical example is a metal. There exists an overlap of the valence band over the conduction band in this material whose conductivity value is in the range of 10^8 to 10^4 Ω cm^{-1}

1.1.2 Semiconductor - The valence band of the material in this category is full of electrons and the conduction band is unoccupied. Hence there is a band gap (region where electrons are forbidden) that separates the valence band from the conduction band. Electrons are able to jump from the valence band to conduction band when they acquire sufficient thermal energy which is required for transport of electric current by electron-hole pair (exciton). Hence, when a potential difference is applied across pure semiconductor and insulator, they exhibit almost the same resistance [1]. The conductivity value of these types of materials is in the range of 104 to 10-8 Ω.

1.1.3 Insulators - These materials have a filled valence band and an unoccupied conduction band with a relatively large band gap (> 4.0 eV) that does not support the movement of electron when the material is thermally or optically irradiated. Conductivity value of this class of material is the poorest and is less than 10-8 Ω.

The band structure of a solid can be illustrated by the magnitude of band gap within the material that an electron is either forbidden or allowed to have. The diffraction of the quantum mechanical wave in the periodic lattice of an atom is the cause of band theory. Many characteristics especially, optical and electronic properties of materials depend on the band structure. Electron occupy orbitals that are in discrete energy levels and if atoms are assembled together to form a molecule a split of the orbitals occur. The resultant effect of this is that molecular orbitals formed are directly proportional to the number of atoms. The combination of a large number of atoms to form a solid material lead to an increasing number of orbitals with a decreasing difference in the energy among them such that the level may eventually become a continuous band of energy instead of the discrete energy level.

Nevertheless, some intervals of energy are void of orbitals irrespective of the number of aggregated atoms and this produced bandgap. Figure 1 represents the energy band gap of metal, semiconductor and insulator.

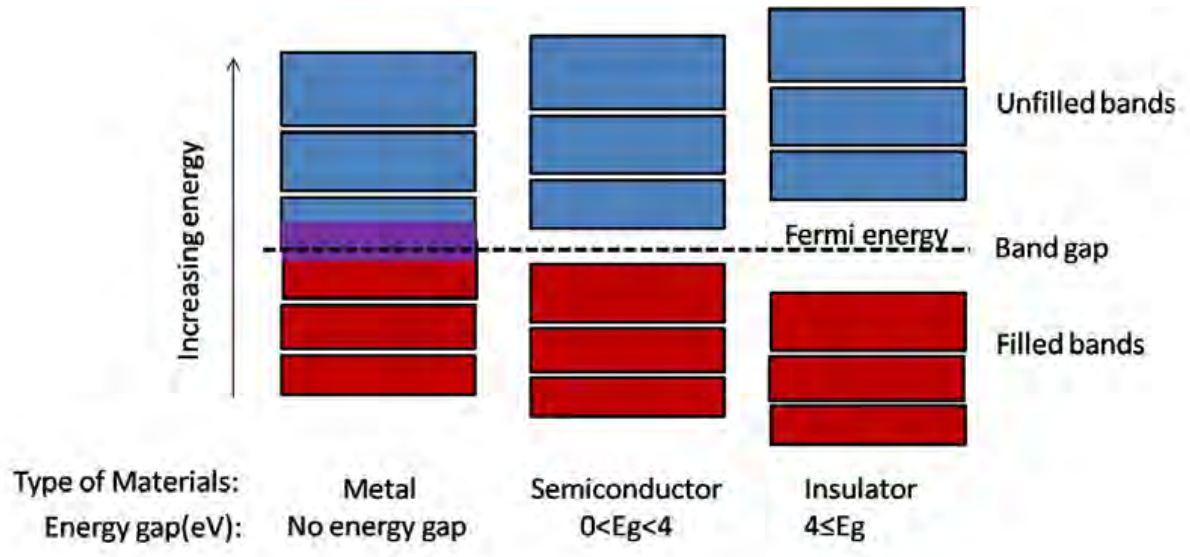

Figure 1.1 Energy band gap of materials

Most of the important semiconductors are isoelectronic. Silicon (Si), germanium (Ge) and diamond (C) are all examples of elemental semiconductors. The compound semiconductors are solids and are a combination of two or more elements that exhibits semiconducting properties. They are grouped as follows: (a) 2 elements; binary alloys, (b) 3 elements; ternary alloys, (c) 4- elements: quaternary alloys Semiconductors materials are generally grouped into; II-VI (12-16) e.g ZnS, CdSe, III-V (13-15) materials e.g GaAs, InP.

Table 1.1 Elements that constitute semiconducting properties

Group 12	Group 13	Group 14	Group 15	Group 16
	B	C		O
	Al	Si	P	S
Zn	Ga	Ge	As	Se
Cd	In		Sb	Te

1.2 Intrinsic Semiconductors

These are semiconductors that are made up of naturally occurring group 16 elements such as Si, Ge, Se, Te and some chemical compounds like GaAs, InSb and a host of others. They are chemically pure and contain equal numbers of excited electrons and holes. The properties of the material dictate the number of charge carriers and not the amount of impurities that is present in the semiconductors. When a semiconductor material is thermally excited, it evokes charge carriers which are made up of electrons in the conduction band and the holes in the valence band. The carriers which are also called intrinsic carriers contain equal number of electrons and holes. For example, in the formation of a silicon crystal, a Si atom with four valence electrons shares electrons covalently with four neighbouring atoms to complete the

bonds. Consequently the silicon four electrons are complemented by four electrons from the neighbours to make eight electrons; an octet [3].

1.2.1 N-type semiconductor

This type of semiconductor is obtained when a pure silicon is doped with any of the group 5 elements; Phosphorus, antimony or arsenic. These elements are pentavalent and only four of the electrons are needed to form covalent bonds with silicon. The fifth electron that is not involved in bonding with neighboring silicon atom is a free electron in the conduction band and this is typical of every impurity. Electron will flow in this material to produce electric current if a potential difference is applied. In short the N-type semiconductor material is a better conductor than pure silicon.

1.2.2 P-type Semiconductor

This type of semiconductor is formed when pure silicon is doped with any of the group 3 elements such that only 3 valence electrons of Si are involved in covalent bonding with neighboring atoms. Hence the forth electron that could not bond causes a hole to be created in the valence bond. Every impurity produces a hole in the valence bond. These holes will cause a flow of electrons when a voltage is applied and an electric current is generated. Impurities atoms are called either donor or acceptor based on the effect they have on the intrinsic semiconductor; they either change the electron or hole concentration

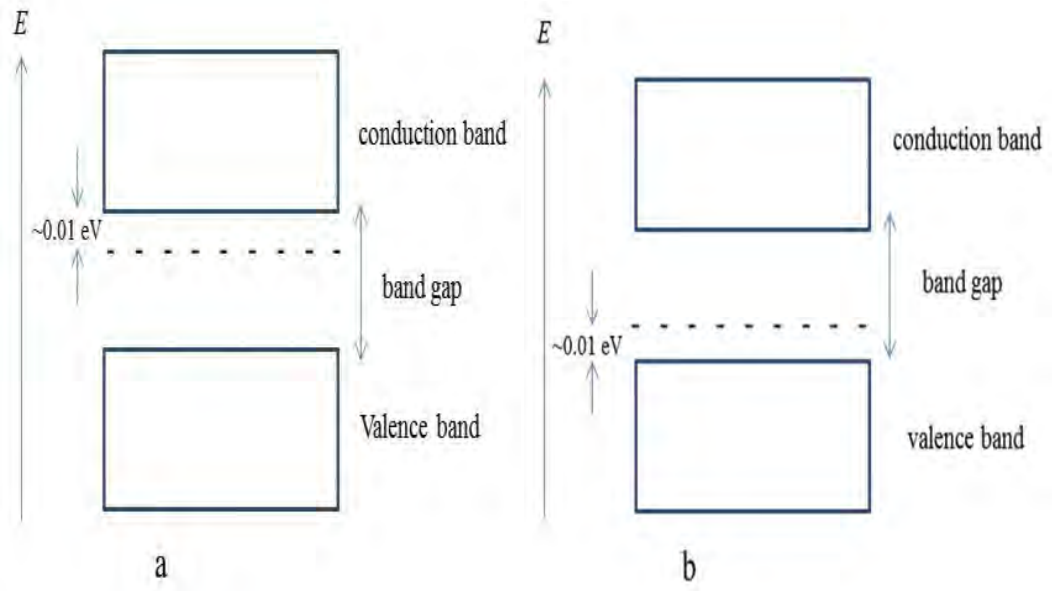

Figure 1.2: Energy band diagrams for (a) P-type (b) N-type semiconductors [4]

1.3 Nanomaterial synthesis

There are two major approaches to the synthesis of nanomaterials and each method has its merits and demerits [5].

1.3.1 Top-down approach

This approach involves materials that go from large molecules to smaller molecules scale down to nanoscale with no atomic level control. There is division of a massive solid into smaller portions. It may involve milling or chemical methods, and volatilization of a solid followed by condensation of the volatilized components. This approach uses traditional methods to guide the synthesis of nanoscale materials. The paradigm proper of its definition generally dictates that in the 'top-down' approach it all begins from a bulk piece of material, which is then gradually or step-by-step removed to form objects in the nanometer-size regime. Well known techniques such as photo lithography and electron beam lithography,

anodization, ion- and plasma-etching, all belong to this type of approach. This approach for nanofabrication was first suggested by Feynman in his famous American Physical Society lecture in 1959 [6].

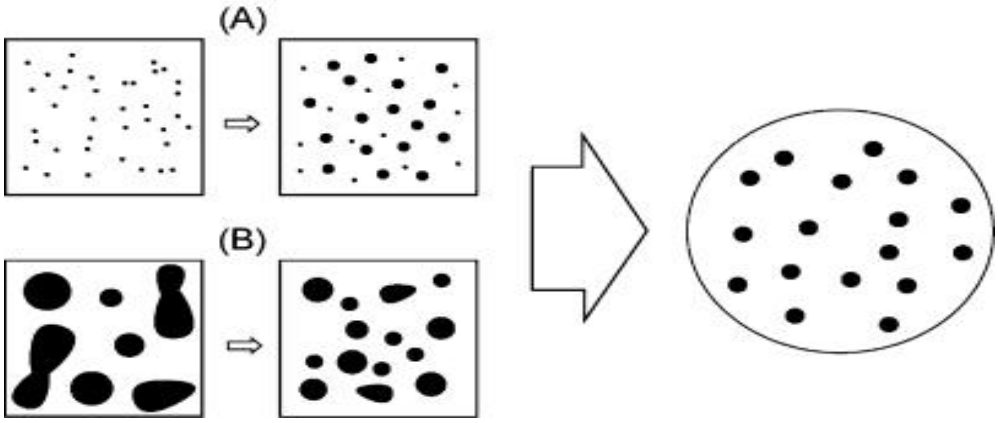

Figure 1.3: Diagram representing bottom up and top down approach [7].

1.3.2 Bottom-up approach

This approach involves the fabrication of nanomaterial from atoms or molecules using the principle of molecular recognition. This approach is far more popular in the synthesis of nanoparticles and it involves the generation of particle from atomic level and it's mainly a chemical process. In this way, instead of starting with large materials and cutting it off to reveal small bits of it, it begins from atoms and molecules that get rearranged and assembled to larger nanostructures. It is the new idea for synthesis in the nanotechnology world as the 'bottom-up' approach allows the creation of diverse types of nanomaterials, and it is likely to revolutionize the way we make materials. It requires a deep understanding of the short-range forces of attraction such as Van der Waals forces, electrostatic forces, and a variety of interatomic or intermolecular forces. Since it is not possible to have various minute particles come together without some attractive force or active field of force in the region, having the

fundamental forces “doing all the work” for you is the key principle underlying this approach This approach is far more popular in the synthesis of nanoparticles.

1.4 Direct and indirect semiconductors

Semiconductors can be classified based on the type of electron transferred from the valence to the conduction band according to their electronic structure. Equation 1 illustrate the kinetic energy of electrons

$$\mathbf{E} = \frac{K^2}{2M_n} \quad \text{..... (1)}$$

M_n represents the effective mass and K stands for the crystal momentum.

In GaAs as an example of semiconductor, the promotion of electron from the valence to the conduction bands needs no change in crystal momentum (vibrational energy) and as such they are called direct band gap semiconductors. Contrarily, in several other semiconductor materials, a change in crystal momentum is associated with excitation of electron from the valence band to the conduction band and this is known as indirect band gap semiconductors and it is worthy to note that the lowest energy electronic transition takes place in an indirect process. For instance in Si and Ge, which are indirect semiconductors, the energy equivalence of the bandgap (Eg) is not enough to promote electrons from the valence band to the conduction band and an additional energy is needed in the form of lattice vibrational energy (phonons). Hence the additional energy required for an electron to undergo a change in crystal momentum for an indirect transition is given by equation 2

$$h\nu = E_g + E_{phonon}, \quad \text{..... (2)}$$

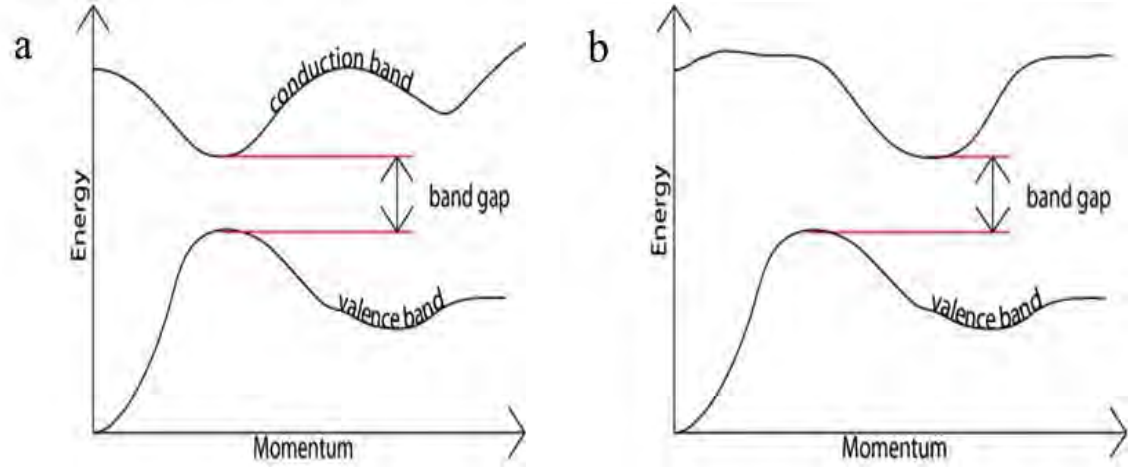

Figure 1.4: Example of bandgap in (a) direct and (b) indirect semiconductors

.

1.5. Quantum confinement

Quantum confinement effect such as blue-shift of absorption that are detected in semiconductor nanocrystals can be described or illustrated by a theoretical framework based on the effective masses of electrons and holes. Just as stated by the effective mass approximation theory, the band gap separating the valence and conduction band is equal to the energy needed to create electron-hole pair in direct band gap materials. The bore radius of an electron-hole pair in a specified material enables the evaluation of the size dependent region of semiconductor nanoparticles. The special localised spectrum can be dramatically influenced if the size is comparable to the Bohr radius of the exciton. The Bohr radius of an exciton represented by aB can be defined by the following equation 3;

$$aB = \frac{\hbar^2 \varepsilon}{e^2}\left(\frac{1}{me} + \frac{1}{mh}\right) \quad \text{.....eq 3}$$

The m_e and m_h stands for the effective mass of electron and effective mass of hole. ε represents the semiconductor's dielectric constant. This is identical with energy quantisation, for example the particle-in-a box phenomenon that cause discontinuous excitation energy state for the particle provided their dimension is equal or comparable to the Bohr radius. The energy gap, E that is dependent of size with physical radius represented by R can be described by equation 4

$$E' = E_g + \Delta E \quad \text{..... (4)}$$

This is identical with energy quantisation for example the particle-in-a box phenomenon that cause discontinuous excitation energy state for the particle provided their dimension is equal or comparable to the Bohr radius.

$$\Delta E = {h\pi^2}/{2R^2}\ [{1}/{m_e} + {1}/{m_h}] - \frac{18e^2}{4\pi\varepsilon o\varepsilon r R} + polarisation$$

Where the semiconductor band gap is denoted by E_g while ΔE correspond to the size-induced shift in the conduction band, R stands for the radius of the particle and ε serves as the dielectric constant.

The polarisation term is known to be very minute hence it can be ignored [8]. One can infer that the band gap of the bulk semiconductor increases as the particle size reduces to the nano dimension [9]. Semiconductor nanoparticles with particles size range of roughly 1-20 nm have unique properties. These unique electronic, optical catalytic and magnetic properties are due to large surface-to-volume ratio and their nanoscopic sizes. When the diameter of a particle approaches the exciton Bohr radius, the hole-electron, charge carrier gets confined

into zero degree of freedom. This significant exciton Bohr radius which is dependent on the material and its dimension is in the range of few to tens of nanometers. Due to geometrical constraints, electrons feel the particle walls and adjust their energy appropriately. The process by which the energy is adjusted is called quantum confinement effect or size effect. The consequence of this is that the continuous band of the solid materials changed to discontinuous or discrete levels and this is accompanied with an increase in band gap. This is diagrammatically shown in Figure 1.5. It is worthy to note that the extent of separation of band is dependent on the particle size, the bandgap and other properties that are related to the bandgap can be tuned. This tunability is the basis of most semiconducting nanoparticle research. The need to miniaturize optical and electrical devices is the soul motivation in nanotechnological research

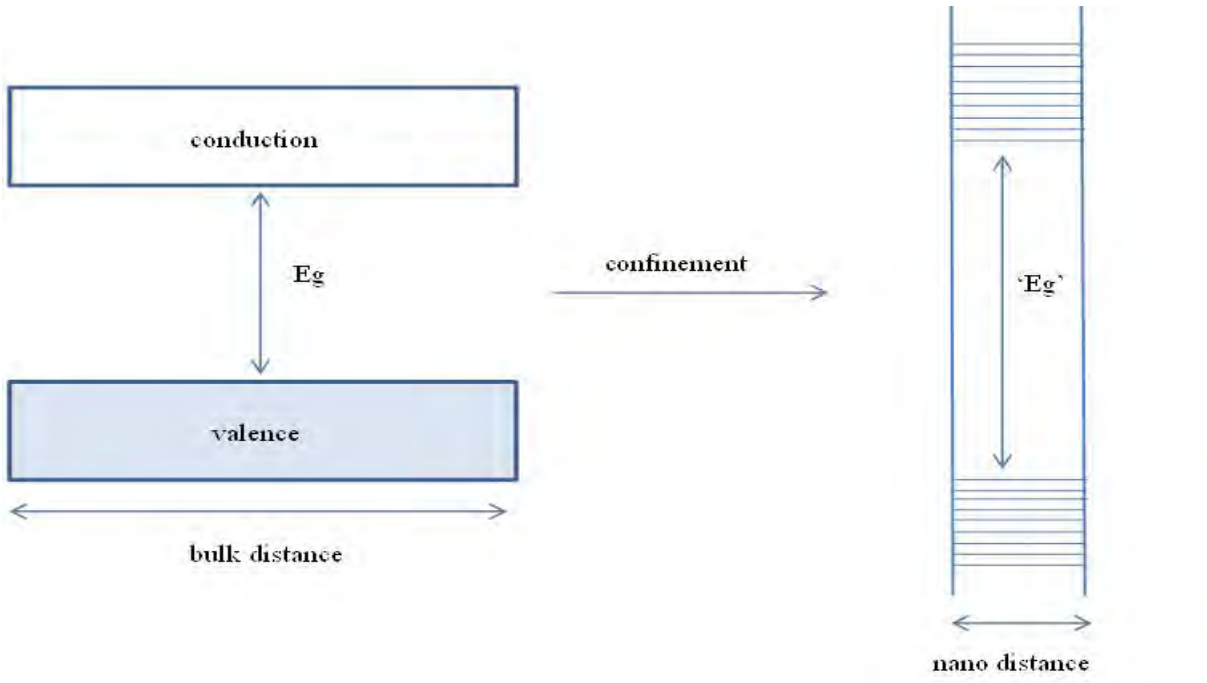

Figure 1.5: A one dimensional spatial electronic diagram for (a) bulk semiconductor (b) semiconductor quantum confined nanocrystal.

1.6 Routes to nanoparticle synthesis

1.6.1 Colloidal Routes

The division of nucleation and growth process as reported by La Mer *et al*. [10] is of central importance to obtaining or accomplishing narrowly dispersed colloids. Monodispersed nanoparticles are characterized by uniform size in a dispersed phase and this can only be attained if nucleation and growth are apparently separated; fast nucleation and slow growth. Solvents with low dielectric constants or stabilizers like syrene/maleic acid copolymer can enhance colloidal growth stability [11]. Colloidal route to nanoparticles synthesis can be undertaken by carrying out precipitation in a homogenous solution or phase in the presence of stabilizers whose function is to prevent agglomeration and additional growth [12-15].

Spenhel *et al*. [14] made the first attempt to prepare nanoparticles of II-VI semiconductor type through colloidal suspension when CdS was synthesized via precipitation of Cd^{2+} by adding H_2S in aqueous solution. Research in colloidal group II-VI semiconductor has witnessed considerable interest. Quite a number of stabilizing or passivating agents have been found in literature for the preparation of colloidal semiconductor within the last few decades. Among which are: inorganic, organic polymers, amines, thiols and polyphosphates [16-25]. The relative growth rates are affected by specific adsorption of surfactant on independent crystallographic planes leading to a means of controlling the nanoparticle shapes. The photoluminescence property of nanoparticles is also controlled by the capping agents or stabilizers. Recently, many studies have been conducted on solution phase synthesis of semiconductors nanoparticles passivated by different surfactant at low temperature. CdS nanowires and nanorods have been synthesized by Dalvand *et al*. [26] via solvothermal method in different solvents such as ethylenediamne, triethylene tetraamine and ethanolamine. The nature of the solvent determines the preferred growth orientation and the

aspect ratio of nanoparticles. CdS nanowires with highest aspect ratio were obtained when ethylenediamine was used while nanorods were prepared with ethanolamine and triethylene tetraamine solvents. Yu *et al*. [27] reported an eco-friendly chemical colloidal method for the preparation of glucose capped CdS nanoparticles and its application on a commercial scale. The advantage of the method is that it is free of the hazardous and toxic stabilizing agents like thiourea, thiophenol and mercaptoacetate [28].

1.6.2 Solvothermal routes

Solvothermal synthesis is a process of transforming reactants or precursors in solution medium and in a closed system usually an aluminium autoclave which is heated to a certain temperature for a particular time and under high pressure. The reaction takes place at a temperature higher than the boiling point of the solvent. After the cooling of the autoclave, the as-prepared product is recovered, dried and ready for analysis. The demerit of this synthetic route is the inability to control the morphology of the nanoparticles; products are amorphous, crystalline solid, nanorods and flower-like [29]. A variety of reaction conditions have been studied and the average temperature range is 160-500 °C with reaction time being between 1 hr and 30 days. In case water is used for synthesis the method is called hydrothermal and the synthesis is usually undertaking below the supercritical temperature of water (340 °C). Based on the experimental conditions, solvothermal synthesis can be heterogenous or homogenous and can exist in subcritical or supercritical condition.

1.6.3 Precursor Routes

The problems associated with the colloidal route to nanoparticle synthesis can be solved by the use of an alternative method that employs organometallic and or metal organic compounds in an anaerobic environment. This method was pioneered by Bawendi *et al*. [30]

and it was through it that quality, monodispersed, crystalline CdSe, CdS, and CdTe nanoparticles were prepared. MeCd dispersed in tri-n-octylphosphine (TOP) and (TOPE) (where E= Se, S, Te) were injected into hot (230-260 °C) coordinating solvent or capping agents, tri-n-octlyphosphine-oxide, TOPO [30]. This initiated a small outbreak of nucleation and subsequently a slow growth and annealing in accordance with Oswald ripening [31]. The role of the coordinating solvent, TOPO, is to act as stabilizer for the colloidal dispersion and electronically cap the surface of the semiconductor nanoparticles. The organic capping agents can be substituted by other groups like amine, pyrimine, tris(2-ethylhexyl)phosphate and 4-(trifluoromethyl)thiophenol.

1.6.4 Single molecule precursor

Single source precursor route was introduced by Brenman *et al*. [32] in the late 80's as a substitute route for synthesis of metal chalcogenide semiconductor nanocrystals. He embarked on the thermolysis of $Cd[Se(C_6H_5)]_2$ using 4-ethylpyridine solvent at high boiling point. Ever since then diakyl-dithiocarbamate complexes of group II-VI and IV-VI semiconductors nanoparticles have been extensively prepared and reported. The single source precursor contains both the organic and the inorganic component; metal and chalcogen source, needed for the preparation of metal chalcogenide nanocrystals. TOPO-capped CdS and CdSe semiconductor nanoparticles have been reportedly prepared by Trinidade and O'Brien from cadmium dithio- and diselenocarbamate complexes [33, 34]. In the experiment, the precursor was dispersed in TOP and injected in hot TOPO which serves as a capping agent. The formation of nanoparticles is in accordance with La Mer mechanism for colloid [35]. The general scheme of growth stages in single source precursor synthesis is shown in Figure 1.6. The decomposition of the precursor is a precondition for the formation of nanoparticles and growth is terminated when the precursor is exhausted. The initial rapid

nucleation at the onset of injection precedes a controlled growth of the nuclei. When the growth of nanoparticles reached the expected size, further growth is terminated by a sudden cooling of the solution. The product which in this case is the nanoparticles is separated with the addition of a solvent which can precipitate it; miscible with the nanoparticles and immiscible with the capping agent preventing aggregation that is due to flocculation. The resultant turbid mixture is subjected to centrifugation to isolate the nanoparticles and the sample is air dried. The already capped nanoparticles are dispersed in appropriate solvent for optical and physical analysis.

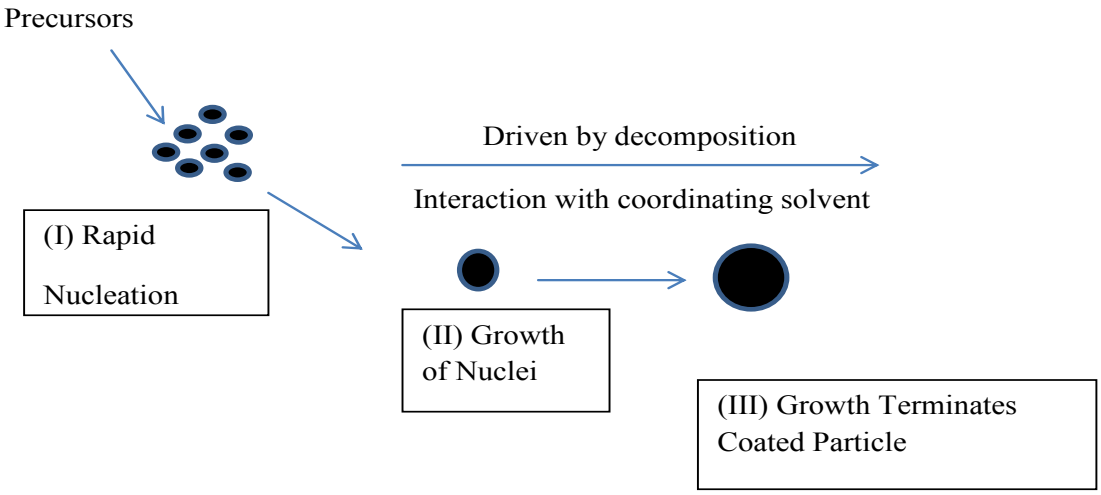

Figure 1.6: Schematic diagram of a one pot synthetic method of nanoparticle synthesis [36].

1.6.5 Requirements of precursors

The needed requirement of a potential single source precursors for the synthesis of metal sulfide are as follows; it must contain the metal and sulfur sources (at least bonded together); it must be air stable and must not oxidize or decompose; under thermal decomposition it must

give metal sulfide as products; in case there is a by-product, it must be un-reactive or volatile. This is why the choice of metal 1,1 dithiolate came up. Dithiolate ligands have the ability to stabilize metal centres. Some dithiolate ligands have other heteroatoms like oxygen, phosphorus. Examples of such are the xanthates, dithiophosphate and these can be a source of impurities in the samples prepared. Oxidations which are a common problem in metal sulfide synthesis should be avoided. 1, 1 dithiolate derivatives like 1-cyano-1-carbo-2, 2-ethylene dithiolate complexes are similar to dithiocarmates complexes which have been used extensively as single source precursors for metal sulfide nanoparticle synthesis. The two ligands similarity is their ability to stabilize a wide range oxidation states unlike xanthates [37]. Oxygen atoms in xanthates have a high electronegativity which will not enable it to form a thioureide resonance analogue form and due to this, it's less liable to stabilize higher oxidation states.

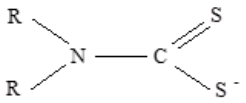

Dithiocarbamate

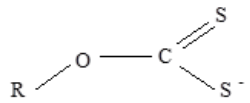

Xanthate

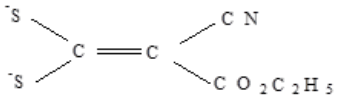

1-cyano-1-carboethoxy-2, 2-ethylenedithiolate

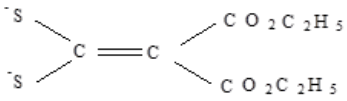

1, 1-diethoxycarbo-2,2-ethylenedithiolate

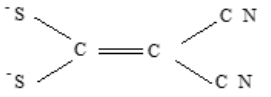

1, 1-dicyano-2,2-ethylenedithiolate

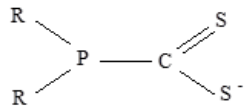

Phosphino dithioformate

Figure 1.7: Selected derivatives of 1, 1 dithiolate ligands

1.6.6 1-cyano-1-carboethoxy-2, 2-ethylenedithiolate

1-cyano-1-carboethoxy-2,2-ethylenedithiolate(CED) is a derivative of 1,1 dithiolate ligand and it has been used in the stabilization of unusually high oxidation state metal ions. Most mononegative 1,1 dithiolates such as ethylxanthate or diethyldithiocarbamate do not give electron delocalization beyond the MS_2 moiety in the complexes of the dithiolates unlike the CED which is a dinegative ligand and it has the ability of expanding electron delocalisation

beyond the MS_2 group [38]. It is prepared by suspending pulverised potassium hydroxide in a solution of ethyl cyanoacetate and carbon disulfide both in equal volume of dioxane. It is difficult to get good single crystal of asymmetrically substituted, CED, of the type $S_2CC(X)(Y)^{2-}$. This is due to the presence of many isomeric species in solution caused by the asymmetrical 1,1 dithiolate ligand and this impedes an extensive detailed characterisation of isolated complexes [39] The chemistry of bidentate ligand, 1-cyano-1-carboethoxy-2,2-ethylenlenedithiolate was extensively researched in the early seventies and there is a renewed attention because of possibility of being applied in organic conductor and solid state materials. Additionally, this ligand is a good chelating agent and can coordinatively react with transition metals to form crystals of many transition elements with different geometrical coordination crystals which have been identified [40-47]. The complexes of 1-cyanocarbo-1-ethoxy-2,2-ethylenlenedithiolate are not soluble in common organic solvent but fairly soluble in high coordinating solvent like DMF and DMSO. There are other ligands like xanthate, dithiocarbamates, and many other rich sulfur sources such as tetramethyl thiuram disulfide, thiosemicarbazide and thioacetamide. A short review on the use of these ligands will be given below.

1.7 Single-source precursors for metal chalcogenide nanoparticles

1.7.1 Complexes of thiosemicarbazide

Thiosemicarbazide also known as 1-aminothiourea or 1-hydrazinecarbothioamide, or N – aminothiourea has a molecular formula of CH_5N_3S. This ligand has been used as a good sulfur source in the synthesis of metal complexes used as precursors for the preparation of nanoparticles. Using novel compounds can be very useful and also open the way for the preparation of nanomaterials to controlled shape, crystallinity and size distribution. Thiosemicarbarzide reacts with mainly transition metals as a ligand because of their ability to

form chelates by coordinating through the sulfur atom. The complexes are prepared by the reaction of thiosemicarbazide with metal salts in methanolic solution. These complexes are moisture and air stable decomposing to metal sulfide during thermolyses and due to this they have been very useful as single source precursors for the synthesis of metal sulfide nanoparticles and thin films. It is noteworthy to examine some of the reported works where thiosemicarbaside ligands have been employed in the synthesis of metal chalcogenide precursors. Mlondo *et al*. [48] reported two thiosemicarbazide complexes which were found effective as single source precursors for the preparation of hexadecylamine (HDA) capped anisotropic CdS nanomaterials on thermal decomposition. The single X-ray structures of these complexes were also obtained; $Cd(NH_2CSNHNH_2)Cl_2]n.H_2O$ (A) and $[Cd(NH_2CSNHNH_2)_2Cl_2]n$ (B). A cadmium acetophenone thiosemicarbazone complex has been exployed as a single source precursor for the synthesis of CdS nanocrystaline and thin films [49]. Single crystals of the complex have also been diffracted.

The effect of growth temperature on the morphologies of these films was observed. PbS nanoparticles were reportedly prepared from the thermal decomposition of bis[bis(thiosemicarbazide)lead(II)], $[Pb(TSC)_2]Cl_2$ (TSC = thiosemicarbazide), using a single source precursor method in the presence of oleylamine and triphenylphosphine as surfactant [50]. The synthesis of ZnS and HgS from $[M(TSC)_2]Cl_2$, has been reported by Sobhani *et al*. [51]. This was achieved from the thermolysis of the thiosemicarbazide complexes as single-source precursor while oleylamine ($C_{18}H_{37}N$) and TPP ($C_{18}H_{15}P$) were employed as surfactants. Nair *et al*. [52] reported the synthesis of thiosemicarbazide complex from the reaction of $CdCl_2.H_2O$ and thiosemicarbazide. The complex, $[Cd(NH_2CSNHNH_2)_2Cl_2]$, formed was thermolysed in tri-n-octyphosphine oxide (TOPO) to produce CdS nanorods. The interrelationship between the decomposition of many single-source precursors and their

morphology has been investigated by Nair *et al*. [53]. Diverse derivatives of thiourea and thiosemicarbazide were employed and it was revealed that the thiosemicarbazide and selenosemicarbazide gave rod shaped CdS and CdSe and this was attributed to a structure directing constituent of semicarbazide released upon decomposition.

1.7.2 Dimorpholinodithioacetylacetonate complexes.

The reaction of morpholine with sulphur and allyl propyl ether at 110 °C gave dimorpholinodithioacetylacetonate ligand which was further reacted with cadmium nitrate to give the corresponding complex, $[Cd(msacmsac)_2(NO_3)_2]$,(msacmsac= dimorpholinodithioacetylacetonate). This complex prepared by Ramasamy *et al*. [54] was the first of its kind and has been used as a single source precursor for the deposition of CdS thin film via an aerosol assisted chemical vapour deposition (AACVD). Hexagonal phase CdS nanorods were obtained from themolysis of the $[Cd(msacmsac)_2(NO_3)_2]$ in oleylamine at 160-240 °C.

1.7.3 Complexes of thiourea

Moloto *et al*. have reported the complexes of cadmium(II) complexes of N, N-diisopropylthiourea and N,N dicyclohexylthiourea and the X-ray crytal sturucture have been determined. The complexes decompose to give a good crystalline CdS. The effect of the temperature of thermolysis on the optical properties and morphology of the particles were also investigated [55]. Dithioubiurea complex with cadmium, $[Cd(NH_2CSNHNHCSNH_2)Cl_2]$, have been reported by Nair *et al*. [56] as precursor for the synthesis of CdS nanoparticles. The precursor was decomposed in trioctylphosphine oxide to give quantum confined CdS nanoparticles with morphology that is dependent on the temperature of injection of the precursor. Apart from the common use of PVP in the synthesis

of nanocomposite, Moloto *et al*. [57] have prepared a thiourea-PVP ligand which was used to synthesize a CdS nanoparticle via a modified single source precursor method with green approach. Other capping agents such as PVA and starch were employed and it was revealed that PVA was the best capping agents with CdS nanoparticle. Co(II) and Ni(II) thiourea and alkylthiourea complexes have been synthesized by Mgabi *et al*. [58]. The metal salts of the selected metals were reacted with thiourea, phenylthiourea and dicyclohexylthiourea ligands in ratio 1:2. The as-prepared complexes are; $[CoCl_2(CS(NH_2)_2)_2]$ (I), $[CoCl_2(CSNHC_6H_5NH_2)_2$ (II) and $[CoCI_2(SC(NHC_6H_{11})_2)_2]$ (III), $[NiCl_2(CS(NH_2)_2)_2]$ (IV), $[NiCl_2(CSNHC_6H_5NH_2)_2]$ (V) and $[NiCl_2(SC(NHC_6H_{11})2)2]$ (VI). These complexes were used as single molecular precursor for deposition of CoS and NiS thin film via aerosol assisted chemical vapour deposition technique AACVD. A simple synthetic route for the preparation of impurity free and star-shaped PbS have been fabricated by Patel *et al*. [59]. He employed a solvothermal route using an environmental benign aminocaproic acid (ACA) mixed with methanolic Pb-thiourea complex as precursors at an annealing temperature of 170 ^oC for 20 h. The as-prepared PbS nanoparticles were characterized with XRD, SEM, and EDX. The results revealed that the star shaped PbS are crystalline with cubic phase and the FTIR study showed that the aminocaproic molecules were attached to the PbS crystals via a lone pair of nitrogen amino head group.

1.7.4 Complexes of Dithiobiuret

Dithiobiuret is an organosulfur compound obtained as the product of a condensation reaction of two molecules of thiourea. Dithiobiuret is extremely toxic and can also be used as an intermediate for pest control chemicals. Ramasamy *et al*. [60] has also synthesized and characterized cobalt complexes of 1,1,5,5-tetramethyl-2,4-dithiobiuret, $[Co\{N(SCNMe_2)_2\}_3]$ (1), and 1,1,5,5-tetraisopropyl-2-thiobiuret, $[Co\{N(SOCNiPr_2)_2\}_2]$. These complexes yielded

cobalt sulfide nanoparticles by thermolysis in hexadecylamine, octadecylamine or oleylamine using single source precursor method. Ramasamy *et al*. [61] also reported the synthesis of zinc and cadmium complexes of 1,1,5,5-tetraalkyl-2-4-dithiobiurets, $[M(N(SCNR_2)_2)_2]$, where [M = Zn, R = methy (1), ethyl (2) and M = Cd, R = methyl (4), ethyl (5)] and 1,1,5,5-tetraalkyl-2-thiobiurets $[M(SON(CNR_2)_2)_2]$ [M = Zn, R = isopropyl (3) and M = Cd, R = isopropyl (6)] were synthesized and the complexes gave their respective metal sulfides on thermolysis using a single source precursor method. Also the zinc cadmium sulfide (ZnxCd1−xS) thin films were prepared by aerosol assisted chemical vapor deposition (AACVD). Ramasamy *et al*. [62] have synthesized a series of nickel(II) complexes of several 1,1,5,5-tetraalkyl-2-thiobiurets and these complexes gave nickel sulphides and thin films were used as single source precursors.

Ramasamy *et al*. [63] have also reported the synthesis of four Iron (III) complexes; 1,1,5,5-tetraalkyl-2-thiobiuret $[Fe(SON(CNiPr_2)_2)_3$ (1), $Fe_2(\mu\text{-}OMe)_2(SON(CNEt_2)_2)_2$ (2), $Fe(SON(CNEt_2)_2)_3$ (3), and $Fe(SON(CNMe_2)_2)_3$ (4)]. The single –crystals X-ray structures of 1, 2 and 4 have been determined and thermogravimetric analysis of the complexes showed decomposition to iron sulfide in one major step. These complexes gave iron sulfide thin film when used as single source precursors. 1, 1, 5, 5-tetraalkyl-2- thiobiuret ligand is prepared by the reaction of N'N-dialylcarbamyl chloride and sodium thiocyanate and dialkylamine. The addition of a solution of this ligand in acetonitrile methanolic solution of metal salts gives metal complexes of thiobiurets [64]. A series of dithiobiuret compounds have been prepared using this method and varieties of metal salts of Co, Ni, Fe, Zn, Cd and In were employed to obtain compounds that are potentially good as single source precursor for synthesis of nanoparticles. The synthesis of nickel(II) and iron(III) thiobiuret were reported by Abdelhady *et al*. [65] and these complexes have been thermolysed in different capping agents;

oleylaminine, octadecene or dodecanethiol, as single source precursor to give Ni_3S_4 and Fe_7S_8 nanoparticles with divergent morphologies.

1.7.5 Complexes of thiuram mono(di)sulfide as precursors

Cadmium complex of tetrametylthiuram disulfide was synthesised by Moloto *et al*. [66]. The complexes were thermolysed as a single source precursor to give HDA-capped CdS nanoparticles. The effect of synthetic parameter; precursor concentration, temperature and capping environment, on the morphology of nanoparticles was investigated. It was revealed that an increase in temperature and precursor concentration increases the particle size while the capping environment also affects the morphology of the nanoparticles. Satyendra *et al*. [67] prepared complexes of Zn(II), Cd(II) and Hg(II) with sulfur donor ligand, tetraethylthiuram disulfide, and thermolysed them as single source precursors in different precursor:surfactant ratio (1:1 and 1:5) to give ZnS, CdS and HgS nanoparticles. He also studied the potency of the complexes, nanoparticles and corresponding Schiff bases against Escherichia coli bacteria. Kolb *et al*. [68] reported the use of tetramethyl thiuram monosulfide as a suitable precursor for the synthesis of nano-size metal sulfide. Although the particles of the metal sulfides obtained are in the nano-regime the particles are devoid of quantum confinement that is typically observed in nanomaterials.

1.7.6 Complexes of xanthate precursors

Xanthate is a salt formed from the reaction of alcohol with carbon disulphide in the presence of an alkali. This compound and its derivatives have been used as single source precursor for the synthesis of metal sulphide nanoparticles. Pradhan *et al*. [69] prepared several metal sulfide with the use of alkyl xanthate, thiocarbamates as single source precursor and Lewis base alkylamine as solvents. The as-prepared metal sulphides nanoparticles are crystalline

despite the low temperature. Bismuth trisxanthate and the dithiocarbamate in ethylene glycol have been used by Koh *et al*. [70] as single source precursors for the synthesis of Bi_2S_3 nanorods and nanotapes. The bismuth xanthate showed a lower decomposition temperature than the dithiocarbamate. It was discovered that precursors that have polymeric structural motif have higher decomposition temperature than the ones that displays dimeric motif. Cusack *et al*. [71] also worked on Zn(II) and Cd(II) ethylxanthates, $[M(S_2COEt)_2TMEDA]$, and establish the structure through single X-ray crystal diffraction. He also prepared $[Cd(S_2COEt)_2(diamine)]$ and obtained CdS through a surfactant assisted single source molecular precursor method using the as-prepared complexes.

Li *et al*. [72] prepared nanorods and faceted CdS nanocrystals from the thermolysis of cadmium ethylxanthate using HDA as capping agent. The influence of reaction condition; temperature and monomer concentration and reaction time, on the morphology and surface states was studied. It was found that the reaction system can change from thermodynamic to kinetic-controlled depending on the how the reaction conditions are varied. Zhang *et al*. [73] have reported the synthesis of Ag_2S nanoparticles through the thermolysis of solventless silver xanthates as single source precursor. It was observed that the control of the Ag_2S depends on the alkyl chain length of the xanthate ligand which serves as the capping agent. Ag_2S nanoparticles from carnaubly xanthate exhibited the smallest diameter of 8.97 nm whereas the product obtained from hexadecylamine and silver octyl xanthate displayed a bigger average diameter of 19.57 nm and 48.37 nm respectively.

1.7.7 Complexes of dithiocarbamate

Dithiocarbamate metal complexes are one of the most studied 1, 1 dithiolate complexes as far as the synthesis of nanoparticles is concerned [74 - 77]. They also have a wide range of usage

in analytical and medicinal chemistry [78 - 80]. It has also been confirmed that they are versatile chelating agents. Several authors have reported the use of dithiocabamates complexes as a precursor for the synthesis of metal sulfide nanoparticles as a result of the effectiveness of the precursor complexes in producing the metal and the chalcogenide on their thermolysis. Ajibade *et al*. did a lot of study on dithiocarbamates metal complexes of the form ML_1L_2 where the ligands L_1 and L_2 represent N-methyl-N-phenyldithiocarbamate and N-ethyl-N-phenyldithiocarmates respectively. They were used to prepare HDA capped metal sulfide nanoparticles and the CdS nanoparticle exhibit sharp absorption edge while crystalline ZnS were revealed with stacking arrangement and HgS displayed TEM images with narrow size distribution [81]. Ajibade and Ejelonu have synthesized ZnS, CdS and HgS nanoparticles from thermolysis of respective metal dithiocarbamates using a single source precursor method. The metal sulfide nanoparticles were further incorporated in polymethyl metharcrylate to prepare the polymernanocomposite of the metal sulfides [82].

1.7.8 Complexes of heterocyclic dithiocarbamate

Apart from the use of alkyl dithiocarbamate metal complexes that have been reported by several authors for the synthesis of nanoparticles via the single source precursor route, heterocyclic dithiocarbamate have also been employed for similar work. Nirmal *et al*. [83] reported the synthesis of CdS nanostructures using cadmium with pyrrolidine dithiocarbamate as single source precursor and HDA as both the solvent and capping agent. Microwave irradiation was used for the decomposition of the precursor at a temperature of 150 ºC and hexagonal CdS nanoparticles were obtained. Nyamen *et al*. [84] synthesized two heterocyclic dithiocarbamato Cd(II) complexes and thermolysed them at different temperature, 80 - 270 °C, and in different amine as capping agent to give different shapes of CdS with nanorod morphology. It was observed that the longer the length of the alkylamine

chain the shorter the length of the rods of the CdS nanoparticles. The binding of the amine on the surface of the nanoparticles as capping agents was also confirmed by the Infra-red spectroscopy.

Nyamen *et al*. [85] also prepared two complexes of Zinc(II); heterocyclic piperidine and tetrahydroquinoline dithiocarbamates and the single X-ray diffraction structure of the latter shows four sulfur atoms bonded to the zinc central metal while the former is dimeric molecule. These complexes were both thermolysed in HDA and TOPO at 180 ºC and 270 °C as single source precursor to produce HDA and TOPO capped ZnS. It was observed from the UV-Vis and photoluminescence spectra that the ZnS are quantum confined. Two more heterocyclic cadmium dithiocarbamate complexes; $[Cd(S_2CNC_5H_{10})_2]$ and $n[Cd(S_2CNC_9H_{10})_2]$ have been synthesized by Mthethwa *et al*. [86] in which they were thermolysed at a temperature of 180 °C to give CdS. Spherical nanoparticles were observed at high concentration and at lower concentration, rods, bipods and tripod shapes evolve.

1.7.9 Adducts as Precursors

Zn(II) and Cd(II) bipyridine addcts of bis(N-phenyldithiocarmate have been synthesized and used for the preparation of HDA capped ZnS and CdS nanoparticles by Onwudiwe *et al*. [87]. The adducts of the complexes were thermolysed at reaction temperature of 180 °C and 220 °C and spherical MS nanoparticles were obtained whose absorption and photuminescence spectra show blue shift and band edges. Pyridyl bis(-ethyl-N-phenyl dithiocarbamato)Zinc(II), $[ZnL_2py]$, and (bis-pyridyl)bis(N-ethyl-N-phenyldithiocarbamato)cadmium(II) complexes have been prepared. Both adducts complexes were used as single source precursors and gave hexadexylamine capped ZnS and CdS on thermolysis at a temperature of 280 ºC. The morphology of the metal sulfide is hexagonal and

optical absorption revealed blue shifted band edges of the metal sulfide particles [88]. Srinivasan *et al*. [89] reported the synthesis of [Cd(thqdtc)$_2$(1,10-phen)], [Cd(thqdtc)$_2$(2,2'-bipy)] and [Cd(thqdtc)$_2$] (where thqdtc =1,2,3,4-tetrahydroquino-linedithiocarbamate). Single crystals X-ray structures of the first two complexes shows that the environment of the central metal is distorted octahedral. The first complex was used as a single source precursor for the synthesis of CdS nanorods that is quantum confined.

Srinivasan *et al*. [90] also worked successful on preparing (1,10-phenanthroline)bis(1,2,3,4-tetrahydroquinolinecarbodithioato-S,S')mercury(II); [Hg(thqdtc)$_2$(1,10-phen)], and obtained the single crystal. The as-prepared [Hg(thqdtc)$_2$(1,10-phen)] was thermolysed for 2 mins at 117 ºC in ethylenediamine and found to be effective single source precursor for the synthesis of hexagonal shaped α-HgS nanosheets. ZnS nanoparticles have been prepared as reported by Srinivasan *et al*. [91] from Zn(thqdtc)$_2$, Zn(thqdtc)$_2$(py) and Zn(thiqdtc)$_2$(py) (i.e 1,2,3,4-tetrahydroquinolinecarbodithioate, thiqdtc = 1,2,3,4-tetrahydroisoquinolinecarbodithioate pyridine adducts) via single source precursor method. The complexes were thermolysed at low temperature in triethylenetetramine (trien) which was used as a capping agent.

1.7.9.1 Dithiophosphinates

Takahashi *et al*. deposited CdS thin layers from the pyrolysis of dimethyldithiophosphinates complex of Cd(II). Good quality ZnS and CdS films were also reportedly grown on silver plated glass substrates [92]. Byrom *et al*. reported the synthesis of Zn(II) and Cd(II) complexes of bis(dithiophosphinate). The X-ray crystal structures were obtained and both compounds have potential as single source precursor for the synthesis of ZnS and CdS nanoparticles and thin film [93].

1.8 Application of nanoparticles

The unique phenomenon of nanoparticles properties (novel electrical, optical, chemical, mechanical, magnetic properties etc) can be selectively controlled by engineering the size, morphology and composition of the particles. These new substances will have entirely different properties from their parent material. Hence industries can reengineer many existing products and design novel product or processes to function at unprecedented levels. Below are some of the applications of nanoparticles.

1.8.1 Renewable energy

The huge resource from the sunlight shining on the earth surface in form of solar energy is remarkable and an hour of incident light from the sun is more than the yearly human consumption of energy [94]. The amount of solar energy the earth receives depends on the season with the summer months having the highest quantity of solar energy [95]. The need to harness these resources that happens to be the best source of renewable energy can be improved successfully with nanotechnology. This can be enhanced because nanoparticles have a surface to volume ratio that can increase solar cell efficiency by exposing a wider surface area to the sunlight unlike the conventional fluid that has poor conversion efficiency. In addition materials like lead-selenide can increase solar cell efficiency due to the fact that they cause more electrons to be released when they are struck by photons of light and consequently increase electricity [96, 97].

1.8.2 Catalytic Applications

The field of nanocatalysis (in which nanoparticles are used to catalyze reactions) has undergone an exponential growth during the past decade. Two types of studies have been carried out; homogeneous catalysis in solution and heterogeneous catalysis in which the

nanoparticles are immobilized on inorganic or organic polymers [98]. Furthermore, the changes in electronic properties arising from quantum confinement in small nanocyrstals also bestow unusual catalytic properties on these particles because nanoparticles have a large surface-to-volume ratio compared to bulk materials. They are therefore used as catalysts [99]. This potential shape dependent catalysis adds to the advantage of using nanoparticles as catalysts. In the course of catalysis, the fact that nanoparticles are small with corners and edges could make their surface atoms unstable during the chemical reaction they catalyze and shape changes could occur. Yates *et al*. [100] showed that there is a decrease in catalytic activity per unit surface area of nickel with the increase in particle size in the hydrogenation reaction of ethene. Modified nanocatalysts have been explored to enhance selectivity and stability and this show that the role of catalysts is more than speeding up reaction rates [101]. Also nanoparticles used as catalysts in combustion engines, have shown properties that render the engine more efficient and therefore more economical.

1.8.3 Biological Application of nanoparticles

Recently, researchers have been conducting investigations on nanoparticles with the aim of commercially exploring their unique, optical, mechanical and electrical properties [102]. Nanoparticles generally, due to their sizes in nanometer regime are biologically-active forms of their conventional source material [103, 104]. The extremely small sizes of quantum dots and small nanomaterials facilitate their absorption through cell membranes [105, 106]. Furthermore these small sizes enable oral, olfactory or dermal application by allowing passage through the cells and translocation via blood and lymph. Experimental cancer treatment has also revealed their capability in crossing blood-brain barrier and this confirms the uniqueness of the size [107]. Quantum dots probes have the capability to track molecules and cells over extended period of time without introducing too much of interference [108].

1.8.4 Targeted drug delivery

One important aspect of the breakthrough in nanotechnology is the ability of the new novel drugs to target specific cells or tissue locations. Today's delivery system is such that the drugs are designed to be able to spot the exact site of ailment. Surface functionalization with ligands that are recognizable by the receptor of the cell's surface is one of the strategies of achieving the delivery of drugs to the target of interest. The selectivity of ligand receptor interaction enables a more exact targeting of site of specific interest [109]. Nanotechnology provides a rare opportunity to overcome another challenge to arrive at this goal in a better way, to make the delivery of the drug at the required location at the right time [110]. It is also anticipated that nanotechnology will bring a dramatic change in the manufacturing industries in the future and this will have a huge impact on life sciences, drug delivery, detection of disease symptoms and the production of therapeutic biomaterials.

1.8.5 Thermal application

Specifically engineered particles could improve the transfer of heat from collectors of solar energy to their storage tanks. They could also enhance the coolant system currently used by transformers in these types of processes with a wide range of active self-assembly mechanisms for nanoscale structures that start from a suspension of nanoparticles in fluid. Addition of nanoparticles in a liquid remarkably enhances the energy transport process of the base liquid [111]. Aerogel insulation is a method of creating a synthetic porous material made from gel in which the fluid has been replaced by gas. The ultra-light material has an internal cross linked features with a number of microscopic pores filled with gas. The absence of vacuum in aerogels prevents the problem of degradation over time. It has both low density and thermal conductivity which attest to its wide applications as insulation materials.

Aerogels are commercially available as fibre composites and their thermal conductivity is around 0.0013W/(mK) [112].

1.8.6 Metal sulfide nanoparticles

1.8.6.1 Zinc Sulfide (ZnS)

ZnS has strong preference for an n-type semiconductor [113] and the band–gap energy is 3.7ev at 300 K. It's also a luminiscenece material, well known for its photoluminescence [114] and electroluminescence [115] and has applications in various fields such as phosphor, solar cells and lasers [116]. In some cases it is used as thin films but it is mostly used in the form of particles. It has been proven that the particle size and distribution play an important role in their applications. The brightness and voltage characteristics depend strongly upon the size of particles using phosphor as an example [117,118].

1.8.6.2 Cadmium sulfide (CdS)

Cadmium sulfide (CdS) is semiconductor which has a direct band gap of 2.4 eV for bulk wurtzite structure, and 3.53 eV for the bulk cubic zinc blende structure [119, 120] and it has been applied to many areas due to the suitability of this band gap and it also has a strong photoresponse in the visible region [121]. CdS nanoparticles have outstanding properties which make it an attractive choice for fucnctional materials and widely used in many fields such as solar, photo dectector photoelectrochemistry, photochromism and electrochromic materials [122-127].

1.8.6.3 Mercury sulfide (HgS)

Mercury sulfide is a member of group II-VI compound semiconductor materials. It crystallizes in two forms; the cubic phase (β–HgS, metacinnabar) and the hexagonal phase

(α–HgS, cinnabar). Very scarce reports are available on nanocrystalline α–HgS and only few reports are available on nanocrystalline β–HgS. HgS has an optical band gap which varies between 1.9 and 2.6 eV, depending upon the composition [128,129]. HgS semiconductors are useful material and are widely used in many fields such as ultrasonic transducers, image sensors, electrostatic image materials and photoelectric conversion devices and light emitting diodes [130]. The HgS thin films have been used in solid-state solar cells, photo-electrochemical cells, storage cells and photoconductors [131]. One-step hydrothermal treatment for the formation of HgS nanostructures with rod-like and dendrites morphologies have been reported [132]. A novel sonochemical method for selective preparation of α-HgS and β-HgS nanoparticles in aqueous solutions under ambient air has also been reported [133].

1.8.7 Polymer nanocomposite

A composite is a blend of two or more substance of interest with distinct physical and chemical properties and identifiable interface. Composites are referred to as nanocomposites when one of the phases has nano dimension morphology for example, nanoparticles, nanowires or nanotubes [134,135]. Nanocomposite can also be defined as a matrix to which nanoparticles have been added to improve a particular property of the material. The increasing need for latest material in the ever developing field of nanotechnology has opened the way for unique ideas concerning the preparation and characterization of semiconductor nanocomposite. This kind of nanomaterials has the advantage of outstanding optical and mechanical and electrical properties of nanoparticles that can be prepared to the required dimension, and depending on their diameter.

Nanocomposites are much different than the conventional composite with the incorporation of nanoparticles in polymer matrix. Metal sulfide nanofillers embedded in polymers have

important barrier effect to reduce the product vulcanization and heat transport during thermal degradation of the polymer and this helps composite with huge thermal stability. It has been reported that the effect of CdS pyrolysis of polystyrene/CdS nanocomposites has been investigated [136, 137]. There is an enhanced thermal stability in the polystyrene/CdS when compared with the virgin polymer. This is due to partially altered mobility of the host (polymer) chain as a result of the encapsulation of the particles in the polymer matrices. Agarwal *et al*. [138] investigated the mechanical properties of ZnS/polymethyl methacrylate prepared by ex-situ process. Different weight percent of ZnS were used with the determination of mechanical properties at different temperature. The mechanical properties were found to increase up till when the ZnS was 6% and a decline set in at 8% of ZnS incorporated in the polymethy metharcrylate matrix. CdS has been reportedly dispersed in polyvinyl alcohol CdS/PVA deposited on a glass substrate by in situ thermolysis of the precursors. This work was credited to Saikia *et al*. [139]. Maitya *et al*. [140] synthesized a poly-capped ZnS nanocrystalline film by a wet chemical process. The polyvinyl pyrolidone encapsulated ZnS nanocrystals were grown into nanopores inside the polymer matrix and on a glass and silicon substrates. The structural, optical and dielectric properties of the films were investigated with different polymer fractions in the films.

1.8.8 Aims and objectives of work

The aim of this work is to prepare metal complexes of Zn(II), Cd(II) and Hg(II) using metal halides and mixed ligands of substituted thiourea, thiuram disulfide and 1,1 dithiolate derivative as precursors to synthesize HDA capped metal sufide nanoparticles and polymer nanocomposites.

Objectives are;

1.To prepare Zn(II), Cd(II), Hg(II) of mixed ligand metal complexes of substituted thiourea (methyl, dimethyl, diethyl and diisopropyl thiourea) and 1,1 dithiolate derivative.

2. To prepare Zn(II), Cd(II), Hg(II) of mixed ligand metal complexes of tetramethyl thiuram disulfide and 1-cyanocarboethoxy-2,2 ethylene dithiolate.

3. To prepare pyridine, 2, 2' bipyridine and 1, 10- phenanthroline adducts of the diisopropyl thiourea parent complexes.

4. To characterize the synthesized complexes with elemental analysis, IR, TGA and NMR.

5. To synthesize HDA capped ZnS, CdS and HgS by the thermolysis of the complexes as single source precursors.

6. To synthesize ZnS and CdS polymer encapsulated nanocomposites via solution casting method using polymethyl methacrylate, polyvinyl alchohol and polyvinyl pyrrolidone as polymer source.

7. To characterize the metal sulfide nanoparticles with XRD, TEM, SEM, EDX, UV-Vis and PL.

1.9 References

1. Kittel, C. *Introduction to solid state physics*, 2002, John Wiley & sons, Inc., Singapore.
2. Young, H. D. freedam, R. A. University Physics, Addison- Wiley Pub, 9th Ed., 1360.
3. Islam, S. S. Semiconductor Physics and Devices, Oxford University press 2006, 1-564.
4. Knowles, K. Introduction to Semiconductors. http://www.doitpoms.ac.uk/tlplib/semiconductors/images/acceptorlevels.jpg. (accessed July 22, 2015)
5. Wang, Y.; Xia, Y. Bottom-up and top-down approaches to the synthesis of monodispersed spherical colloids of low melting-point metals. *Nano Lett*. **2004**, *4*, 2047-2050
6. Feynman, R. P.; Leighton, R. B.; Sands, M. The Feynman lectures on physics, Reading MA: Addison Wesley Publishers; **1961**, (1).
7. Bohua, S.; Henry, H. X. M. Mechanical nano-resonators at ultra-high frequency and their potential applications. *S. Afr. J. Sci*, **2008**, *104*, 169-171.
8. Hullavarad, N.V.; Hullavarad, S. S.; Karulkar, P. C. Cadmium sulphide (CdS) nanotechnology: Synthesis and applications. *J. Nanosci. Nanotechnol*. **2008**, *8*, 3272-3299.
9. Pan, H.; Feng, Y. P. Semiconductor nanowires and nanotubes: Effects of size and surface-to-volume ratio. *ACS Nano*. **2008**, *2*, 2410-2414.
10. La Mer, V. K.; Dinegar, R. H. Theory, production and mechanism of formation of monodispersed hydrosols. *J. Am. Chem. Soc*. **1950**, *72*, 4847-4852.

11. Samoilova, N.; Kurskaya, E.; Krayukhina, M.; Askadsky, A.; Yamskov, I. Copolymers of maleic acid and their amphiphilic derivatives. *J. Phys. Chem. B*, **2009** *19*, 3395-3403.

12. Chestnoy, N.; Harris, T. D.; Hull, R.; Brus, L. E. Luminescence and photophysics of cadmium sulfide semiconductor clusters: The nature of the emitting electronic state *J. Phys. Chem.* **1986**, *90*, 3393-3399.

13. Brus. L. E.; Electronic wavefunctions in semiconductor clusters. *J. Phys. Chem.* **1986** *90*, 2555-2560.

14. Spenhel, L.; Hasse, H.; Weller, H.; Henglein, A. Surface modification and stability of strong luminescent CdS particles. *J. Am. Chem. Soc.* **1987**, *109*, 5649-5655.

15. Spenhel, L.; Weller, H.; Henglein, A. Photochemistry of semiconductor colloids. 22. Electron injection from illuminated CdS into attached TiO_2 and ZnO particles *J. Am. Chem. Soc.* **1987**, *109*, 6632-6635.

16. Manyar, H. G.; Iliade, P.; Bertinetti, L.; Coluccia, S.; Berlier, G. Structural and spectroscopic investigation of ZnS nanoparticles grown in quaternary reverse micelles. *J. Colloid Interf. Sci.* **2011**, *354*, 511-516.

17. Ashtapurte, S. S.; Deshpande, A.; Marathe, S.; Wankhede, M. E.; Chimanpure, J.; Pasricha, R.; Urban, J.; Haram, S. K.; Gosavi, S. W.; Kulkarni, S. K. Synthesis and analysis of ZnO and CdSe nanoparticles. *Pramana J. Phys.* **2005**, *65*, 615-620.

18. Sondi, I.; Siiman, O.; Matijevic, E. Synthesis of CdSe nanoparticles in the presence of aminodextran as stabilizing and capping agent. *J. Colloid Interf. Sci.* **2004**, *275*, 503-507.

19. Pattabi, M.; Saraswathi, A. B. Effect of precursor concentration on the particle size of mercaptopropionic acid-capped CdS nanoparticles. *J. New Mat. Electr. Sys.* **2007**, *10*, 43-47.

20. Knowles, K. E.; Tice, D. B.; McArthur, E. A.; Solomon, G. C.; Weiss, E. A.; Chemical control of the photoluminescence of CdSe quantum dot-organic complexes with a series of para-substituted aniline ligands. *J. Am. Chem. Soc.* **2010**, *132*, 1041-1050.

21. Rohwer, L. E. S.; Martin, J. E. Luminescence decay of broadband emission from CdS quantum dots. *J. Lumin.* **2007**, *127*, 499-507.

22. Mehta, S. K.; Chaudhary, S.; Kumar, S.; Singh, S. Facile synthesis, growth mechanism, and optical properties of CdSe nanoparticles in self-assembled micellar media and their efficient conjugation with proteins. *J. Nanopart. Res.* **2010**, *12*, 1697-1709.

23. Zhang, P.; Gao, L. Synthesis and characterization of CdS nanorods via hydrothermal microemulsion**.** *Langmuir*. **2003**, *19*, 208-2010.

24. Chen, M.; Xie, Y.; Lu, J.; Xiong, Y.; Zhang, S.; Qian, Y. T.; Liu, X. Synthesis of rod-, twinrod-, and tetrapod-shaped CdS nanocrystals using a highly oriented solvothermal recrystallization technique. *J. Mater. Chem.* **2002**, *12*, 748-753.

25. Gao, F.; Lu, Q. Y.; Xie, S. H.; Zhao, D. Y. A Simple route for the synthesis of multi-armed CdS nanorod-based materials, *Adv. Mater.* **2002**, *14*, 1537-1540.

26. Dalvand, P.; Mohammadi, M. R.; Fray, D. J. One-dimensional cadmium sulfide (CdS) nanostructures by the solvothermal process: Controlling crystal structure and morphology aided by different solvents. *Mater. Lett.* 2011, *65*, 1291-1294.

27. Yu, D.; Chen, Y.; Li, B.; Chen, X. Nanocubes of PbS with visible luminescence synthesized by sulfonated polymer as stabilizer and modifier at room-temperature *Mater. Lett.* **2009**, *63*, 2317-2320.

28. Bansal, P.; Jaggi, N.; Rohilla, S. K. Green synthesis of CdS nanoparticles and effect of capping agent concentration on crystallite size. *Res. J. Chem. Sci.* **2012**, *2*, 69-71.

29. Huang, W.; Xu, Z.; Liu, R.; Ye, X.; Zheng, Y. Tungstenic acid induced assembly of hierarchical flower-like MoS {2spheres}. *Mater. Res. Bull*. **2008**, *43*, 2799-2805.

30. Murray, C. B.; Norris, D. J.; Bawendi, M. G. Synthesis and characterization of nearly monodisperse CdE (E = sulfur, selenium, tellurium) semiconductor nanocrystallites. *J. Am. Chem. Soc*. **1993**, *115*, 8706-8715.

31. Malik, M. A.; O'Brien, P.; Revaprasadu, N. Semiconductor nanoparticles: Their properties, synthesis and potential for application. *S. Afr. J. Sci*. **2000**, *96*, 55-60.

32. Brenmam, J. G.; Siegrist, T.; Carrol, P. J.; Stuczinsky, M.; Brus, L.E.; Steigerwald, M. L. The preparation of large semiconductor clusters via the pyrolysis of molecular precursor. *J. Am. Chem. Soc*. **1989**, *111*, 4141-4143.

33. Trindade, T.; O'Brien, P. Novel single molecule precursor routes for direct synthesis of CdSe nanocrstallite. *Adv. Mater*. **1996**, *8*, 161-163.

34. Trindade, T.; O'Brien, P. Synthesis of CdS and CdSe nanocrystallite using a novel single source molecule precursor approach. *Chem. Mater*. **1997**, *9*, 523-530.

35. Jonson, T.; La Mer, V. K. Theory production and mechanism of formation of monodispersed hydrosols. *J. Am. Chem. Soc*. **1947**, *69*, 1184-1192.

36. Malik, M. A.; O'Brien, P.; N. Revaprasadu. Precursor routes to semiconductor quantum dots. Phosphorus Sulfur Silicon Relat Elem**. 2005**, *180*, 689-712.

37. Hogarth, G. Transition metal dithiocarbamates. *Prog. Inorg. Chem.* 2005, *53*, 71-561

38. Kalbacher, B. J.; Bereman R, D. Preparation and magnetic properties of cobalt(II) and cadmium(II) complexes of the dianion of cyclopentadienedithiocarboxylic acid. Inorg. Chem **1973**, *12*, 2997-3000

39. Liu, C. W.; Liaw, B. J.; Wang, L-C.; Liou, L-S.; Keng.; T-C. Dithiolate cluster of copper(I): Utilization of all possible coordination sites of 1-(deithoxylphosphinyl) -1-cyanoethylene-2-2-dithiolate. *J. Chem. Soc. Dalton Trans*. **2002**, 1058-1065.

40. Liu, S-G.; Liu, Y-Q.; Li, Y-F.; Zhu, D-B.; Crystal structure, spectral anld electrochemical properties of [TBA], [Ni(i-MNT),], [TBA] [Ni(i-MNT),], [TBA],[Ni(i-MNS),] and related bis (1,2-dithiolene) metal complexes. *Synthetic Met*. **1996**, *83*, 131-140.

41. Liu, C. W.; Staples, R. J.; Fackler, J. P. Copper(I) 1,1-dithiolate cluster transformations. Synthesis of $[Bu_4N]6[Cu_6(S,i\text{-}MNT)_6]$, *i*-MNT=$[S_2CC(CN)_2]^-$,from $[Bu_4N]_4[Cu_8(i\text{-}MNT)_6]$ with sulfur. Reaction of the cyclic hexanuclear complex with phosphine to give the tetrahedral $[Bu_4N]_4[Cu_4(i\text{-}MNT)_4]$ which oxidizes in solution to give the homocubane $[Bu_4N]_4[Cu_8(i\text{-}MNT)_6]$ and $[Bu_4N]_2[Cu(i\text{-}MNT)_2]$ *Coord. Chem. Rev.* **1998**, *174*, 147-177.

42. Kirmse R. Single crystal ESR study of copper(II)-bis(1,1-dicyanoethylene-2,2-dithiolate) *Chem. Phys. Lett.* **1973**, *23*, 83-86

43. Sansiviero, M. T. C.; Alves, O. L. Thermal decomposition in air of $[Bu_4N]_2[Zn(imnt)_2]$ (bis(1,1-dicyanoethylene-2,2- ditiolate)zincate II of bis(tetrabutilamonium)and morphological investigation. *Mater. Lett.* **2000**, *45*, 217-223.

44. Liu, Y.; Pan, Q.; Peng, Z.; Li, D.; Zhou, Y. Spectroscopic and theoretical studies on cobalt (II) complex of maleonitriledithiolate and 5-nitro-1,10-phenanthroline. *Spectrochimica Acta Part A*. **2007**, *68*, 78-84

45. Davidovich, R. L.; Stavila, V.; Whitmire, K. H. Stereochemistry of lead(II) complexes containing sulfur and selenium donor atom ligands. *Coord. Chem. Rev.* **2010**, *254*, 2193-2226.

46. Kong, L. Q.; Dou, J. M.; Li, D. C.; Wang, D. Q. Syntheses and crystal structures of two isomeric crown ether lead(II) bis(dithiolate) complexes $[K(18C6)]_2[Pb(i\text{-}mnt)_2]$. *J. Mol. Struct.* **2006**, *785*, 186-191.

47. Ihlo, L.; Bottcher, R.; Olk, R. M.; Kirmse, R. A single-crystal electron paramagnetic resonance ^{13}C and ^{1}H electron nuclear double resonance study of tetra-n-butylamonium-bis(1,2-dithiocyanoethylene 1,2-dithiolate)aureate(II) $[(n\text{-}C_4H_9)_2]$ [Au II$(mnt)_2$ *Inorg*. *Chim*. *Acta*. **1998**, *281*, 160-164

48. Mlondo, S. N.; Revaprasadu, N.; Christian, P.; Helliwell, M.; O'Brien, P. Cadmium thiosemicarbazide complexes as precursors for the synthesis of nanodimensional crystals of CdS. *Polyhedron*. **2009**, *28*, 2097-2102.

49. Palve, A. M; Joshi, P. V; Puranik, V, Shivram, S. Garje, S. S, Synthesis and X-ray single crystal structure of a cadmium(II) acetophenone thiosemicarbazone complex and its use as a single-source precursor for the preparation of CdS nanocrystallites and thin films. *Polyhedron*. **2013**, *61*, 195-201.

50. Salavati-Niasaria, M.; Sobhanib, M. A.; Davara, F. Synthesis of star-shaped PbS nanocrystals using single-source precursor. *J*. *Alloys Compd*. **2010**, *507*, 77-83.

51. Sobhani, A; Salavati-Niasari, M; Sobhani, M. Synthesis, characterization and optical properties of mercury sulphides and zinc sulphides using single-source precursor. *Mater*. *Sci*. *Semicond*. *Process*. **2013**, *16*, 410-417.

52. Nair, P. S. Radhakrishnan, T.; Revaprasadu, N.; Kolawole, G. A.; O'Brien, P. A single-source route to CdS nanorods. *J*. *Chem*. *Soc*. *Chem*. *Comm*. **2002**, 564-565.

53. Nair, P. S.; Scholes, G. D. Thermal decomposition of single source precursors and the shape evolution of CdS and CdSe nanocrystals. *J*. *Mater*. *Chem*. **2006**, *16*, 467-473.

54. Ramasamy, K.; Malik, M. A.; O'Brien P.; Raftery, J. The synthesis and structure of a cadmium complex of dimorpholinodithioacetylacetonate and its use as single source precursor for CdS thin films or nanorods. *Dalton Trans*. **2009**, 2196-2200

55. Moloto, N.; Revaprasadu, N.; Moloto, M. J.; O'Brien, P.; Helliwell, M. *N*, *N*'-diisopropyl- and N,N'-dicyclohexylthiourea cadmium(II) complexes as precursors for the synthesis of CdS nanoparticles. *Polyhedron*. **2007**, *26*, 3947-3955.

56. Nair, P. S; Radhakrishnan, T; Revaprasadua, N; Kolawole, G. A Paul O'Brien, P $Cd(NH_2CSNHNHCSNH_2)Cl_2$: a new single-source precursorfor the preparation of CdS nanoparticles. Polyhedron. **2003**, *22*, 3129-3135.

57. Xaba, T.; Moloto, M. J.; Moloto, N. The effect of water-soluble capping molecules in the "green" synthesis of CdS nanoparticles using the (Z)-2-(pyrrolidin-2-ylidene) thiourea ligand. *Mater*. *Lett*. **2015**, *146*, 91-95.

58. Mgabi, L. P.; Dladla, B. S.; Malik, M. A.; Shivram S.; Garje, J. Akhtar, N. Revaprasadu N. Deposition of cobalt and nickel sulfide thin films from thio- and alkylthio-urea complexes as precursors via the aerosol assisted chemical vapour deposition technique. *Thin Solid Films*. **2014**, *564*, 51-57.

59. Patel, J. D.; Mighri, F.; Ajji, A. Aminocaproic acid mixed methanolic lead-thiourea complex precursor and its thermal decomposition to star-shaped lead sulfide crystals. *Mater*. *Lett*. **2012**, *74*, 183-186

60. Ramasamy, K; Maneerprakorn, W; Malik, M. A; O'Brien, P. Single-molecule precursor-based approaches to cobalt sulfide nanostructures. Size-controlled synthesis of monodisperse Ag_2S nanoparticles by a solventless thermolytic method *Phil. Trans. R. Soc. A*. **2010**, *368*, 4249-4260.

61. Ramasamy, K; Malik, M. A.; Helliwell, M.; Raftery, J.; O'Brien, P. Thio- and Dithio-biuret precursors for zinc sulfide, cadmium sulfide, and zinc cadmium sulfide thin films. *Chem*. *Mater*. **2011**, *23*, 1471-1481.

62. Ramasamy, K; Malik, M. A; O'Brien, P.; Raftery, J; Helliwell, M.; Nickel sulfide thin films from thio- and dithiobiuret precursors *Chem*. *Mater*. **2010**, *22*, 6328-6340

63. Ramasamy, K; Malik, M. A; Helliwell, M; Tuna, F.; O'Brien, P. Iron thiobiurets: single-source precursors for iron sulfide thin films. *Inorg. Chem*. **2010**, *49*, 8495-8503.

64. Ramasamy, K.; Malik, M. A.; O'Brien, P.; Raftery, J. Metal complexes of thiobiurets and dithiobiurets: Novel single source precursors for metal sulfide thin film nanostructures. *Dalton Trans*. **2010**, *39*, 1460-1463

65. Abdelhady, A. L.; Malik, M. A.; O'Brien, P.; Tuna, F. Nickel and iron sulfide nanoparticles from thiobiurets. *J*. *Phys*. *Chem*. *C*. **2012**, *116*, 2253-2259.

66. Moloto, N, Revaprasadu, N, Musetha, P. L Moloto, M. J. Effect of temperature, precursor concentration and capping group on the shape of CdS nanoparticles. *J*. *Nanosci*. *Nanotechnol*. **2009**, 9, 4760-4766.

67. Shukla, S. N.; Gaur, P.; Rai, N. Complexes of tetraethylthiuram disulphide with group 12 metals: Single-source precursor in metal sulphide nanoparticles synthesis. *Appl. Nanosci*. **2015**, *5*, 583-593.

68. Kolb, M. A.; Maier, W. F.; Stowe, K.V. High-throughput syntheses of nano-scaled mixed metal sulphides. *Catal. Today*. **2011**, *159*, 64-73.

69. Pradhan, N.; Katz, B.; Efrima, S. Synthesis of high-quality metal sulfide nanoparticles from alkyl xanthate single precursors in alkylamine solvents. *J. Phys. Chem. B*. **2003**, *107*, 13843-13854.

70. Koh, Y. W.; Lai, C. S.; Du, A. Y.; Tiekink, E.R.T.; Loh. K.P. Growth of bismuth sulfide nanowire using bismuth trisxanthate single source precursors. *Chem. Mater.* **2003**, *15*, 4544-4554.

71. Cusack, J.; Drew, M. G. B.; Spalding, T. G. Syntheses and spectroscopy of diamine complexes of Zn(II) and Cd(II) ethylxanthates and the molecular structures of

[$M(S_2COEt)_2TMEDA$]: Formation of CdS nanoparticles from [$Cd(S_2COEt)_2$] and [$Cd(S_2COEt)_2TMEDA$]. *Polyhedron*. **2004**, *23*, 2315-2321.

72. Li, Y.; Li, X.; Yang, C.; Li, Y.; Controlled synthesis of CdS nanorods and hexagonal nanocrystals. *J. Mater. Chem.* **2003**, *13*, 2641-2648.
73. Zhang, C.; Zhang, S.; Yu, L.; Zhang, Z.; Zhang, P.; Wu, Z. Size-controlled synthesis of monodisperse Ag_2S nanoparticles by a solventless thermolytic method .*Mater. Lett.* **2012**, 85, 77-80.
74. Onwudiwe, D. C.; Ajibade, P. A.; Zn(II), Cd(II) and Hg(II) complexes of *N*-methyl-*N*-phenyl dithiocarbamate as single-source precursors for the synthesis of metal sulfide nanoparticles. *Mater*. *Lett*. **2011**, *65*, 3258-3261.
75. Srinivasan N. Synthesis and characterization of functionalized dithiocarbamates: New single-source precursors for CdS. *Superlattices Microstruct*. **2014**, *65*, 227-239.
76. Nirmal, R. M.; Pandian, K.; Sivakumar, K. Cadmium(II) pyrrolidine dithiocarbamate complex as single source precursor for the preparation of CdS nanocrystals by microwave irradiation and conventional heating process. *Appl. Surf. Sci.* **2011**, *257*, 2745-2751.
77. Birri, A.; Harvey, B.; Hogarth, G.; Subasi, E.; Ugur, F. Allyl palladium dithiocarbamates and related dithiolate complexes as precursors to palladium sulphides. *J*. *Organomet*. *Chem*. **2007**, *692*, 2448-2455.
78. Stary, J.; Kratzer, K. Stability and distribution constants of thallium(I) dithiocarbamates. *J*. *Radioanal*. *Nucl*. *Chem*. *Lett*. **1992**, *165*, 137-143.
79. Monser, L.; Adhoum, N. A. Modified activated carbon for the removal of copper, zinc, chromium and cyanide from wastewater. *Sep. Purif. Technol.* **2002**. *26*, 137-146.

80. Caruso, F.; Chan, M. L.; Rossi, M. A Short Pb.Pb separation in the polymeric compound bis(pyrrolidinecarbodithioato)lead(II) and a conformational pathway interconversion for the "Pb(II)S(4)" framework. *Inorg. Chem*. **1997**, *36*, 3609-3615.

81. Ajibade, P. A.; Onwudiwe, D. C.; Moloto, M. K. Synthesis of hexadecylamine capped nanoparticles using group 12 complexes of *N*-alkyl-*N*-phenyl dithiocarbamate as single-source precursors. *Polyhedron*. **2011**, *30*, 246-252.

82. Ajibade, P. A.; Ejelonu, B. C. Group 12 dithiocarbamate complexes: Synthesis, spectral studies and their use as precursors for metal sulfides nanoparticles and Nanocomposites. *Spectrochim*. *Acta Part A*. **2013**, *113*, 408-414.

83. Nirmal, R. M.; Pandian, K.; Sivakumar K. Cadmium(II) pyrrolidine dithiocarbamate complex as single source precursor for the preparation of CdS nanocrystals by microwave irradiation and conventional heating process. *Appl. Surf. Sci*. **2011**, *257*, 2745-2751.

84. Nyamen, L. D.; Revaprasadu, N.; Pullabhotla, R. V. S. R.; Nejo, A.; Ndifon, P. T. Malik, M. A.; O'Brien, P. Synthesis of multi-podal CdS nanostructures using heterocyclic dithiocarbamato complexes as precursors. *Polyhedron*. **2013**, *56*, 62-70.

85. Nyamen, L. D.; Nejo, A. A.; Pullabhotla, V. S. R.; Ndifon, P. T.; Malik, M. A.; Akhtar, J.; O'Brien, P.; Revaprasadu N. The syntheses and structures of Zn(II) heterocyclic piperidine and tetrahydroquinoline dithiocarbamates and their use as single source precursors for ZnS nanoparticles. *Polyhedron*. **2014**, *67*, 129-135.

86. Mthethwa, T.; Pullabhotla, V. S. R. R.; Mdluli, P. Wesley-Smith, S J.; Revaprasadu, N. Synthesis of hexadecylamine capped CdS nanoparticles using heterocyclic cadmium dithiocarbamates as single source precursors. *Polyhedron* **2009**, *28*, 2977-2982.

87. Onwudiwe, D. C.; Strydom, C. A. The bipyridine adducts of N-phenyldithiocarbamato complexes of Zn(II) and Cd(II); synthesis, spectral, thermal decomposition studies and use as precursors for ZnS and CdS nanoparticles, *Spectrochim. Acta Part A*. **2015**, *135*, 1080-1089.

88. Onwudiwe, D. C.; Strydom, C. A.; Oluwafemi, O. S.; Hosten, E.; Jordaan, A. Synthesis, spectral and thermal studies of pyridyl adducts of Zn(II) and Cd(II) dithiocarbamates, and their use as single source precursors for ZnS and CdS nanoparticles. *Dalton Trans*. **2014**, *43*, 8703-8711.

89. Srinivasan, N.; Thirumaran, S.; Ciattini, S. Synthesis and crystal structures of diimine adducts of Cd(II) tetrahydroquinolinedithiocarbamate and use of (1,10-phenanthroline)bis(1,2,3,4-tetrahydroquinolinecarbodithioato-S,S')-Cadmium(II) for the preparation of CdS nanorods. *J. Mol. Struct*. **2012**, *1026*, 102-107.

90. Srinivasan, S.; Thirumaran, S.; Ciattini, S. Synthesis of α-mercury sulfide nanosheets from(1,10-phenanthroline)bis(1,2,3,4-tetrahydroquinolinecarbodithioato-S, S')mercury(II*). J. Mol. Struct*. **2014**, *1076*, 382-386.

91. Srinivasan, N.; Thirumaran S. Synthesis of ZnS nanoparticles from pyridine adducts of zinc(II) dithiocarbamates. *C. R. Chim.* **2014**, *17*, 964-970

92. Takahashi, Y.; Yuki, R.; Sugiura, M.; Motojima, S.; Sugiyama K. Vapor deposition of thin cadmium sulfide layers using thermal decomposition of dithiolatocadmium complexes. *J. Cryst. Growth*. **1980**, *50*, 491-497.

93. Byrom, C.; Malik, M. A.; O'Brien, P.; White, A. J. P.; Williams, D. J. Synthesis and X-ray single crystal structures of bis(diisobutyldithiophosphinato)cadmium(II) or zinc(II): Potential single-source precursors for II/VI materials. *Polyhedron*. **2000**, *19*, 211-215.

94. Kiehl, J.; Trenberth, K. Earth's annual global mean energy budget. *Bull*. *Am*. *Meteorol*. *Assoc*. **1997**, *78*, 197-208.

95. Gardner G. Alternative energy and nanotechnology .PCOST project. **2008**, 1-11

96. Lewis N. Toward cost-effective solar energy use. *Sci*. **2007**, *315*, 798-801.

97. Calixto-Rodriguez, M.; García, H. M.; Nair, T. S.; Nair, P. K. Antimony chalcogenide/lead selenide thin film solar cell with 2.5% conversion efficiency prepared by chemical deposition ECS. *J*. *Solid State Sci*. *Technol*. **2015**, *4*, Q9-Q16.

98. Burda, C.; Chem X.; Narayanan, R. A.; Mostafa, E. L. Chemistry and properties of nanocrystals of different shapes. *Chem*. *Rev*. **2005**, *105*, 1025-1102.

99. Narayanan, R.; El-Sayed, M. A. Effect of nanocatalysis in colloidal solution on the tetrahedral and cubic nanoparticle shape: Electron-transfer reaction catalyzed by platinum nanoparticles. *J*. *Phys*. *Chem*. *B*. **2004**, *108*, 5726-5733.

100. Yates, D. J. C.; Sinfelt, J. H. The catalytic activity of rhodium in relation to state of dispersion. *J*. *Catal*. **1967**, *8*, 348-358.

101. Gellman, J.A.; Shukla N. Nanocatalysis; More than speed. *Nat*. *Mater*. **2009**, 8, 87-88.

102. Mazzola, L. Commercializing nanotechnology. *Nat. Biotechnol.* **2003**, *21*, 1137-1143

103. Wagner, M. K.; Li, F.; Li, J.; Li, X. F.; Le X. C. Use of quantum dots in the development of assays for cancer biomarkers. *Anal. Bioanal. Chem.* **2010**, *397*, 3213-3224.

104. Armstead, A. L.; Li, B. Nanomedicine as an emerging approach against intracellular pathogens. *Int. J. Nanomed*. **2011**, *6*, 3281-3293.

105. Buzea, C.; Pacheco, I. I.; Robbie, K. Nanomaterials and nanoparticles: Sources and toxicity. *Biointerphases*. **2007**, *2*, MR17-MR71.

106. Hopkins, L. E.; Patchin, E. S.; Chiu, P. L.; Brandenberger, C.; Smiley-Jewell, S.; Pinkerton, K. E. Nose-to-brain transport of aerosolised quantum dots following acute exposure. *Nanotoxicology*. **2014**, *8*, 885-893.

107. Malam, Y.; Lim, E. J. Seifalian, A. M. Current trends in the application of nanoparticles in drug delivery. *Curr*. *Med*. *Chem*. **2011**, *18*, 1067-1078.

108. Taton, T. A. Nanostructures as tailored biological probes. *Trends Biotechnol*. 2002**,** *20*, 277-279**.**

109. Kayser, O.; Lemke, A.; Hernández-Trejo. N. The impact of nanobiotechnology on the development of new drug delivery systems. *Curr. Pharm. Biotechnol*. **2005**, *6*, 3-5.

110. Kaparissides, C.; Alexandridou, S.; Kotti K.; Chaitidou S. Recent advances in novel drug delivery systems. *J. Nanotechnol. Online*. **2006**, 2, 1-11

111. Singh A. K. Thermal conductivity of nanofluids. *Defence Sci*. *J*. **2008**, *58*, 600-607

112. Jelle, B. P.; Gustavsen, A.; Baetens, R. The path to the high performance thermal building insulation materials and solutions of tomorrow. *J. Build Phys*. **2010**, *34*, 99-123.

113. Sooklal, K.; Cullum, B.; Angel, S. M.; Murphy, C. J. Photophysical properties of ZnS nanoclusters with spatially localized Mn^{2+}. *J*. *Phys*. *Chem*. **1996**, *100*, 4551-4555.

114. Falcony, C.; Garcia, M.; Ortiz, A.; Alonso. J. C. Luminescent properties of ZnS: Mn films deposited by spray pyrolysis *J*. *Appl*. *Phys*. **1992**, *72*, 1525-1527.

115. Tang, W.; Cameron, D.C. Electroluminescent zinc sulfide devices produced by sol gel. *Thin Solid Films*. **1996**, *280*, 221-222.

116. Celikkaya, A.; Akinc, M. Preparation and mechanism of formation of spherical submicrometer zinc sulfide powders. *J*. *Am*. *Ceram*. *Soc*. **1990**, 73, 2360-2365.

117. Faria, S. Electroluminescent characteristics of small particle size phosphors. *J. Electrochem. Soc.* **1988**, *135*, 2627-2630.

118. Voltage dependence and particle size distribution of electroluminescent phosphors. *J. Electrochem. Soc.* **1960**, *107*, 20-26.

119. Zeiri, L.; Patla, I.; Acharya, S.; Golan, Y.; Efrima, S. Raman spectroscopy of ultranarrow CdS nanostructures. *J. Phys. Chem. C.* **2007**, *111*, 11843-11848.

120. Cao, H.; Wang, G.; Zhang, S.; Zhang, X.; Rabinovich, D.; Growth and optical properties of wurtzite-type CdS nanocrystals. *Inorg. Chem.* **2006**, *45*, 5103-5108.

121. Sun, Z. X.; Li, F. X.; Xu, L.; Liu, S. P.; Zhao, M. L.; Xu, B. B. Effects of Dawson-type tungstophosphate on photoelectrochemical responses of cadmium sulfide composite film. *J. Phys. Chem. C.* **2012**, *116*, 6420-6426.

122. Monk, P. M. S.; Duffy, J. A.; Ingram, M. D. Elecreochromic display devices of tungsticoxide containing vanadium oxide or cadmium sulfide as a light-sensitive layer. *Electrochim. Acta.* **1993**, *38*, 2759-2764.

123. Ding, S.N.; Xu, J. J.; Shan, D.; Gao, B. H.; Yang, H. X.; Sun, Y. M; Cosnier, S. Electrochromic response and electrochemiluminescence of CdS nanocrystals thin film in aqueous solution. *Electrochem. Commun.* **2010**, *12*, 713-716.

124. Jie, J. S.; Zhang, W. J.; Jiang, Y.; Meng, X. M.; Li, Y. Q.; Lee, S. T. Photoconductive characteristics of single-crystal CdS nanoribbons, *Nano Lett.* **2006**, *6* 1887-1892.

125. Shalom, M.; Hod, I.; Tachan, Z.; Buhbut, S.; Tirosh, S.; Zaban, A. Quantum dot based anode and cathode for high voltage tandem photo-electrochemical solar cell. *Energy Environ. Sci.* **2011**, *4*, 1874-1878.

126. Li, T. L.; Lee, Y- L.; Teng, H. High-performance quantum dot-sensitized solar cells based on sensitization with $CuInS_2$ quantum dots/CdS heterostructure, *Energy Environ Sci.* **2012**, *5*, 5315-5324.

127. Ke, D. N.; Liu, S. L.; Dai, K.; Zhou, J. P.; Zhang, L. N.; Peng, T. Y. CdS/regenerated cellulose nanocomposite films for highly efficient photocatalytic H_2 production undervisible light irradiation. *J. Phys. Chem. C*. **2009**, *113*, 16021-16026.

128. Kale, S. S.; Lokhande, C.D. Preparation and characterization of HgS films by chemical deposition. *J. Mater. Chem. Phys*. **1999**, *59*, 242-246.

129. Sharma, N. C.; Pandya, D. K.; Sehgal, H. K.; Chopra, K .L. Electroless deposition of epitaxial $Pb_{1-x}Hg_xS$ films. *Thin Solid Films*. **1979**, *59*, 157-164.

130. Perakh, M.; Ginsberg, H. Deposition of thin films of HgS from colloidal solutions. *Thin Solid Films*. **1978**, *52*, 195-202.

131. Qin, D. Z.; Ma, X. M.; Yang, L. Zhang, L. Biomimetic synthesis of HgS nanoparticles in the bovine serum albumin solution. *J. Nanopart. Res*. **2008**, *10*, 559-566.

132. Sheikhiabadi, P. G.; Davar, F.; Salavati-Niasari, M. The single source preparation of rod-like mercury sulfide nanostructures via hydrothermal method. *Inorganica Chimica. Acta*. **2011**, *376*, 271-277.

133. Wang, H.; Zhu, J. J. A sonochemical method for the selective synthesis of a-HgS and b-HgS nanoparticles. *Ultrason. Sonochem*. **2004**, 11, 293-300.

134. Lu, C.; Guan, C.; Liu, Y.; Cheng, Y.; Yang, B. PbS/Polymer nanocomposite optical materials with high refractive index. *Chem. Mater.* **2005**, *17*, 2448-2454.

135. Casciato, M. J.; Levitin, G.; Hess, D. W.; Grover, M. A. Synthesis of optically active ZnS–carbon nanotube nanocomposites in supercritical carbon dioxide via a

single source diethyldithiocarbamate precursor. *Ind*. *Eng*. *Chem*. *Res*. **2012**, *51*, 11710-11716.

136. Kuljanin-Jakovljevic, J.; Marinovic´-Cincovic, M.; Stojanovic´, Z.; Krkljesˇ, A.; Abazovic´, N. D.; Comor, M. I. Thermal degradation kinetics of polystyrene/cadmium sulfide composites. *Polym*. *Degrad*. *Stabil*. **2009**, *94*, 891-897.

137. Marcilla, A.; Beltra, ´M. Kinetic study of thermal decomposition of polystyrene and polyethylene-vinyl acetate graft copolymers by thermogravimetric analysis. *Polym*. *Degrad*. *Stabil*. **1995**, *50*, 117-124.

138. Agarwal, S.; Dinesh, P.; Saxena, N. S. Effect of ZnS nanofiller and temperature on mechanical properties of Poly(methyl methacrylate). *J. Appl. Polym. Sci*. **2013**, *123*, 2431-2438.

139. Saikia, D.; Saikia, P. K.; Gogoi, P. K.; Das M. R.; Sengupta, P.; Shelke, M. V. Synthesis and characterization of CdS/PVA nanocomposite thin films from a complexing agent free system. *Mater. Chem. Phys.* **2011**, *131*, 223-229.

140. Maitya, R.; Maitia, U. N.; Mitrab, M. K.; Chattopadhyaya, K. K. Synthesis and optical characterization of polymer-capped nanocrystalline ZnS thin films by chemical process. *Physica E*. **2006**, *33*, 104-109.

CHAPTER 2

2. Experimental

2.1 Chemicals

Zinc chloride, cadmium chloride, mercury chloride, potassium hydroxide, cyanoacetate, dioxane, carbon disulfide, diethyl ether, thiuram disulfide, methyl thiourea, dimethyl thiourea, diethyl thiourea, diisopropyl thiourea methanol, ethanol, toluene, acetone, deuterated dmso were all purchased from Sigma and Aldrich and used without further purification.

2.2 Physical measurements

2.2.1 ^{1}H and ^{13}C-NMR spectroscopy

NMR spectra were recorded on a 600 MHz Bruker Avance III NMR spectrometer using deuterated DMSO as solvent. 1H- NMR and 1C-NMR spectra were referenced to the solvent signal and the chemical shifts are reported comparative to Me_4Si.

2.2.3 Infrared spectroscopy

Infrared spectra analysis of the samples was done using KBr discs on a Perkin Elmer Paragon 2000 FTIR spectrophotometer, in the range 4000 - 350 cm^{-1}

2.2.4 Thermogravimetry analysis

Thermogravimetry analysis measurements were taken using a SDTQ 600 thermal instrument. Samples were contained within alumina crucibles and heated at a rate of 10 °C min^{-1} from room temperature to 700 °C under flowing nitrogen.

2.2.5 Melting point determination

Gallenkamp melting point apparatus was used to record the melting point.

2.2.6 Elemental analysis

Electrochemical analysis for CHNS was performed using a Fission elemental analyser. Samples to be analysed are placed in a tin container that is dropped in a furnace at 1000 ºC and this led to the ejection of oxygen from the furnace. The samples were subjected to burning and decomposed into combustion gasses (carbon monoxide, water vapour, nitrogen and sulfur dioxide) which were isolated and analysed using a gas chromatography column to ascertain the amount of each element present in the analyte.

2.3 Synthesis

2.3.1 Synthesis of ligand, dipotassium 1-cyano-1-carboethoxylethylene-2,2- dithiolate.

Pulverized potassium hydroxide (0.1 mol) was suspended in dioxan (50 mL) and a solution of ethyl cyanoacetate (0.05 mol) and carbon disulfide (0.05 mol) in dioxan (25 mL) was added with stirring and cooling to maintain a temperature of 15 - 20 ºC. After the addition the suspension was stirred for another 20 mins and diluted with 125 mL of ether. The yellow precipitate was filtered washed with dioxan-ether (1:1) and dried in vacuo over NaOH and P_2O_5 [1, 2].

2.3.2 Synthesis of (1-cyano-1-carboethoxyethylene-2,2-dithiolato–κS,S')–bis(N,N'-dimethylthiourea–κS)zinc(II): $[Zn(mtu)_2ced]$ (1)

In a typical experiment a mixture of $ZnCl_2$ (0.6814 g, 0.005 mol) was dissolved in 40 mL of absolute methanol and refluxed for 3 h with (0.9015 g 0.01 mol) of methylthiourea dissolved in 40 mL of methanol. The solution was concentrated to half of its original (40 mL) volume

and K_2ced (1.417 g, 0.005 mol) was dissolved in 20 mL of distilled water and added to the refluxing mixture. The initial colourless mixture changes to milky yellow and the reaction was further refluxed for 12 h. The milky yellow product obtained by filtration was washed twice with ice cold methanol, water and diethyl ether. It was also re-dissolved in acetone and filtered to remove KCl which is the by - product of the reaction. The acetone was concentrated to obtain the product.

[Zn(mtu)$_2$(ced)]: (Yield: 1.16 g, 59 %; M.p. 208 - 210 ºC). Anal. calc. for $C_{10}H_{17}N_5O_2S_4Zn$ (432.93): C, 27.74; H, 3.95; N, 16.17; S, 29.62. Found: C, 27.68; H, 3.98; N, 16.21; S, 29.60. Selected IR, *v*(cm−1): 2200 (C≡N), 1462 (C=S_2), 1681 (C=O), 373 (M-S).

^{1}H-NMR (DMSO) δ = 1.14 (t, 3H, CH_3), 4.02 (q, 2H, -OCH_2)

^{13}C-NMR (DMSO) δ = 203.69 (C=S), 168.68 (C=O), 122.94 (C≡N), 59.29 (-OCH_2).

2.3.3 Synthesis of (1-cyano-1-carboethoxyethylene-2,2-dithiolato-κS,S)-bis(N,N'-methylthiourea–κS)cadmium (II): [Cd(mtu)$_2$ced] (2).

$CdCl_2$ (0.916 g, 0.005 mol) was dissolved in 40 mL of methanol and added to methylthiourea (0.9015 g, 0.01 mol) dissolved in 20 mL of methanol. The solution was refluxed for 3 h after which it was concentrated to half of its original volume (40 mL). K_2ced (1.417 g, 0.005 mol) dissolved in water was added to the mixture. The reaction was further refluxed for 12 h. The product was filtered and washed twice with ice cold methanol, water and ether. The product was re-dissolved in acetone and KCl removed with filtration after which the acetone was removed in vacuo to obtain the precipitate.

[Cd(mtu)$_2$(ced)]: (Yield: 1.34 g, 77%; M.p. 217 - 219 ºC). Anal. calc. for $C_{10}H_{17}N_5O_2S_4Cd$ (479.94): C, 23.42; H, 3.57; N, 14.59; S, 26.72. Found: C, 23.39; H, 3.58; N, 14.62; S, 26.70. Selected IR, *v*(cm^{-1}): 2199 (C≡N), 1652 (C=O), 1412 (C=S2), 376 (M–S).

^{1}H-NMR (DMSO) δ = 1.12 (t, 3H- CH_3) 4.02 (q, 2H, -OCH_2)

^{13}C-NMR (DMSO) δ = 203.69 (C=S_2), 168.68 (C=O), 122.94 (C≡N), 59.29 (-OCH_2).

2.3.4 Synthesis of (1-cyano-1-carboethoxyethylene-2,2-dithiolato-κS,S')–bis(N,N'-methylthiourea–κS)mercury(II): [Hg(mtu)$_2$ced] (3).

$HgCl_2$ (1.3575 g, 0.005 mol) was dissolved in 40 mL of methanol and added to methylthiourea (0.9015 g, 0.01 mol) dissolved in 20 mL of methanol. The solution was refluxed for 3 h after which it was concentrated to half of its original volume (30 mL). K_2ced (1.417 g, 0.005 mol) dissolved in water was added to the mixture. The reaction was further refluxed for 12 h. The product was filtered and washed twice with ice cold methanol, water and ether. The product was re-dissolved in acetone and KCl removed with filtration after which the acetone was removed in vacuo to obtain the precipitate.

[Hg(mtu)$_2$(ced)]: (Yield: 2.63 g, 74%; M.p. 247 - 249 ºC). Anal. calc. for $C_{10}H_{17}N_5O_2S_4Hg$ (568.12): C, 21.14; H, 3.01; N, 12.33; S, 22.57. Found: C, 21.11; H, 3.09; N, 12.31; S, 22.23.

Selected IR, ν(cm^{-1}): 2232 (C≡N), 1732 (C=O), 1489 (C=S_2), 1681 (C=O), 388 (M–S).

^{1}H-NMR (DMSO) δ =1.28 (t, 3H, CH_3), 4.30 (q, 2H, -OCH_2).

^{13}C-NMR (DMSO) δ = 14.01 (-CH_3).

2.3.5 Synthesis of (1-cyano-1-carboethoxyethylene-2,2-dithiolato-κS,S')-bis(N,N'-dimethylthiourea–κS)zinc (II): [Zn(dmtu)$_2$ced] (4)

In a typical experiment a mixture of $ZnCl_2$ (0.6814 g, 0.005 mol) was dissolved in 40 mL of absolute methanol and refluxed for 3 h with (1.042 g, 0.01 mol) of dimethylthiourea dissolved in 40 mL of methanol. The solution was concentrated to half of its original (40 mL) volume and K_2ced (1.417 g, 0.005 mol) was dissolved in 20 mL of distilled water and added to the refluxing mixture. The initial colourless mixture changes to milky yellow and the reaction was further refluxed for 12 h. The milky yellow product obtained by filtration

was washed twice with ice cold methanol, water and diethyl ether. It was also re-dissolved in acetone and filtered to remove KCl which is the by - product of the reaction. The acetone was concentrated in vacuo to obtain the product.

[$Zn(dmtu)_2(ced)$]: (Yield: 1.79 g, 66%; M.p. 211 - 213 ºC). Anal. calc. for $C_{12}H_{21}N_5O_2S4Zn$ (460.98): C, 31.27; H, 4.59; N, 15.19; S, 27.82. Found: C, 30.79; H, 5.06; N, 15.53; S, 27.65

Selected IR, *v*(cm−1): 2209 (C≡N), 1705 (C=O), 1448 (C=S2), 394 (M–S).

^{1}H-NMR (DMSO) δ = 3.98 (q, 2H, -OCH_2) 1.15 (t, 3H, CH_3)

^{13}C-NMR (DMSO) δ = 14.62 (-CH_3), 58.41 (-OCH_2), 90.91 (C=C), 120.88 (C≡N), 163.92 (C=O), 206.32 (C=S_2).

2.3.6 Synthesis of (1-cyano-1-carboethoxyethylene-2,2-dithiolato-κS,S')-bis(N,N'-dimethylthiourea–κS) cadmium(II): [$Cd(dmtu)_2ced$] (5)

$CdCl_2$ (0.916 g, 0.005 mol) was dissolved in 40 mL of methanol and added to dimethylthiourea (1.042 g, 0.01 mol) dissolved in 40 mL of methanol. The solution was refluxed for 3 h after which it was concentrated to half of its original volume (40 mL) and K_2ced (1.417 g, 0.005 mol) dissolved in distilled water was added to the mixture. The reaction was further refluxed for 12 h. The product was filtered and washed twice with ice cold methanol, water and ether. The product was re-dissolved in acetone and KCl removed with filtration after which the acetone was removed in vacuo to obtain the precipitate.

[$Cd(dmtu)_2(ced)$]: (Yield: 2.54 g, 73%; M.p. 219 - 221 ºC). Anal. calc. for $C_{12}H_{21}N_5O_2S_4Cd$ (508): C, 28.37; H, 4.17; N, 11.75; S, 21.51. Found: C, 28.74; H, 3.78; N, 11.90; S, 22.49

Selected IR, *v*(cm^{-1}): 2209 (C≡N), 1629 (C=O), 1473 (C=S2), 377 (M–S).

^{1}H-NMR (DMSO) δ = 4.01 (q, 2H, -OCH_2) 1.16 (t, 3H, CH_3)

^{13}C-NMR (DMSO) δ = 14.59 (-CH_3), 58.91 (-OCH_2), 90.58 (C=C), 121.28 (C≡N), 165.96 (C=O), 207.72 (C=S_2).

2.3.7 Synthesis of (1-cyano-1-carboethoxy-2, 2-ethylendithiolato-κS,S')-bis(N,N'-diethylthiourea-κ S)Hg(II): [Hg(dmtu)$_2$ced] (6).

$HgCl_2$ (1.358 g, 0.005 mol) was dissolved in 40 mL of methanol and added to dimethylthiourea (1.042 g, 0.01 mol) dissolved in 40 mL of methanol. The solution was refluxed for 3 h after which it was concentrated to half of its original volume (40 mL) and K_2ced (1.417 g, 0.005 mol) dissolved in water was added to the mixture. After a period of 15 mins the colour of the mixture changed to grey and finally to black. The reaction was refluxed further for 12 h. The product was filtered and washed twice with ice cold methanol, water and ether. The product was re-dissolved in acetone and KCl removed with filtration after which the acetone was removed in vacuo to obtain the precipitate.

[Hg(dmtu)$_2$(ced)]: (Yield: 2.74 g, 61%; M.p. 211 - 212 ºC). Anal. calc. for $C_{12}H_{21}N_5O_2S_4Hg$ (596.12): C, 24.17; H, 3.55; N, 11.74; S, 21.51 Found: C, 24.45; H, 3.83; N, 12.27; S, 21.29

Selected IR, ν(cm^{-1}): 2202 (C≡N), 1649 (C=O), 1457 (C=S_2), 378 (M–S).

^{1}H-NMR (DMSO) δ = 4.02 (q, 2H, -OCH_2) 1.15 (t, 3H, CH_3)

^{13}C-NMR (DMSO) δ = 14.59 (-CH_3), 58.91 (-OCH_2), 90.58 (C=C), 121.28 (C≡N), 165.96 (C=O), 207.72 (C=S_2).

2.3.8 Synthesis of (1-cyano-1-carboethoxyethylene-2,2-dithiolato-κS,S')-bis(N, N'-diethylthiourea – κS)zinc(II): [Zn(detu)$_2$ced] (7)

In a typical experiment a mixture of $ZnCl_2$ (0.6814 g, 0.005 mol) was dissolved in 40 mL of absolute methanol and refluxed for 3 h with (1.3223 g 0.01 mol) of diethylthiourea dissolved in 40 mL of methanol. The solution was concentrated to half of its original (40 mL) volume and K_2ced (1.417 g, 0.005 mol) dissolved in 20 mL of distilled water was added to the refluxing mixture. The initial colourless mixture changes to milky yellow and the reaction was further refluxed for 12 h. The milky yellow product obtained by filtration was washed

twice with ice cold methanol, water and diethyl ether. It was also re-dissolved in acetone and filtered to remove KCl which is the by-product of the reaction. The acetone was concentrated in vacuo to obtain the product.

[$Zn(detu)_2(ced)$]: (Yield: 1.42 g, 54.9 %; M.p. 211 - 212 ºC). Anal. calc. for $C_{16}H_{29}N_5O_2S_4Zn$ (517.08): C, 37.17; H, 5.65; N, 13.54; S, 24.80. Found: C, 37.31; H, 5.70; N, 14.63; S, 24.55

Selected IR, $\nu(cm^{-1})$: 2204 (C≡N), 1462 ($C=S_2$), 1681 (C=O), 373 (M–S).

^{1}H-NMR (DMSO) δ = 1.12 (t, 3H, CH_3) 3.95 (q, 2H, -OCH_2)

^{13}C-NMR (DMSO) δ = 14.61 (-CH_3), 58.40 (-OCH2), 90.91 (C=C), 120.83 (C≡N), 163.92 (C=O), 206.30 ($C=S_2$).

2.3.9 Synthesis of (1-cyano-1-carboethoxyethylene-2,2-dithiolato-κS,S')-bis (N,N'-diethylthiourea – κS)cadmium(II): [$Cd(detu)_2ced$] (8)

$CdCl_2$ (0.916 g, 0.005 mol) was dissolved in 40 mL of methanol and added to diethylthiourea (1.322 g, 0.01 mol) dissolved in 40 mL of methanol. The solution was refluxed for 3 h after which it was concentrated to half of its original volume (40 mL). K_2ced (1.417 g, 0.005 mol) dissolved in water was added to the mixture. The reaction was further refluxed for 12 h. The product was filtered and washed twice with ice cold methanol, water and ether. The product was re-dissolved in acetone and KCl removed with filtration after which the acetone was removed in vacuo to obtain the precipitate.

[$Cd(detu)_2(ced)$]: (Yield: 2.0 g, 77.3%; M. p. 231 - 233 ºC). Anal. calc. for $C_{16}H_{29}N_5O_2S_4Cd$ (564.10): C, 34.06; H, 5.18; N, 12.42; S, 22.73. Found: C, 34.22; H, 5.36; N, 12.67; S, 22.91

Selected IR, ν(cm−1): 2206 (C≡N), 1463 ($C=S_2$), 1651 (C=O), 372 (M–S).

^{1}H-NMR (DMSO) δ = 1.12 (t, 3H, CH_3), 3.99 (q, 2H, -OCH_2)

^{13}C-NMR (DMSO) δ = 14.57 (-CH_3), 58.49 (-OCH_2), 90.25 (C=C), 121.57 (C≡N), 163.92 (C=O), 208.15 ($C=S_2$).

2.3.10 Synthesis of (1-cyano-1-carboethoxyethylene-2,2-dithiolato-κ,S'S)-bis(N, N'-diethylthiourea –κS)mercury(II): [Hg(detu)$_2$ced] (9)

$HgCl_2$ (1.3575 g, 0.005 mol) was dissolved in 40 mL of methanol and added to diethylthiourea (0.9015 g, 0.01 mol) dissolved in 20 mL of methanol. The solution was refluxed for 3 h after which it was concentrated to half of its original volume (40 mL). K2ced (1.417 g, 0.005 mol) dissolved in water was added to the mixture. The reaction was further refluxed for 12 h. The product was filtered and washed twice with ice cold methanol, water and ether. The product was re-dissolved in acetone and KCl removed with filtration after which the acetone was removed in vacuo to obtain the precipitate.

[Hg(detu)$_2$(ced)]: (Yield: 2.1 g, 64.0%; M.p. 344 - 346 ºC). Anal. calc. for $C_{16}H_{29}N5O_2S_4Cd$ (652.29): C, 29.46; H, 4.48; N, 10.73; S, 19.66. Found: C, 29.12; H, 4.07; N, 10.98; S, 19.39. Selected IR, *v*(cm−1): 2188 (C≡N), 1458 (C=S_2), 1651 (C=O), 375 (M-S).

^{1}H-NMR (DMSO) δ = 1.13 (t, 3H, CH_3) 4.02 (q, 2H, -OCH_2)

^{13}C-NMR (DMSO) δ = NA (Not available).

2.3.11 Synthesis of (1-cyano-1-carboethoxy-2,2-ethylenedithiolato-κS,S')–bis(N,N'-diisopropylthiourea-κS)zinc(II): [Zn(diptu)$_2$ced] (10)

$ZnCl_2$ (0.6815 g, 0.005 mol) in a hot methanol (40 mL) was added to a heated solution of diisopropylthiourea (1.6028 g, 0.01 mol) in methanol (40 mL). The solution was refluxed for 5 h and later concentrated to half of its original volume (30 mL). K_2ecda (1.417 g, 5.00 mmol) dissolved in water was slowly added to the mixture and stirred further for 12 h. The product, a white yellowish coloured material, was filtered and washed twice with ice cold methanol, water, ether and air dried.

[Zn(diptu)$_2$(ced)]: (Yield: 1.34 g, 77%; M.p. 208-210 ºC). Anal. calc. for $C_{20}H_{37}N_5O_2S_4Zn$ (573.19): C, 34.06; H, 5.18; N, 12.42; S, 22.73. Found: C, 34.22; H, 5.36; N, 12.67; S, 22.91

Selected IR, *v*(cm−1): 2196 (C≡N), 1374 (C=S_2), 1615 (C=O), 412 (M–S).

^{1}H-NMR (DMSO) δ = 3.98 (q, 2H, -OCH_2) 1.14 (t, 3H, CH_3)

^{13}C-NMR (DMSO) δ = 14.39 (-CH_3), 58.34 (-OCH_2), 90.86 (C=C), 120.86 (C≡N), 163.88 (C=O), 206.30 (C=S_2).

2.3.11 Synthesis of [Zn(diptu)$_2$(ced)(py)] (11)

[Zn(diptu)$_2$(ced)] (0.8598 g, 0.015 mol) was refluxed in 20 mL hot pyridine at 80 ºC for 3 h. The pyridine solution was removed by filtration and the resulting whitish yellow precipitate was rinsed with water followed by ethanol.

[Zn(diptu)$_2$(ced)(py)]: (Yield: 1.03 g, 71%; M.p. 207-209 ºC). Anal. calc. for $C_{25}H_{42}N_6O_2S_4Zn$ (653.30): C, 45.96; H, 6.63; N, 12.86; S, 19.63. Found: C, 45.51; H, 6.47; N, 12.81; S, 20.04.

Selected IR, v(cm−1): 2196 (C≡N), 1374 (C=S_2), 1615 (C=O), 412 (M-S).

^{1}H-NMR (DMSO) δ = 3.95 (q, 2H, -OCH_2) 1.14 (t, 3H, CH_3)

^{13}C-NMR (DMSO) δ = 14.61 (-CH_3), 58.41 (-OCH_2), 90.90 (C=C), 120.87 (C≡N), 164.00 (C=O), 206.35 (C=S2); C_5H_5N(py) δ = 149.46, 124.19.

2.3.12 Synthesis of [Zn(diptu)$_2$(ced)(bpy)] (12)

[Zn(diptu)$_2$(ced)] (1.1464 g, 0.002 mol) was dissolved in 40 mL hot chloroform and refluxed with 2, 2’ bipyridine (0.3120 g 0.002 mol) dissolved in 20 mL of hot chloroform. The resulting mixture was refluxed for 4 h at a mild temperature of around 70º C and filtered while hot. The precipitate was washed with chloroform, diethyl ether and air dried.

[Zn(diptu)$_2$(ced)(bpy)]: (Yield: 1.27 g, 68 %; M.p. 209 - 211 ºC). Anal. calc. for $C_{30}H_{45}N_7O_2S_4Zn$ (729.37): C, 49.40; H, 6.21; N, 13.44; S, 17.58. Found: C, 49.02; H, 5.85; N, 13.16; S, 17.20.

Selected IR, ν(cm^{-1}): 2196 (C≡N), 1374 (C=S2), 1615 (C=O), 412 (M–S), 1521 (bipy).

^{1}H-NMR (DMSO) δ = 3.99 (q, 2H, -OCH_2) 1.14 (t, 3H, CH_3)

^{13}C-NMR (DMSO) δ = 14.61 (-CH_3), 58.38 (-OCH_2), 91.12 (C=C), 122.42 (C≡N), 163.89 (C=O), 206.24 (C=S2); C_6H_4(bpy) δ = 122.42, 127.08, 141.43, 148.40

2.3.13 Synthesis of [Zn(diptu)$_2$(ced)(phen)] (13)

Complex 13, [Zn(diptu)$_2$(ced)(phen)], was prepared by the same synthetic procedure adopted in complex 3 but 1,10 phenanthroline (0.5406 g, 0.002 mol) was used instead of 2,2 bipyridine .[Zn(diptu)$_2$(ced)(phen)]: (Yield: 1.34 g, 77%; M.p. 230-232 ºC). Anal. calc. for $C_{32}H_{45}N_7O_2S_4Zn$ (753.39): C, 51.02; H, 6.02; N, 13.01; S, 17.02. Found: C, 51.11; H, 5.79; N, 13.35; S, 17.28.

Selected IR, ν(cm^{-1}): 2197 (C≡N), 1629 (C=O), 1373 (C=S_2), 421 (M–S).

Yield: 1.59 g (75.1 %), m. p. 315-317 ºC.

^{1}H-NMR (DMSO) δ = 1.13 (t, 3H, CH_3), 3.97 (q, 2H, -OCH_2)

^{13}C-NMR (DMSO) δ = 14.62 (-CH_3), C-N (56.06) 58.35 (-OCH_2), 90.12 (C=C), 125.95 (C≡N), 163.91 (C=O), 206.65 (C=S_2); C_6H_4(phen) δ = 125.95, 127.39, 140.09, 149.08.

2.3.14 Synthesis of (1-cyano-1-carboethoxy-2,2-ethylenedithiolato-κS,S')-bis(N,N'-diisopropylthiourea–κS)cadmium(II): [Cd(diptu)$_2$ced] (14).

$CdCl_2$ (0.7332 g, 0.004 mol) was dissolved in 25 mL of methanol and added to diisopropylthiourea (1.2822 g, 0.008 mol) dissolved in 25 mL of methanol and refluxed for 4 h. A yellowish solution was obtained which was concentrated to half its original volume and a solution of Potassium 1-cyano-1-carboethoxy-2,2-ethylenedthiolate (K_2ced) dissolved in 10 mL of distilled water was slowly added to the mixture and stirred at room temperature further

for 8 h. The yellow solution obtained was concentrated in vacuo, filtered and the precipitate washed with water, methanol, diethyl ether and air dried.

[Cd(diptu)$_2$(ced)]: (Yield: 1.27 g, 68%; M.p. 202-203 ºC). Anal. calc. for $C_{16}H_{29}N_5O_2S_4Cd$ (620.21): C, 34.06; H, 5.18; N, 12.42; S, 22.73. Found: C, 34.22; H, 5.36; N, 12.67; S, 22.91.

Selected IR, ν(cm^{-1}): 2201 (C≡N), 1623 (C=O), 1463 (C=S2), 351 (M–S),

^{1}H-NMR (DMSO) δ = 1.05 (t, 3H, CH_3) 4.02 (q, 2H, -OCH_2)

^{13}C-NMR (DMSO) δ = 14.61 (-CH_3), 58.40 (-OCH_2), 90.92 (C=C), 120.82 (C≡N), 163.93 (C=O), 206.30 (C=S_2).

2.3.15 Synthesis of [Cd(diptu)$_2$(ced)(bpy)] (15)

[Cd(diptu)$_2$(ced)] (1.2404 g, 0.002 mol) was dissolved in 40 mL hot chloroform and refluxed with 2, 2’ bipyridine (0.3120 g, 0.002 mol) dissolved in 20 mL of hot chloroform. The resulting mixture was refluxed for 4 h at a mild temperature of around 70º C and filtered hot. The precipitate was washed with chloroform, diethyl ether and air dried.

[Cd(diptu)$_2$(ced)(bpy)]: (Yield: 1.27 g, 68%; M.p.205-206 ºC). Anal. calc. for $C_{30}H_{45}N_7O_2S_4Cd$ (776.38): C, 46.41; H, 5.84; N, 12.63; S, 16.52. Found: C, 46.02; H, 5.57; N, 12.18; S, 16.55.

Selected IR, ν(cm^{-1}): 2198 (C≡N), 1629 (C=O), 1439 (C=S2), 403 (M–S),

^{1}H-NMR (DMSO) δ = 4.37 (q, 2H, -OCH_2) 1.09 (t, 3H, CH_3)

^{13}C-NMR (DMSO) δ = 14.44 (-CH_3), 56.06 (-OCH_2), 91.00 (C=C), 122.38 (C≡N),

C_6H_4(bpy) δ = 122.38, 126.32, 140.24, 149.46.

2.3.16 Synthesis of [Cd(diptu)$_2$(ced)(phen)] (16)

[Cd(diptu)$_2$(ced)] (1.2404 g 0.002 mol) was dissolved in 40 mL hot chloroform and refluxed with 1, 10-phenanthroline (0.3604 g, 0.002 mol) dissolved in 20 mL of hot chloroform. The

resulting mixture was refluxed for 4 h at a mild temperature of around 70º C and filtered hot. The precipitate was washed with chloroform, diethyl ether and air dried.

[Cd(diptu)$_2$(ced)(phen)]: (Yield: 1.34 g, 77%; M.p. 211-212 ºC). Anal. calc. for $C_{32}H_{45}N_7O_2S_4Cd$ (800.21): C, 48.01; H, 5.66; N, 12.24; S, 15.96. Found: C, 48.21; H, 5.39; N, 12.50; S, 16.13.

Selected IR, ν(cm^{-1}): 2198 (C≡N), 1625 (C=O), 1374 (C=S$_2$), 398 (M–S),

^{1}H-NMR (DMSO) δ = 3.37 (q, 2H, -OCH$_2$) 1.06 (t, 3H, CH$_3$)

^{13}C-NMR (DMSO) δ = 14.69 (-CH$_3$), C-N (56.06) 58.35 (-OCH$_2$), 90.12 (C=C), 125.42 (C≡N), C$_6$H$_4$(phen) δ = 125.42, 127.25, 140.17, 149.89.

2.3.17 Synthesis of [Zn(Me$_4$tds)ced] (17)

ZnCl$_2$ (0.681 g, 0.005 mol) dissolved in 30 mL of methanol was added to tetramethyl thiuram disulfide (1.202 g, 0.005 mol) dissolved in 30 mL of methanol. The mixture was refluxed for 4 h. It gave a colourless solution and K$_2$ced (1.417 g, 0.005 mol) dissolved in 30 mL methanol was added. The colour changed immediately to whitish yellow and the reaction was refluxed further for 8 h. The product was filtered hot and re-dissolved in acetone to remove KCl by-product. The precipitate was recovered by allowing the acetone to evaporate at room temperature and the product was washed with methanol and diethyl ether.

[Zn(Me$_4$tds)ced]: (Yield: 1.59 g (75.1%), m. p. 315-317 oC). Anal. calc. for $C_{12}H_{17}N_3O_2S_6Zn$ (490.89): C, 29.44; H, 3.55; N, 9.01; S, 39.97. Found: C, 29.33; H, 3.49; N, 8.56; S, 39.08.

Selected IR, v(cm^{-1}): 2245(C≡N), 1732 (C=O), 1455 (C=S$_2$), 382 (M–S).

^{1}H-NMR (DMSO) δ = 1.05(t, 3H -NH-CH$_3$) 4.02 (q, 2H, -OCH$_2$)

^{13}C-NMR (DMSO) δ = 203.69 (C=S), 168.68 (C=O), 122.94 (C≡N), 59.29 (-OCH$_2$).

2.3.18 Synthesis of [Cd(Me_4tds)ced] (18)

$CdCl_2$ (0.917 g, 0.005 mol) dissolved in 30 mL of methanol and added to tetramethyl thiuram disulfide (1.202 g, 0.005 mol) dissolved in 30 mL of methanol. The mixture was refluxed for 4 h. K_2ced (1.417 g, 0.005 mol) dissolved in 30 mL methanol was added. The colour changed immediately to yellow and the reaction was refluxed further for 8 h. The product was filtered hot and the residue dissolved in acetone to remove the KCl. The filtrate was concentrated in vacuo and the final yellow product was washed with methanol and diethyl ether.

[Cd(Me_4tds)ced]: (Yield: 1.58 g (72.8%), m. p. 337-339 ºC). Anal. calc. for $C_{12}H_{17}N_3O_2S_6Cd$ (540.87): C, 26.35; H, 3.29; N, 8.13; S, 35.40. Found: C, 26.62; 3.17; N, 7.77; S, 35.47.

Selected IR, ν(cm^{-1}): 2233 (C≡N), 1512 (C=S2), 384 (M–S), 1600 (C=O).

^{1}H-NMR (DMSO) δ = 1.27 (t, 3H, -OCH_2CH_3), 4.09 (q, 2H, -OCH_2)

^{13}C-NMR (DMSO) δ = 208 (C=S), 164 (C=O), 121.37 (C≡N), 90.6 (C=C), 14.6 (-CH_3), 58.5 (-OCH_2).

2.3.19 Synthesis of [Hg(Me_4tds)ced] (19).

$HgCl_2$ (1.357 g, 0.005 mol) was dissolved in 40 mL of methanol and was added to tetramethyl thiuram disulfide (1.202 g, 0.005 mol) dissolved in 30 mL of methanol and refluxed for 4 h. The resultant colourless solution changed to brown on adding K_2ced (1.417 g, 0.005 mol) dissolved in 30 mL of methanol. The brown colour changed to grey and finally to black. The reaction was further refluxed for 8 h, filtered and the product dissolved in acetone to remove KCl by-product. The solvent was concentrated in vacuo, filtered and the final product washed with methanol and diethyl ether.

[Hg(Me_4tds)ced] (Yield: 1.9 g (91.6%), m. p. 309-311ºC). Anal. calc. for $C_{12}H_{17}N_3O_2S_6Hg$ (628.94): C, 22.95; H, 2.76; N, 6.64; S, 30.44. Found: C, 22.90; H, 2.72; N, 6.68; S, 30.50.

Selected IR, *v*(cm−1): 2244(C≡N), 1492 (C=S2), 449 (M–S), 1738 (C=O).

^{1}H-NMR (DMSO) δ = 4.35 (q, 2H, -OCH_2), 1.23 (t, 3H-CH_3).

^{13}C-NMR (DMSO) δ = NA.

2.4 References

1. Jensen, K. A.; Henriksen, L. Studies of thioacids and their derivatives. *Acta Chemica Scandinavica*, **1968**, *22*, 1107-1128.
2. Ajibade, P. A.; Osuntokun, J. Synthesis and characterization of hexadecylamine capped ZnS, CdS, and HgS nanoparticles using heteroleptic single molecular precursors. J. Nanomater. **2014**, *782526*, 1-7.

CHAPTER 3

3.Characterization of metal complexes

3.1 Introduction

The chemistry of substituted derivatives of thiourea has stimulated a lot of interest due to its diversity of binding sites, capability of being used as reagents for separation of metal ions [1] and biological activity such as; antibacterial [2, 3], antifungal [4] and antiviral [5] agents. Thiourea ligand mode of coordination is through S as donor (neutral ligand) or as deprotonated ligands in a monodentate (usually S-bonded) or through bidentate (as N, S-coordinated) mode [6]. Substistuted thioureas have been used as source of sulfur for the synthesis of metal sulfide nanoparticles [7, 8]. Thiourea is a useful ligand for the synthesis of metal complexes. In most cases it bonds via sulfur atom to the central metal and for this reasons, thiourea complexes are employed in the synthesis of nanoparticles as single source precursor because they provide a template for the establishment of a chalcogenide bond although, there has been an example of exceptional cases where the bond is through the nitrogen atom [9]. The general structure of substituted thiourea is shown in Figure 3.1.

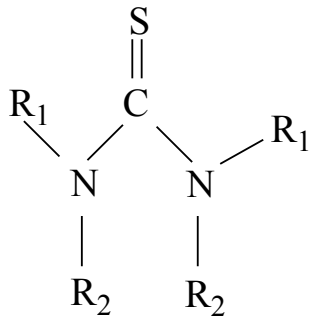

R_1 = H; R_2=CH_3, - N methyl thiourea, R_1 = R_2=CH_3, - N, N dimethylthiourea

R_1 = R_2 =C_2H_5, - N, N diethyl thiourea, R_1= R_2= C_3H_7, - N, N diisopropyI thiourea.

3. 1: Structure of alkyl substituted thiourea.

Other ligands used in this work as source of sulfur are tetramethyl thiuram disulfide and 1-cyano-1-carboethoxy-2, 2-ethylenedithiolate, Figure 3.2. More details about these ligands have been provided in chapter one.

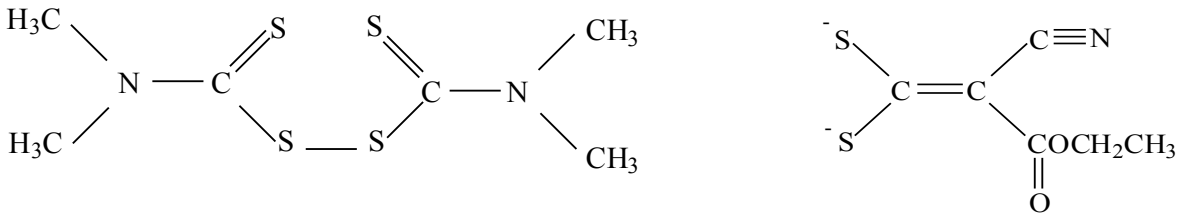

3.2: Tetramethyl thiuram disulfide (Me4tds). (b) 1-cyano-1-carboethoxy -2,2-ethylenedithiolate (CED).

This chapter contains the characterization of metal complexes and some of their adducts. It describes the details of the IR, ^{1}H and ^{13}C-NMR analysis of the metal complexes synthesized in this work. Zn(II), Cd(II) and Hg(II) thiourea or tetramethyl thiuram disulfide with 1-cyano-1-carboethoxy-2,2-ethylene dithiolate metal complexes have been were discussed and the coordination of the ligands to the central metals established. The substituted thiourea ligands used are methy, dimethyl, ethyl and diisopropyl thiourea. The characterization of adducts of the parent complexes of Zn(II) and Cd(II) synthesised through reactions with nitrogen donor ligands (pyridine, 2,2'-bipridine and 1, 10 - phenthroline) have been also described. The thermogravimetric analysis of the complexes was also described. The metals decomposed to their respective metal sulfide on thermal degradation and this confirms their potential as prescursor for the synthesis of metal sulfide nanoparticles.

3.2 Results and discussion

3.2.1 Metal complexes of 1-cyano-1-carboethoxy-2, 2-ethylenedithiolato–κS,S'–bis(N-methylthiourea–κS)M(II) (where M = Zn or Cd or Hg)

The complexes were isolated by reacting the metal salts of Zn(II), Cd(II) and Hg(II) with N-methylthiourea and ced in a 1:2:1 molar ratio. The products of the reactions are formulated as four coordinate species: $[Zn(mtu)_2ced]$, $[Cd(mtu)_2ced]$ and $[Hg(mtu)_2ced]$, in which the metal ions are coordinated to two molecules of N' methylthiourea acting as monodentate ligand and one molecule of ced acting as chelating bidentate ligand through the sulfur atoms. A representative equation for the formation of the complexes is shown in Scheme 3.1. The complexes were characterized by melting point, elemental analyses, IR, ^{1}H-NMR and ^{13}C-NMR spectroscopy. The complexes are not soluble in methanol, ethanol, hexane, chloroform, benzene and diethyl ether but they are sparingly soluble in highly coordinating solvents such as DMF and DMSO.

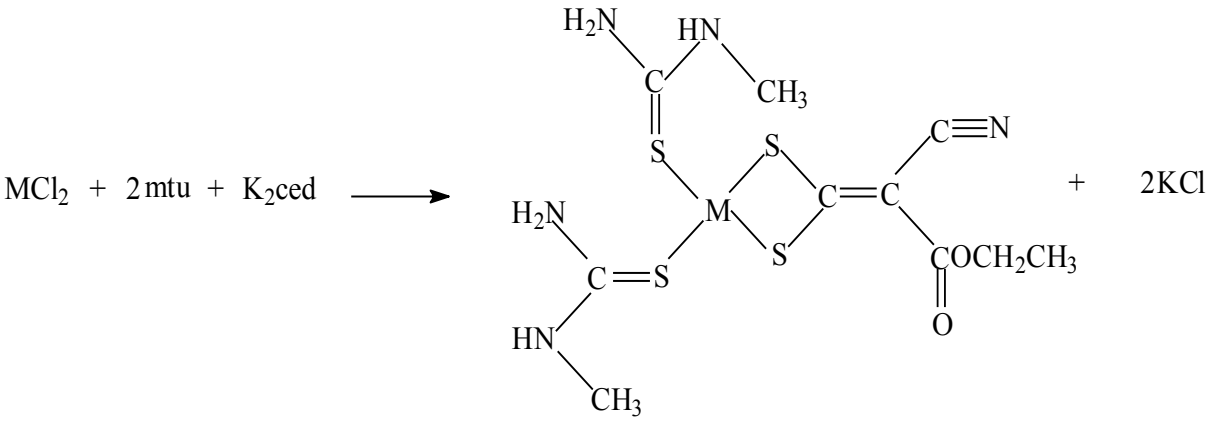

Scheme 3.1: Synthesis of $[M(mtu)_2(ced)]$, (M = Zn, Cd, Hg).

3.2.2 Infrared spectra studies of the metal complexes: $[M(mtu)_2(ced)]$

The IR spectra of the free ligands and their respective metal complexes were assigned on careful comparison. The IR spectra of complexes **1-3** show vibrational bands that are typical of the mixed coordinated ligands of methyl thiourea and ced. For the thiourea complexes, distinct vibration bands are observed at 624, 1513, 1618, 3412 cm^{-1} (**1**) 620, 1571, 1623, 3310 cm^{-1} (**2**), and 650, 1500, 1632, and 3200 cm^{-1} (**3**) which can be assigned to *ν*(C=S), ν(C-N), and *ν*(N-H) vibrations respectively [10]. The corresponding bands of the free thiourea ligand appeared at around 700, 1500, 1600 and 3235 cm^{-1} for *ν*(C=S), ν(C-N) and *ν*(N-H) vibrations sequentially. The thione ligand, (>C=S), on complexation exhibits red shift in its vibrational frequency due to electron donation or sulfur donation of electron to the metal center which enhance or promote π back donation to the thione π* orbital. Invariably, this leads to the decrease in strength of the carbon sulfide bond [11]. Contrarily, the *ν*(N-H) band experiences a blue shift in wavenumber which corresponds or indicates an increase in the strength of the *ν*(N-H) bond of the complex relative or compared to the free or pure ligand.

This is due to the electron donation from sulphur [12]. There exists a low frequency shift in C=S and a high frequency shift in the *ν*(N-H) vibration when these values are compared to free thiourea. The red shifting of the *ν*(C=S) bond of the free ligand confirmed that methylthiourea is coordinated to the metal ions via sulfur atoms [13, 14].

Selected vibrational bands that constitute the main region of interest in 1-cyano-1-carboethoxyl- 2,2-ethylenedithiolate complexes arising from *ν*(C≡N), *ν*(C=O), *ν*(C=CS_2), *ν*(C-S) are; in the ranges of 2188-2244, 1645-1700 cm^{-1}, 1412-1492 cm^{-1}, 1165-1116 cm^{-1} respectively [15]. In the uncoordinated K_2ced ligand these stretching vibrations are observed around 2161, 1680, 1441 and 1148 cm^{-1} while in the metal complexes, they are observed at 2198, 1630 , 1459 and 1148 cm^{-1} (**1**) for [Zn(mtu)$_2$ced]; 2199, 1652, 1412 and 1174 cm^{-1} (**2**) for [Cd(mtu)$_2$ced] and 2232 , 1732 , 1489, 1201 cm^{-1} (**3**) for [Hg(mtu)$_2$ced]. The appearance of bands around 1165 cm^{-1} in the complexes is indicative of a bidentate mode of coordination of ced through sulfur atoms [16]. The υ(M-S) was observed at 376, 396 and 388 cm^{-1} in [Zn(mtu)$_2$ced], [Cd(mtu)$_2$ced] and [Hg(mtu)$_2$ced] respectively. The presence of these vibrational frequencies confirms the coordination of the ions to the sulfur atoms [13, 14]. Some selected spectra for the ligands and the complexes are presented in Table 3.1.

Table 3.1: Some selected infra-red spectroscopy frequency of [M(mtu)$_2$ced]

Complexes	*ν*(N-H) (cm^{-1})	*ν*(C≡N) (cm^{-1})	*ν*(C=O) (cm^{-1})	*ν*(C=S_2) (cm^{-1})	*ν*(C–S)) (cm^{-1})	*ν*(C=S) (cm^{-1})	*ν*(M–S) (cm^{-1})
[Zn(mtu)$_2$ced]	3274	2198	1630	1459	1148	671	376
[Cd(mtu)$_2$ced]	3363	2199	1652	1412	1174	671	396
[Hg(mtu)$_2$ced]	3310	2232	1732	1489	1201	670	388

3.2.3 ^{1}H and ^{13}C-NMR spectra of [M(mtu)$_2$ced] (where M = Zn, Cd and Hg)

The complexes are dissolved in in DMSO-d_6 and the data of the chemical shift signals from ^{1}H and ^{13}C-NMR spectra are all consistent with the proposed structures for the complexes. Characteristic chemical shift that are diagnostic of thiourea and ced were shown in the resonance signals. In the ^{1}H-NMR of the complexes **1-3**, the N-H signals of thiourea appeared at 7.97, 7.86 and 7.60 ppm respectively. The N-H show less intensity of the signal on coordination and this led to a downfield shift relative with position in free N-methylthiourea. The deshielding can be attributed to increase in π electron density in the C-N bond on coordination [17]. The existence of *ν*(N-H) indicated that the thiourea ligand is coordinated to the central metal atom through the sulfur atom. Reports on crystal structures of substituted thiourea derivatives confirm the coordination of thiourea to metal center through sulfur [18, 19]. ^{1}H-NMR spectra of complexes **1-3** reveals a quartet in a low field (chemical shift 3.70-4.14) and a triplets (chemical shifts 1.26-1.35) which is in agreement with OCH_2CH_3 moiety [20]. The ^{13}C-NMR exhibits 6 set of signals that are characteristic of K_2ced ligands and they are C=S, C=O, C≡N, C=C, OCH_2, CH_3. These signals appear in complexes 1-3 at 206, 163, 120.74, 90.00, 58.8, 14.59 ppm (**1**) 206.8, 160. 28 121.5, 90.1, 58.32 ppm, 14.55 (**2**) and 58.55, 14.40 ppm (**3**) for C=S, C=O, C≡N, C=C, OCH_2, CH_3 sequentially. Some of the resonance signals are not available for complex 3 which is a mercury complex due to the poor solubility in DMSO-d6.

3.2.4 Thermal study of [M(mtu)$_2$ced] (Where M = Zn and Cd)

The thermogravimetric (TGA), DTG and DSC of the complexes were measured under a flow of nitrogen to study the thermal behaviour of the complexes. The TGA and DTG of complexes, (**1**) & (**2**) are shown in Figure 3.3 (a) and (b). [Zn(mtu]$_2$ced] shows a two stage decomposition profile and the DTG presented a maximum decomposition temperature of 202

ºC. The decomposition of the complex led to the formation of ZnS. The weight loss found was 58.6% and the calculated was 62.5%.

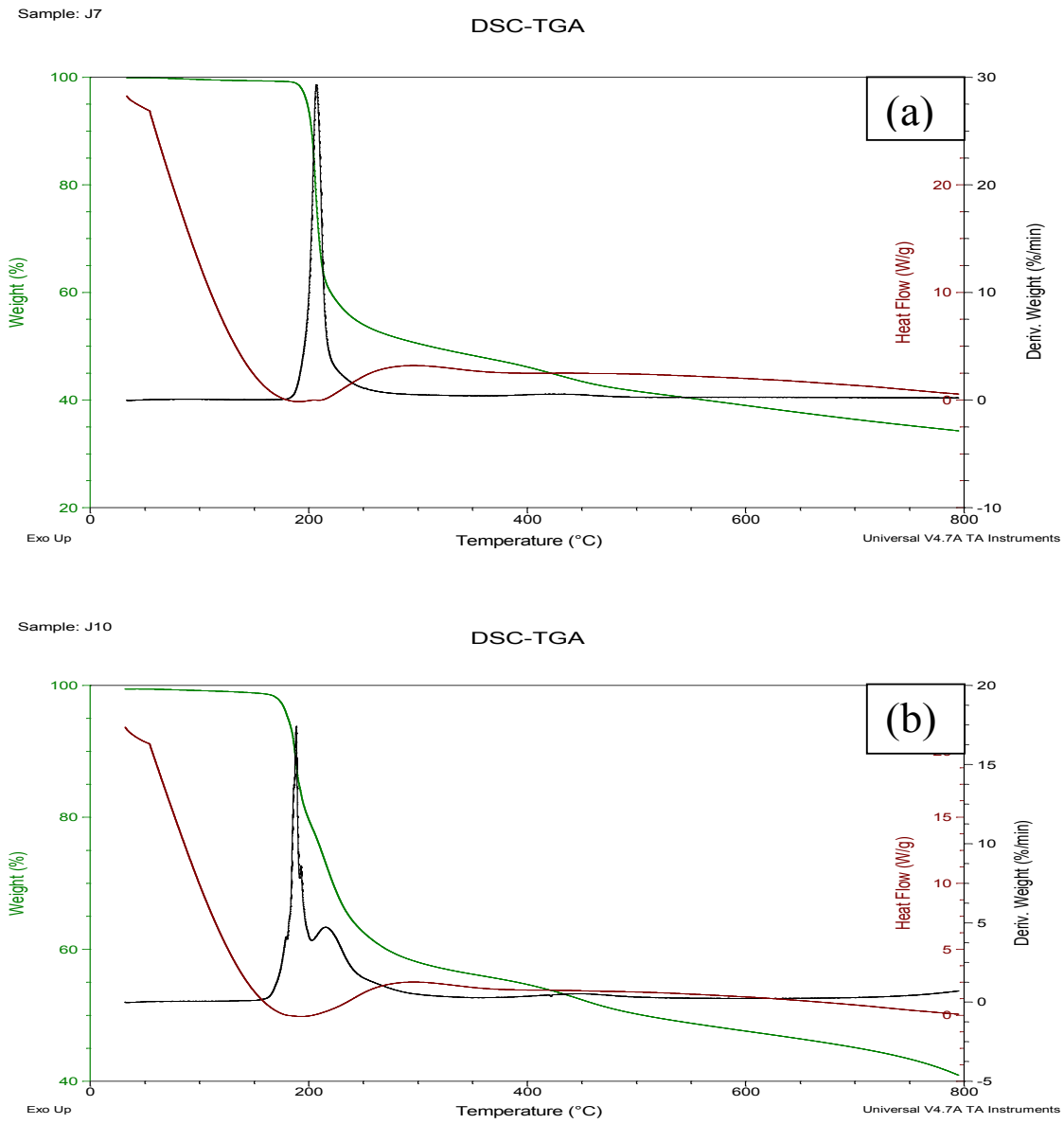

3. 3: TGA/DTG of (a) [Zn(mtu)$_2$ced] and (b) [Cd(mtu)$_2$ced]

The TGA reveals that the product of thermal decomposition is ZnS and this confirms the suitability of [Zn(mtu)$_2$ced] as a good precursor for thermolysis to obtain ZnS nanoparticles; (Found calcd. weight loss) 58.6% for (**1**) and calculated was 62.5%. Complex 2 has a similar decomposition profile and like (**1**), it does not have a plateau. The DTG have a maximum is 210º C. Decomposition started around 135 ºC and extended till around 600 ºC with a loss of fragments around 250 ºC which is most likely to be the thiourea moiety. Similar results have been found in literature [21]. The sharp DTG is likely due to melting of the complex.

The percentage of the complex that decomposed was 66% with only 34% left although this is close to the calculated amount of 30.10 % mass of CdS left residue left after the decomposition around 43 % and it's close to the calculated amount of 35%. Generally for thiourea complexes on decomposition, they either volatilize leaving a negligible amount of residue or decompose to afford the respective metal sulfide. This is why sometimes the expected decomposition residue may not correspond with the calculated values [22]. There are actually three stages of degradation, the first one occurred between 60 and 200 ºC (less than 200 ºC) lead to loss of trapped solvent with loss of about less than 4% of the total weight of the complex.

3.3 Metal complexes of 1-cyano-1-carboethoxy-2, 2-ethylenedithiolato–κS,S'–bis(N, N-dimethylthiourea–κS)M(II) (where M = Zn or Cd or Hg)

The synthesis of heteroleptic Zn(II), Cd(II) and Hg(II) complexes formed by the reaction of the respective metal salts, N, N dimethylthiourea (dmtu) and 1-cyano 1-carboethoxy-2,2 ethylene dithiolate (ced) in the mole ratio of 1:2:1 afforded the formation of the three precursors formulated as [Zn(dmtu)$_2$ced] and [Cd(dmtu)$_2$ced] and [Hg(dmtu)$_2$ced]. The complexes are air stable based on the analytical and spectroscopic data. The complexes are

insoluble in most common organic solvents but slightly soluble in high coordinating solvents like DMF and DMSO. A typical equation for the formation of the complexes is shown in Scheme 3.2.

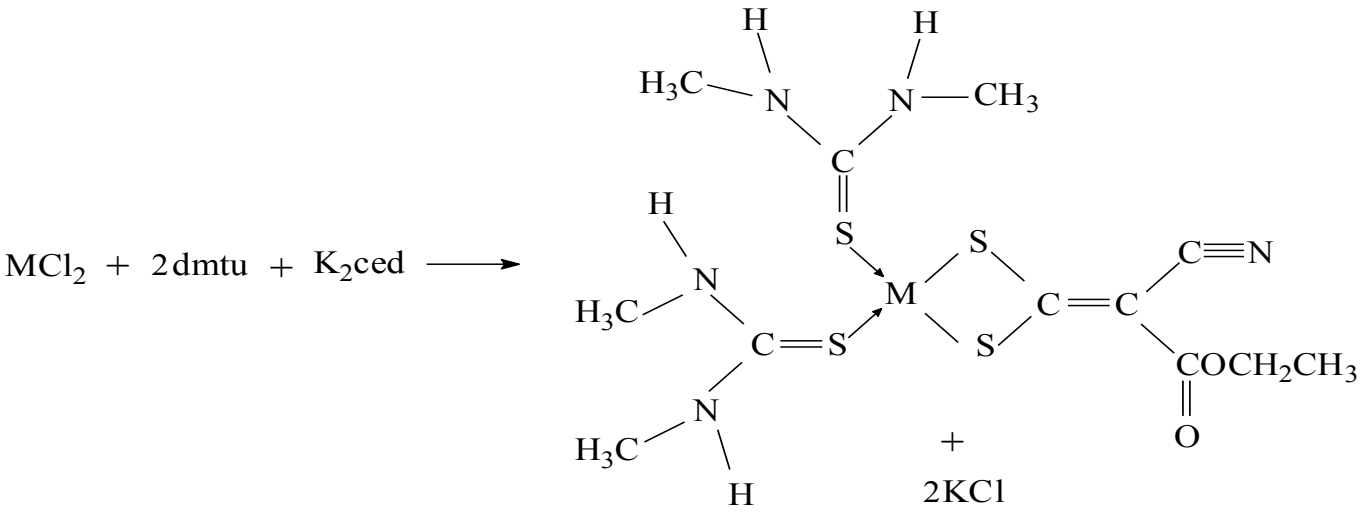

Scheme 3.2: Synthesis of $[M(dmtu)_2(ced)]$, M= (Zn, Cd and Hg)

3.3.1 Infrared spectra studies of the metal complexes: $[M(dmtu)_2(ced)]$

FT-IR spectra of the complexes $[Zn(dmtu)_2ced]$ (**4**), $[Cd(dmtu)_2ced]$ (**5**) and $[Hg(dmtu)_2ced]$ (**6**) showed all the characteristics bands for ced and dimethyl thiourea. There are three characteristics bands that are typical of thiourea ligands and they normally appear in frequency regions; v(C=S) located around 700 cm^{-1}, v(C-N) at around 1500 cm^{-1} and the v(N-H) is identified around 3200 cm^{-1} while the N-H bending vibration is noticeable around 1600 cm^{-1} [23, 24]. For the $[Zn(dmtu)_2ced]$, $[Cd(dmtu)_2ced]$ and $[Hg(dmtu)_2ced]$ these bands are observed at; [622, 1570, 1613, 3414] cm^{-1}, [623, 1557, 1607, 3403] $cm^{-1}$and [617, 1618,

1637, 3237] cm^{-1} respectively for the v(C=S), v(C-N), N-H bending vibrations and the v(N-H). It is worthy of note that a low frequency shift in the v(C=S) band, accompanied with a high frequency shift in the N-H and (C-N) bands in thiourea complexes as related to the uncoordinated ligands is indicative of the presence of thione form in the solid state [25].

Four main regions are of interest in 1-cyano-1-carboethoxy-2,2-ethylenedithiolato (ced) complexes namely: the 2188-2244 cm^{-1} which is due to v(C≡N); 1645-1700 cm^{-1} which is due to v(C=O); 1412-1492 cm^{-1} due v($C=CS_2$) and 1116-1165 cm^{-1} due to v(C-S) of the chelated ced^{2-} [16, 26]. In the metal complexes, these stretching vibrations were observed at 2209, 1705, 1448 and 1188 cm^{-1} for [$Zn(dmtu)_2$ced] (4), 2209, 1629, 1473 and 1165 cm^{-1} for [$Cd(dmtu)_2$ced] (**5**) and [2024, 1637, 1472, 1138] for [$Hg(dmtu)_2$ced] (**6**). The *ν*(M-S) stretching vibrations occur as a weak band at region of low intensity at 376 and 396 cm^{-1} and 400 cm^{-1} for [$Zn(dmtu)_2$ced] and [$Cd(dmtu)_2$ced] respectively. The presence of these weak bands confirmed bonding between the metal and the sulfur atoms [17, 27]. Table 3.2 shows selected IR spectra of the complexes.

Table 3.2: Some selected infra-red spectroscopy frequency of [$M(dmtu)_2$ced]

Complexes	*ν*(N-H) (cm^{-1})	*ν*(C≡N) (cm^{-1})	*ν*(C=O) (cm^{-1})	*ν*($C=S_2$) (cm^{-1})	*ν*(C–S) (cm^{-1})	*ν*(C=S) (cm^{-1})	*ν*(M–S) (cm^{-1})
[$Zn(dmtu)_2$ced]	3275	2209	1705	1448	1188	671	394
[$Cd(dmtu)_2$ced]	3244	2209	1629	1473	1165	670	377
[$Hg(dmtu)_2$ced]	3362	2241	1599	1459	1191	670	424

3.3.2 ^{1}H and ^{13}C-NMR spectra of [M(dmtu)$_2$ced] (where M = Zn, Cd and Hg)

The Zn(II) complex showed characteristics chemical shift that are typical of thiourea and ced. The singlet peak at δ 7.37 ppm in the ^{1}H-NMR can be assigned to the proton of the N-H of the thiourea group. The signal of the N-H of the thiourea is observed to be less intense on coordination and shifted downfield relative to the position of the uncoordinated ligand. The deshielding can be ascribed to an increase in π electron density in the C-N bond on coordination [28]. The emergence of N-H signal is an indication that the thiourea ligand is bonded to the central metal via the thione group [29]. Other peaks at δ 3.98 and 1.15 ppm are due to quaternary protons of (OCH_2) and triplet's protons of (CH_3) respectively. Other prominent peaks are 2.5 and 3.5 ppm and are due to solvent (DMSO) and moisture (H_2O) respectively. The ^{13}C-NMR spectra of [Zn(dmtu)$_2$ced] shows resonance signals corresponding to ced for; C-S (206.32), C=O (163.92), C≡N (121.88), C=C (90.91), -OCH_2 (58.41) and CH_3 (14.62) δ in ppm for the carbons of ced and thiourea group. A marginal coordination induced downfield shift of the C-S carbon is indicative of the (S, S) coordinated nature of the ced^{2-} [30]. A peak observed at δ 7.34 ppm can be assigned to the N-H protons of the thiourea group in [Cd(dmtu)$_2$ced] (**5**). The peaks at δ 4.01 and 1.16 ppm in the ^{1}H-NMR of the complex can also be assigned to the quaternary protons of OCH_2 and triplet protons of CH_3 respectively. The ^{13}C-NMR of this complex (**5**), shows a peak at δ C-S (207.84), C=O (165.89), C≡N (121.34), C=O (90.44), -OCH_2 (58.86) and CH_3 (14.59) ppm typical of coordinated ced functionalities [31].

3.3.3 Thermal study of [M(dmtu)$_2$ced] (Where M = Zn and Cd)

The TGA, and DTG of [Zn(dmtu)$_2$(ced)] (**4**) and [Cd(dmtu)$_2$ced] (**5**) are shown in Figure 3.5 (a & b). The decomposition of complex (**4**), Figure 3.4(a) took place in two stages. The first stage started at 196 ºC and ended at 240 ºC while decomposition of complex (**5**) started at around 150 ºC with an expulsion of trapped solvent (less than 2% of the complex) below 200 ºC. The DTG maximum for complex (**4**) is at 200 ºC and it is observed that a significant fragment of the complex probably thiourea moiety is lost at around 250 ºC. The mass of the complex (**4**) lost is around 57% while the amount remaining about 42%. This is close to the weight of ZnS. Complex (**5**) represented by Figure 3.4(d) has a maximum DTG of 210 ºC and this shows that it is stable. The TGA of (**5**) reveals that the 68% of weight loss occurred with almost 32% residue obtained. This is close to the calculated residue of 28.4%. The suitability of the complex as precursor for CdS synthesis is confirmed.

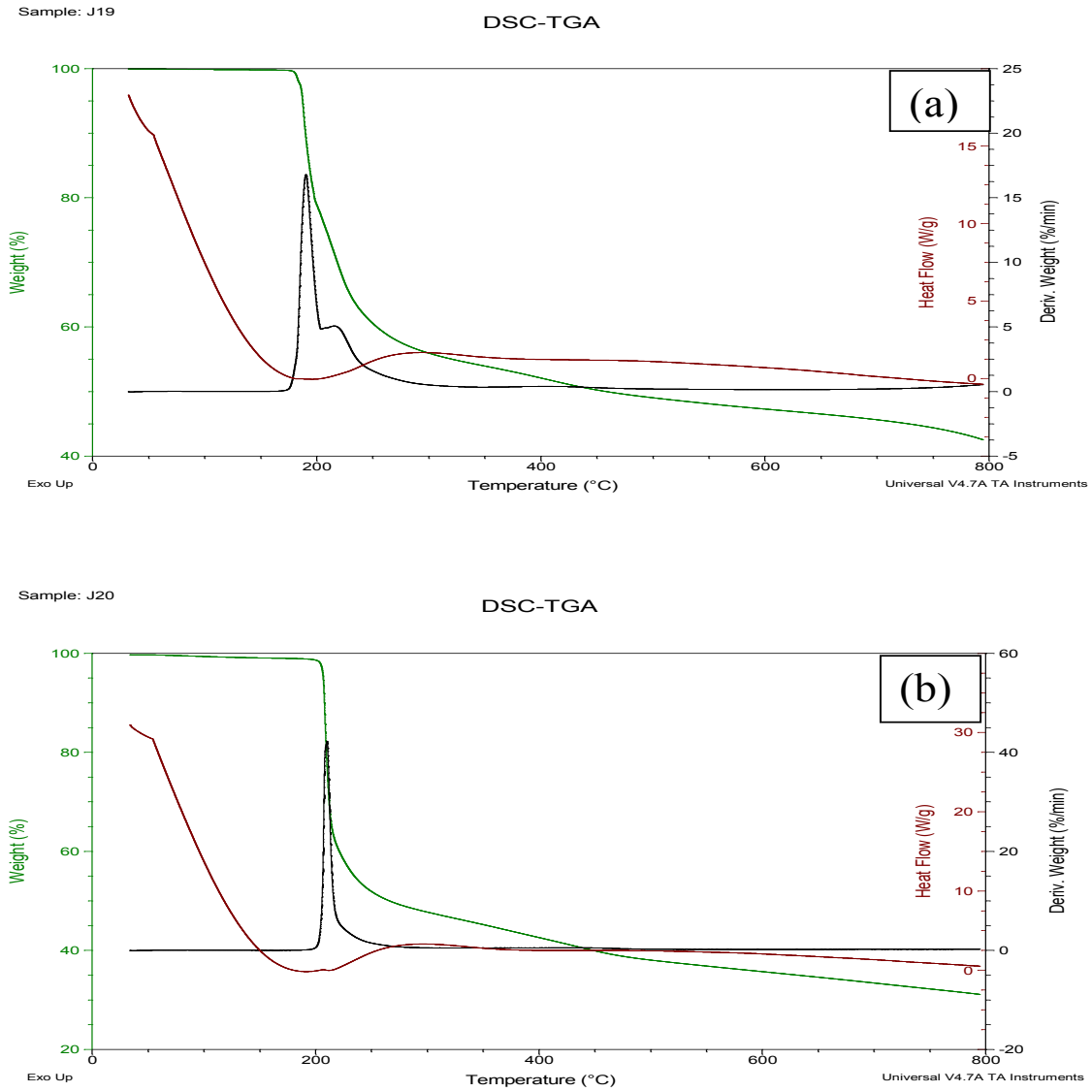

Figure 3.4: TGA/DTG of (a) $Zn(dmtu)_2$ and (b) $[Cd(dmtu)_2ced]$.

3.4 Metal complexes of 1-cyano-1-carboethoxy-2, 2-ethylenedithiolato–κS,S'–bis(N, N-diethylthiourea–κS)M(II) (where M = Zn, Cd, Hg) (7), (8) and (9)

These complexes are formulated as $[M(detu)_2ced]$ (where M = Zn, Cd and Hg) and the synthetic method used in the preparation is the same as with the previous complexes above, (**1**-**6**). The complexes were characterized with elemental analysis, IR, ^{1}H- and ^{13}C-NMR spectroscopy. The substituted thiourea in these complexes is the N, N diethylthiourea which is a monodentate ligand and the second ligand, 1-cyano-1-carbethoxy-2, 2-ethylenedithiolate, is a bidentate chelating ligand. The mode of coordination to the central metal is through four sulfur atoms. The complexes are formulated as four coordinate species consisting of two molecules of monodentate diethythiourea and one molecule of bidentate ced. This central metal displays MS_4 chromophore. Substituted thiourea compounds are known to form stable complexes and have been reportedly used as single source precursors for the preparation of semiconductor nanoparticles [32, 33]. Formation of the complexes can be represented as shown in Scheme 3.3. All the three complexes are not soluble in the common organic solvents although they are sparingly soluble in DMF and DMSO. They also decompose in the temperature range of 200-400 ºC.

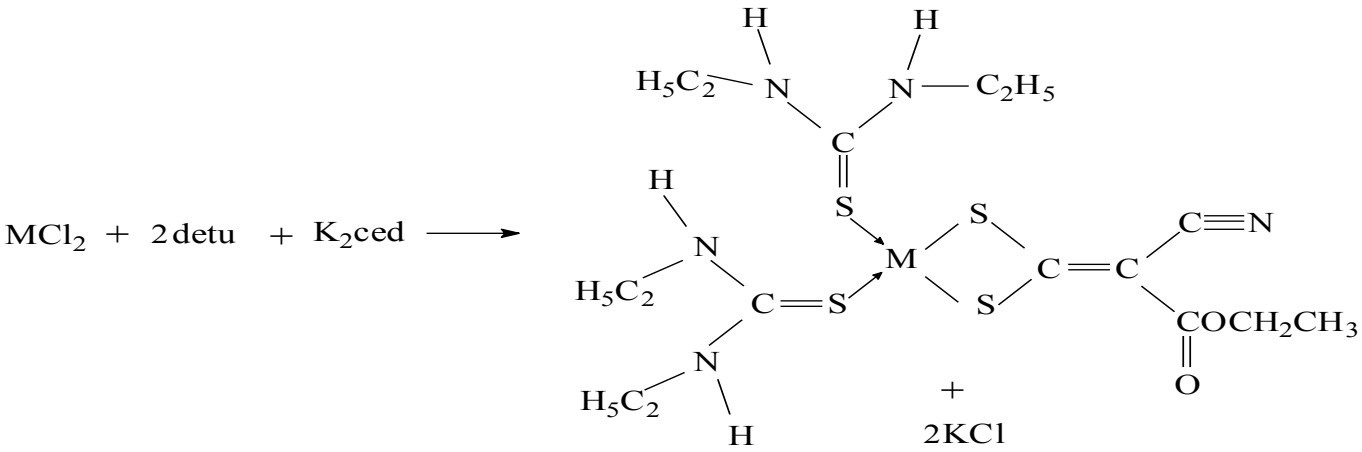

Scheme 3.3: Synthesis of $[M(detu)_2(ced)]$, M= (Zn, Cd and Hg)

3.4.1 Infrared spectra studies of the metal complexes: [M(detu)$_2$(ced)]

Like the previously discussed bonding of the substituted thiourea mixed ligand complexes with ced, there are diagnostic characteristics bands for thiourea and ced which are clearly revealed by the IR spectra of the complexes. For the diethylthiourea the bands are observed in the free ligand in three frequency regions; ν(C=S) located around 600 cm^{-1}, ν(C-N) bands observed around 1500 cm^{-1} and the ν(N-H) found around 3200 cm^{-1}. But in the complexes these bands appear at (619, 1515, 3288) cm^{-1} (**7**), (621, 1522, 3294) cm^{-1} (**8**) and (652, 1572, 3362) cm^{-1} (**9**).

Table 3.3: Some selected infra-red spectroscopy frequency of [M(detu)$_2$ced]

Complexes	ν(N-H) (cm^{-1})	ν(C≡N) (cm^{-1})	ν(C=O) (cm^{-1})	ν(C=S$_2$) (cm^{-1})	ν(C–S) (cm^{-1})	ν(C=S) (cm^{-1})	ν(M–S) (cm^{-1})
[Zn(detu)$_2$ced]	3275	2200	1681	1462	1193	670	373
[Cd(detu)$_2$ced]	3275	2206	1651	1463	1176	666	372
[Hg(detu)$_2$ced]	3362	2188	1656	1458	1191	669	375

The occurrence of N-H vibrational bands in all the complexes confirms the bonding of the diethyl thiourea ligand to the metals via sulfur atom [34]. The stretching vibrations that appear at 794 cm^{-1} in the free diethylthiourea shifted to about 620 cm^{-1} in the metal complexes. The red shifting of the ν(C=S) bond of the free ligand confirm that diethylthiourea is coordinated to the metal ions through the sulfur with a reduction of π-electron density of the ν(C=S) bond. For the K$_2$ced ligand of the complex, the most important vibrational modes of the dipotassium 1-cyano-1-ethoxy-2,2-ethylenedithiolate ligands are; 2161 cm^{-1} due to ν(C≡N); 1681 cm^{-1} due to ν(C=O); 1360 cm^{-1} due ν(C=CS$_2$) and 1160 cm^{-1} due to ν(C-S). The assignment of these vibrations frequencies are based on literature source

[27, 35, 36]. These were observed in the metal complexes at (2200, 1681, 1462, 1193) cm^{-1} for complex (7); (2206, 1651, 1463 and 1176) cm^{-1} for complex (8) and (2188, 1656, 1458, 1191) cm^{-1} for complex (9) characteristic of CED complexes in a chelating and bidentate bridging mode [37]. The appearance of a band around 1165 cm^{-1} which is due to the vibrations of the *ν*(C-S) suggests a bidentate mode of chelation of ced via sulfur atoms [21]. The *ν*(M-S) was observed at 373, 372 and 375 in [Zn(detu)$_2$ced], [Cd(detu)$_2$ced] and [Hg(detu)$_2$ced] respectively.

3.4.2 ^{1}H and ^{13}C-NMR spectra of [M(detu)$_2$ced] (where M = Zn, Cd and Hg)

In the ^{1}H-NMR spectra of the diethyl thiourea complexes, the N-H singlet peaks were observed at 7.27, 7.48 and 7.87 ppm chemical shifts for complexes **7**, **8** and **9**. These signals appear to be less than the chemical shift assigned to N-H in the free ligand. This is due to the coordination of the diethyl thiourea ligand to the central metal ions. The deshielding can be attributed to an increase in π electron density in the C-N bond upon coordination of the ligand [38]. The CH_3 and CH_2 signals of the free ligand are observed at 1.07 ppm and 3.35 ppm and these were revealed in the complexes at around 1.04 and 3.35 ppm for complexes (**7**), (**8**) and (**9**).

Coordinated ced ligand exhibits a low field quartet and triplets due to the OCH_2 and the CH_3 of the ethoxy moiety. These quartet signals due to OCH_3 are observable at (3.95- 3.99 δ ppm) and 1.13 -1.15 δ ppm) in complexes (**7**), (**8**) and (**9**). The ^{13}C-NMR spectra of complexes (**7**) and (**8**) show chemical shifts corresponding to the carbon atoms of ced and the thiourea although most of the chemical shift of the thiourea carbon atoms were masked by that of the ethoxy moiety of the 1,1 dithiolate derivative. The carbon atoms of the ethoxy moiety exhibited chemical shifts at (14.53, 58.83, 90.91, 120.83, 163.92, 206.32) δ ppm (**7**) and

(14.53, 58.32, 90.84, 120.76, 163.87, 206.23) δ ppm (**8**) which are resonance signals corresponding to CH_3, -OCH_2, C=C, C=N, C=O, C-S_2 of the ethoxy moiety [39]. It is worth noting that the chemical shift signals at around 39.74 and 14.54 ppm attributed to CH_2 and CH_3 resonance is due to the presence of diethyl thiourea ligand. Complex (**9**), with mercury as the central atom, showed only chemical shift at 54.41, 39.47 and 14.51 ppm as signals from chemical shift that is due to OCH_2, CH_2 and CH_3 chemical shifts.

3.4.3 Thermal study of [M(detu)$_2$ced] (Where M = Zn and Cd)

The thermal degradation of complexes [Zn(detu)$_2$ced] (**7**) and [Cd(detu)$_2$ced] (**8**) are depicted in Figure 3.5(a & b). The complex (**7**) begins to decompose at about 100 ºC with expulsion of trapped solvent. The decomposition continued till around 260 ºC with the DTG maximum at about 218 ºC. At the final stage of decomposition about 67% of the sample has decomposed leaving behind about 33% as residue which correspond to the mass of the CdS. For the [Cd(detu)$_2$ced] (**9**), the DTG reveals 3 stages of decomposition, the first between 50-100 ºC which is due to expulsion of trapped solvent in the sample. The second one occurred between 180-230 ºC which is due to the loss of thiourea fragments and the final one around 280 ºC. About 60% of the sample decomposed at the final stage with expected residue that corresponds to the mass of CdS. Generally mercury metal complexes are volatiles on decomposition leaving almost no residues and due to these the TGA and DTG are not presented here.

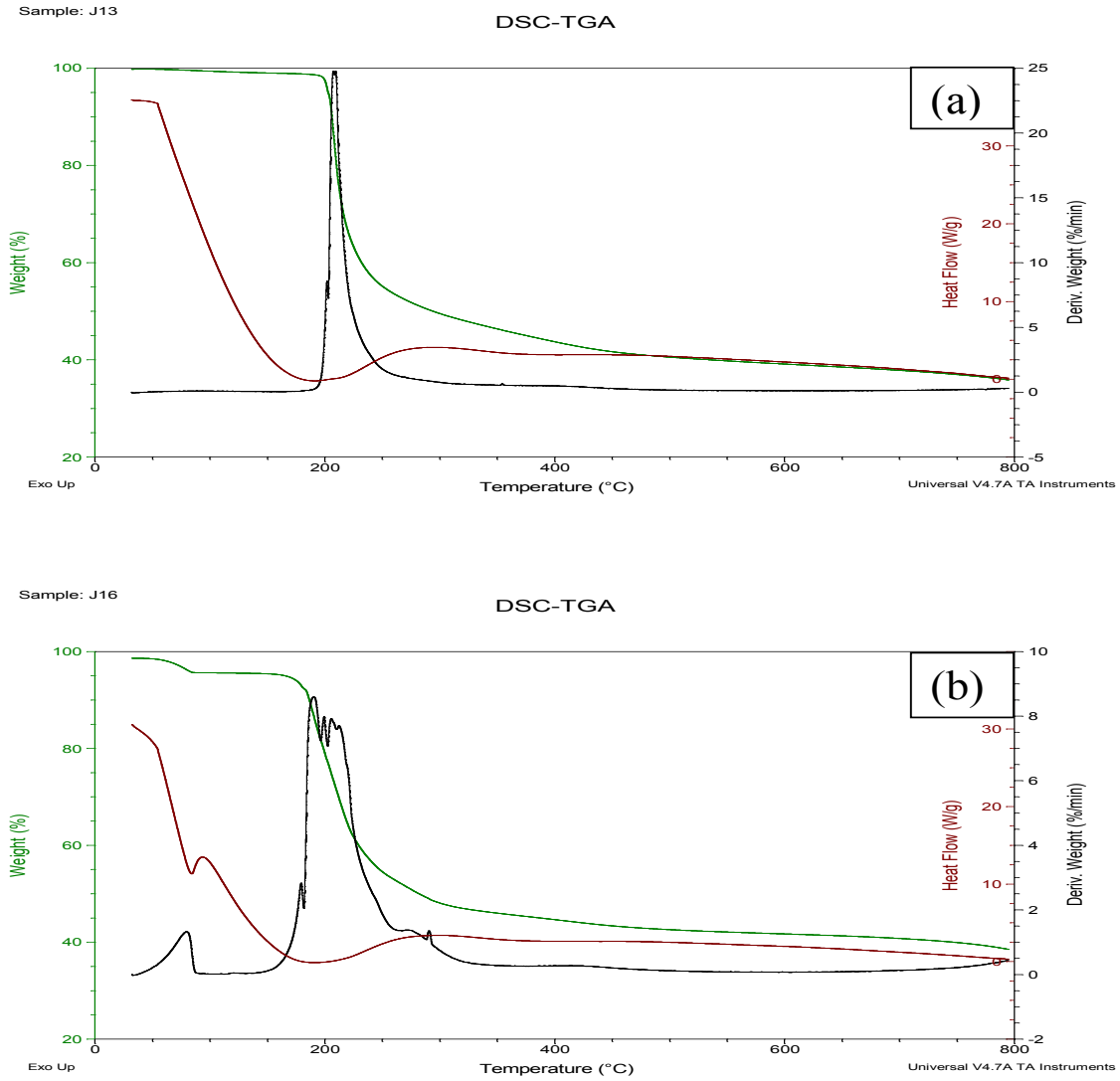

Figure 3.5: TGA/DTG of (a) [Zn(detu)$_2$ced] and (b) [Cd(detu)$_2$ced].

.

3.5 Adducts of 1-cyano-1-carboethoxyethylene-2,2-dithiolato–κS,S'–bis(N,N'-diisopropylthiourea–κS)Zn(II):[M(diptu)2ced/py/N-N] (where = Zn, py = pyridine, N-N = 2, 2 bipyridine or 1,10 phenanthroline) (10-13)

The parent complex $[Zn(diptu)_2ced]$ represented by (**10**) was synthesized by the reaction of $ZnCl_2$ with diisopropyl thiourea and a slow addition of dipotassium 1-cyano-1-carbethoxyl-2,2-ethelene dithiolate in molar ratio of 1: 2: 1. It afforded the formation of the parent precursor complex (**10**) which was further reacted with pyridine, 2, 2' bipyridine or 1, 10 phenanthroline, in molar ratio 1:1 to give the respective adducts (**11**), (**12**) and (**13**) via addition reaction. Pyridine is a monodentate ligand while 2, 2' bipyridine are 1, 10 phenanthroline are bidentate nitrogen donor ligands and the isolated products are Zn(II) adducts that are insoluble in water and other organic solvents but slightly soluble in strong coordinating solvents such as DMF and DMSO..

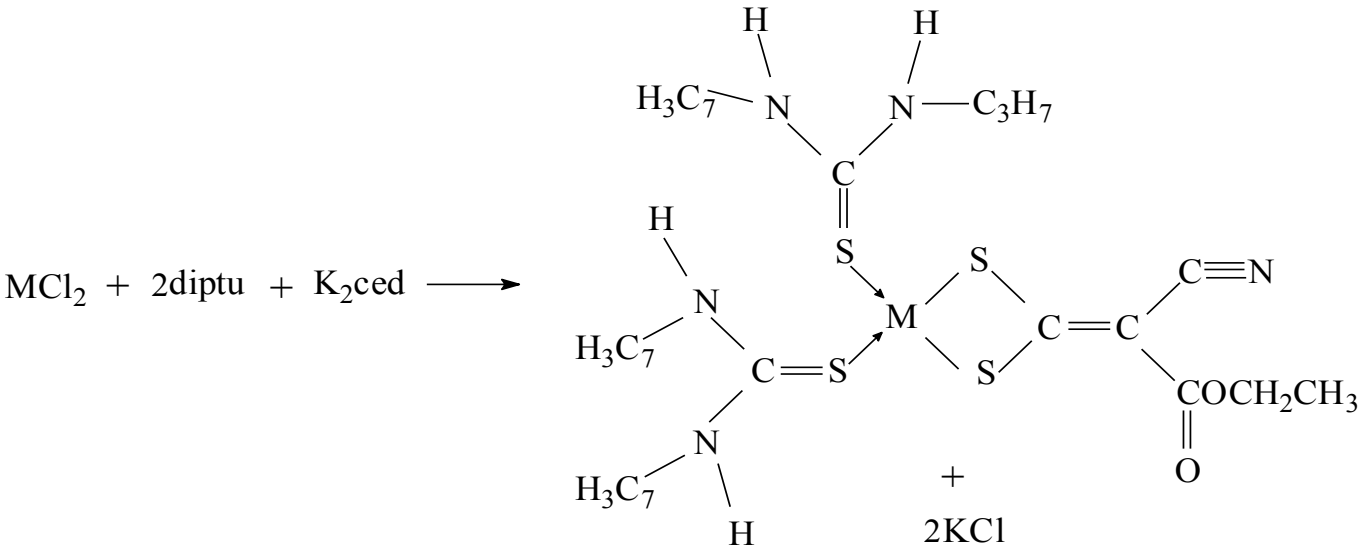

(Where M = Zn)

Scheme 3.4: Synthesis of $[M(diptu)_2ced]$ (where M= Zn).

The coordination geometry around the Zn metal is increased from four to five by pyridine adducts formation to give a MS_4N chromophore and to six in the synthesis of 2, 2' bipyridine

and 1, 10 phenanthroline adducts to produce a MS_4N_2 chromophore. The sulfur and the nitrogen atoms are electron rich and donate electron to the metal centre. The ced^{2+} is a cationic ligand and it shares electrons with the divalent central metal (Zn^{2+} or Cd^{2+}) while the thiourea is a chalcogen source and donates a pair of electron to the central metal.

3.5.1 Infrared spectra studies of the metal complexes: [Zn(diptu)$_2$(ced)/py/N-N]

The IR spectra of the Zn(II) mixed ligand complexes exhibit frequency bands associated with important functionalities of diisopropyl thiourea and ced. The thiourea ligand is expected to have a set of peaks at four frequency regions; *v*(C=S) at around 600 cm^{-1}, *v*(C-N) at around 1500 cm^{-1}, N-H bending vibration observed around 1600 cm^{-1} and N-H that is noticeable around 3200 cm^{-1} [40]. For the parent complex [Zn(diptu)$_2$(ced)], and the adducts; [Zn(diptu)$_2$(ced)(py)], [Zn(diptu)$_2$(ced)(bpy)], [Zn(diptu)2(ced)(phen)], these vibrational frequencies are observed at (617, 638, 629, 639) cm^{-1}, (1515, 1518, 1518, 1518) cm^{-1} , (1616, 1606, 1614, 1622) cm^{-1} and (3414, 3225, 3263, 3070) cm^{-1} for *v*(C=S), *v*(C-N), N-H bending vibration and N-H respectively. A low frequency shift in C=S and a high frequency shift in N-H confirms the coordination of the Zn^{2+} to the diisopropyl thiourea ligand. The appearance of N-H vibration in the complex is also a proof that thione form of the ligand is in solid state [41, 42]. The infrared spectra of the 1-cyano-1-carboethoxy-2, 2-ethylenedithiolate complexes is expected to have strong absorption in the following region; 2188-2244 cm^{-1}, 1645-1700 cm^{-1} 1116-1165 cm^{-1} due to *v*(C≡N), *v*(C=O) and *v*(C-S) respectively [43].

In the uncoordinated ced^{-2} ligand, these stretching vibrations are observed around 2174, 1681 and 1160 cm^{-1} while in [Zn(diptu)$_2$ced] they appeared at 2196, 1615 and 1173 cm^{-1}. In the adducts: They are observed at 2198, 1616, 1173 cm^{-1}, for the [Zn(diptu)$_2$(ced)(py)], at 2198,

1606, 1166 cm^{-1} for [Zn(diptu)$_2$(ced)(bpy)] and 2197, 1620, 1169 cm^{-1} for [Zn(diptu)$_2$(ced)(phen)] respectively. Typical characteristic band due to pyridine adducts is observed in [Zn(diptu)$_2$(ced)(py)] at 1606 cm^{-1} [44]. Ring frequencies related to 2, 2' bipyridine and 1, 10 phenanthroline adducts are in the range of 1600-1000 cm^{-1}. For [Zn(diptu)$_2$(ced)(bpy)], there is a noticeable band at 1597 cm^{-1} due to the v(C=N) in the 2, 2'-bipyridine ring, and this was observed in the free 2,2 bipyridine at 1579 cm^{-1}, while [Zn(diptu)$_2$(ced)(phen)] shows characteristic peak at 1622 and 1518 cm^{-1} as against 1608 cm^{-1} and 1512 cm^{-1} that were observed in the free 1,10 phenanthroline [45]. The positive shift may be due to the ring current arising from electron delocalization after the chelate formation [46]. The v(C=C) and v(C=N) modes of 1,10 phenanthroline in [Zn(diptu)$_2$(ced)(phen)] appear at 1510 and 1683 cm^{-1} while in the free 1,10 phenanthroline the values are 1500 cm^{-1} and 1600 cm^{-1} sequentially [47]. The shift to higher wavenumber on coordination can be ascribed to the interaction between Zn^{2+} and the nitrogen atom of the 1, 10 phenanthroline.

Table 3.4: Some selected infra-red spectroscopy frequency of [Zn(diptu)$_2$ced/py/N-N**]**

Complexes	*ν*(N–H) cm^{-1}	*ν*(C≡N) cm^{-1}	*ν*(C=O) cm^{-1}	*ν*(C=S$_2$) cm^{-1}	*ν*(C–S) cm^{-1}	*ν*(C=S) cm^{-1}	*ν*(M–S) cm^{-1}
[Zn(diptu)$_2$(ced)]	3417	2196	1615	1374	1173	650	412
[Zn(diptu)$_2$(ced)(py)]	3225	2198	1606	1369	1166	638	422
[Zn(diptu)$_2$(ced)(bpy)]	3447	2198	1607	1375	1173	651	411
[Zn(diptu)$_2$(ced)(phen)]	3422	2197	1629	1373	1167	637	421

3.5.2 ^{1}H and ^{13}C-NMR spectra of [Zn(diptu)$_2$ced/py/N-N]

The ^{1}H-NMR of the parent compound, [Zn(diptu)$_2$ced], displays triplet at δ 1.14 ppm for the CH_3 and quartet at δ 3.98 ppm for the –OCH_2 protons of the ethoxy group of ced. The solvent peak ($DMSO_6$) and moisture (H_2O) peak are observed at δ 2.40 ppm and 3.37 ppm respectively. The N-H resonant peak appears at δ 7.8 ppm. The ^{13}C-NMR of the parent complex, [Zn(diptu)$_2$ced], shows peaks at δ; 14.39, 58.34, 90.86, 120.86, 169.88 and 206.30 ppm and these peaks correspond to the CH_3, OCH_2, C=C, C=N, C=O, C-S which are characteristic peaks of the ced [48]. For the pyridine adduct of the parent complex, [Zn(diptu)$_2$ced(py)], a triplet at δ 1.27 ppm for CH_3 and a quartet at 3.95 ppm for –OCH_2 protons of the ethoxy of ced are identified. Solvent peaks for $DMSO_6$ and (H_2O) appeared at δ 2.49 and 3.36 ppm while the N-H peak of the thiourea is also present at δ 7.8 ppm. For the ^{1}H-NMR of the complex (**11**), the pyridine hydrogen resonances are found shifted to the lower field relative to the free pyridine. The signals observed at 7.42, 7.82 and 8.57 ppm are assigned to the protons of pyridine ring. ^{13}C-NMR spectrum of [Zn(diptu)$_2$ced(py)] showed peaks are at δ; 14.61, 58.41, 90.90, 120.87, 164.00, 206.35 ppm and these can be attributed to the carbon atoms of CH_3, OCH_2, C=C, C=N, C=O and C-S_2 sequentially. Peaks at δ; 149.46 and 124.19 ppm can be assigned to carbon atoms of the pyridine moiety [49].

The ^{1}H-NMR spectrum of [Zn(diptu)$_2$ced(bpy)] adduct shows signals of triplets at δ 1.13 ppm for CH_3 and quartet at δ 3.99 ppm for –OCH_2 protons of the ced group or moiety. The N-H resonance was observed at 7.81 ppm and the peaks which appear at δ 8.31-8.69 ppm are due to the ring protons of 2, 2' bipyridine [50]. The ^{13}C-NMR of the adduct complex, [Zn(diptu)$_2$ced(bpy)], show peaks around δ 14.61, 58.38, 91.12, 122.42, 163.89 and 206.34 ppm that correspond to CH_3, OCH_2, C=C, C≡N, C=O and C-S carbons of the ced ligand [51] as reported in the literature. A slight downfield shift confirms the bidentate (S, S) coordinated

property of ced ligand. The signals between δ 140.09-149.09 ppm are predicted as due to 2, 2'- bipyridine carbons. The ^{1}H-NMR of [Zn(diptu)$_2$(ced)(phen)] adducts shows triplet resonant signals at δ 1.13 ppm, a quartet at δ 3.97 ppm and these are due to the protons of the CH_3 and -OCH_2 of the ced group.

The presence of 1, 10 - phenanthroline is also established in the molecular structure of the as-prepared Zn(II) adduct complexes by the two peaks observed at 8.91 and 8.93 ppm in the complexes and they can be ascribed to the ring protons of 1, 10 - phenanthroline. Protons of the uncoordinated, 1, 10 - phenanthroline are seen at δ 9.19, 7.65, 8.47 and 7.81 ppm. All the protons were observed to have shifted downfield in ^{1}H-NMR spectrum of the 1, 10 - phenanthroline adduct of the complex and this is attributable to the coordination of the metal ion to the N donor ligand [51]. The ^{1}H NMR data of the [Zn(diptu)$_2$ced(phen)] exhibit or show the presence of quartet at low field (3.95-3.97) ppm and a triplets at (2.48-2.49) ppm, which are consistent with the OCH_2CH_3 moiety. The ^{13}C-NMR of the adduct, [Zn(diptu)$_2$ced(phen)], show signals at δ 14.62, 56.06, 58.35, 90.12, 125.95, 163.91, 206.65 ppm which correspond to the presence of important features such as CH_3, OCH_2, C=C, C≡N, C=O and C-S carbons of the CED group sequentially [52]. Four signals are observed in the region δ = 125.92-149.3 ppm; 125.95, 127.39, 129.64 and 149.08 pp, which are due to the ring carbons of 1, 10 - phenanthroline. Resonance of these carbon are down shielded in the coordinated complex when compared to that of the free 1, 10 - phenanthroline. These shifts are diagnostic signals of coordinated 1, 10 - phenanthroline [53]

3.5.3 Thermal analysis of [Zn(diptu)$_2$ced/py/N-N]

Thermogravimetry analysis (TGA and DTG) of the complexes gave an insight into their decomposition behaviour. The TGA and DTG of the parent complex, [Zn(diptu)$_2$ced] (**10**), adducts; [Zn(diptu)$_2$ced(py)] (**11**) [Zn(diptu)$_2$ced(bpy)] (**12**) and [Zn(diptu)$_2$ced(phen)] (**13**) are given in Figure 3.6 (a & b) and 3.7 (c & d) sequentially. Complex (**10**) undergoes two-step decomposition as shown in Figure 3.7 (a).

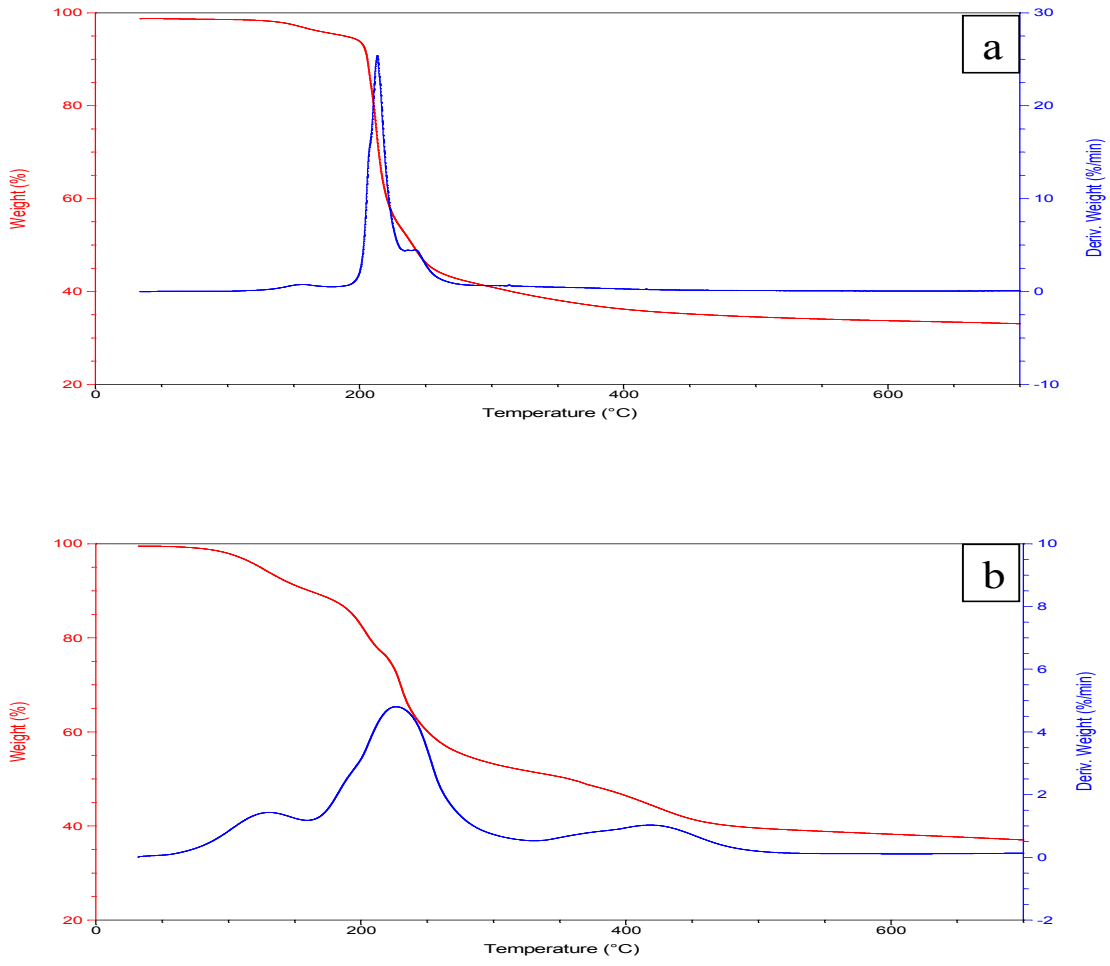

Figure 3.6: TGA/DTG of (a) [Zndiptu)$_2$ced] and (b) Zn(diptu)$_2$ced(py)

The decomposition started around 90 ºC and ended at around 250 ºC accompanied with about 64% weight loss. About 36% of residue remained which correspond to the weight of ZnS. The inflection point is detected at 210 ºC; point of greatest rate of change on the weight loss curve. It is also referred to as the first derivative peak temperature. Decomposition profile of $[Zn(diptu)_2(ced)py]$ and $[Zn(diptu)_2(ced)py]$ are similar although the peak decomposition temperatures are 219 ºC and 228 ºC respectiely. Both complexes show continuous loss of mass till around 470 ºC and only about 65.3% and 67.24% of mass respectively remained at 520 ºC degrees. The calculated mass of ZnS left as residue from complexes $[Zn(diptu)_2(ced)_2py]$ and $[Zn(diptu)_2(ced)py]$ are 34.7% and 32.8% respectively which is in agreement with the weight of ZnS.

The $[Zn(diptu)_2(ced)phen]$ complex appear to have a different decomposition behaviour from the other adducts and it is the most thermally stable of all the complexes. The decomposition is accompanied by expulsion of solvent at around 120 ºC. The thermogram showed constant mass left at about 490 ºC. At this temperature, about 68.6% of the weight of the complex has decomposed leaving only 31.4% as the resultant weight of the residue and this corresponds to the weight of ZnS. The DTG depicts peak decomposition at around 250 ºC followed by loss of other fragments of the complex around 390 ºC which can be attributed to loss of different moieties of the ligands that make up the complex. The products of the thermal decomposition of the complexes being ZnS has confirmed the suitability of the parent complex and its nitrogen donor adducts for the preparation of ZnS nanoparticles like many other 1, 1 dithiolate complexes such as xanthate, and dithiocarbamates, dithiophosphate and dithiophosphinates. Thermally the 1, 10 - phenanthroline adduct is the most stable of all the complexes and comparatively the order of stability of the complexes is as follows; $[Zn(diptu)_2(ced)phen] > [Zn(diptu)_2(ced)bpy] > [Zn(diptu)_2(ced)py] > [Zn(diptu)_2(ced)]$. The

decomposition profiles of the four precursors show that they are potential good material for the preparation of ZnS nanoparticle. The weights of the products of all the thermal decompositions are invariable in agreement with the calculated weight of ZnS in the complex.

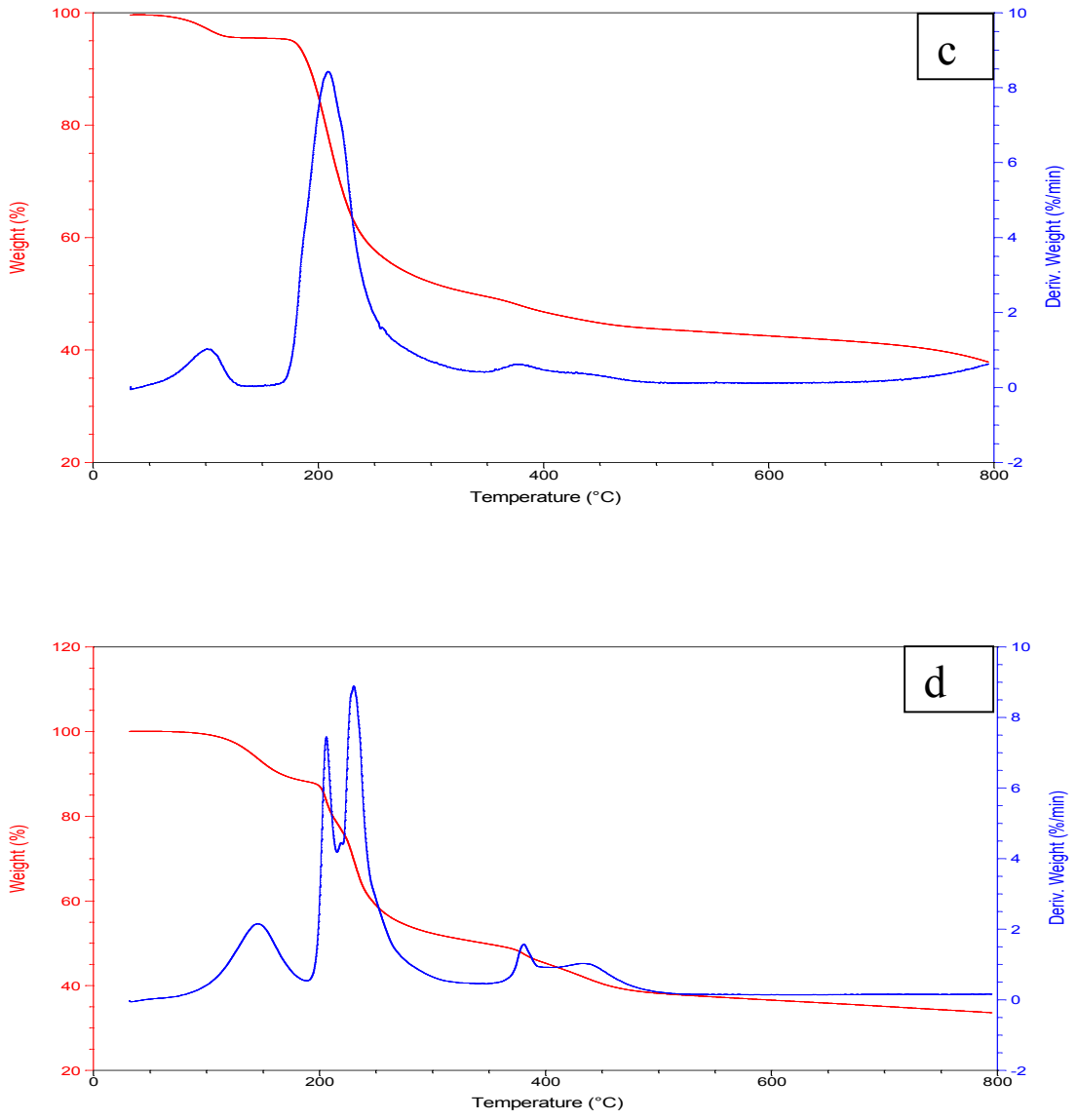

Figure 3.7: TGA/DTG of (c) [Zn(diptu)$_2$bpy] and (d) Zn(diptu)$_2$(phen)

3.6 1-cyano-1-carboethoxyethylene-2,2-dithiolato–κS,S'–bis(N,N'-diisopropylthiourea–κS)Zn(II):[Cd(diptu)$_2$ced/N-N] (where = N-N = (where N-N = 2,2 bpy or 1,10 phen) (14, 15 and 16)

Reaction of cadmium chloride, diisopropylthiourea and dipotassium 1-cyano-1-carboethoxyl-, 2-ethylenedithiolate in mole ratio 1:2:1 leads to the formation of the precursor complex, [Cd(diptu)$_2$(ced)]. Further reaction of the complex formed in mole ratio 1:1 with 2, 2' bipyridine and 1, 10 - phenanthroline respectively resulted in the formation of the adducts and the coordination numbers changed from four to six (from MS_4 to MS_4N_2 where M = Cd). All compounds are air stable and insoluble in most solvent but are soluble in polar coordinating solvent such as DMSO and DMF. The analytical data are consistent with the proposed formulation of the complexes.

3.6.1 Infrared spectra studies of the metal complexes: [Zn(diptu)2(ced)//N-N]

The FTIR spectra of diisopropyl thiourea, CED, the metal complexes and adducts measured in the region of 4000 - 350 cm^{-1}. Table 1 contains a summary of the relevant FTIR data. The four vibrational peaks associated with uncoordinated thiourea ligands are observed at around 700 cm^{-1}, 1500 cm^{-1}, 1600 cm^{-1} and 3200 cm-1 for frequency bands of C=S, C-N, N-H vibration at N-H respectively. These bands appear at [618, 1566, 1632, 3412] cm^{-1}, [622, 1517, 1626, 3415] cm^{-1} and [618, 1514, 1625, 3415] cm-^{1} for complexes [$CdCl_2$(diptu)$_2$(ced)], [$CdCl_2$(diptu)$_2$(ced)bpy] and [$CdCl_2$(diptu)$_2$(ced)phen] respectively. There are three main region of interest in the 1-cyano-1-carboethoxylethylene-2, 2'-dithiolate complexes namely; the 2188 - 2244 cm^{-1} region, which is due to *v*(C≡N); the 1645-1700 cm^{-1} region which is due to v(C=O); and the 1116-1165 cm-1 region which is ascribed to v(C-S) of the chelated ced^{2-} [54]. In the uncoordinated ced^{2-} ligand these stretching vibrations were observed around 2174, 1681 and 1160 cm^{-1} while in the parent metal complex

[Cd(diptu)$_2$ced] they were observed at 2204, 1616 and 1167 cm^{-1}. In the adducts, they were observed at 2198, 1626, 1168 cm^{-1} for [Cd(diptu)$_2$(ced)(bpy)], and 2198, 1625, 1143 cm^{-1} for [Cd(diptu)$_2$(ced)(phen)] respectively.

The *v*(C=N) ring of the 2,2'- bipyridine which appeared at 1579 cm^{-1} in the complex shifted to a higher energy of 1517 cm^{-1} in the [Cd(diptu)$_2$(ced)(bpy)]. This positive shift may be due to the ring current arising from electron delocalization after the chelate formation [55, 56]. The thioureide band which appeared at 1463 cm^{-1} in the [Cd(diptu)$_2$(ced)] is shifted to 1439 cm^{-1} in the corresponding 2, 2' bipyridine adduct complex [57]. The appearance of a new band in the region 1023 - 1015 cm^{-1} in the bipyridine adduct which was absent in the free 2, 2'-bipyridine is due to adduct formation [58]. The occurrence of a single weak to strong band in the region 930 - 935 cm^{-1} for v(C–S) in these complexes indicates symmetrical bonding of the sulfurs [59], and these bands appeared at 930, 922 and 921 cm^{-1} in complexes [CdCl$_2$(diptu)$_2$(ced)], [CdCl$_2$(diptu)$_2$(ced)(bpy)] and [CdCl$_2$(diptu)$_2$(ced)(phen)] respectively.

Table 3.5: Some selected infra-red spectroscopy frequency of [Cd(diptu)$_2$(ced)/NN]

Complexes	*v*(N–H) cm^{-1}	*v*(C≡N) cm^{-1}	*v*(C=O) cm^{-1}	*v*(C=S$_2$) cm^{-1}	*v*(C–S) cm^{-1}	*v*(C=S) cm^{-1}	*v*(M–S) cm^{-1}
[Cd(diptu)$_2$(ced)]	3412	2201	1623	1463	1167	670	351
[Cd(diptu)$_2$(ced)(bpy)]	3415	2198	1626	1439	1168	622	403
[Cd(diptu)$_2$(ced)(phen)]	3415	2198	1625	1374	1143	618	398

The lowering of the v(C-N) values when compared with the parent complexes may be ascribed to the change in coordination geometry from tetrahedral to octahedral, which leads

to reduction in vibration frequency. The spectra of [Cd(diptu)(ced)(phen)], contains peaks at around 1625, 1517 and 736 cm^{-1} which are typical of 1,10 - phenanthroline complexes [60]. The frequency at 351, 403 and 398 cm^{-1} in complexes [$Cd(diptu)_2(ced)$], [$Cd(diptu)_2(ced)(bipy)$] and [$Cd(diptu)_2(ced)(phen)$] respectively [61, 62], can be ascribed to the metal-sulfur (M-S bond).

3.6.2 ^{1}H and ^{13}C-NMR spectra of [$Zn(diptu)_2ced$/N-N] (where N-N =2,2 bpy or 1,10 phen)

The spectrum of the parent complex, [$Cd(diptu)_2ced$], displays resonance signals of all the ligands associated with the central metal. Singlet peak at 7.20 ppm is assignable to the N-H vibration and this is noticeable at δ 7.75 ppm and 8.22 ppm in the 2, 2'-bipyridine and 1, 10-phenanthroline adducts of the parent complex respectively. There are additional signals that are typical of 2, 2'-bipyridine and 1, 10- phenanthroline ligand in the complex. These signals confirm the 2, 2'-bipyridine and 1, 10- phenanthroline moiety in adducts. The resonance signals observed in the downfield region of 8.21-8.86 ppm and 8.82- 8.84 are due to the proton present in the 2, 2' bipyridine and 1, 10 phenanthroline moieties of [$Cd(diptu)_2ced(bpy)$], [$Cd(diptu)_2ced(phen)$]. Chemical shifts at signals around (3.41- 3.43) ppm and 1.09 ppm as well as δ (3.95-3.98) ppm and 1.17 ppm can be ascribed to the OCH_2 and CH_3 protons of the ethoxy group of [$Cd(diptu)_2ced(bpy)$], and [$Cd(diptu)_2ced(phen)$] adduct respectively. The signals of all the ligands in the complexes are shifted partially or slightly from their positions in the respective pure ligands. The ^{1}H NMR spectrum of [$Cd(diptu)_2ced(bpy)$] displays signals for triplets at δ 1.09 ppm for CH_3 and quartet at δ 4.37 for $–OCH_2$ protons of the ced group or moiety. The CH_3 of the diisopropyl thiourea ligand exhibits a signal at δ 2.48 ppm and another signal at δ 7.77 ppm which is due to the N-H resonance. The signals observed at δ 8.21-8.86 ppm are due to the ring protons of 2, 2'-

bipyridine. The ^{13}C-NMR of parent complex, adducts have poor solubility and as such not all the resonance signals are completely resolved.

The parent complex shows chemical shifts at δ 14.60, 58.35 163.89 and 206. 31 ppm which are assignable to CH_3, OCH_2, C=O and C-S while adducts exhibit additional peaks at δ 125, 140.24-149.49 ppm and δ 125- 127, 140-149 ppm which are attributable to the carbon atoms of 2, 2' bipyriddine and 1, 10-phenanthroline rings of the adducts. The ^{13}C-NMR of the complex, [Cd(diptu)$_2$cedbpy], show peaks around δ 14.61, 58.38, 90.99, 122.42, 163.89 and 206.34 ppm that correspond to CH_3, OCH_2, C=C, C≡N, C=O and C-S carbons of the ced ligand while a slight down field shift confirms the bidentate (S,S) coordinated property of ced ligand. The signals δ 140.09 and 149.09 ppm are between δ 137- 149 ppm and are predicted as 2, 2' bipyridine carbons. ^{1}H NMR spectrum of [Cd(diptu)$_2$(ced)(phen)] shows resonant signals for triplets δ 1.06 ppm and quartet at 3.37 ppm which are due to CH_3 and $-OCH_2$ of the ced moiety respectively. The signal at δ 2.48 ppm is ascribed to the CH_3 of the diptu and the peak due to the N-H is found at δ 8.22 ppm.

^{13}C-NMR resonance signals displays chemical shift at 14.69 ppm which is due to the CH_3 of the ced group. Peaks in the range of δ 125.42-149.89 ppm are due to the carbon ring of the 1, 10 phenanthroline. Other peaks that appear to be missing are due to poor solubility of the as prepared adduct in DMSO-d_6. Resonance signals observed in the range of δ 8.22-8.84 in the ^{1}H NMR spectrum of the as prepared, [Cd(diptu)$_2$(ced)(phen)], are due to the ring protons of 1,10- phenanthroline peaks which are observed at 8.91 and 8.93 ppm in the as-prepared complexes and they can be ascribed to the protons of 1,10- phenanthroline. Protons of the un-coordinated 1, 10 -phenanthroline are seen at δ 9.19, 7.65 8.47 and 7.81 ppm.

3.6.3 Thermal study of [Cd(diptu)$_2$ced/N-N] (where N-N =2,2 bpy or 1,10 phen)

The thermal study of the complexes, [Cd(diptu)$_2$(ced)], [Cd(diptu)$_2$(ced)(bpy)], and [Cd(diptu)$_2$(ced)(phen)] are shown in Figures 3.8 a, b and c. The TGA and DTG curves are represented by (i) and (ii). In Figure 3.8a, the peak observed around 70 ºC could be ascribed to the extrusion of the entrapped solvent. The decomposition of the complex occurred at 180 ºC and continued till around 280 ºC, losing about 67% of the complex. This decomposition stage has its maximum rate around 195 ºC, as shown by the DTG, and the resultant residue corresponded to the calculated mass of CdS. In Figure 3.8b, [Cd(diptu)$_2$(ced)(bpy)], the TGA curve also showed a sharp decomposition step which started around 200 ºC and continued till around 320 ºC with 66.24% loss of the sample. The DTG curve showed that this step is resolvable into two sub steps with peaks at around 210 and 250 ºC. At the end of this decomposition step, 33.75% residue was left which corresponds to CdS.

The decomposition profile of [Cd(diptu)$_2$(ced)(phen)] is shown in Figure 3.8c. These compounds appeared to have the highest thermal stability, with decomposition onset at approximately 210 ºC. The DTG showed a peak at 230 ºC, and a shoulder at 280 ºC, which could be ascribed to the expulsion of ligands fragments with close decomposition temperature. Afterwards a plateau appeared in the TGA which reveals no change in mass with increase in temperature. At this stage about 61.05% of the sample was decomposed with 38.95 % left as residue which corresponds to the mass of CdS, as given by the stoichiometry calculation.

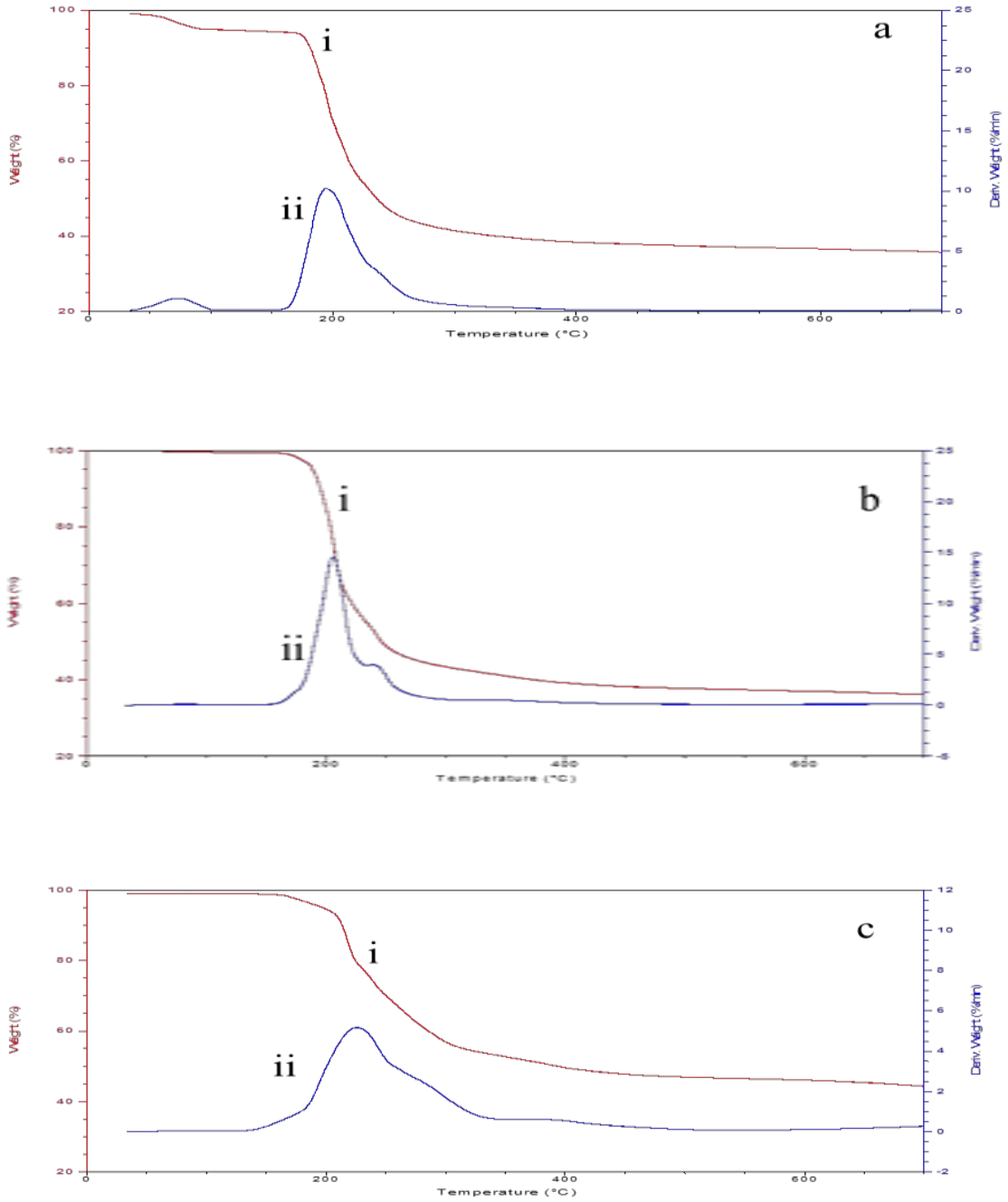

Figure 3.8: (a), (b) and (c) showing TGA (i) and (ii) DTG curves for the decomposition of [Cd(diptu)$_2$(ced)] [Cd(diptu)$_2$(ced)(bpy)] and [Cd(diptu)$_2$(ced)(phen)] complexes respectively.

3.7 1-cyano-1-carboethoxyethylene-2,2-dithiolato–κS,S'(tetramethylthiuramdisulfideκS) M(II) :[M(Me$_4$tds)ced/N-N

Reaction of one molar equivalent of Me$_4$tds and ced with one mole of $ZnCl_2$, $CdCl_2$, and $HgCl_2$ at room temperature gave the respective metal complexes. All compounds are air-stable and insoluble in most solvents but some are soluble in polar coordinating solvents such as DMSO and DMF. The formation of the compounds is shown in scheme 1. The analytical and spectroscopic data are consistent with the proposed formulation for the complexes.

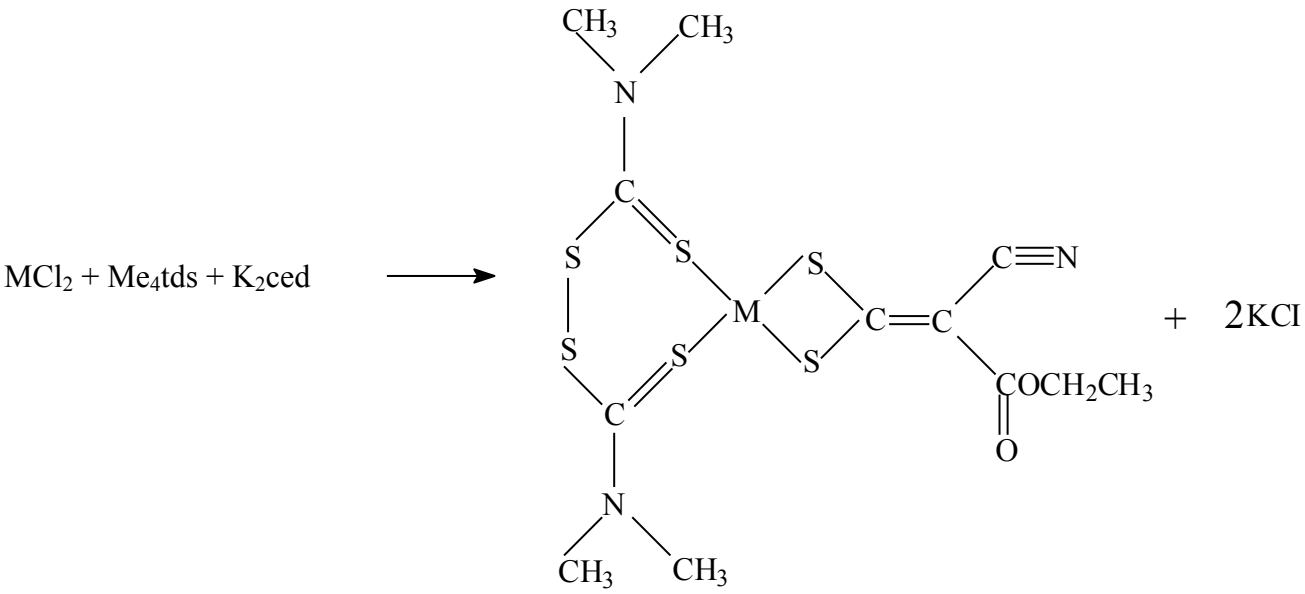

M = Zn, Cd, Hg

Scheme 3.6: Synthesis of the metal complexes

3.7.1 Infrared spectra studies of the metal complexes: [M(Me$_4$tds)ced] (M = Zn, Cd, Hg)

The IR of the metal complexes synthesized from ecda and tetramethylthiuram disulfide show characteristic changes in the functional group when compared with the spectra of the ligands. The ecda has four important absorptions frequencies which are: 2161 cm^{-1} due to ν(C≡N);

1681 cm^{-1} due to *v*(C=O); 1360 cm^{-1} due *v*(C=CS_2) and 1160 cm^{-1} due to *v*(C-S) [63]. These stretching vibrations were observed in the metal complexes at: 2245, 1732, 1438 and 1142 cm-^{1} for [Zn(Me_4tds)ced]: 2233, 1600, 1512 and 1147 cm^{-1} for [Cd(Me_4tds)ced] and 2244 , 1738 , 1492, 1191 cm^{-1} for [Hg(tmtd)ced] respectively. There are four vital bands in thiuram disulfide metal complexes and they appear in the region of 800-1510 cm^{-1}. A strong thioureide C-N band, the band at 1200 cm^{-1} which is due to C-N vibration of the alkyl group, the band responsible for the C=S stretching mode around 973 cm^{-1} and the band around 822 cm^{-1} that can be ascribe to the stretching C-S mode. All these band are observable in [Zn(Me_4tds)(ced)], [Cd(Me_4tds)(ced)] and [Hg(Me_4tds)(ced)] at vibration frequencies of ;1520, 1512, 1530 cm^{-1}; 1200, 1209, 1201 cm^{-1}; 973, 95 , 965 cm $^{-1}$; 822, 820, 830 cm^{-1} respectively. The absorption bands assigned to M-S in these complexes are observed at 384, 449 and 416 cm^{-1} for [Zn(Me_4tds)(ced)], [Cd(Me_4tds)(ced)] and [Hg(Me_4tds)(ced)] respectively.

Table 3.6: Some selected infra-red spectroscopy frequency of [M(Me_4tds)ced]

Complexes	*v*(C≡N) (cm^{-1})	*v*(C=O) (cm^{-1})	*v*(C=S_2) (cm^{-1})	*v*(C–S) (cm^{-1})	v(C=S) (cm^{-1})	*v*(M–S) (cm^{-1})
[Zn(Me_4tds)ced]	2245	1732	1138	1142	970	382
[Cd(Me_4tds)ced]	2233	1600	1512	1147	957	384
[Hg(Me_4tds)ced]	2244	1738	1492	1170	-	449

3.7.2 ^{1}H and ^{13}C-NMR spectra of [M(Me_4tds)ced] (M = Zn, Cd, Hg)

The ^{1}H-NMR of the Zn complex show a triplet at δ 1.05 and a quartet at δ 4.02 ppm which can be assigned to CH_3 and OCH_2 of the ced^{2-} . The ^{13}C-NMR spectrum of [Zn(Me4tds)ced], show peaks around δ 203.69, 168.68, 122.94, 59.29, and 18.51 ppm corresponding to C-S,

C=O, C≡N, -OCH_2, and CH_3 respectively for carbon of the ced^{2-} . The ^{1}H-NMR spectra of the Cd complex contained a triplet at δ 1.27 ppm for the -CH_3 protons of the tetramethyl thiuram disulfide (Me_4tds) and the ester group of the ecda ligand. The protons of the -OCH_2 group are observed as a quartet at 1.27-4.09 ppm. The ^{1}H-NMR spectra of this complex, [Hg(Me_4tds)ced], show triplet peaks 1.05 and 4.35 for –CH_3 protons of the thiuram disulfide and ced^{2-}. The other peaks at 2.5 and 3.4 pmm are due to solvent peaks of $DMSO_6$ and water. The complex is partially soluble in $DMSO_6$ and hence the spectrum was very weak. The complex was run for solid state on 600MHz NMR but the complex could not be used for calibration and all effort to do it proved abortive. As a result of this, the ^{13}C-NMR was not reported.

3.8 Conclusion

The chapter contains the characterization of nineteen complexes that were synthesied in this work. Six ligands were used in all for the synthesis of the various metal complexes and these ligands are; four substituted thiourea ligands (methyl, dimethyl, diethyl and diisopropyl thiourea), tetramethyl thiuram thiourea and 1-cyano-1-carboethoxyl-2,2 ethylene dithiolate, ced, Nine complexes were synthesized from the reaction of the susbstited thiourea with ced and the reaction of tetramethyl thiuram disulfide with ced also gave 3 complexes. Apart from the six ligands mentioned above, 3 nitrogen donor ligands, (pyridine, 2,2'-bipyridine and 1,10-phenanthroline), were also employed for the synthesis of 7 adducts complexes. The detailed IR and the coordination compound chemistry of the complexes were highlighted. The bonding between the different substituted thiourea ligands and the central metal atoms was through sulfur for all the complexes as this was confirmed from the IR study. The 1, 1 diothiolate ligand, ced, also chelate with the central metal atoms in a bidentate mode as revealed from the IR spectra. The ^{1}H and ^{13}C-NMR also shows resonance signals that were

typical of the coordinated ligands. TGA studies showed that the complexes are all stable and that they are all potential single source precursors for the synthesis of metal sulphide nanoparticles via a single source precursor route based on the TGA and DTG of some of the metal complexes. The decomposition temperatures of the 1, 10- phenenthroline and 2, 2'-bipyridine adducts indicated enhanced stability of these adducts compared with other parent complexes. The coordination geometry around the central metal ion were formulated to be MS_4, MS_4N and MS_4N_2 respectively for the complexes, the pyridine, the 2, 2'-bipyridine and 1, 10–phenanthroline adducts. All the complexes were further thermolysed in HDA to sysnthesize HDA capped metal sulfide nanoparticles and the details of which are described in chapter four and five.

3.9 References

1. Bourne, S.; Koch, K. R. Intramolecular hydrogen-bond controlled unidentate co-ordination of potentially chelating N-acyl-N′-alkylthioureas: Crystal structure of cis-bis(N-benzoyl-N′-propylthiourea) dichloroplatinum(II). *J. Chem. Soc., Dalton Trans*. **1993**, 2071-2072.
2. Bielenica, A.; Stefańska, J.; Stępień, K.; Napiórkowska, A.; Augustynowicz-Kopeć, E.; Sanna, G.; Madeddu, S.; Boi, S.; Giliberti, G.; Wrzosek, M.; Marta Struga, M. Synthesis, cytotoxicity and antimicrobial activity of thiourea derivatives incorporating 3 (trifluoromethyl)phenyl moiety. *Eur. J. Med. Chem*. **2015**, *101*, 111-125.
3. Khawar, M.; Imtiaz-ud-Din, R.; Badshah, A.; Gielen, M.; Ebihara, M.; Vos, D.; Ahmed S.; Synthesis, structural characterization and in vitro cytotoxicity and antibcteria activity of some copper(I) complexes with N, N′-disubstitutedthiourea. *J. Inorg. Biochem*. **2009**, *103*, 1135-1144.
4. Abbas, S. Y.; El-Sharief, M. A.; Basyouni, W. M.; Fakhr, I. M. I.; El-Gammal E. W Thiourea derivatives incorporating a hippuric acid moiety: Synthesis and evaluation of antibacterial and antifungal activity. *Eur. J. Med. Chem*. **2013**, *64*, 111-120.
5. Dolan, N.; Gavin, D. P.; Eshwika, A.; Kavanagh, K.; McGinley, J.; Stephens J. C. Synthesis, antibacterial and anti-MRSA activity, in vivo toxicity and a structure–acrelationship study of a quinoline thiourea. *Bioorg. Med. Chem Lett.* **2016**, *26*, 630-635.
6. Spenceley, J. E.; Henderson, W.; Lane, J. R.; Saunders, G. C. Isomerism in platinum(II) complexes of asymmetrically 1,3-disubstituted thiourea dianion ligands. *Inorg. Chim. Acta*. **2015**, *425*, 83-91.
7. Patel, J. D.; Mighri, F.; Ajji, A. Aminocaproic acid mixed methanolic lead–thiourea complex precursors and its thermal decomposition to star-shaped lead sulfide crystals *Mater. Lett*. **2012**, *74*, 183-186.

8. Patel, J. D.; Mighri, F.; Ajji, A.; Chaudhuri T. K.; Morphology and size control of lead sulfide nanoparticles produced using methanolic lead acetate trihydrate-thiourea complex via different precipitation techniques. *Mater. Chem. Phys.* **2012**, *132*, 747-755.
9. Rivest. R. Coordination complexes of titanium(IV) halides: III. Preparation and infrared spectra of the complexes of titanium tetrachloride with urea, thiourea and some of their derivatives. *Can. J. Chem*. **1962**, *40*, 2234-2242.
10. Singh, A.; Bharty, M. K.; Bharati, P.; Bharti, A.; Singh, S.; Singh, N. K. Synthesis, spectral, thermal and structural characterization of a hexanuclear copper(I) cluster and a cobalt(III) complex of 1-ethyl-3-phenyl-thiourea. *Polyhedron*. **2015**, *85*, 918-925.
11. Al-Maythalony, B. A.; Monim-ul-Mehboob, M.; Altaf, M.; Wazeer, M. I. M.; Isab, A. A.; Altuwaijri, S.; Ahmed, A.; Dhuna V.; Bhatia G.; Dhuna K.; Kamboj, S. S. Some new $[(thione)_2Au(diamine)]Cl_3$ complexes: Synthesis, spectroscopic characterization, computational and *in vitro* cytotoxic studies. *Spectrochim. Acta Part A*. **2013**, *115*, 641-64.
12. Wang, X.; Guo, Z.; Towards the rational design of platinum(II) and gold(III) complexes as antitumour agents. *J. Chem*. *Soc*. *Dalton Trans*. **2008**, *12*, 1521-1532.
13. Yan, Z.; Voloshin, Y.Z.; Varzatskii, O.A.; Kochubey, D.I.; Vorontsov, I. I.; Yurii, N.; Bubnov, Y.N. Synthesis and structure of monoribbed-functionalized disulfide iron(II) clathrochelates and their coordination as the ligands toward platinum(II) and platinum(IV) ions. *Inorg*. *Chim*. *Acta*. **2009**, *362*, 149-158.
14. Altaf, M.; Stoeckli-Evans, H.; Batool, S. S.; Isab, A. A.; Ahmad, S.; Saleem, M.; Awan, S. A.; Shaheen, M. A. Mercury(II) complexes of pyrrolidinedithiocarbamate, crystal structure of bis{[μ2-(pyrrolidinedithiocarbamato-S,S′) (pyrrolidinedithiocarbamato-S, S′)mercury(II)]}. *J. Coord. Chem*. **2010**, *63*, 1176-1185.

15. Alkam, H. H.; Kanan, K. M.; Hadjikostas, C. C. Syntheses and characterization of some homoleptic (1,1-dithiolato)copper(II) and nickel(II) complexes, and mixed-ligand (1,1-dithiolato)nickel(II) chelates containing nitrogenous bases. Crystal structures of tetrabutylammonium(1-cyano-1-chlorophenyl-2,2-ethylenedithiolato) copper(II), [(2,20-bipyridine)(1-cyano-1-phenyl-2,2-ethylenedithiolato)nickel(II)], and 5-amino-4-(4-chlorophenyl)-[1,2] dithiole-3-thione. *Polyhedron*. **2005**, *24*, 2944-2954.
16. Pakawatchai, C.; K. Sivakumar, K.; H.-K. Fun, Bis(N,N'-dimethylthiourea-S)silver(I) perchlorate and tris(N,N'-dimethylthiourea-S)silver(I) perchlorate. *Acta Cryst.* **1996**, *C52*, 1954-1957.
17. Fourati, M.; Chaabouni, M.; Pascal, J. L.; Potter, J. Synthesis and vibrational analysis of new anhydrous oxochloroperchlorato complexes of titanium. IV. *J. Mol. Struct*. **1986**, *143*, 147-150.
18. Burrows, A. D.; Harrington, W. R.; Mahon, M. F. Dichlorobis(1,3-dimethylthiourea-κS)zinc(II). *Acta. Cryst. E*. **2004**, *60*, m1317 - m1318.
19. Ahmad, S.; Sadaf, H.; Akkurt, M.; Sharif, S.; Khan, I. U. Bis(1,3-dibutylthiourea)dicyanidomercury(II). *Acta Crystallogr. Sect. E*: **2009**, *65*, m191-m1192.
20. Singh, S.; Rai, S. K. Spectroscopic and Conducting Properties of Some Heterobimetallic Complexes Formed with 1-ethoxycarbonyl-1-cyanoethylene-2, 2-dithiolate. IV, *Synth. React. Inorg. Met.-Org. Chem*. **2000**, *30*, 281-305.
21. Chetana, P. R.; Srinatha, B. S.; Somashekar, M. N.; R. S. Policegoudra, R. S. Synthesis, spectroscopic characterisation, thermal analysis, DNA interaction and antibacterial activity of copper(I) complexes with N, N'- disubstituted thiourea. *J. Mol. Struct*. **2016**, *1106*, 352-365.
22. Mgabi, L. P.; Dladla, B. S.; Malik, M. A.; S. Garje, S. S.; Akhtar, J.; Revaprasadu, N. Deposition of cobalt and nickel sulfide thin films from thio- and alkylthio-urea complexes

as precursors via the aerosol assisted chemical vapour deposition technique. *Thin Solid Films*. **2014**, *564*, 51-57.

23. Isab, A. A.; Nawaz, S.; Saleem, M.; Altaf, M.; Monim-ul-Mehboob, M.; Ahmad, S.; Evans, H. S. Synthesis, characterization and antimicrobial studies of mixed ligand silver(I) complexes of thioureas and triphenylphosphine; crystal structure of {[Ag(PPh_3)(thiourea)(NO_3)]$_2$. [Ag(PPh_3)(thiourea)]$_2$(NO_3)$_2$}. *Polyhedron*, **2010**, *29*, 1251-1256.
24. Malik, M. R.; Vasylyeva, V.; Merz, K.; Metzler-Nolte, N.; Saleem, M.; Ali, S. A.; Isab, A. A.; Munawar, K. S.; Ahmad, S. Synthesis, crystal structures, antimicrobial properties and enzyme inhibition studies of zinc(II) complexes of thiones. *Inorg. Chim. Acta*. **2011**, *376*, 207-211.
25. Isab, A. A.; Fettouhi, M.; Ahmad, S.; Ouahab, L. Mixed ligand gold(I) complexes of a phosphines and thiourea and X-ray structure of (thiourea-κS)(tricyclohexylphosphine)κS)(tricyclohexylphosphine)gold(I)chloride. *Polyhedron*, **2003**, *22*, 1349-1354.
26. Cummings, S. D.; Eisenberg, R. Luminescent platinum(II) bis(1,1-dithiolate) complexes. *Inorg. Chim. Acta*. **1996**, *242*, 225-231.
27. Yan, Z.; Voloshin, Y. Z.; Varzatskii, O. A.; Kochubey, D. I.; Vorontsov, I. I.; Yurii, N.; Bubnov, Y. N. Synthesis and structure of monoribbed-functionalized disulfide iron(II) clathrochelates and their coordination as the ligands toward platinum(II) and platinum(IV) ions. *Inorg. Chim. Acta*. **2009**, *362*, 149-158.
28. Singh, N.; Gupta, S.; Nath, G. Preparation, spectroscopic investigation and antibacterial activity of some organomercury(II) and organotin(IV) dithiocomplexes. *Appl. Organomet. Chem*. **2000**, *14*, 484-492.

29. Singh, M. K.; Das, A.; Paul, B. Synthesis and structural characterization of mixed ligand complexes of nickel(II) with 1-cyano-1-carboethoxyethylene-2,2-dithiolate and some nitrogen. *Trans. Met. Chem*. **2007**, *32*, 732-736.

30. Nadeem S., Rauf M. K., Ahmad S., Ebihara M., Tirmizi S. A., Bashir S. A., Badshah A.: Synthesis and characterization of palladium(II) complexes of thioureas. X-ray structures of $[Pd(N,N'\text{-dimethylthiourea})_4]Cl_2.2H_2O$ and $[Pd(tetramethylthiourea)_4]Cl_2$. *Trans*. *Met*. *Chem*. **2009**, *34*, 197-202.

31. Malik, M. R.; Rüffer, T.; Lang, H.; Isab, A. A.; Ali, S.; Ahmad, S.; Stoeckli-Evans, H. Structural characterization of dicyanidobis-(N,N-dimethylthiourea-κS)Cadmium(II). *J. Struct. Chem*. **2013**, *54*, 810-814.

32. Moloto, N.; Revaprasadu, N.; Moloto, M.J. O' Brien, P.; Raftery, J. N, N'-diisopropylthiourea and N, N'-dicyclohexylthiourea zinc(II) complexes as precursors for the synthesis of ZnS nanoparticles. *S. Afri. J. Sci*. **2009**, *105*, 7-8.

33. Moloto, M. J.; Malik, M. A.; O'Brien P.; Motevalli, M.; Kolawole, G. A. Synthesis and characterization of some N-alkyl/aryl and N, N′-dialkyl/aryl thiourea cadmium(II) complexes: The single crystal X-ray structures of $[CdCl_2(CS(NH_2)NHCH_3)_2]n$ and $[CdCl_2(CS(NH_2)NHCH_2CH_3)]$. *Polyhedron*, **2003**, *22*, 595-603.

34. Ali, S.; Malik M.R.; Isab, A. A.; Ahmad S. Synthesis and spectroscopic characterization of cadmium (II) complexes of thiones and thiocyanate. *J*. *Coord*. *Chem*. **2009**, *62*, 475-480.

35. Singh, N.; Gupta, S. Solid state electrical conductance properties of some new bimetallicoordination polymers derieved from bis (1-ethoxylcarbonyl-1-cyanoethylene- 2, 2-dithiolato) cuprate(II) ion. *Synth. Met*. **1999**, *107*, 167-174.

36. Singh, N.; Gupta, S. Magnetic and electrical properties of new inorganic complex based materials derived from bis(1-ethoxycarbonyl-1-cyanoethylene-2,2-dithiolato)metalate(II) ions. *Int*. *J*. *Inorg*. *Mater*. **2000**, *2*, 427-435.

37. Hadjikostas, C. C.; Alkam, H. H.; Bolos, C. A.; Christidis, P. C. Synthesis and spectroscopic investigation of some mixed-ligand nickel(II) chelates containing phosphines and 1,1-dithiolate ligands. Crystal structure of [(1,2-bis(diphenylphosphino)ethane)- 1,1-dicyano-2,2-ethylenedithiolato]nickel(II). *Polyhedron*. **2001**, *20*, 395-401.
38. Swaminathan, K.; Irving, H. M. N. H. Infrared absorption spectra of complexes of thiourea. *J. Inorg. Nucl. Chem*. **1964**, *26*, 1291-1294.
39. Zuleta, J. A.; Bevilacqua, J. M.; Proserpio, D. M.; Harvey, P. D.; Eisenberg, R. Spectroscopic and theoretical studies on the excited state in diimine dithiolate complexes of platinum(II). *Inorg. Chem.* **1992**, *31*, 2396-2404.
40. Jing-Han, H.; Xiao, Hui, F.; Xiao-Li, D.; Tai-Bao, W. Synthesis, crystal structure, and biological activity of a new Cu(I) complex of the N-phenyl-N -(2-Nitrobenzoyl)-thiourea. *Phosphorus*, *Sulfur*, *Silicon Relat*. *Elem*. **2010**, *185*, 2558-2562.
41. Malik, M. R.; Vasylyeva, V.; Merz, K.; Metzler-Nolte, N.; Saleem, M, Ali, S.; Isab, A. A, Munawar, K. S.; Ahmad, S. Synthesis, crystal structures, antimicrobial properties and enzyme inhibition studies of zinc(II) complexes of thiones. *Inorg*. *Chim*. *Acta*. **2011**, *376*, 207-211.
42. Han, A.; Ozturk I. I; Banti, C. N.; Kourkoumelis, N.; Manoli, N. M.; Tasiopoulos, A. J; Owczarzak, A. M., Kubicki, M.; Hadjikakou, S. K. Antimony(III) halide compounds of thioureas: Structures and biological activity. *Polyhedron*. **2014**, *79* 151-160.
43. Singh, N.; Gupta, S. Complex salt and heterobimetallic complexes derived from bis(1-ethoxycarbonyl-1-cyanoethylene-2,2-dithiolato) diargentate(I) ion: preparation, spectroscopic investigation and electrical conductance properties. *Polyhedron*. **1999**, *18*, 1265-1271.
44. Valarmathi P.; Thirumaran, S.; Ragi P.; Ciattini, S. Synthesis and spectral studies on nitrogen donor adducts of bis(4-ethylpiperazinecarbodithioato-S,S′)M(II) (M = Zn, Cd) and use of

adducts of cadmium dithiocarbamate for the preparation of cadmium sulfide. *J. Coord. Chem*. **2011**, *64*, 4157-4167.

45. Thirumaran, S.; Ramalingam, K.; Bocelli, G.; Righi, L. XPS, single crystal X-ray diffraction and cyclic voltammetric studies on 1, 10-phenanthroline and 2, 2'-bipyridine adducts of bis(piperidinecarbodithioato-S,S')cadmium(II) with CdS_4N_2 environment- A stereochemical and electronic distribution investigation. *Polyhedron*, **2009**, *28*, 263-268.
46. Seminara, A.; Giuffrida, S.; Musumei, A.; Fragala, I. Polynuclear complexes of lanthanides with nickel and copper schiff bases as ligands. *Inorg. Chim. Acta*. **1984**, *95*, 201-205.
47. Yin, H.; Wang, C.; Xing, Q. Synthesis and characterization of 2,2 bipyridine adducts of bis(N,N-dialkylcarbodithioato-S,S')Zn(II) and crystal structure of (2,2'bipyridine)bis (N,N-diethylcarbadithioato-S,S')Zn(II)and(2,2'bipyidine) bis (pyrrolinedinecarbodithioato–S,S')Zn(II). *Ind. J. Chem*. **2004**, *43*, 1911-1914.
48. Sarkar, B.; Liaw, B. J.; Fang, C. S.; Liu, C. W. Phosphonate- and ester-substituted 2-cyanoethylene-1,1-dithiolate clusters of zinc: Aerial CO_2 fixation and unusual binding patterns. *Inorg. Chem.* **2008**, *47*, 2777-2785.
49. Srinivasan, N; Thirumaran, S.; Ciattini S. Effect of phenyl and benzyl group in heterocyclic dithiocarbamates on the ZnS4N chromophore: Synthesis, spectral, valence-bond parameters and single crystal X-ray structural studies on (pyridine)bis(1,2,3,4 tetrahydroquinolinedithiocarbamato)- zinc(II) and (pyridine) bis(1,2,3,4 tetrahydroisoquinolinedithiocarbamato)zinc(II). *J. Mol. Struct*. **2009**, *921*, 63-67.
50. Subha, P. V.; Valarmathi, P.; Srinivasan, N.; Thirumaran, S.; Saminathan, K. Effect of size of metal ion on MS_4N_2 chromophore: Synthesis, spectral and single crystal X-ray structural studies on (2,2'-bipyridine)bis(N-cyclohexyl-N methyldithiocarbamato)M(II) (M = zinc, cadmium). *Polyhedron*. **2010**, *29*, 1078-1082.

51. Singh, N.; Gupta, S.; Nath, G. Preparation, spectroscopic investigation and antibacterial activity of some organomercury(II) and organotin(IV) dithio complexes. *Appl*. *Organometal*. *Chem*. **2000**, *14*, 484-492.

52. Khaled, S.; Mohammed, Z. A.; Firdous, G. K.; Shaikh, K. A. Synthesis, characterization, and photophysical studies of some novel ruthenium(II) polypyridine complexes derived from benzothiazolyl hydrazones. *Int. J*. *Inorg*. *Chem*. **2013**, 212435-212443.

53. Frechette, M.; M.; Butler, I. R.; Hynes, R.; Detellier, C. Structures in solution and in the solid state of the complexes of lanthanum(III) with 1,10-phenanthroline. X-ray crystallographic and proton, carbon-13, oxygen-17 and lanthanum-139 solution NMR studies. *Inorg. Chem*. **1992**, *31*, 1650-1656.

54. Jensen, K. A.; Henriksen, L. Studies of thioacids and their derivatives, Acta Chem. Scand., *22*, **1968**. 1107-1128.

55. Ajibade, P. A.; Osuntokun, J.; Synthesis and characterization of hexadecylamine capped ZnS, CdS, and HgS nanoparticles using heteroleptic single molecular precursors. *J. Nanomater*. **2014**, *782526*, 1-7.

56. Cummings, S. D.; Eisenberg, R. Luminescent platinum(II) bis(1,1-dithiolate) complexes. *Inorg*. *Chim*. *Acta*. **1996**, *242*, 225-231.

57. Inskeep, R. G. Infrared spectra of metal complex ions below 600 cm^{-1}. The spectra of the tris complexes of 1, 10 phenanthroline and 2, 2' bipyridine with the transition metals iron (II) through zinc(II). *J. Inorg. Nucl. Chem*. **1962**, *24*, 763-776.

58. Reddy, H. K.; Reddy, P. S. Mixed ligand Zn(II) and Cadmium(II) complexes with alkyl xanthate and 2, 2' bipyridyl. *Indian J. Chem*. *Sect*. *A*. **2001**, *40*, 1118-1120.

59. Oliveira, A. M.; Chagas, A. P.; Airoldi, C. Synthesis, characterization and thermochemistry of adducts of zinc, cadmium and mercury halides with N, N'-dimethylformamide. *Inorg. Chem*. **1983**, *22*, 136-140.

60. Rodríguez, A.; Sousa-Pedrares, A.; García-Vázquez, J. A.; Romero, J.; Antonio Sousa A. Electrochemical synthesis and characterization of zinc(II) complexes with pyrimidine-2-thionato ligands and their adducts with N, N donors. *Polyhedro*n. **2009**, *28*, 2240-2248.
61. Yamad, Y.; Shimoi, M.; Ouchi, A. Adducts of Bis(O,O'-Dlythyl Dithiophosphato) cobalt(II) with some amines and triphenylphosphine. *Chem. Lett.* **1978**, *7*, 867-870.
62. Nakamoto, K. **1978**, Infrared and raman spectra of inorganic and coordination compounds, 3rd Edn, Wiley-Interscience, New York.
63. Victoriano, L. I.; Gnecco J. A.; Carbacho, H. V. Oxidation of tetramethylthiuram sulfide(II) dithiocarbamate with ferric chloride. *Polyhedron*. **1996**, *15*, 1315-1321.

CHAPTER 4

4. Sythesis and Characterization of Metal Sulfide Nanoparticles

4.1 Introduction

Physical and chemical properties of materials deviate from the bulk with reduction of size to nanometer range. Among different classes of materials, nanostructured semiconductors have been studied due to their novel properties and practical applications [1-5]. The unusual change in properties of nanoparticles from the bulk is induced by two factors; the increase in surface to volume ratio which makes surface and interface effects dominant over volume effects and the change in electronic structure which gave rise to increase in bandgap [6]. Invariably, a lot of effort has been applied to control the size, morphology and crystallinity of these material with the objective to tune their physical properties. Bawendi and coworker [7] pioneered the use of organometallic compounds for controlled synthesis of semiconductor nanoparticles, but the hazardous nature of the starting materials call for the need for safer synthetic routes. This led to the development of single source precursor route for the synthesis of semiconductor nanoparticles. This method avoids the use of volatile and hazardous compounds at high temperatures and leads to nanoparticles with homogeneous distribution of metal ions at molecular level [8-12].

The objective of nanochemistry is to establish a cost-effective well manageable, safe, high yielding route to nanoparticles synthesis that enables the nature of the precursor to plays a relevant function. Only some few groups of single source precursor were good enough or successful in the deposition and synthesis of nanoparticles like the metalorganics, hydrides, chlorides and other volatile compound in solid, liquid and gaseous states. A quest for novel precursors with satisfactory volatility, solubility and the potential or capability of deposit of

nanoparticles or thin films devoid of contaminants is a herculean task for nanochemistry [13, 14].

Nanoparticles need to be passivated because the absence of organic stabilizers or passivation of the surfaces of nanoparticles leads to aggregation of nanoparticles. Hence organic passivation agents are commonly used to prevent them from aggregation by capping the surfaces. Appropriate surface passivation by suitable stabilizers also has an influence on the chemical and physical properties of the nanomaterials [15]. The choice of hexadecylamine as a preferred capping agent in this work arose from the fact that it is an effective capping agent with good selectivity [16]. It decreases the growth rate, size of nanoparticles and improves the photoluminescence quantum efficiency by effectively passivating the surface defects while behaving as nonradiative relaxing centre. These properties are attributable to its high electron donating ability and capping density as a result of its small stereochemical interference [17, 18].

4.1 Experimental

4.1.1 Synthesis of HDA capped metal sulfide nanoparticles

In a typical experiment, about 0.4 g of the precursor complex, [M(mtu)2(ced)] (M=Zn, Cd and Hg), was dissolved in 10 mL of trioctylphosphine oxide (TOP). The obtained solution was then injected into 4 g of hot HDA at a temperature of 180 °C. A subsequent decrease in temperature of 20-30 °C was observed and the solution was allowed to stabilize at 180 °C. A further heating was done for 60 min and the reaction was terminated. The solution was then allowed to cool to about 70 °C, and about 100 mL methanol was added to remove the excess HDA. The flocculent precipitate formed was centrifuged and the supernatant was decanted, after which the isolated solid was dispersed in toluene. The above centrifugation and isolation

procedure was repeated three times for the purification of the prepared metal sulfide nanoparticles.

4.2 Physical Measurements

4.2.1 UV-Vis

The systematic changes in the electronic structure as a function of size is one of the most extensively studied properties of semiconductor nanoparticles. UV-visible spectroscopy is used to probe the quantum confinement effect and also for calculating the optical band gap of the semiconductor nanomaterials. The UV-vis of the metal sulfide nanoparticles were recorded on Perking Elmer Lambda 25 spectrophotometer in toluene from 200-800 cm^{-1}

4.2.2 Photoluminescence spectroscopy (PL)

This is simple, contactless, nondestructive method of probing electronic structure. The photoluminescence measurement of the nanoparticles was carried out with Perkin Elmer LS 45 Fuorimeter.

4.2.3 X-ray diffraction (p-XRD)

P-X-ray diffraction study is employed for the identification of, purity and crystalline phase of material. It is a simple non- destructive technique and it is established on constructive interference of X-rays and sample. Powder X-ray diffractogram of nanoparticles were recorded on a Bruker D8 Advanced, equipped with a proportional counte using Cu Kα radiation (λ=1.5405 A, nickel filter). Samples of nanoparticles were loaded on flat steel or rubber sample holder and scanned from 10 to 80º. The diffraction peaks at various 20 values were compared with the documented standards in JCPDS.

4.2.4 Scanning electron Microscope and energy dispersive X-ray (SEM/EDX)

Scanning electrom microscope (SEM) is an important instrument employed for inspecting the topographies of sample materials and it also reveals the chemical composition information. Scanning electron microscope (SEM) was done using JOEL JSM-6390 LVSEM at a rating voltage of 15-20 kV at different magnifications as indicated on the SEM images. Energy dispersive spectra were processed using energy dispersive X-ray analysis (EDX) attached to a Jeol, JSM-6390 LV SEM with Noran system six software formations near the surface.

4.2.5 Tansmission electron Microscopy (TEM)

Transmission electron microscopy (TEM) is used to determine the shape, size and size distribution of nanoparticles samples. It is the fisrt method used for this determination. TEM has the advantages of high magnification of spatial information in the signal by as little as 50 times to as much as a factor of 106. It also has the capability of providing both image and diffraction information from a single sample. The transmission electron microscopy (TEM) images were obtained using a ZEISS Libra 120 electron microscope operated at 120 kV.

In this chapter, the use of metal complexes presented in chapter three as single source precursors to synthesize HDA capped metal sulfide nanopartricles are described. The nanoparticles were characterized by absorption and photoluminescence spectroscopy to determine their optical properties. Their structural and morphological properties were also studied with XRD, SEM, EDX and TEM.

4.3 Results and Discussion

4.4 Characterization of ZnS, CdS and HgS nanoparticles from [M(mtu)$_2$ced] precursor (M = Zn, Cd, Hg)

4.4.1 X-ray Diffraction studies

Figure 4.1(a) shows the XRD pattern of the ZnS nanoparticles formed from the thermolysis of complex (1) at 120 ºC for 60 mins. It displays the characteristic XRD peaks of cubic phase ZnS with obvious (1 1 1), (2 2 0) and (3 1 1) crystal plane reflections corresponding to 2θ = 28.5º, 47.6º, 56.4º and comparable to JCPDS card no. 5-566) [19]. Figure 4.1(b) shows the diffractogram of CdS with peaks that are relatively broad and this clearly indicates that small nanocrystals are present in the sample. In the case of CdS nanoparticles, the XRD pattern shows that the as-prepared nanoparticles are in cubic crystalline phase. According to the JCPDS card no. 80-0019, the diffraction peaks correspond to (1 1 1), (2 2 0), (3 1 1), (3 3 1) and (4 2 2) crystal plane [20]. The diffraction peaks of HgS represented by Figure 4.1(c) reveals peaks at 2θ = 26.9 º, 30.68 º, 43.82 º, 51.86 º, 62.55 º, 70.06 º that corresponds to; (1 1 1), (2 0 0), (2 2 0), (3 1 1), (2 2 2), (4 0 0), (3 3 1) planes of HgS (metacinnabar) and are in agreement with JCPDS card no. 00-006-0261 [21]. There is the formation of smaller ZnS and CdS nanoparticles than those of the HgS as this can be ascribed to the relatively broader diffraction peaks of the first two metal sulfides. Surface passivation is revealed by the elongation of the XRD patterns [22, 23].

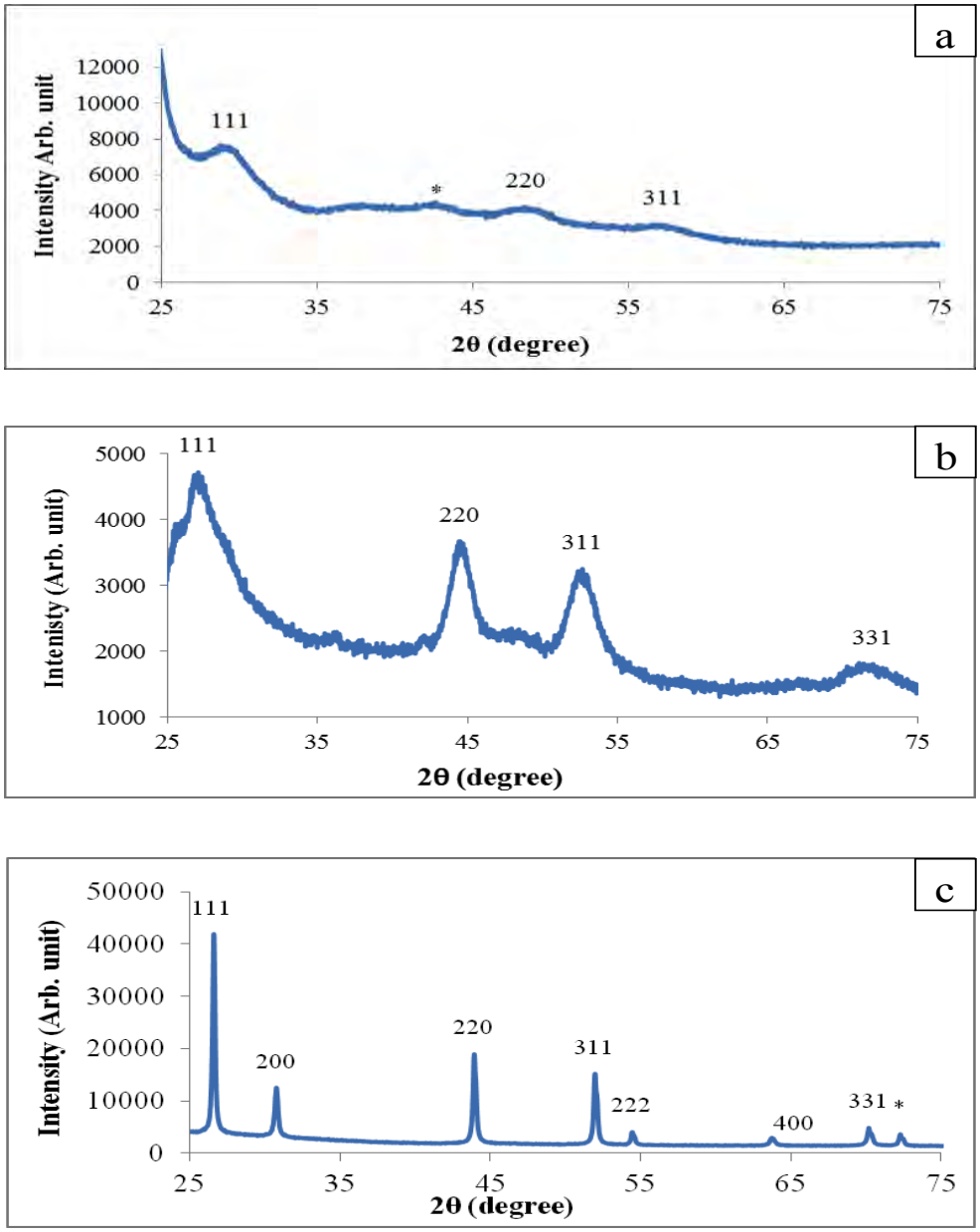

Figure 4.1: XRD pattern of HDA capped (a) ZnS (b) CdS and (c) HgS nanoparticles from the thermolysis of [Zn(mtu)2(ced)] [Cd(mtu)2(ced)] and [Hg(mtu)$_2$(ced)] at 180 °C

4.4.2 Transmission Electron Microscopy (TEM) studies of nanoparticles from [M(mtu)$_2$ced]

TEM micrographs of metal sulfide nanocrystals synthesized from [Zn(mtu)$_2$(ced)] (**1**), [Cd(mtu)$_2$(ced)] (**2**) and [Hg(mtu)$_2$(ced)] (**3**) are presented in Figure 4.2. The micrograph of

ZnS showed dot and rod shaped morphology while that of CdS is spheroid shaped and the TEM micrograph of HgS displayed a rounded shape of agglomerated nanoparticles. The spacing between the nanocrystals indicates that an organic material, in this case HDA, is likely to be the capping agent of the metal sufilde nanoparticles [24, 25]. The particles size of the HDA capped ZnS are in the range of 4.14 - 4.63 nm; those of CdS in the range of 6.14 - 11 nm while HgS nanocrystals have much more bigger sizes with range between 39.29 - 59.94 nm as can be seen in Figure 4.2 (a-c).

4.3.3 Scanning Electron Microscopy (SEM) AND EDX of MS from [M(mtu)$_2$ced]

The microstructure of the metals sufide nanocrystals was examined by scanning electron microscopy (SEM). The SEM micrograph of HDA capped ZnS, CdS and HgS obtained by the thermolysis of complexes: [Zn(mtu)$_2$(ced)] (**1**), [Cd(mtu)$_2$(ced)] (**2**) and [Hg(mtu)$_2$(ced)] (**3**) are displayed in Figure 4.3(i-iii). The images from ZnS, Figure 4.3 (i), can be described as rough and coagulated, while the images from CdS are like spheroids at Figure 4.3(ii) b higher magnification and that of HgS have crumbs-like shapes both in Figure 4.3iii (a) low and (b) higher magnifications. The elemental composition of the HDA capped metal sulfide nanoparticles formed were confirmed by energy dispersive X-ray (EDX) analysis as shown in Fig 4.3(c) The EDX spectra show peaks corresponding to the respective metal and sulfur with only a noticeable contaminant being phosphorus and presumably from tri-n-octylphosphine (TOP) in which the precursor metal complexes were dispersed prior to injection into hot hexadecylamine (HDA). The morphology of the particles is nearly spherical. The smaller particles can be easily seen clinging to the surface of the big particles.

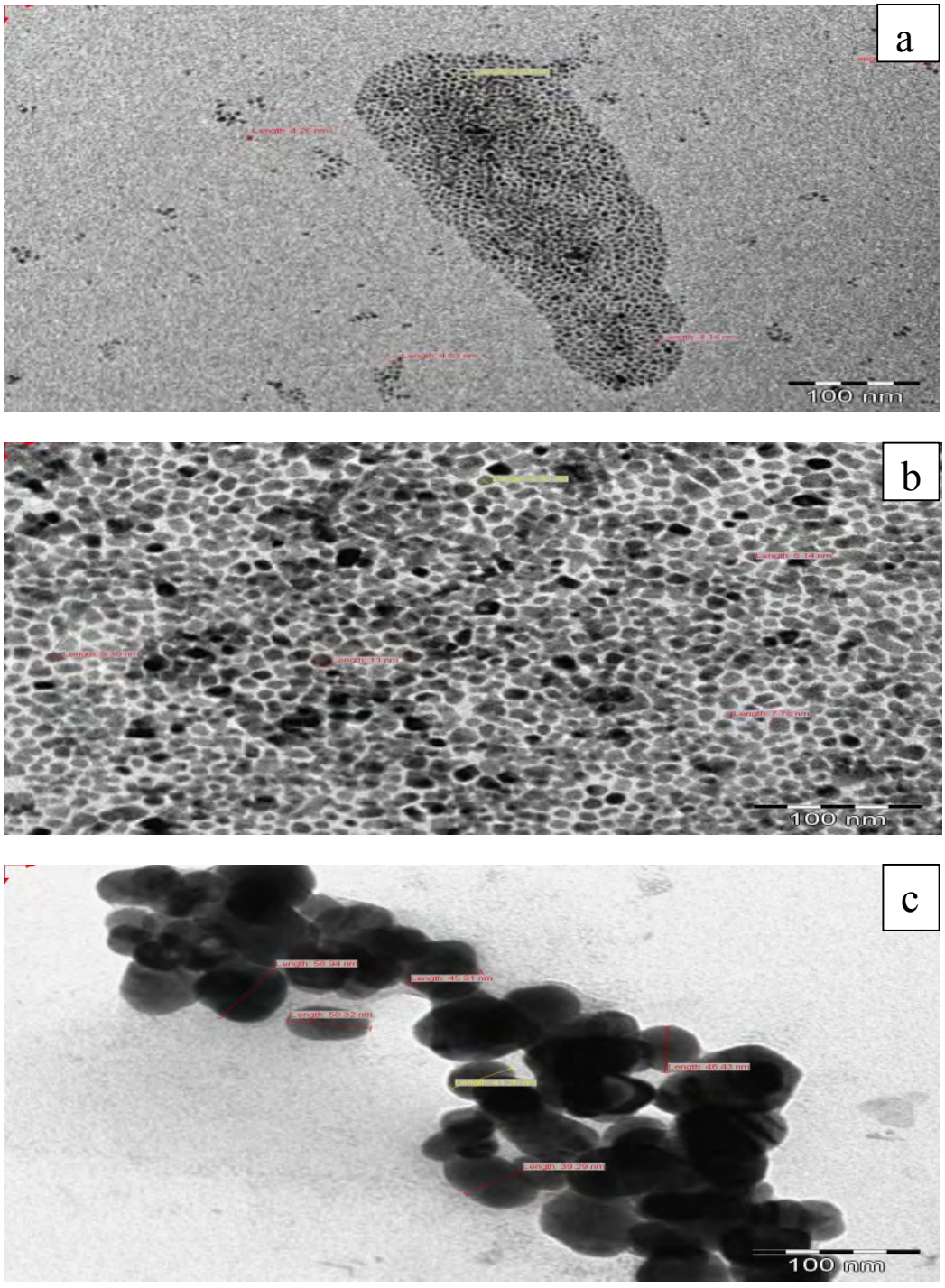

Figure 4. 2: TEM photograph of (a) ZnS, (b) CdS and (c) HgS nanoparticles obtained from the thermolysis of [Zn(mtu)2(ced)], [Cd(mtu)2(ced)], and [Hg(mtu)2(ced)] at 180 º

Because SEM can often only determine the particle size of secondary particles, it is assumed that the secondary particles of metal sulfides consist of the primary particles which are in the nanometer range, as estimated by effective mass approximation (EMA).

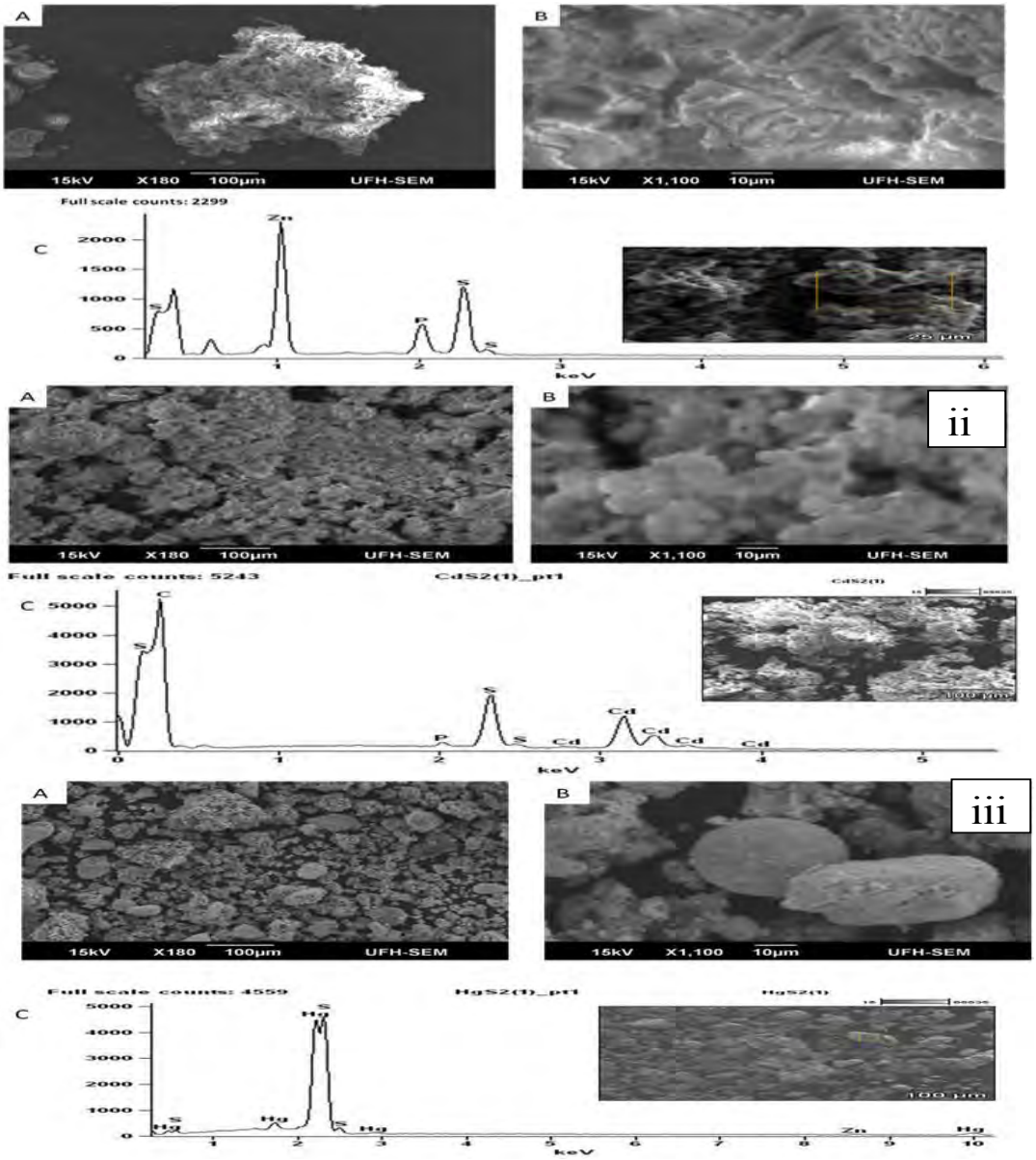

Figure 4.3: The SEM micrograph of (i) ZnS, (ii) CdS and (iii) HgS nanoparticles from [Zn(mtu)2ced], [Cd(mtu)$_2$ced] and [Hg(mtu)$_2$ced] complexes, at 180 ºC (a) low magnification, (b) high magnification (c) EDX spectrum of these sample.

4.4.4 Absorption and luminescence Studies.

UV-visible spectroscopy measures electronic transitions from the ground state to the excited state and it's a vital technique for monitoring the optical properties of quantum sized nanoparticles. Normally, the wavelength at the maximum exciton absorption (λ max) decreases as the size of the nanoparticles decreases, as a consequence of quantum confinements of the photogenerated electron hole carriers [26]. UV-Visible absorption spectra for ZnS nanoparticles prepared from dissolution in toluene at room temperature exhibits absorption peak at approximately 285 nm (4.35 eV) Figure 4.4(a) i. The absorption peak is significantly blue shifted compared to the bulk value 345 nm (3.6 eV) absorption wavelength of the bulk [27]. The photoluminescence property of ZnS nanoparticles was investigated at room temperature. It was observed that the PL spectrum shows a blue emission peak centered at 327 nm, Figure 4.4 (b) i. This indicates a slight blue shift from the bulk and can be ascribed to quantum confinement of the ZnS nanoparticles. CdS has an excitonic feature at 467 nm. This showed a clear appearance of blue-shift of the absorption peaks relative to the bulk CdS (515 nm) [28]. This observation actually indicates that the CdS nanoparticles are quantum confined. The photoluminescence spectra of the CdS showed broad emission peaks which correspond to large size distribution or the presence of anisotropic particles. The emission maximum was observed at 459 nm, Figure 4.4 (b) ii. The as-prepared nanoparticles are 56 nm blue shifted relative to the bulk CdS, 515 nm [29, 30].

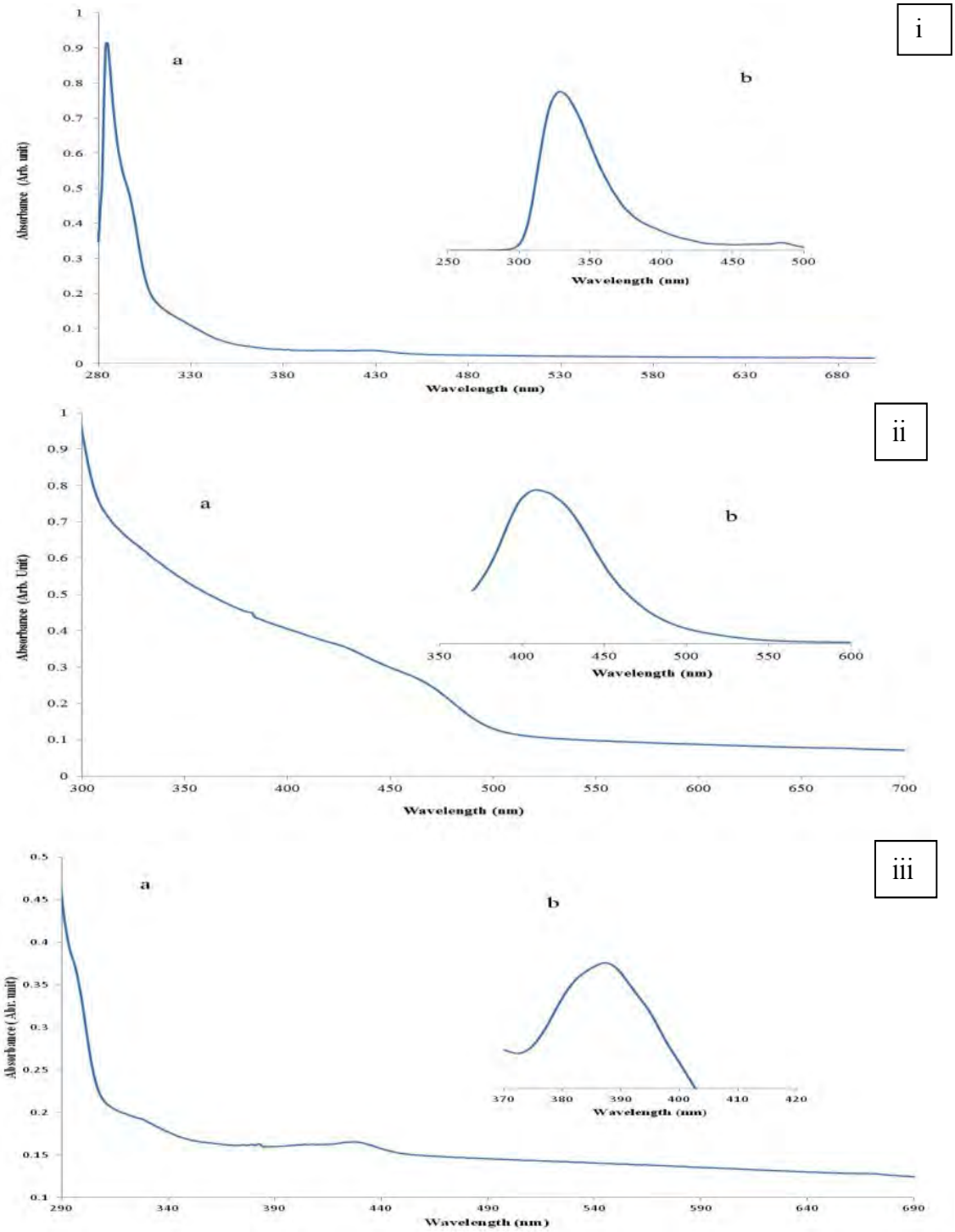

Figure 4.4: Absorption and emission spectra of the nanoparticles (a) Absorption and (b) emission spectra of HDA capped, ZnS (i), CdS (ii) and HgS (iii) nanoparticles synthesized from their respective metal complexes $[M(mtu)_2ced]$.

This can be ascribed to quantum size effect of the CdS. In the case of HgS nanoparticles, Figure 4.4(a) iii, the absorption spectra of the HgS nanoparticles, derived from the thermolysis of [Hg(mtu)$_2$(ced)] exhibited an absorption maximum at 425 nm and photoluminescence emission maximum at 387 nm as shown in Figure 4.4(a) iii. The HgS nanoparticles is blue shifted compared to the bulk, 616 nm [31].

4.5 Synthesis of HDA capped ZnS, CdS and HgS nanoparticles from [M(dmtu)$_2$ced] (where M = Zn, Cd or Hg).

The synthesis of the above listed nanoparticles were carried out according to the procedure reported earlier for the synthesis of [M(mtu)$_2$ced] in section 4.1.1 but the [M(dmtu)$_2$ced was used as the precursor.

4.5.1 XRD studies of HDA capped ZnS, CdS and HgS

Figure 4.5 shows typical XRD patterns nanoparticles. The ZnS diffractogram shows main peaks at 2θ values of 28.80º, 48.66º and 57.34º which can be indexed to miller indices of (1 1 1), (2 2 0) and (3 1 1) respectively. The assigned diffraction peaks is indicative of the formation of cubic sphalerite phase of ZnS, Figure 4.5(b) [32]. The XRD spectrum of CdS, Figure 4.5(b) reveals three main diffraction peaks of CdS nanoparticles and they are broadened as a result of very small size of the crystallites. The diffraction peaks at 2θ values; 26.75° (1 1 1), 44.85° (2 2 0) and 52.93° (3 1 1) correspond to as cubic CdS phase (Powder Diffraction JCPDS File no.10-454) [33].

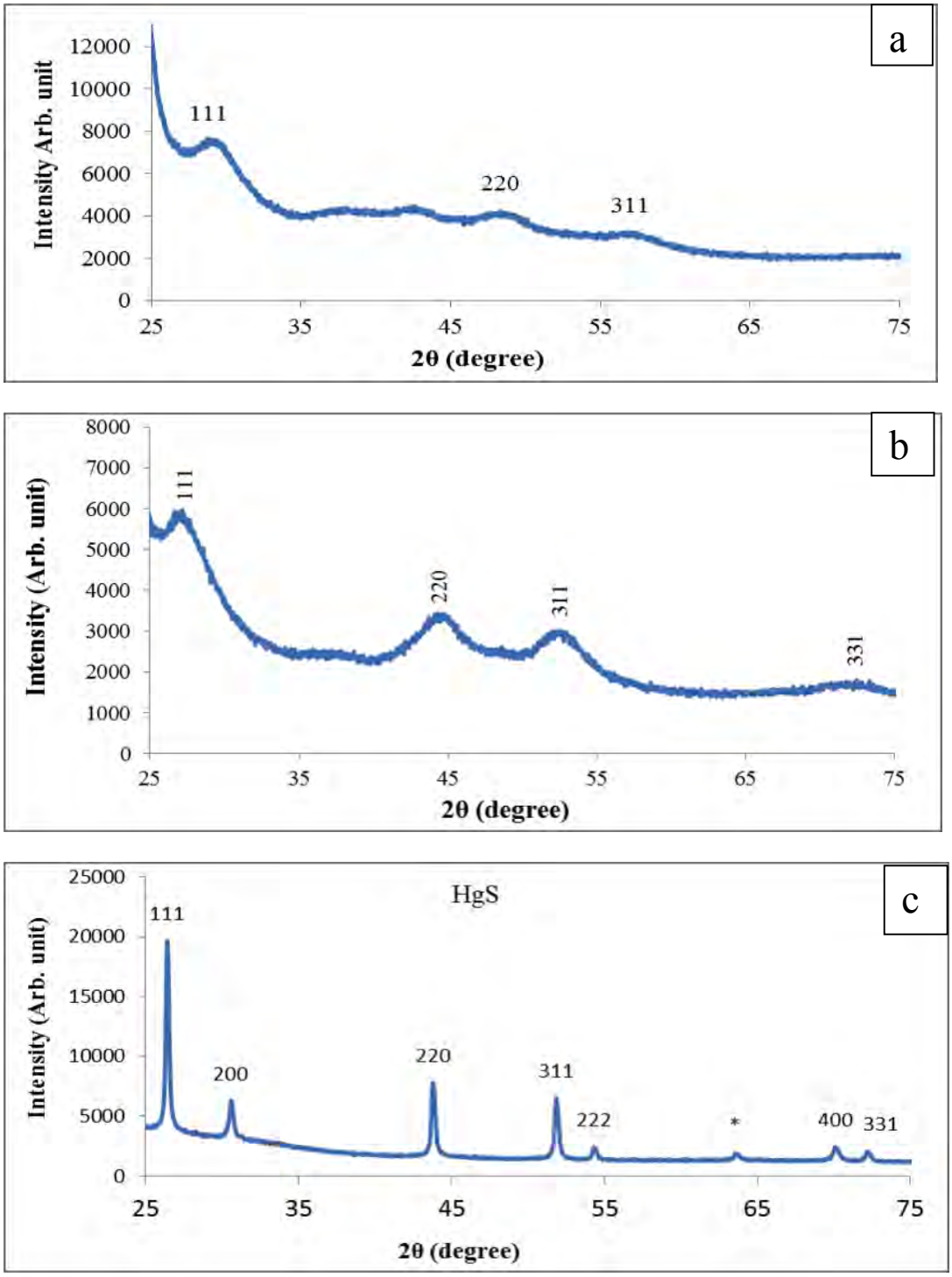

Figure 4.5: XRD pattern of HDA capped ZnS (a), CdS (b) and HgS (c) nanoparticles obtained from the thermolysis of respective $[Zn(dmtu)_2(ced)]$, $[Cd(dmtu)_2(ced)]$ and $[Hg(dmtu)_2(ced)]$ at 180 ºC.

The HgS diffractogram exhibits the characteristic peaks of the nanocrystals with discernible peaks at 2 θ = 26.38º, 30.51º, 43.72º, 51.83º, 54.30º. These values can be indexed to the following miller indices; (1 1 1), (2, 0 0), (2 2 0), (3 1 1) and (2 2 2) respectively. The diffractogram matches the cubic ß-HgS (metacinnabar) with no reflection peaks due to impurities according to JCPDS 06-0261 [31]. The sizes of the ZnS and CdS crystallites were estimated from the XRD pattern using the Scherrer's equation [34]. They were found to be 4.23 and 4.8 nm which agrees slightly with the range obtained from the TEM analysis (4.33 - 8.14 nm and 4.09 - 7.78 nm). The XRD peaks of the all the metal sulfide discussed are elongated and this is a confirmation of surface passivation of the nanocrystal [35].

4.5.2 Transmission Electron Microscopy (TEM) studies of nanoparticles from [M(dmtu)$_2$ced].

TEM images of ZnS, CdS and HgS nanoparticles from the precursors; [Zn(dmtu)$_2$(ced)], [Cd(dmtu)$_2$(ced)] and [Hg(dmtu)$_2$(ced)] are shown in Figure 4.6(a-c). The ZnS spectrum reveals ellipsoidal and rod shaped nanoparticles; the CdS are rod-like shaped while the HgS are rice-like shaped. The spacing between the nanocrystals is suggestive of the use of organic compound with donor electrons as a capping agent [36]. The sizes of ZnS, CdS and HgS nanoparticles are 4.33-7.21, 4.95-7.78 6.44-15.70 nm respectively. The crystallinity of the lattice planes observed in the XRD analysis is confirmed by the TEM analysis [37]. It is observed that the morphology of the ZnS and CdS nanoparticles is not the same with the one obtained from the precursor complex of the methyl thiourea. Spherical, (ZnS), and cube, (CdS), shaped morphology are revealed when methyl thiourea were used as precursor while with dimethyl thiourea rod shaped morphology were obtained for both ZnS and CdS nanoparticles.

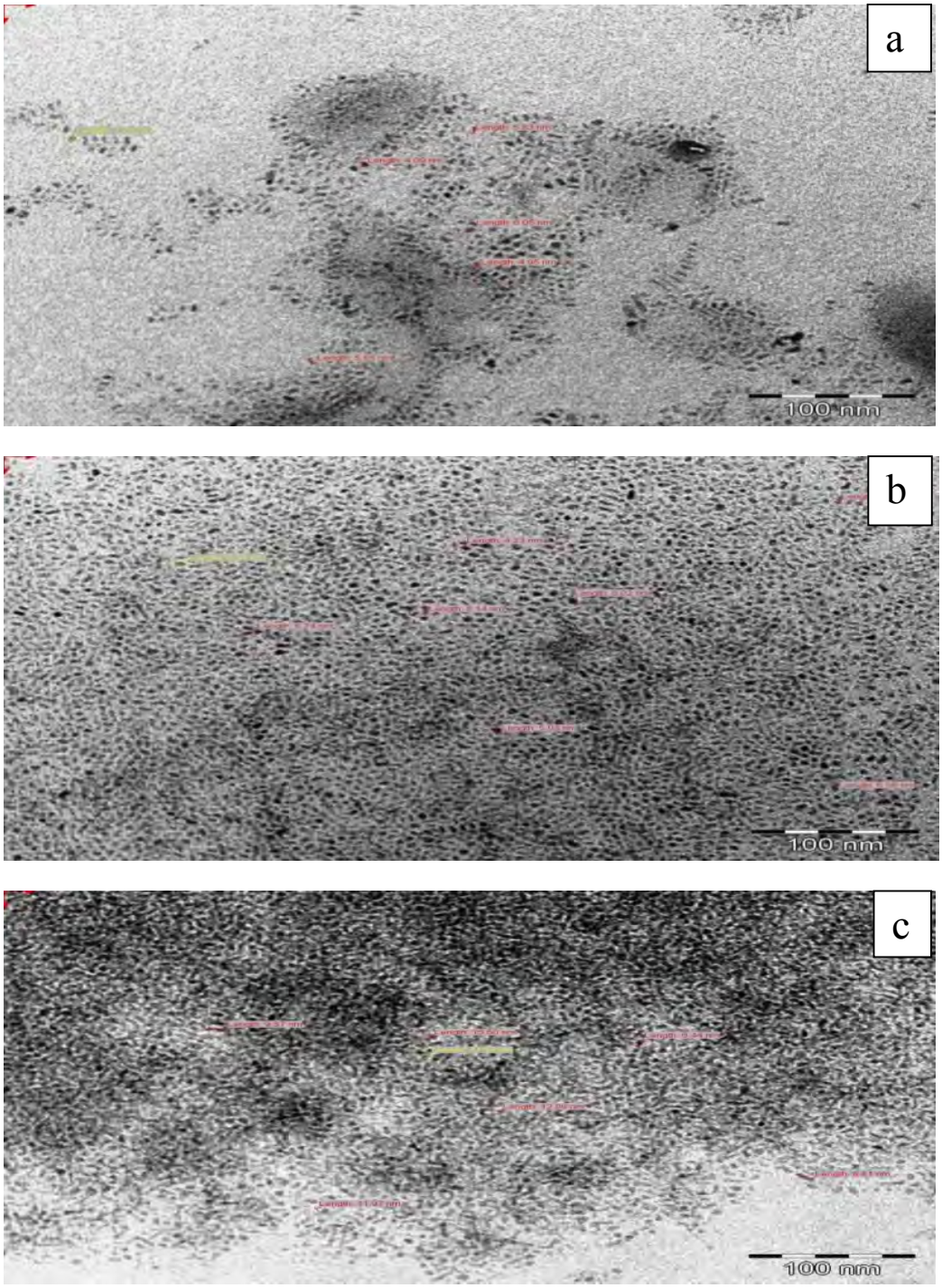

Figure 4.6: TEM photograph of (a) ZnS, (b) CdS and (c) HgS nanoparticles obtained from the thermolysis of $[Zn(dmtu)_2(ced)]$, $[Cd(dmtu)_2(ced)]$ and $[Hg(dmtu)_2(ced)]$ at 180 ºC.

:

4.5.3 Scanning Electron Microscopy (SEM) of ZnS, CdS and HgS nanoparticles from [M(dmtu)$_2$ced]

SEM images of ZnS, CdS and HgS nanoparticles are shown in Figure 4.7(i-iii). The SEM images of CdS showed well-arranged dense sphere-like shapes of approximately 3 μm in diameter. The surfaces of all the metals sulfides are slightly rough at lower magnification and smooth at higher magnification. The samples are aggregated as a result of the sample preparation from isolated dry powder. Despite the fact that the organic moieties are the same for these as-synthesized nanoparticles their morphologies are different, most likely because it is influenced by the chemistry of the central metal [31]. The elemental composition of the metal sulfide nanoparticles formed was confirmed by the energy dispersive X-ray analysis (EDX). The EDX spectra of ZnS, CdS and HgS nanoparticles are depicted in Figure 4-7(c), and the presence of Zn, Cd, Hg and S can be observed in all except that Phosphorus appear to be visible in the ZnS and CdS nanoparticles spectra possibly as a contaminant from the use of tri-n-octyl phosphine which served as a medium in which the precursor complexes were dispersed prior to injection in a hot coordinating solvent, HDA. The peaks from the EDX are consistent with the formation of the respective metal sulfide nanoparticles.

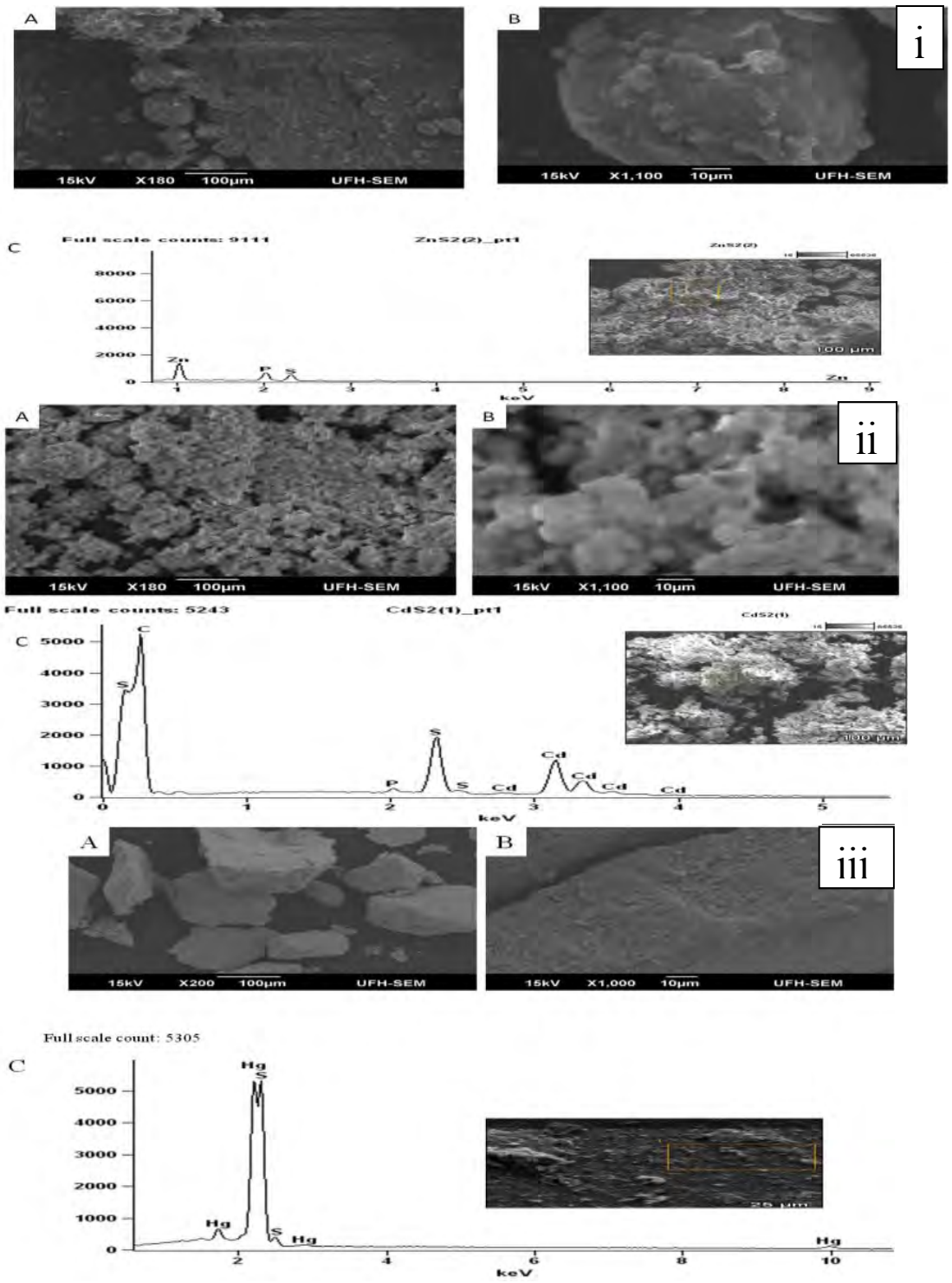

Figure 4.7: The SEM micrograph of (i) ZnS, (ii) CdS and (iii) HgS nanoparticles from [Zn(dmtu)$_2$ced] [Cd(dmtu)$_2$ced], [Hg(dmtu)$_2$ced] complexes, at 200 ºC (a) low magnification, (b) high magnification (c) EDX spectrum of the these samples.

4.5.4 Optical studies of ZnS, CdS and HgS from [M(dmtu)$_2$ced] (where M= Zn, Cd or Hg]

Figure 4.8a and b shows the absorption and photoluminescence spectra of ZnS, CdS and HgS. The absorption spectra of ZnS, CdS and HgS showed a characteristic absorbance band with a maximum located at a wavelength of 287 nm (4.32 eV) relative to bulk 340 nm (3.6 eV). Generally, the absorbance band appears at shorter wavelength when compared to the bulk. This significant observation has been explained as a result of quantum confinement [38, 39]. The absorption spectrum of the as-synthesized CdS nanoparticles Fig 4.8iia shows an absorption inflection point at around 429 nm (2.89 eV), which can be assigned to the excitonic absorption feature of CdS. The band gap has a blue shift of about 86 nm, in comparison with the value of the bulk 515 nm (2.40 eV) [40]. Thus, indicating the quantum confinement of the as-prepared CdS nanoparticles which has been similarly reported in literature [41]. The absorption spectrum of HgS also showed a quantum confinement that is characteristics of nanodispersed semiconductor nanoparticles. The bulk band gap of HgS is 620 nm (2.0 eV) and the as-prepared showed a significant blue shift in the absorption edge to 393 nm (3.15 eV). The spectrum also exhibits a second peak at 336 nm and this observation is suggestive of a highly monodispersed nanoparticles [42]. The tailing of the absorption features in CdS and HgS is due to particle sizes [43].

The photoluminescence (PL) spectra of ZnS, CdS and HgS nanoparticles, Figure 4.8(b) i-iii obtained at excitation wavelength of 250, 340 and 393 nm respectively show emission bands at 3.83 eV (323 nm), 3.06 eV (405 nm) and 3.17 eV (393 nm) for ZnS, CdS and HgS nanoparticles sequentially are in the locality of the band gap obtained from their absorption spectra. Hence, they are due to band to band transition. PL is commonly used for band gap, band-to-band investigations and also impurity level detection.

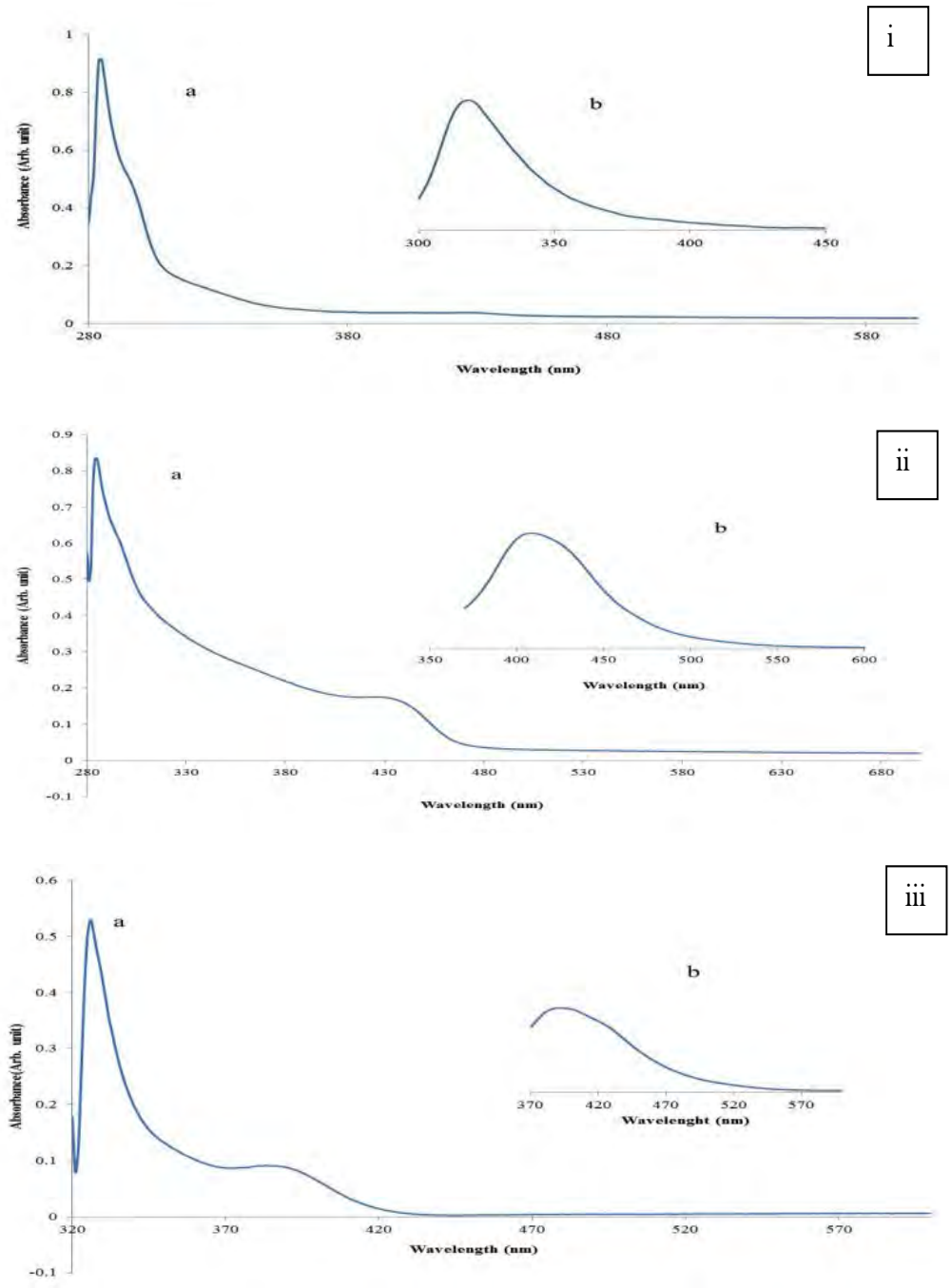

Figure 4.8: Absorption and emission spectra of the nanoparticles (a) Absorption and (b) emission spectra of HDA capped, ZnS (i), CdS (ii) and HgS (iii) nanoparticles synthesized from their respective metal complexes [$M(dmtu)_2ced$].

4.6 Synthesis of HDA capped MS nanoparticles from [M(detu)$_2$ced]

Similar procedure to the synthesis of ZnS, CdS and HgS from the complex represented by [M(detu)$_2$ced] has been reported in section 4.1.1.

4.6.1 XRD patterns of HDA capped ZnS, CdS and HgS nanoparticles from [M(detu)$_2$ced] (where M= Zn, Cd or Hg).

Typical XRD patterns of the as-prepared HDA capped ZnS, CdS, and HgS nanoparticles prepared by the thermolysis of [Zn(detu)$_2$ced], [Cd(detu)$_2$ced] and [Hg(detu)$_2$ced] respectively at 120 ºC are shown in Figure 4.9. In the XRD pattern of ZnS nanoparticles, three reflection peaks were observed at 2θ of 28.1º, 32.2º, 47.3º and 56.4º indexed to (1 1 1), (2 0 0), (2 2 0) and (3 1 1) planes, in the XRD diffractogram of the ZnS nanoparticles corresponding to the zinc blende structure (cubic, β-ZnS) [44, 45]. The broadening of the three diffraction peaks is also observed and this suggests that the dimension of the ZnS nanoparticles is very small. The average size as estimated from the XRD using Sherrer formula is 9.9 nm. The XRD pattern of the CdS shows three main reflection patterns from (1 1 1), (2 2 0) and (3 1 1) which can be indexed to 2θ values of 26.87°, 44.48° and 52.54°. The CdS nanoparticles on comparing with the data of JCPDS file card no 10-454, are identified as β-CdS which belong to cubic crystal system [46]. The mean size of CdS has been estimated to be 7.7 nm. The broadening of the peaks is as a result of the small particle size of the nanocrystals. The HgS has peaks at diffraction angles of 26.59°, 30.81°, 43.98°, 51.99°, 54.61°, 63.81°, 70° and 72.52° corresponding to the miller indices (111) (200) (220), (311), (222), (400), (331) and (422). These are comparable to the planes of HgS (metacinnabar system) and are in good agreement with JCPDS 00-006-0261 [47]. Surface passivation is revealed by the elongation of the XRD pattern [23]. The small sizes of the particles can be confirmed by the relative broadening of the peaks.

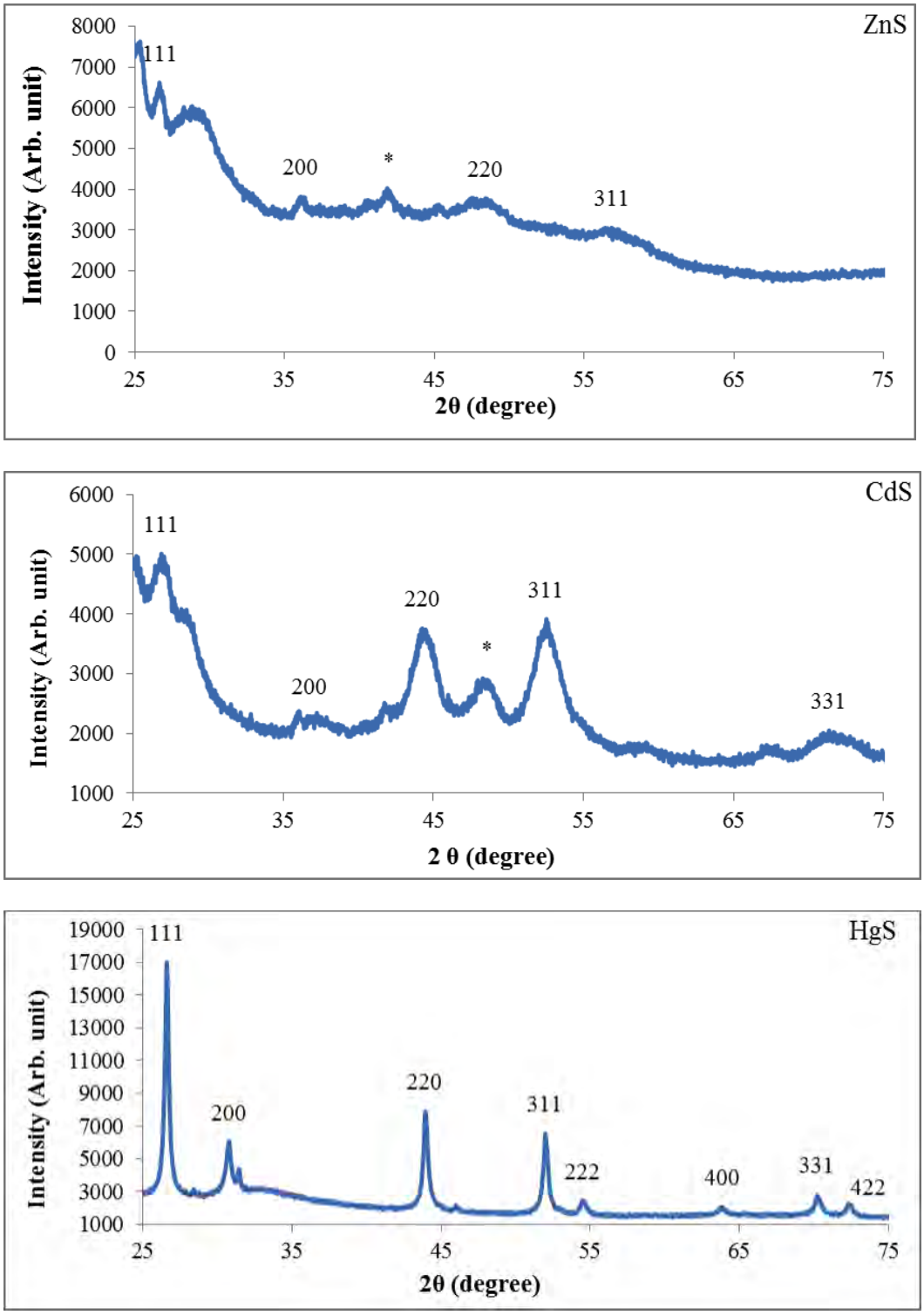

Figure 4.9: XRD pattern of HDA capped ZnS, CdS and HgS nanoparticles obtained from the thermolysis of $[Zn(detu)_2(ced)]$, $[Cd(detu)_2(ced)]$ and $[Hg(detu)_2(ced)]$ at 120 ºC

4.6.2 Transmission Electron Microscopy (TEM) studies of nanoparticles from [M(detu)$_2$ced]

The TEM image of ZnS nanoparticles shown in Figure 4.10 (a) reveals that small particles aggregated into secondary particles because of their extremely small sizes and higher surface energy with average crystallite sizes of ZnS being 2.69-4.66 nm. The morphology of the ZnS is dot and rod shaped. CdS nanoparticles in a way have a spheroid and rod shaped unagglomerated and it's uniformly monodispersed as can be seen in Figure 4.10(b). There is an observed trend in the morphology of ZnS and CdS nanoparticles as the thiourea alkyl substitutents were changed from methyl to dimethly to diethyl. One can infer from the TEM images that symmetrical (dimethyl, diethyl) substituted thiourea ligands in the complexes gave rod shaped ZnS and CdS nanoparticles and assymetrical substituted thiourea (methyl) gave spherical and cube shaped for ZnS and CdS nanoparticles respectively. Rod shapped nanoparticles being anisotropic have higher surface to volume ratio and invariably possesses higher energy per atom [48]. They have beneficial properties for application in chemical stability and exhibits enhanced catalytic activity compared with spherical shaped nanoparticles [49]. The size of the CdS nanoparticles was estimated to be between 4.88-7.68 nm. The HgS nanoparticles, Figure 4.10(c) appear to be spherical in shape and equally monodispersed although some part of it seems to be agglomerated. The average size of HgS nanoparticles is in the range of 8.34 -11.10 nm. It is hard to determine the exact dimension of HgS particles by only observing the TEM image because the extremely small particles aggregate to secondary particles [50].

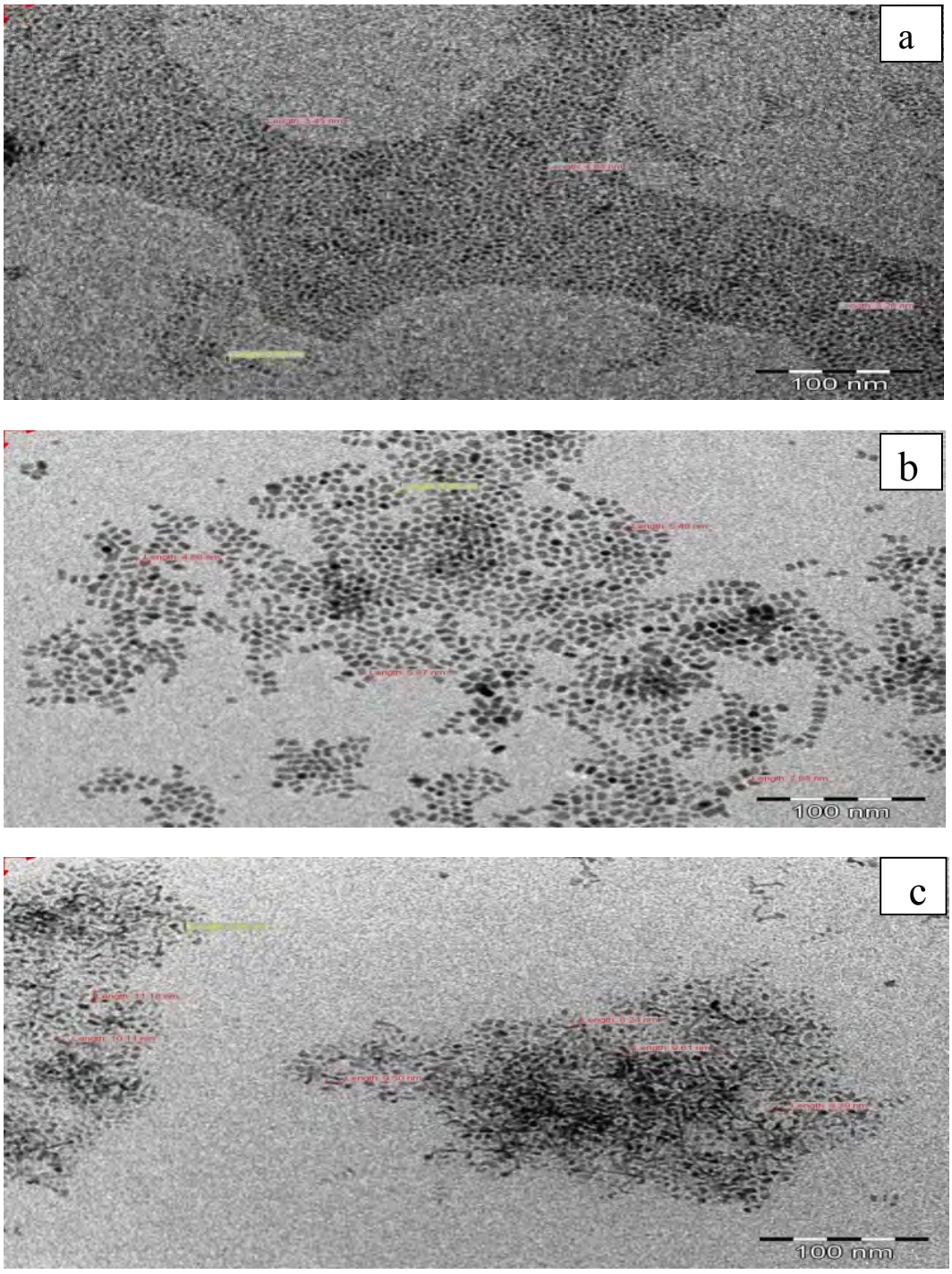

Figure 4.10: TEM photograph of (a) ZnS, (b) CdS and (c) HgS nanoparticles obtained from the thermolysis of $[Zn(detu)_2(ced)]$, $[Cd(detu)_2(ced)]$ and $[Hg(detu)_2(ced)]$ at 120 ºC.

4.6.3 Scanning Electron Microscopy (SEM) of ZnS, CdS and HgS from [M(detu)$_2$ced]

The ZnS nanoparticles at lower magnification showed a rough surface which appeared to be smooth at higher magnification as shown in Figure 4.11(b). A good growth environment of the nanoparticles can be revealed by the similarity and uniformity of the spheres and this also indicate good crystallinity of the sphere from other aspects [51]. At higher magnification the large particles were observed to be aggregates of the nanoparticles as seen in the SEM images of ZnS, and CdS and HgS nanoparticles, (Figure 4.11(b)). The EDX of the nanoparticles; ZnS, CdS and HgS showed peaks of Zn and S, Cd and S, Hg and S respectively with the appearance of phosphorus peaks in ZnS and CdS as the only noticeable contaminant from tri-n-octyl phosphine (TOP) in which the precursor metal complexes were dispersed prior to injection into the hot hexadexylamine (HDA).

4.6.4 Absorption and Photoluminescence studies.

The absorption spectrum of ZnS nanoparticles obtained from the thermolysis of [Zn(detu)$_2$ced] also shows quantum size effect which are characteristic of nanodispersed semiconductors nanoparticles. The absorption peak showed a broad close to band edge emission observed at 287 nm (4.32 eV) as shown in Figure 4.12(a) i. This peak exhibited a blue shift of about 53 nm compared to the bulk 340 nm (3.65 eV) [35]. The photoluminescence emission maximum appeared at 331 nm (3.74 eV) which is relatively blue shifted compared to the bulk ZnS (340 nm) [52]. The absorption spectrum of CdS, Figure 4.12 (a) ii, also shows quantum size effects which are characteristic of nanodispersed semiconductors.

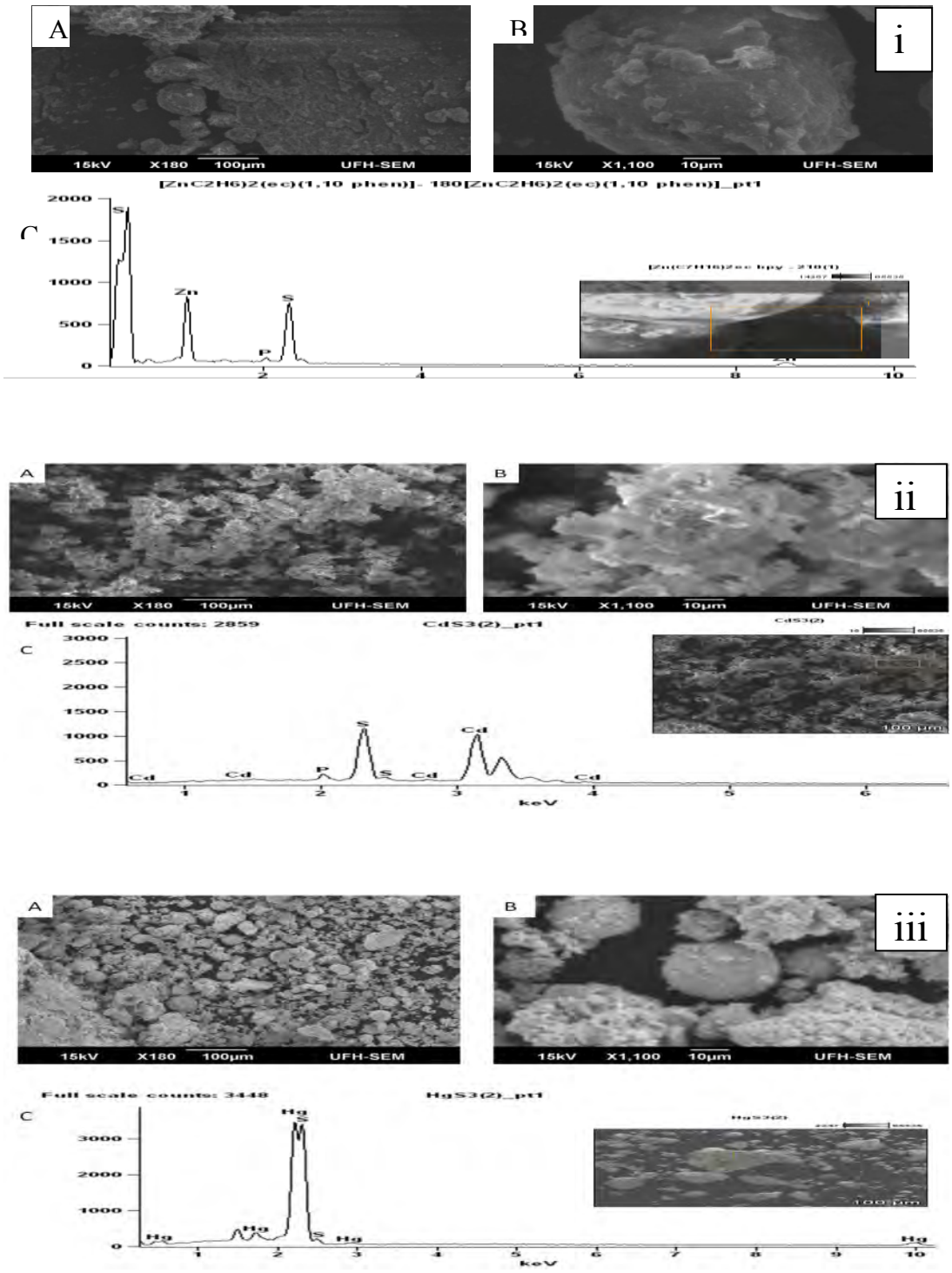

Figure 4.11: The SEM micrograph of (i) CdS, (ii) ZnS and (iii) HgS nanoparticles from [Zn(detu)$_2$ced], [Cd(detu)$_2$ced] and [Hg(detu)$_2$ced] complexes, at 120 ºC at; (a) low magnification, (b) high magnification (c) EDX spectrum of the these samples

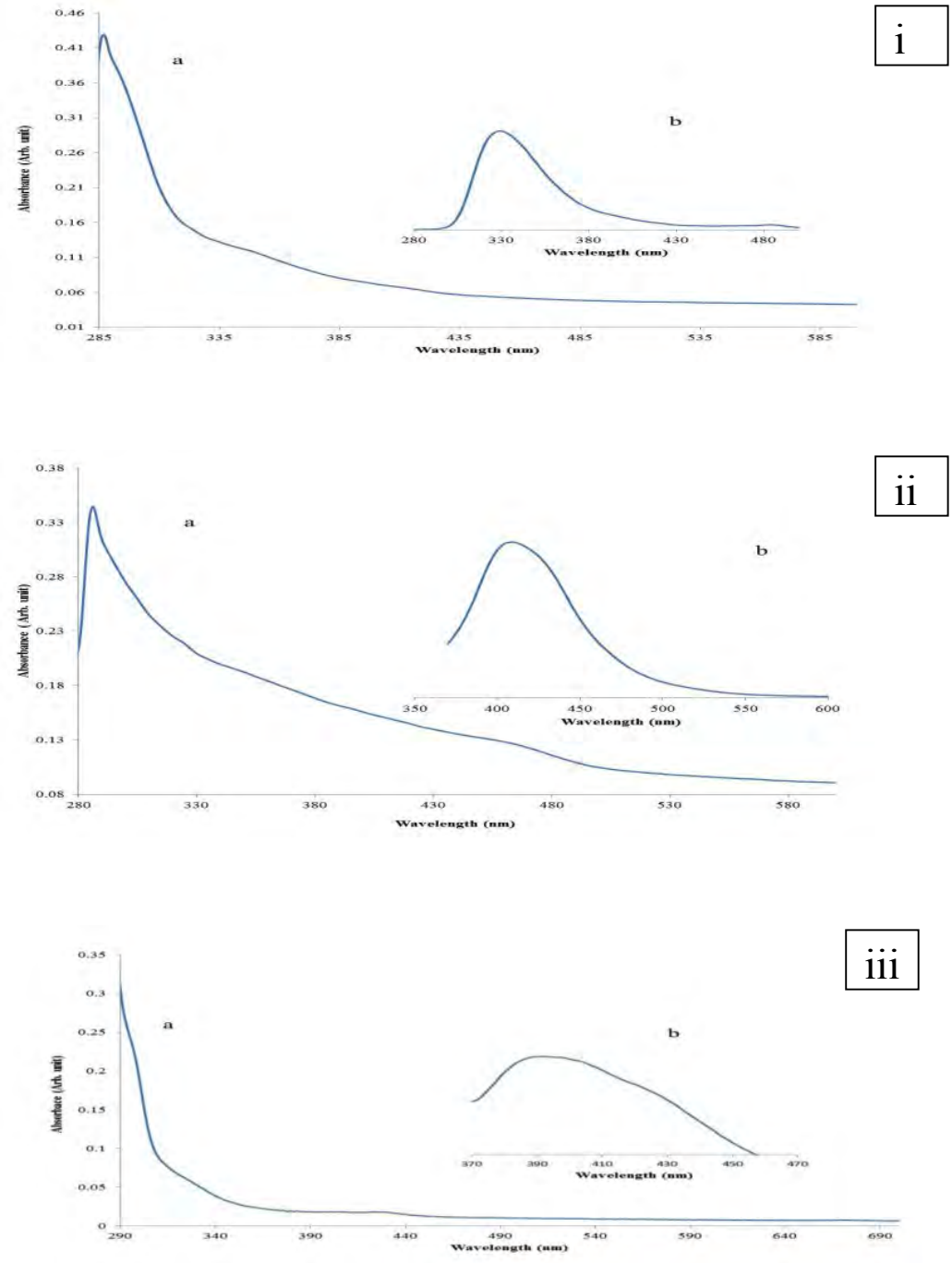

Figure 4.12: Absorption and emission spectra of the nanoparticles (a) Absorption and (b) emission spectra of HDA capped, (i) ZnS, (ii) CdS and (iii) HgS nanoparticles synthesized from their respective metal complexes $[M(detu)_2ced]$.

The synthesized CdS shows a blue shift in the absorption peak at 467 nm (2.65 eV) compared with the bulk CdS (515 nm, 2.14 eV) [53]. The photoluminescence spectrum shows an emission maximum at around 458 nm which is also a significant blue shift from the band edge of the bulk (515) nm as shown in Figure 4.12(b) ii. The absorbance spectrum of HgS reveals presence of excitonic feature at 430 nm (2.88 eV) with a typical tailing of the absorption band and an emission maximum at 390 nm (3.17eV), Figure 4.12 (a,b) iii, as compared to the bulk HgS 620 nm (2.0 eV) [54]. This showed quantum confinement with a significant blue shift from the band edge compared with the bulk.

4.7 Synthesis of metal sulfide nanoparticles obtained from tetramethylthiuram disulfide [M(Me_4(tds)(ced)] (where M = Zn, Cd, Hg)

4.7.1 X-ray diffraction studies of HDA-capped ZnS, CdS, HgS derived from [M(Me_4tds)ced]

The powder XRD patterns of the ZnS, CdS and HgS nanoparticles are shown in Figures 4.13(a-c). For ZnS, Figure 4.13(a), the three peaks with 2θ values 26.78º, 44.43º and 52.36º correspond to the presence of hexagonal ZnS. The indicator is the peak value 26.78º plane which corresponds to (1 0 1) and is in good agreement with Joint committee of powder diffraction standard (JCPDS-75-1534) data belonging to hexagonal ZnS [55] and the presence of 52.36º which suggest the hexagonal phase of ZnS [56]. The XRD pattern of CdS is shown in Figure 4.13(b) and show a single phase sphalerite crystal structure. The 2θ values are: 26.9º, 36.16º, 43.6º, and 51.83º that can be indexed to the following planes: (1 1 1), (2 0 0), (2 2 0) and (3 1 1) planes of the cubic phase β-CdS (JCPDS 80-0019). The peak broadening of XRD pattern indicates that small nanocrystals are present.

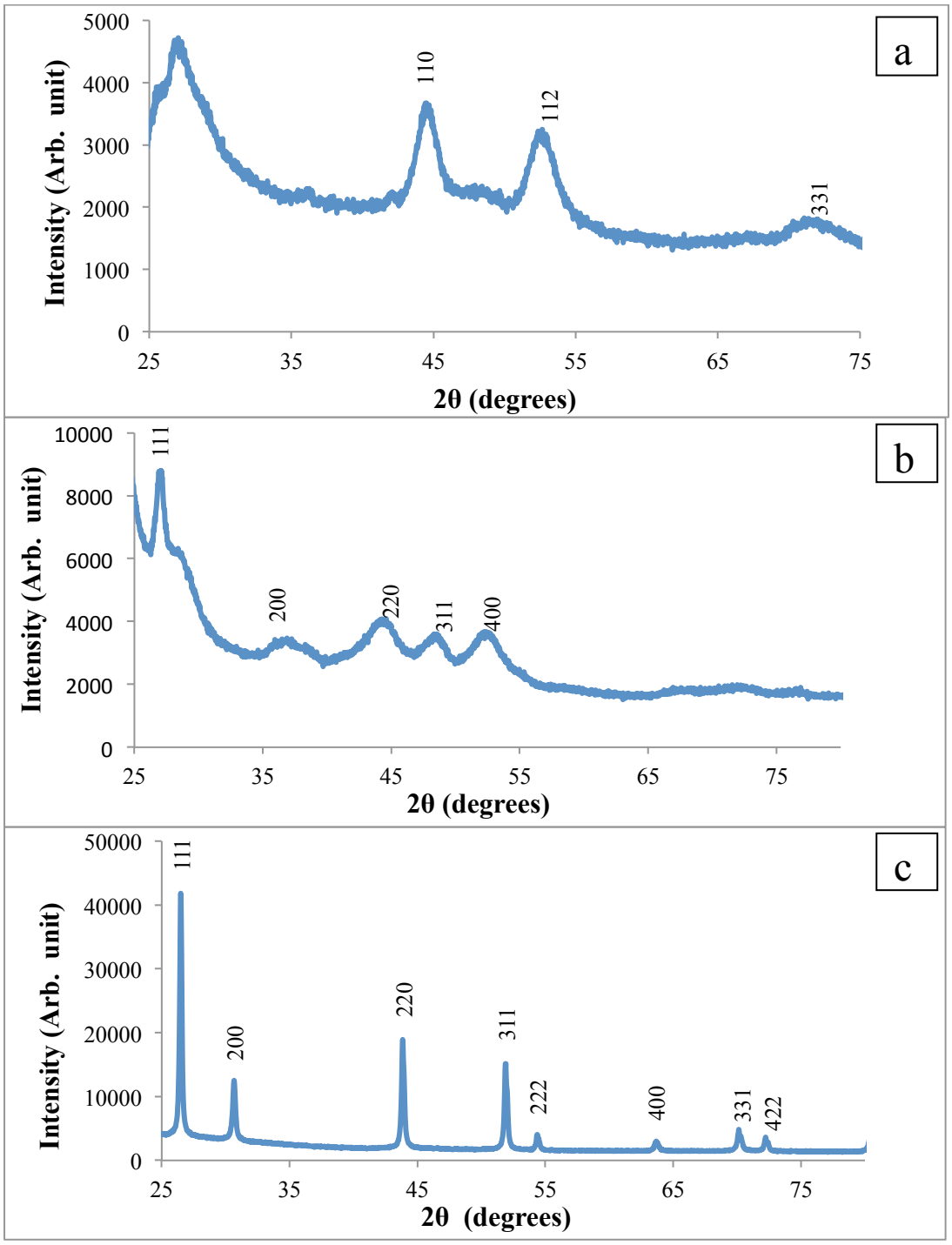

Figure 4.13: XRD patterns of ZnS, CdS, and HgS nanoparticles synthesized from [M(Me_4tds)ced] (where M= Zn, Cd, Hg).

The listed peaks as observed in the XRD pattern of HgS, Figure 4.13(c), are at 2θ = 26.49º, 30.64º, 43.85º, 51.89º and 54.33º. They match the peaks of known metaccinabar [57/52]. The peaks are intense and all orient along the planes (1 1 1), (2 0 0), (2 2 0), (3 1 1), (4 0 0). All these peaks are to be indexed to face-centered cubic HgS.

4.7.2 Transmission electron microscopy (TEM) studies of nanoparticles from [M(Me$_4$tds)ced].

TEM images of the ZnS, CdS and HgS nanoparticles synthesized from [M(Me4tds)ced] (M = Zn, Cd, Hg) respectively are presented in Figure 4.14(a-c). It is observed that the particles of the ZnS in Figure 4.14(a) are dot shaped and the particles are evenly distributed.

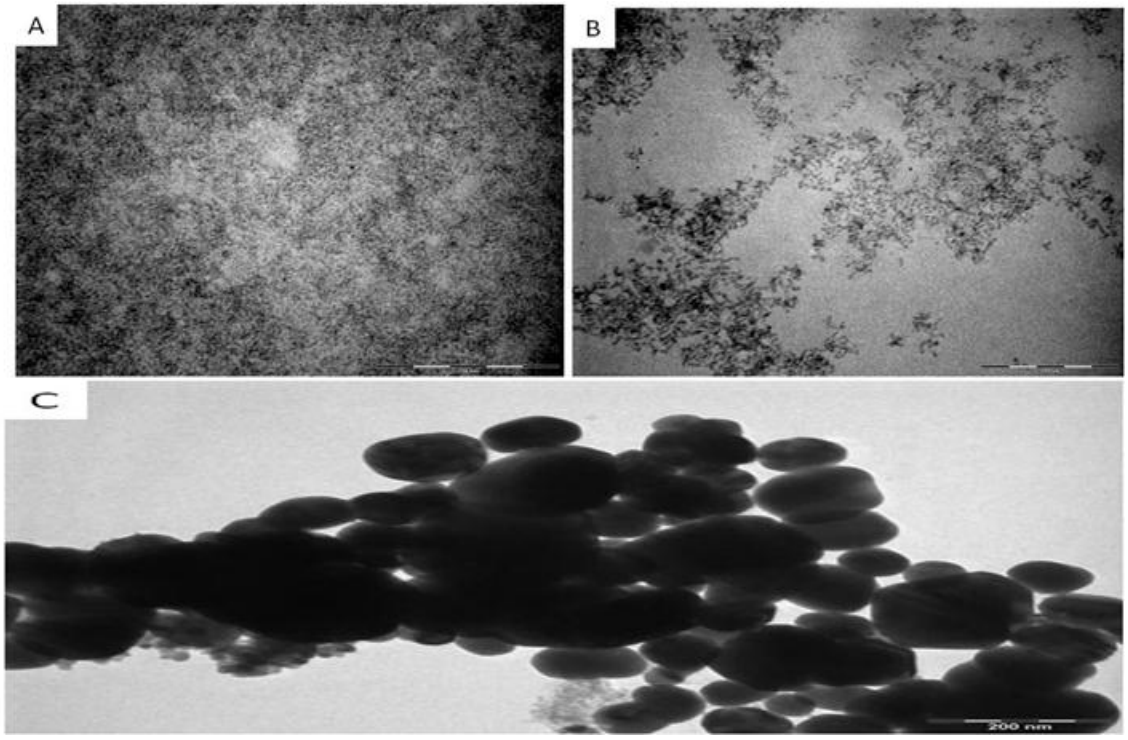

Figure 4.14: TEM photograph of (A) ZnS, (B) CdS and (C) HgS nanoparticles obtained from the thermolysis of [Zn(Me4tds)(ced)], [Cd(Me4tds)(ced)] and [Hg(Me4tds)(ced)] at 120 ºC.

The CdS particles display a spherical shaped morphology while in the HgS sample, agglomerated oval shaped particles were observed. TEM showed that the product was composed of 40% isolated particles and 60% agglomerated particles. The average size of HgS nanoparticles is in about 60 nm.

4.7.3 Scanning electron microscopy (SEM) studies of nanoparticles from [M(Me$_4$tds)ced].

The microstructure of the nanocrystals was examined by scanning electron microscopy (SEM) and the elemental compositions of the nanoparticles formed were confirmed by energy dispersive X-ray (EDX) analysis as shown in Figure 4.15. Zinc and sulfur are the main composition of the sample with traces of phosphorus that is an impurity. The phosphorus is from the trioctyl phosphine in which the precursor material was discharged. At higher magnification, the surface of ZnS nanoparticles appears smooth and spherical while the CdS showed flowery morphology intercalated with granular-like shaped materials and the HgS nanoparticles appear to be a combination of granules and flowery material.

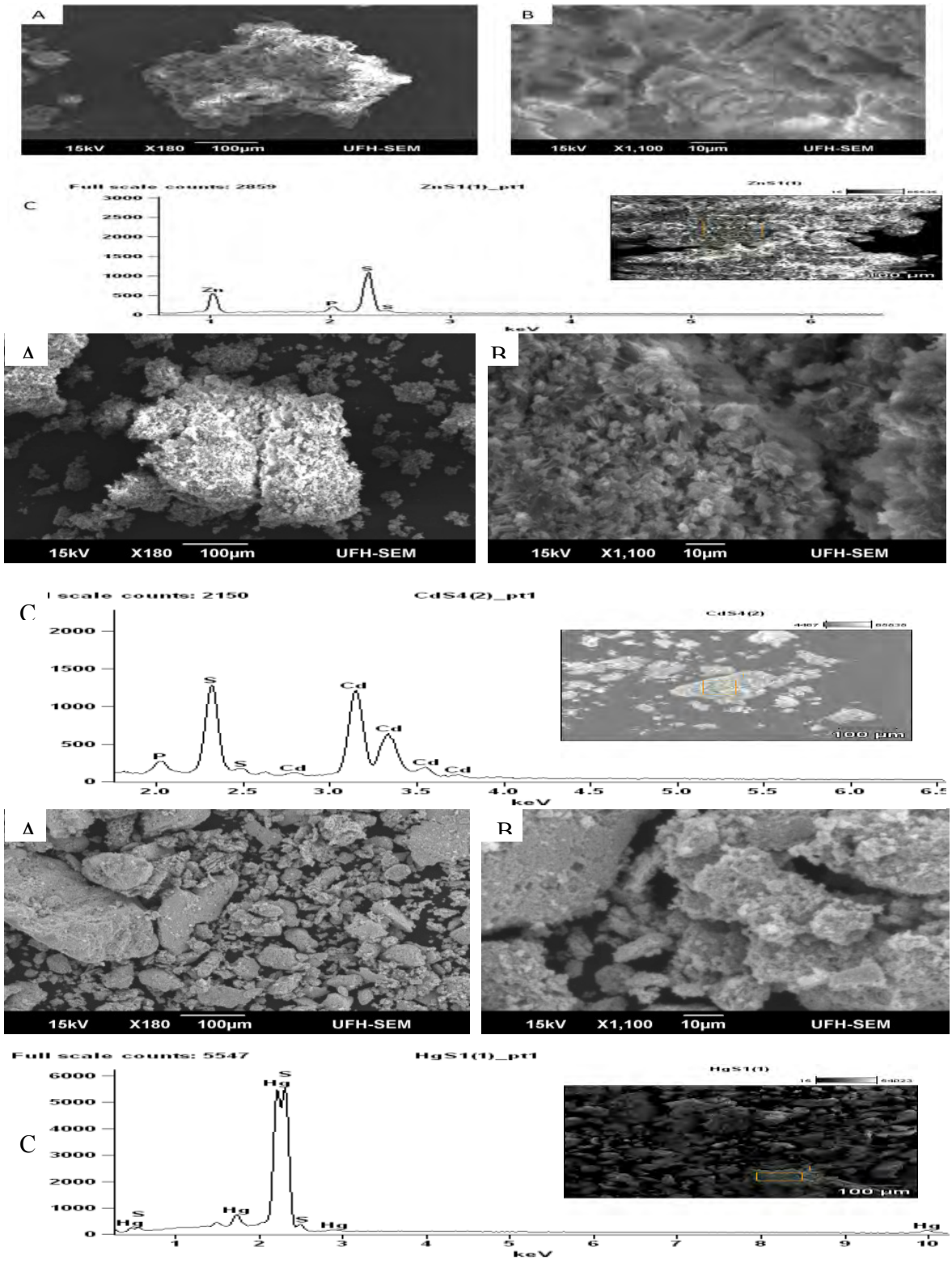

Figure 4.15: SEM photograph of (A) ZnS, (B) CdS and (C) HgS nanoparticles obtained from the thermolysis of [Zn(Me4tds)(ced)], [Cd(Me4tds)(ced)] and [Hg(Me4tds)(ced)] at 120 ºC

4.7.4 Optical property of metal sulfide (MS) derived from [M(Me_4tds)ced] (M = Zn, Cd and Hg)

UV-Visible spectra analysis has served as a useful technique for the characterization of semiconductor nanoparticles, which exhibit quantum size effect. The quantum size effect is caused by the photo-generated electron-hole pairs. The UV-Visible absorption spectrum of semiconductor nanoparticles depends on their size and the absorption maximum decreases with the nanoparticle size [57]. The UV-Vis absorption spectra (Figure 3.16(a) i-iii showed that the absorption peaks of analyzed ZnS, CdS and HgS particles are at 288, 439 and 296 nm respectively, a relative blue-shift to the band gap of the bulk which are at 340, 515 and 563 nm respectively [50, 58]. The peak positions can be related to the mean diameter of the particles, smaller diameter meaning lower wavelength. The results showed the effect of quantum confinement [59]. The absorption shift represents a change in band gap along with exciton features, which can be used as a measure of particle size and size distribution. The calculated gap for the ZnS, CdS, and HgS particles are = 3.78, 2.82, and 3.89 eV respectively.

In semiconductor nanoparticles, the position of absorption band edge can be taken as indicator of their sizes. The approach has proven very useful since the result obtained from this method has not been affected by the presence of aggregates. The electronic coupling between particles in an aggregate is sufficiently weak so that the resultant spectrum is determined by the primary particles only [60]. Brus equation [61] was used to calculate the particle size from the absorption edge. From the characteristic absorption spectra, the size of CdS and ZnS nanoparticles were estimated to be about 5.68 and 7.88 nm in diameter.

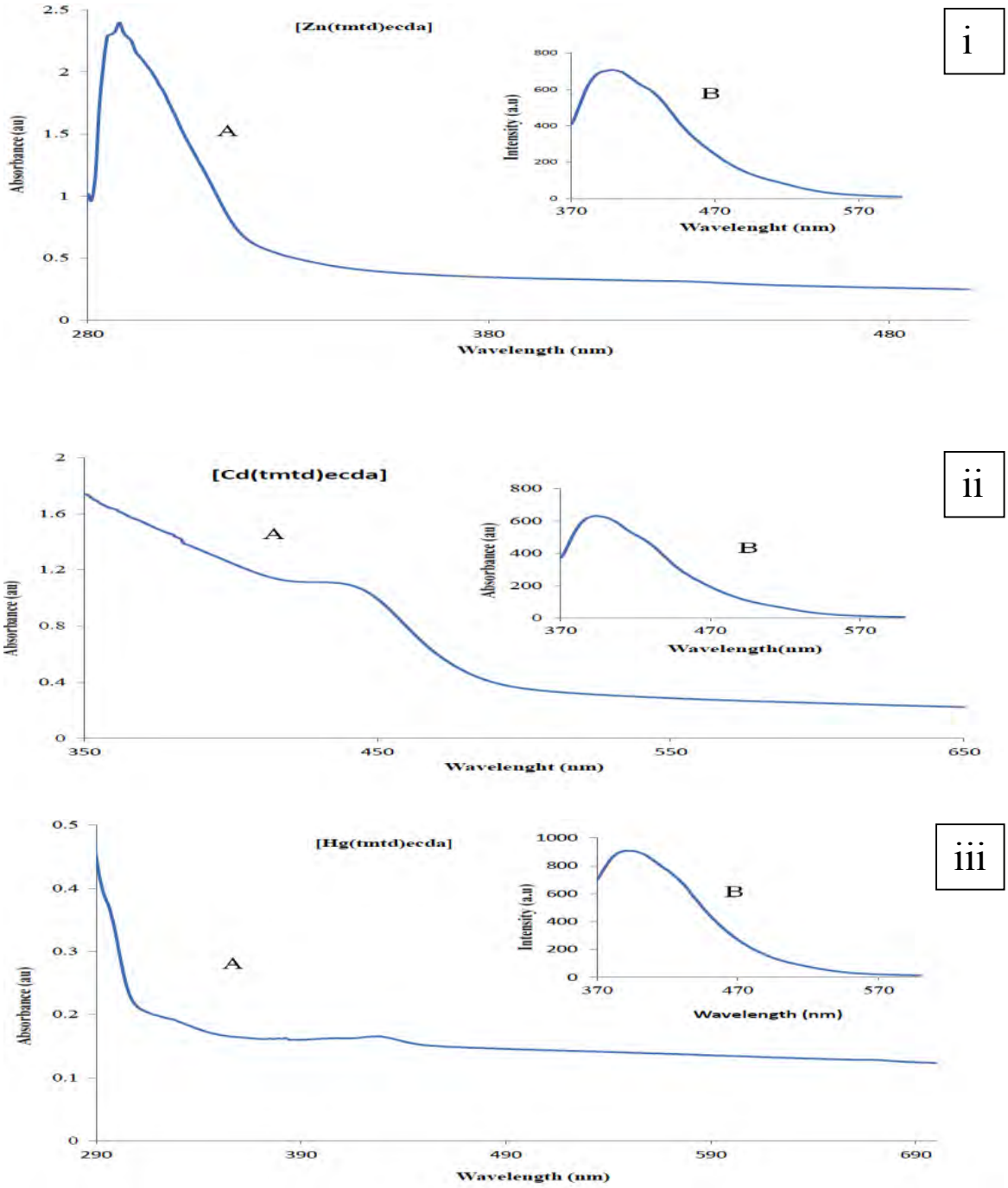

Figure 4.16: Optical absorption (a) and corresponding photoluminescence spectra (b) of HDA capped ZnS, CdS, and HgS nanoparticles synthesized from [M(Me_4tds)ced].

The photoluminescence spectra of the as–prepared ZnS, CdS and HgS from their respective complexes were recorded at room temperature at an excitation wavelength of 370 nm and they exhibit emission peak maxima at 398, 394 and 393 nm respectively. The ZnS is red shifted with respect to the bulk and CdS and HgS are blue shifted compared with their bulk materials.

4.8 Conclusion

In the synthesis of the ZnS, CdS and HgS, 3 different substituted thiourea complexes were used as single source precursors and these gave different morphologies of ZnS and CdS nanoparticles. Although the thermolysis in HDA was conducted at either 120 ºC or 180 ºC the same growth time of 1 h was employed. For the ZnS and CdS from methyl thiourea spherical and cube shaped morphologies were obtained. The precursor complexes with dimethyl thiourea substituent gave both rod shaped ZnS and CdS nanoparticles. ZnS and CdS synthesized from diethyl thiourea gave spherical shaped and a combination of rod and spherical shaped for ZnS and CdS respectively. Lastly the precursor complex with tetramethythiuram disulfide ligand generated rod shaped morphology for both ZnS and CdS nanoparticles.

Narrowing down our analysis on ZnS and CdS because of the conspicuous observation one can infer that all the symmetrical substituted thiourea (dimethyl and diethyl) gave rod shaped CdS nanoparticles while the asymmetrical substituted thiourea (methyl) produced a cube shaped CdS nanoparticles. The particle size of ZnS nanoparticles from diethyl thiourea exhibit the smallest particle sizes with an average crystallite size of 2.69 - 4.66 nm when compared with 4.14 - 4.63 nm and 4.33 - 7.21 nm observed from methyl and dimethyl thiourea precursor complexes. The relevance of this revealation is that symmetrical

substituted thiourea ligand will have a better application in catalysis because rod shaped nanoparticles have enhanced catalytic acativity than the spherical shaped nanoparticles. This is due to the facts that they have higher surface to volume ratio and invariably there are higher energy per atom. Generally anisotropic nanoparticles have enhanced catalytic activity than isotropic (spherical ones.

4.8 References

1. Malik, M. A.; Revaprasadu, N.; O'Brien, P. Air-stable single source precursors for the synthesis of chalcogenide semiconductor nanoparticles. *Chem*. *Mater*. **2001**, *13*, 913-920.
2. Trindade, T.; O'Brien, P.; Zhang, X.M. Synthesis of CdS and CdSe nanocrystallites using a novel single-molecule precursors approach. *Chem. Mater*. **1997**, *9*, 523-530.
3. Green, M.; Prince, P.; Gardener, M.; Steed J. mercury(II) *N*,*N*′-Methyl-phenylethyl-dithiocarbamate and its use as a precursor for the room-temperature solution deposition of β-HgS thin films. *Adv. Mater*. **2004**, *16*, 994-1030.
4. Matchett, M.A.; Viano, A. M.; Adolphi, N. L.; Stoddard, R. D.; Buhro, W. E.; Conradi, M. S.; Gibbons, P. C. A sol-gel route to crystalline cadmium phosphide nanoclusters. *Chem*. *Mater*. **1992**, *4*, 508-511.
5. Lazell, M.; O'Brien, P. A novel single source precursor route to self-capping CdS quantum dots. *Chem*. *Commun*. **1999**, 2041-2042.
6. A. P. Alivisatos, Perspective on the physical chemistry of semiconductor nanocrystal. *J. Phys*. *Chem*. **1996**, *100*, 13226-13239.
7. Murray, C. B.; Norri, D. J; Bawendi, M. G. Synthesis and character of nearly monodisperse CdE (E=S, Se, Te). *J. Am*. *Chem*. *Soc*. **1993**, *115*, 8706-8715.
8. Pickett, N. L.; O'Brien, P. Synthesis of semiconductor nanoparticles using single source precursor methods. *Chem*. *Rec*. **2001**, 461-479.
9. Rees Jr, W. S.; Kräuter, G. Preparation and characterization of several group 12 element (Zn, Cd)-*bis*(thiolate) complexes and evaluation of their potential as precursors for 12-16 semiconducting materials. *J. Mater*. *Res*. **1996**, *11*, 3005-3016.
10. Thurston, J. H.; Ely, T. O.; Trahan, D.; Whitmire, K. H. Nanostructured bimetallic oxide ion-conducting ceramics from single source molecular precursors. *Chem. Mater*. **2003**, *15*, 4407-4416.

11. Pohl, I .A. M.; Westin, L. G.; Kritikos, M. Preparation, Structure, and properties of a new giant manganese oxo-alkoxide wheel, $[Mn_{19}O_{12}(OC_2H_4OCH_3)_{14}(HOC_2H_4OCH_3)_{10}]\cdot HOC_2H_4OCH_3$. *Eur. J. Chem*. **2001**, *7*, 3438-3445.

12. Thurston, J. H.; Whitmire, K. H. Molecular precursors for ferroelectric materials: Synthesis and characterization of $Bi_2M_2(\mu\text{-}O)(sal)_4(Hsal)_4(OEt)_2$ and $BiM_4(\mu\text{-}O)_4(sal)_4(Hsal)_3(O^iPr)_4$ (sal = $O_2CC_6H_4O$, Hsal = $O_2CC_6H_4OH$) (M = Nb, Ta). *Inorg. Chem*. **2003**, *42*, 2014-2023.

13. Palgrave, R. G.; Parkin, I. P. Aerosol assisted chemical vapor deposition using nanoparticle precursors: A route to nanocomposite thin films. *J. Am. Chem. Soc*. **2006**, *128*, 1587-1597.

14. Boadi, N. O.; Malik, M. A.; O'Brien, P. Awudza, J. A. M. Single source molecular precursor routes to lead chalcogenides. *Dalton Trans*., **2012**, *41*, 10497-10506

15. Aldana, J.; Wang, Y. A.; Peng, X. Photochemical instability of CdSe nanocrystals coated by hydrophilic thiols. *J. Am. Chem. Soc*. **2001**, *123*, 8844-8850.

16. Jin, M.; Guannan, H.; Zhang, H.; Zeng, J.; Xie, Z.; Xia, Y. Shape-controlled synthesis of copper nanocrystals in an aqueous solution with glucose as a reducing agent and hexadecylamine as a capping agent. *Ang. Chem. Inter. Ed*. **2011**, *50*, 10560-10564.

17. Mthethwa, T.; Pullabhotla, V. S. R.; Mdluli, P. S., Wesley-Smith, J.; Revaprasadu, N. Synthesis of hexadecylamine capped CdS nanoparticles using heterocyclic cadmium dithiocarbamates as single source precursors. *Polyhedron*, **2009**, *28*, 2977-2982.

18. Park, J. Y.; Aliaga, C.; Renzas, R. J.; Lee, H.; Somorjai, G. The role of organic capping agents layers of platinum nanoparticles in catalytic activity of CO oxidation. *Catal. lett*. **2009**, *129*, 1-6.

19. Srinivasan, N.; Thirumaran, S.; Ciattini, S. Preparation of ZnS nanosheets from (2,2'-bipyridine)bis(1,2,3,4-tetrahydroquinolinecarbodithioato-S,S')zinc(II). *Spectrochim. Acta A*. **2013**,102, 263-268.

20. Chen, D.; Weng S. Chemical effects of size quantization of CdS nanoparticles. *Sci. China B*. **1996**, *39*, 646-653.

21. Downs, R. T.; Hall-Wallace, M. The American mineralogist crystal structure database. *Am*. *Miner*. **2003**, *88*, 247-250.

22. Dhanam, M.; Devasia, D. P.; Kavitha, B.; Maheswari, B. Structural and optical analysis of CdS nanocrystals prepared by low temperature thermolysis. *Dig*. *J*. *Nanomater*. *Biostruct.* **2010**, *5*, 587-592.

23. Sharma, M.; Kumar, S.; Pandey, O. P. Photo-physical and morphological studies of organically Passivated core-shell zns nanoparticles. *Dig*. *J*. *Nanomater*. *Biostruct*. **2008**, *3*, 189-197.

24. Mirnaya, T. A.; Asaula V. N.; Volkov, S. N.; Tolochko, A. S.; Melnik, D. A.; Klimusheva, G. A. Synthesis and optical properties of liquid crystalline nanocomposites of cadmium octanoate with CdS quantum dots. *Phys. Chem. Sol. State*. **2012**, *13*, 131-135.

25. Yordanov, G. G.; Gicheva, G. D.; Bochev, B. H.; Dushkin, C. D.; Eiki Adachi. The effects of temperature and carboxylic acid ligand on the growth of nanocrystalline CdSe in a hot paraffin matrix. *Colloids Surf. A*. **2006,** *273*, 10-15.

26. Brus, L. E. Electronic wave functions in semiconductor clusters: Experiment and theory. *J. Phys. Chem.***1986**, *90*, *12*, 2555-2560.

27. Moloto, N; Revaprasadu, N; Moloto, M. J; O'Brien P; Raftery, J. N, N'- diisopropylthiourea and N, N'-dicyclohexylthiourea zinc(II) complexes as precursors for the synthesis of ZnS nanoparticles. S. Afr. J Sci. 2009, *105*, 258-263.

28. Nyamen, L. D.; Pullabhotla, V. S. R.; Nejo, A. A.; Ndifon, P.; Revaprasadu, N. Heterocyclic dithiocarbamates: Precursors for shape controlled growth of CdS nanoparticles. *New J. Chem*. **2011**, *35*, 1133-1139.

29. Bera, P; Kim, C.-H; Seok, S. I. High-yield synthesis of quantum-confined CdS nanorods using a dimeric cadmium(II) complex of S-benzyldithiocarbazate as single-source molecular precursor, *Solid State Sci*. **2010**, *12*, 435-532.
30. Lazell, M; O'Brien P. Synthesis of CdS nanocrystals using cadmium dichloride and trioctylphosphine sulfide. *J. Mater. Chem*., **1999**, *9*, 1381-1382.
31. Onwudiwe, D. C.; Ajibade, P. A. Zn(II), Cd(II) and Hg(II) complexes of N-methyl-N-phenyl dithiocarbamate as single-source precursors for the synthesis of metal sulfide nanoparticles. *Mater. Lett*. **2011**, *65*, 3258-3261.
32. Biswas, S.; Kar, S. Fabrication of ZnS nanoparticles and nanorods with cubic and hexagonal crystal structures: a simple solvothermal approach. *Nanotechnology*, **2008**, *19*, 045710-045720.
33. Rodriguez, P.; Munoz-Aguirre.; N, San-Martin Martinez, E.; Gonza lez de la Cruz, G.; Tomas, S. A.; Zelaya Angel, O. Synthesis and spectral properties of starch capped CdS nanoparticles in aqueous solution. *J. Cryst. Growth*, **2008**, *310*,160-164.
34. Monshi, A.; Foroughi, M. R.; Monshi M. R. Modified Scherrer equation to estimate more accurately nano-crystallite size using XRD. *World J. Nano Sci. Eng.* **2012**, *2*, 154-160.
35. Dhanam, M.; Devasia, D. P.; Kavitha, B.; Maheswari, B. Structural and optical analysis of CdS nanocrystals prepared by low temperature thermolysis. *Dig. J. Nanomater. Biostruct*. **2010**, 5, 587-592.
36. Mirnaya, T. A.; Asaula, V. N.; Volkov, S. V.; Tolochko, A. S.; Melnik, D. A.; Klimusheva, G. V. Synthesis and optical properties of liquid Crystalline Nanocomposites of Cadmium Octanoate with CdS Quantum Dots. *Physics and Chemistry of Solid State*, **2012**, *13*,131-135.
37. Revaprasadu N, Mlondo S. N. Use of metal complexes to synthesize semiconductor nanoparticles. *Pure Appl. Chem.* **2006**; *78*, 1691-1702.

38. Bochev, B.; Yordanov, G.; Room temperature synthesis of thioglycolate-coated zinc sulfide(ZnS) nanoparticles in aqueous medium and their physicochemical characterization. *Colloids Surf. A*. **2014**, *441*, 84-90.
39. Yoffe, A.D. Low-dimensional systems: quantum size effects and electronicproperties of semiconductor microcrystallites (zero-dimensional systems) andsome quasi-two-dimensional systems. *Adv. Phys*. **1993**, *42*, 173-266.
40. Chowdhury, P. S; Ghosh, P; Patra, A. Study of photophysical properties of capped CdS Nanocrystals. *J. Lumin*. **2007**, *124*, 327-322.
41. Lazell, M and O'Brien, P. Synthesis of CdS nanocrystals using cadmium dichloride and trioctylphosphine sulphide. *J. Mater. Chem*. **1999**, *9*, 1381-1382.
42. Murray, C. B.; Norris, D. J.; M. G. Bawendi, M. J. Synthesis and characterization of nearly monodisperse CdE (E = sulfur, selenium, tellurium) semiconductor nanocrystallites. *J. Am. Chem. Soc*. **1993**, *115*, 8706-8715
43. Ajibade. P. A. Onwudiwe, D. C. Moloto, M. J. Synthesis of hexadecylamine capped nanoparticles using group 12 complexes of N-alkyl-N-phenyl dithiocarbamate as single-source precursors. *Polyhedron*, **2011**, *30*, 246-252.
44. Spanhel, L.; Haase, H.; Weller, H.; Henglein, A. Photochemistry of colloidal Semiconductors. 20. Surface modification and stability of strong luminescing CdS particle. *J. Am. Chem. Soc.* **1987**, *109*, 5649-5655.
45. Denzler, D.; Olschewski, M.; Sattlera, K. Luminescence studies of localized gap states in colloidal ZnS nanocrystals. *J. Appl. Phys*. **1998**, *84*, 2841-2845.
46. Nguyen, T. T.; Nguyen-Duc, T. K.; Pham T. H.; Nguyen, H. T. Luminescence properties of Zinc nanoparticles and porous nanosphere synthesized via co-precipitation and hydrothermal route *E-J. Surf. Sci. Nanotech*. **2011**, *9*, 521-525.

47. Onwudiwe, D. C.; Ajibade, P. A. ZnS, CdS and HgS nanoparticles via alkyl-phenyl dithiocarbamate complexes as single source precursors. *Int. J. Mol. Sci.* **2011**, *12*, 5538-5551.

48. Sajanlal, P. R.; Sreeprasad, T. S.; Samal, A. A.Pradeep, T Anisotropic nanomaterials: structure, growth, assembly and functions. *Nano Rev.* **2011**, 2: 5883.

49. Khalavka, Y.; Becker, J.; So¨nnichsen, C. Synthesis of rod-shaped gold nanorattles with improved plasmon sensitivity and catalytic activity. *J. Am. Chem. Soc.* **2009**, *131*, 1871-1875.

50. Xu, W.; Wang. Y.; Xu, R.; Liang, S.; Zhang, G.; Yin, D. Synthesis and fluorescence spectrum analysis of CdS nanocrystals. *J. Mater. Sci.* **2007**, *42*, 6942-6945.

51. Sahraei, R.; Aval, G. M.; Baghizadeh, M. L.; Rachti, A.; Goudarzi, M. L.; Ara, M. Investigation of the effect of temperature on the growth mechanism of nanocrystalline ZnS thin films. *Mater. Lett*. **2008**, *62*, 4345-4348.

52. Downs, R.T.; Hall-Wallace, M. The American mineralogist crystal structure database. *Am. Miner*. **2003**, *88*, 247-250.

53. Pandey, G.; Sharma, H. K. A. New Approach of Synthesis of Micro/Nanoscale HgS Spheres. *Synthesis and React. Inorg. Met.-Org. Nano-Met. Chem*. **2010**, *40*, 312-318.

54. Yin, Y.; Xu, X.; Ge, X.; Lu, Y.; Zhang, Z. Synthesis and characterization of ZnS colloidal particles via γ-Radiation. *Radiat. Phys.Chem*. **1999**, *55*, 353-356.

55. Kole, A. K.; Kumbhakar, P. Cubic-to-hexagonal phase transition and optical properties of chemically synthesized ZnS nanocrystals. *Results Phys*. **2012**, *2*, 150-155

56. Thomas, P. J.; Christian, P.; Daniels, S.; Li, Y.; Wang, Y. S.; O'Brien, P. Nanorods of CoP, CdS, and ZnS. *Pure Appl. Chem*. **2006**, *78*, 1651-1665.

57. Calandra, P. Goffredi, M.; Liveri, V. T. Study of the growth of ZnS nanoparticles in water/AOT/n-heptane microemulsions by UV-absorption spectroscopy. *Colloids Surfaces A*. **1999**, *160*, 9-13.

58. John R.; Sasi, S. F. Optical structural and morphological studies of bean-like ZnS nanostructures by aqueous chemical method. *Chalcogenide Lett*. **2010**, *7*, 269-273.

59. Zhao, X. W.; Komuro, S.; S. Fujita, S.; Isshiki, H., Aoyagi, Y.; Sugano, T. Size control of Si nanocrystallites formed in amorphous Si matrix by Er-doping, *Mat. Sci. Engin. B*. **1998**, *15*, 154-157

60. Mehta, S. K.; Kumar, S.; Gradzielski, M. Growth, stability, optical and photoluminescent properties of aqueous colloidal ZnS nanoparticles in relation to surfactant molecular structure. *J. Colloid Interf. Sci.* **2011**, *360*, 497-507.

61. Brus, L. E. Electron-electron and electron-hole interactions in small semiconductor crystallites: the size dependence of the lowest excited electronic state. *J. Chem*. *Phys*. **1984**, *80*, 4403-4409.

CHAPTER 5

5. Synthesis and characterization of ZnS and CdS nanoparticles from 1-cyano-1-carboethoxy-2,-2-ethylenedithiolato–κS,S'–bis(N,N'-diisopropylthiourea–κS)M(II) and their nitrogen heterocyclics adducts as single source precursors (M = Zn and Cd).

5.1 Introduction

1, 1 dithiolate derivatives are chelating ligands that form stable complexes with many transition metals [1, 2]. These ligands have been known to have high affinity for metals such zinc and cadmium as this can be buttressed by the use of the ligand as scavengers for the above mentioned elements in biological media. Among these are: dithiocarbamates, xanthates with varying length of alkyl groups that have been duly reported [3, 4]. Several of these complexes have been explored as precursors for the synthesis of metal sulfide nanoparticles and thin films [5-7]. 1,1 dithiolate complexes of Zn(II) and Cd(II) are to some extent unsaturated and will react with nitrogenous ligand bases to form adducts [8, 9]. The parent complexes of the divalent transition metals with four-coordinate geometry are known to expand their coordination number by intermolecular association, or by adduct formation with solvents or appropriate ligands of equivalent litigating strength or by polymerization [10]. The propensity for increase in coordination number is exhibited by the ease with which Zn and Cd of 1, 1 dithiolate ligands react with nitrogen, oxygen sulfur and phosphorus donors [11, 12]. Original polymeric structures in 1, 1 dithiolate compounds are broken to monomeric adducts by their reaction with Lewis bases. Hence, 1, 1 dithiolate ligands form stable trigonal-bipyramidal or unstable six coordinate geometry adducts upon reaction with nitrogen based ligands. Thermolysis of heteroleptic 1, 1 dithiolate complexes give particles with non-spherical morphologies [13] and this is attributable to non-similar mechanism of formation

due to change in decomposition profile of the compounds [14]. It is worthy of note that the addition of neutral nitrogen donor ligands in the precursor complexes promotes the axial growth direction of nanoparticles or enhances the synthesis of anisotropic nanoparticles.

An insight in the thermal behaviour of metal complexes provides useful information about their potential applications [15]. Despite the fact that the products of decomposition of most chalcogenide compounds are chalcogen metals, the major drawback militating against their usage as precursor is poor volatility. One approach to enhance their performance as precursors is to form more (branched) complex compounds. The metal centers of five or six coordinate geometry of metal complexes show increased density. These adduct have thermal properties that reveals increased volatility on the addition of nitrogen donor Lewis base as ligands. Effects of pyridine and other polypyridine nitrogen donor ligands in heterocyclic derivative of 1, 1 dithiolate have been reported in literature [16, 17]. Ligands play important role in the decomposition of coordination compounds due to several properties such as volatility; basicity (the ability of donor atoms electron to interact with metals), induced inductive and mesomeric effect, number of donor atoms and the number of atoms which participate in coordinative bond [18]. Hence, this ultimately influences the decomposition profile of the compound and also enhances their use as precursor complex in the preparation of metal sulfide nanoparticles [19, 20].

Chapter 5 consists of two main sections. Section 1 is about the synthesis and characterization of 1-cyano-1-carboethoxy-2,2-ethylenedithiolato–κS,S'-bis(N,N'-diisopropylthiourea–κS)zinc(II) complexes and their nitrogen donor ligands as adducts (pyridine and polypyridine). These complexes were thermolysed at 180 ºC and used for the synthesis of four different ZnS nanoparticles; ZnS1, ZnS2 ZnS3 and ZnS4. Section 2 contains the

synthesis of the Cd(II) analogue complex of Zn(II), 1-cyano-1-carboethoxy-2,2-ethylenedithiolato–κS,S'–bis(N, N'-diisopropylthiourea–κS)cadium(II) and its nitrogen donor adducts. The three Cd(II) complexes were also used as single source precursors for the synthesis of CdS nanoparticles. Seven complexes were reported in all, in this chapter; four Zn(II) and three Cd(II) (made up of two parent complexes and 5 adducts). All the complexes were prepared from the metal salts of zinc or cadmium, diisopropyl thiourea and 1,1 dithiolate derivatives and their pyridine and two polypyridine adducts (2, 2' bipyridine and 1,10 phenanthroline).

5.1.1 Synthesis of HDA capped metal sulfides nanoparticles

0.6 g of the precursor complex, was dissolved in 7 mL of tri-n-octylphosphine (TOP) and then injected into a three-necked flask containing 6 g of hot HDA at a temperature of 180 ºC with vigorous stirring under nitrogen. A subsequent decrease in temperature of 15 - 25 ºC was observed. The solution was heated gradually and the temperature was allowed to stabilize at 180 ºC. After 60 mins, the yellowish solution obtained was allowed to cool to about 70 ºC and methanol was added to precipitate the nanoparticles. The flocculent precipitate formed was centrifuged and the supernatant was decanted, after which the isolated solid was dissolved in toluene. The above centrifugation and isolation procedure was repeated three times for the purification of the prepared cadmium sulfide nanoparticles. A similar procedure was adopted for the preparation of HDA capped ZnS and CdS nanoparticles. ZnS1, ZnS2, ZnS3 and ZnS4 are HDA capped nanoparticles obtained from the thermolysis in HDA of precursor complexes $Zn(diptu)_2(ced)]$, $[Zn(diptu)_2(ced)(py)]$, $[Zn(diptu)_2(ced)(bpy)]$ and $[Zn(diptu)_2(ced)(phen)]$ respectively while CdS1, CdS2 and CdS3 nanoparticles were equally obtained from $[Cd(diptu)_2(ced)]$, $[Cd(diptu)_2(ced)(bpy)]$ and $[Cd(diptu)_2(ced)(phen)]$ sequentially.

5. 2 Characterization of the nanoparticles from Zn(II) complex and its adducts

5.2.1 Structural studies

5.2.2 X-ray diffraction studies of the nanoparticles

Figure 5.1 represents the XRD diffraction pattern of as-prepared ZnS1, ZnS2, ZnS3 and ZnS4 nanoparticles. All the zinc sulfide nanoparticles exhibit three diffraction peaks except for ZnS2 which shows additional peaks that is suggestive of a mixture of crystalline phases. The diffraction peaks appeared at 2θ of 28.31º, 47.54º and 56.16º; 26.40º, 28.14º, 35.58º, 41.20º; 44.43º, 47.49º, 56.19º; 23.72º, 28.09º, 47.01º and 55.41º; 28.03º, 47.05º and 56.10º for ZnS1, ZnS2, ZnS3 and ZnS4 respectively. The XRD peaks were indexed by comparing the observed data with the standard JCPDF 80-0020. The 2θ values correspond to (111), (220) and (311) planes sequentially and they can be indexed to cubic phase of ZnS. ZnS2 nanoparticles from the pyridine adducts is observed to possesses additional peaks at 2θ = 26.40º, 35.58º, 41.20º that can be indexed to (002), (102) and (103) miller indices of hexagonal ZnS. It is a most likely confirmation that ZnS2 is a mixture of both cubic (zinc blende) and hexagonal (wurtzite) phase nanoparticles. Similar results have been reported in the literature [21, 22]. The broadening of the XRD peaks is due to the nanocrystalline nature of the as-prepared nanoparticles. The particle sizes were also estimated using Schereer equation from the most intense peaks. The sizes obtained are 2.3 nm, 3.7 nm 3.8 nm and 4.5 nm respectively for ZnS1, ZnS2, ZnS3 and ZnS4 respectively.

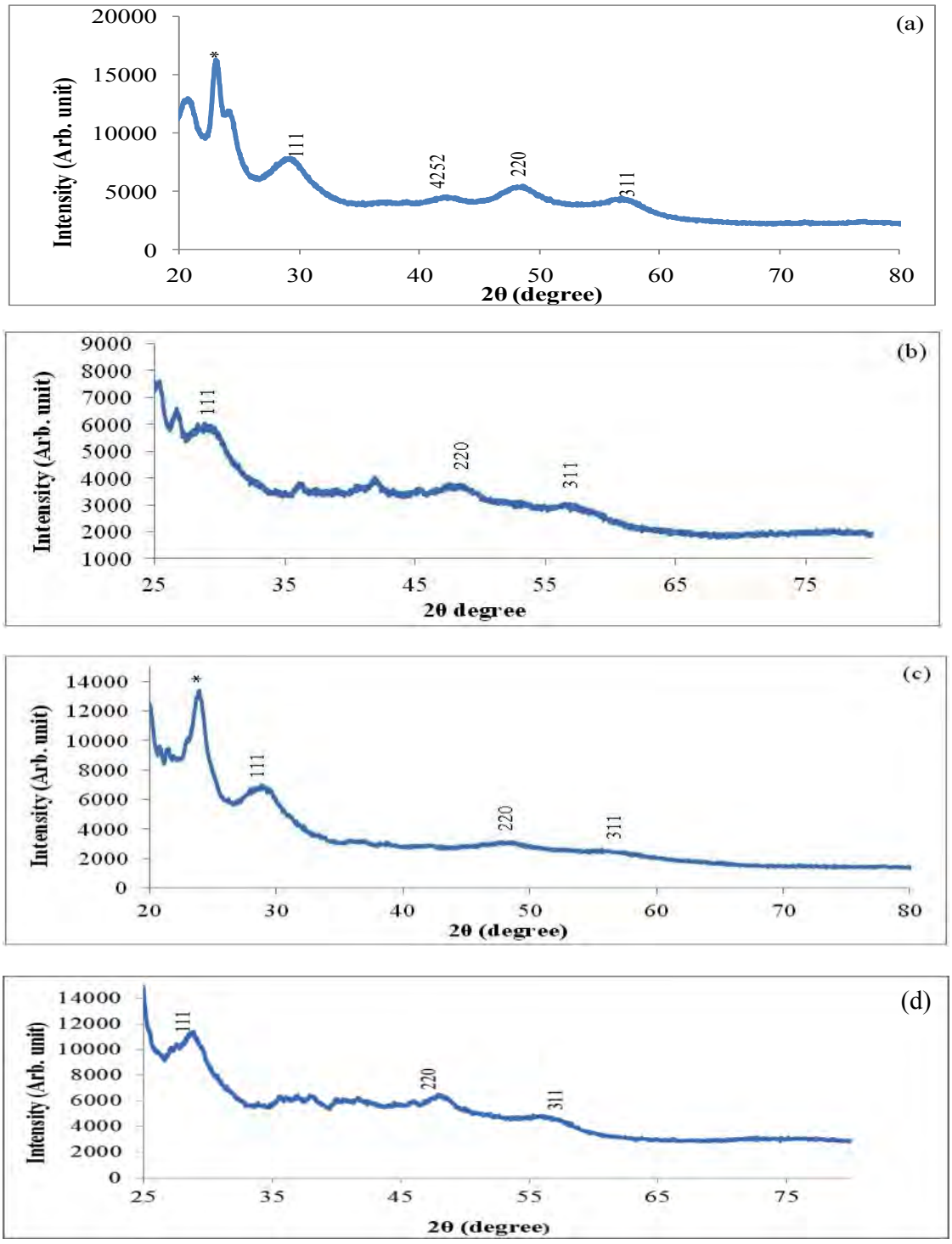

Figure 5.1: The XRD patterns of (a) ZnS1, (b) ZnS2 and (c) ZnS3 and (d) ZnS4

5.2.3 Tranmission electron microscrope (TEM) studies of ZnS nanoparticles

Typical TEM micrograph of ZnS1, ZnS2, ZnS3 and ZnS4 nanoparticles obtained from the as-prepared complexes [Zn(diptu)ced] (**10**), [Zn(diptu)ced(py)] (**11**), [Zn(diptu)ced(bpy)] (**12**), [Zn(diptu)ced(phen)] (**13**) are shown in Figure 5.2. From these micrographs, it is evident that the nanoparticles have slightly different morphologies. The ZnS1 nanoparticles, from the parent complex appear roughly spherical with particle sizes of 1.92-3.42 nm. ZnS from the pyridine adducts gave rod shaped morphology with diameter size of 2.63-3.91 nm and length of about 10.5 nm. The ZnS3 and ZnS4 from the 2, 2' bipyridine and 1, 10 phenanthroline adducts also gave anisotropic particles whose particle sizes are in the rage of 2.3-3.72 nm and 2.98-4.74 nm respectively. ZnS2 has a different morphology from the rest of the metal sulfide nanoparticles and this can be explained by the presence of pyridine which might have altered the thermal decomposition profile of the precursor complex. Similar results have been reported in the literature for CdS and ZnS nanoparticles and it is most likely that the ligand can affect the shape of nanoparticles [23, 24]. The enhacement of axial growth of the metal sulfide nanoparticles can b attributed to he incorporation of nitrogen donor ligand in the precursors of he nanoparticles [25].

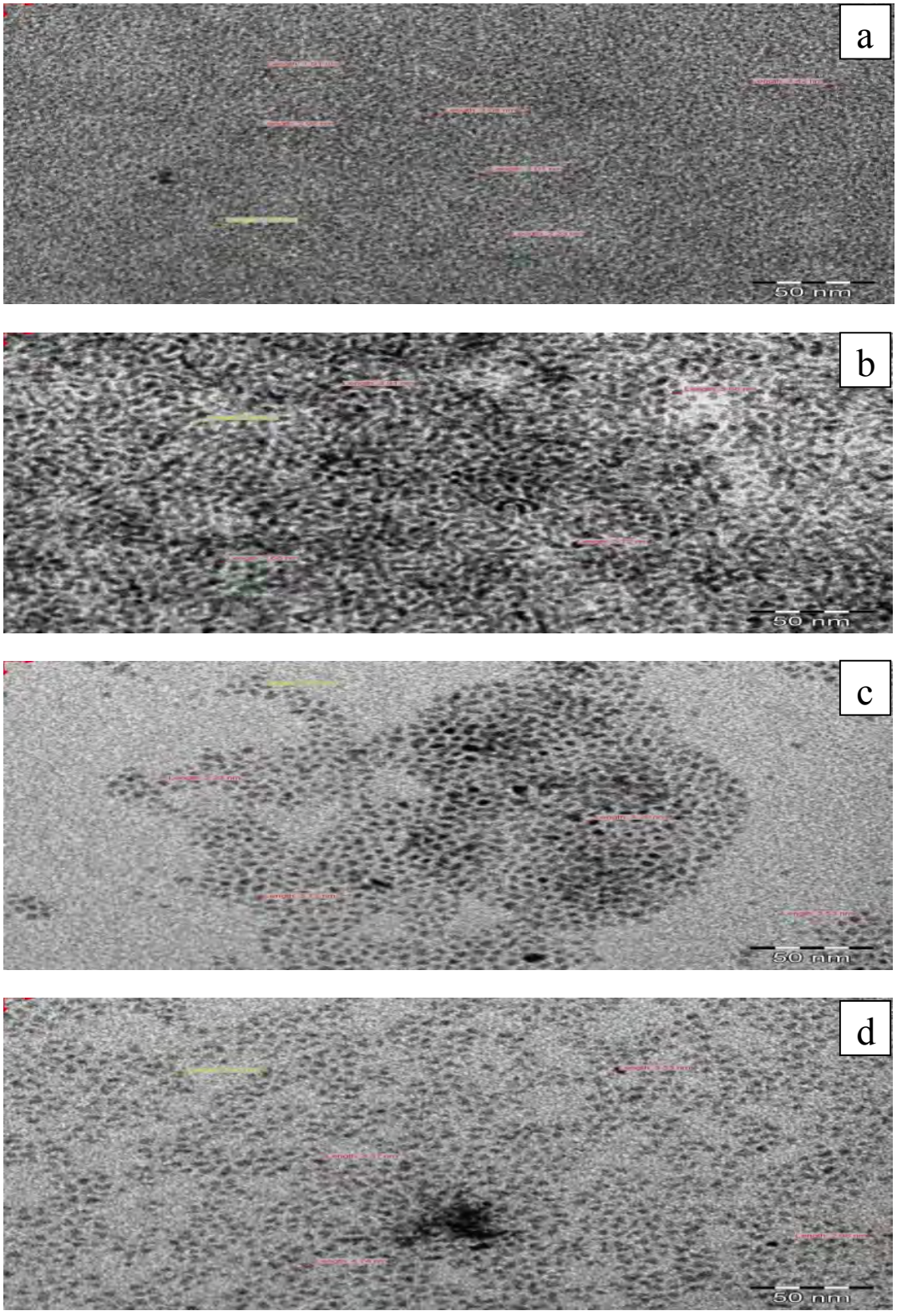

Figure 5.2: TEM micrograph of (a) ZnS1, (b) ZnS2 (c) ZnS3 and ZnS4

5.2.4 Scanning electron microscopy of ZnS nanoparticles

Figure 5.3(a-f) shows the SEM micrograph of ZnS1, ZnS2, ZnS3 and ZnS4 respectively. The monograph of ZnS1 from complex ZnS1 displayed at lower magnification while flower-like images of the nanoparticle can be observed at higher magnification. The SEM image of ZnS2 shown in Fig 5.3(b) reveals paricles that exhibit a wooly-like morphology at lower magnifications and close to flower-like (petal-like) shapes at higher magnification.

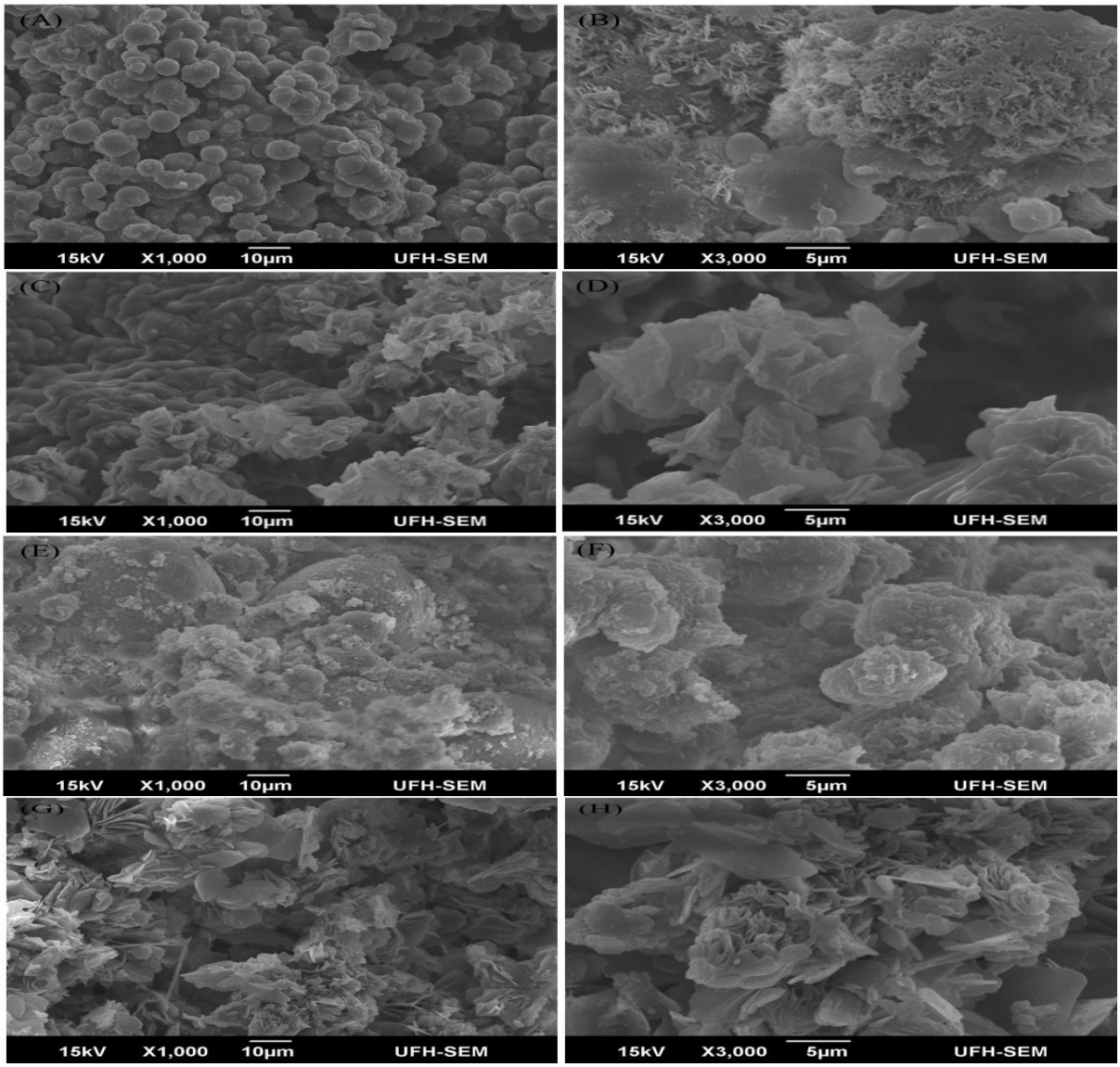

Figure 5.3: SEM micrographs of ZnS1, ZnS2, ZnS3 and ZnS4

The as-synthesized ZnS3 and ZnS4 obtained from complexes 3 and 4, polypydine adducts, displayed remarkable morphology both at the lower and higher magnification. At lower magnification, a clearly visible combination of cloud-like shapes intercalated with flower-like shapes are observed while the morphology at higher magnification is more of flowery flakes. It's worthy of note that the change to flowery morphology is more pronounced in the ZnS obtained from the adduct complexes.

5.2.5 Optical spectra of the ZnS nanoparticles

The behaviour of semiconductor nanocrystals can only be understood better with optical absorption study. The band gap which can be defined as the distance between the valence band and conduction band is an important characteristic of semiconductor materials. The optical absorption spectra of ZnS1, ZnS2, ZnS3 and ZnS4 nanoparticles in the range of 200-800 nm are shown in Figure 5.4. It is obvious that all the spectra are devoid of absorption in the visible region (800-390 nm). Absorption edge or excitonic absorption appeared at shorter wavelength in the UV region at 296, 322, 325 and 326 nm for ZnS1, ZnS2, ZnS3 and ZnS4 nanoparticles respectively. The apparent exhibition of blue shift in all the ZnS is a reflection of increase in band gap due to quantum confinment effect. Bulk ZnS being a direct band gap material has a band gap of approximately 3.66 eV [26]. The blue shift in the absorption edge corresponds to increase in effective band gap of the material. The absorption edge of the ZnS nanoparticles which is equivalent to the bandgap energy is calculated to be 4.19 eV, 3.89 eV, 3.81 eV, and 3.80 eV for ZnS1, ZnS2, ZnS3 and ZnS4 respectively. The band gap values are slightly reduced from ZnS1 to ZnS4 due to increase in the particle sizes of the metal sulfide synthesized from the various precusor complexes.

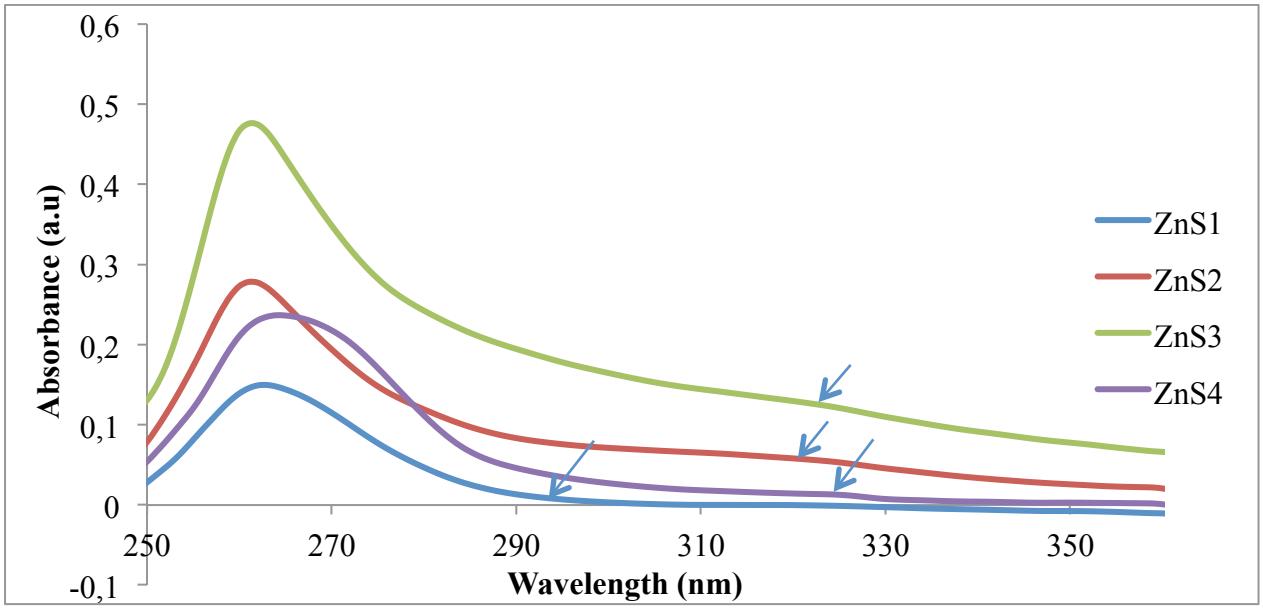

Figure 5.4: UV-Vis spectra of ZnS1, ZnS2 and ZnS3 and ZnS4

5.2.6 Photoluminescence studies of ZnS

Photoluminescence spectra of the as-prepared samples ZnS1, ZnS2, ZnS3 and ZnS4 in the range of 250 - 600 nm are shown in Figure 5.5(a). All the samples except the ZnS4 show two different emission peaks at; 296.2, 296.3, 296.5 nm for the low intensity narrow emission peaks and 384.5, 385.8 387.51 and 395.5 nm for the broad centered emision peaks of ZnS1, ZnS2, ZnS3 and ZnS4 respectively. The emission peaks around 296 nm can be ascribed to spontaneous emission orginating from band to band transition while the broad emission peaks at around 384.5 nm could emanate from surface states [27, 28]. PL with multiple emission peaks have been earlier reported in literature [29]. The inset diagram in Figure 5.4(b) contains the emission peaks that are blue shifted relative to ZnS bulk [30].

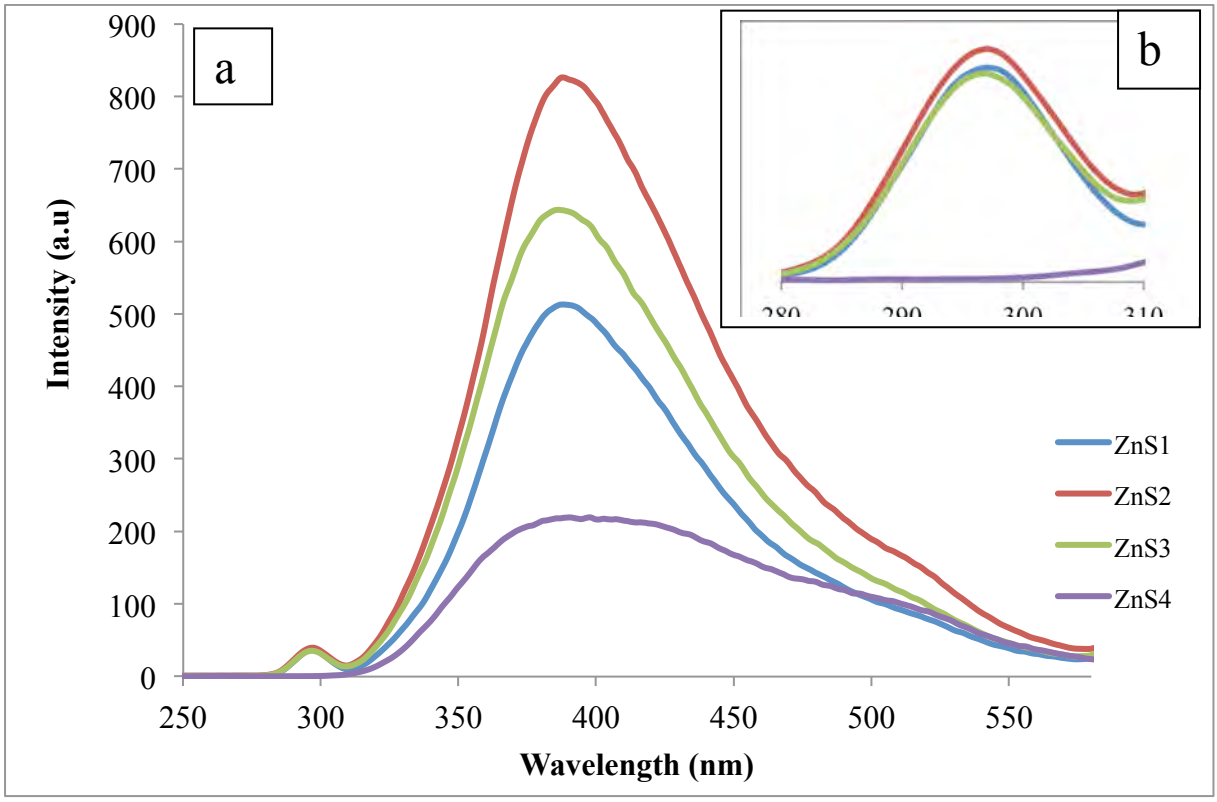

Figure 5.5: PL spectra of HDA-capped ZnS1, ZnS2, ZnS3 and ZnS4

Table 5.1: Particle sizes and band gap values of HDA-capped ZnS nanoparticles

Nanoparticles	Particle size from XRD (nm)	Particle size from TEM (nm)	Absorption peaks (nm)	Band gap Eg (eV)
ZnS1	2.3	1.91 - 2.23	296	4.19
ZnS2	3.7	2.63 - 3.91	322	3.89
ZnS3	3.8	2.23 - 3.72	325	3.81
ZnS4	4.5	2.98 - 4.75	326	3.80

5.3 Structural and optical studies of HDA capped CdS nanoparticles from [Cd(diptu)$_2$ced/N-N] (where N-N is bpy or phen)

5.3.1 X-ray diffraction studies of the CdS nanoparticles

Figures 5.6 (a), (b) and (c) show the X-ray diffractogram of HDA-capped nanoparticles synthesized from [Cd(diptu)$_2$(ced)], [Cd(diptu)$_2$(ced)(bpy) and [Cd(diptu)$_2$(ced)(phen)]. In the XRD patterns, the peaks which occurred at 2θ values of [24.56º, 26.5º, 36.95º, 44.0º, 48.2º, 52.0º], [24.13º, 26.89º, 36.63º, 44.16º, 48.29º, 52.26º], and [25.20º, 26.85 º, 28.54º, 37.36º, 44.18º, 48.32º, 52.26º] for the CdS obtained from the precursor complexes (1), (2) and (3) respectively, correspond to (1 0 0), (0, 0 2), (1 0 2), (1 1 0), (1 0 3) and (1 1 2) Miller indices. These peaks are characteristic of hexagonal CdS nanoparticles [32]. Figure 5.6(c) shows an additional peak at 2θ value of 28.54º which corresponds to Miller index for crystalline plane of (1 0 1) [33-35] and they correlate with the standard reference (JCPDS 01-080-0006). The broadness of the XRD patterns indicates small crystallite size of the sample and elongation of the XRD pattern in case of capped nanoparticles shows surface passivation [35, 37]. The average particle sizes of CdS1, CdS2 and CdS3 nanoparticles are; 5.1, 4.58 and 7.92 nm respectively as calculated from the full-width at half maximum (FWHM) of the most intense peak using Scherrer's equation [38, 39]. CdS1, CdS2 and CdS3 represents the nanoparticles obtained from the thermolysis of precursors complexes [Cd(diptu)$_2$(ced)], [Cd(diptu)$_2$(ced)(bpy) and [Cd(diptu)$_2$(ced)(phen)] respectively in HDA.

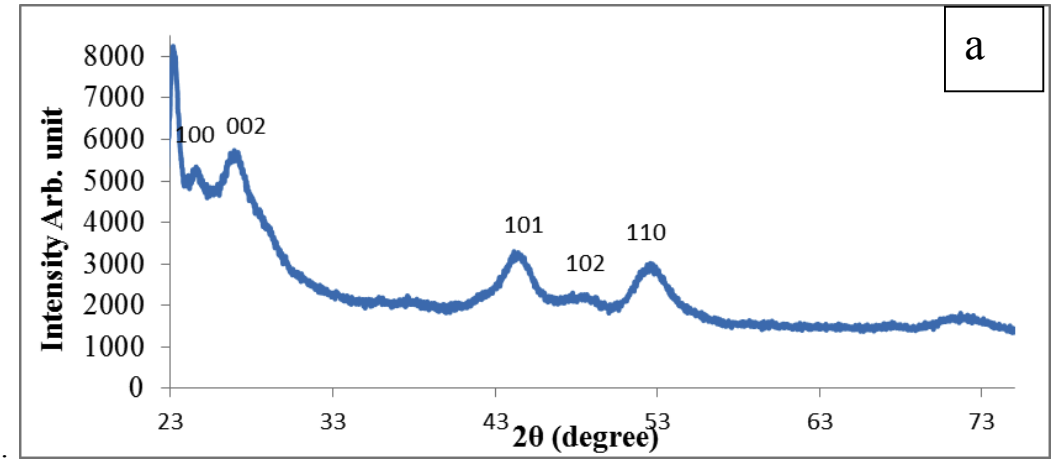

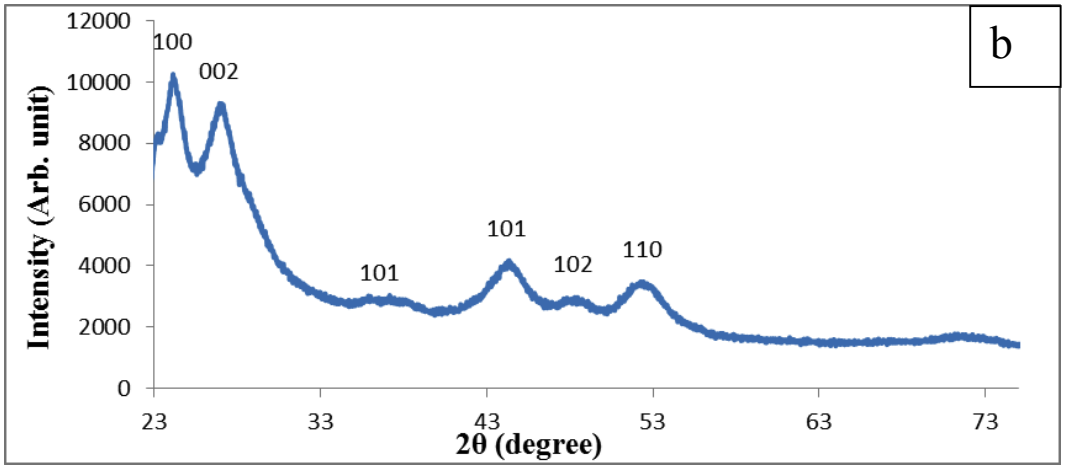

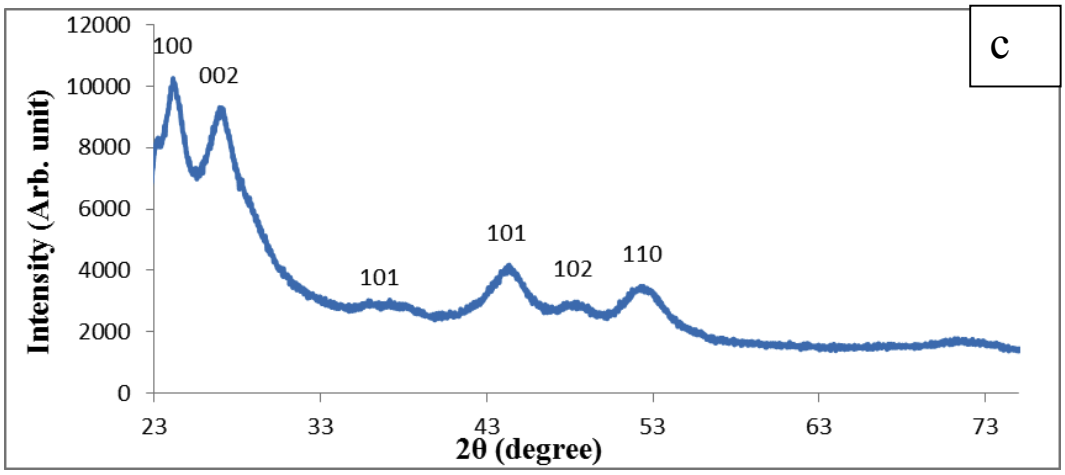

Figure 5.6: The XRD patterns of (a) CdS1, (b) CdS2 and (c) CdS3.

5.3.3 Transmission electron microscopy (TEM) studies of HDA capped CdS nanoparticles

In order to further investigate the structure of CdS nanoparticles, TEM analysis was carried out on the samples and Figure 5.7(a-c) show TEM images of CdS1, CdS2, and CdS3 respectively. The TEM micrograph showed that the as-synthesized CdS nanoparticles are monodispersed and well defined.

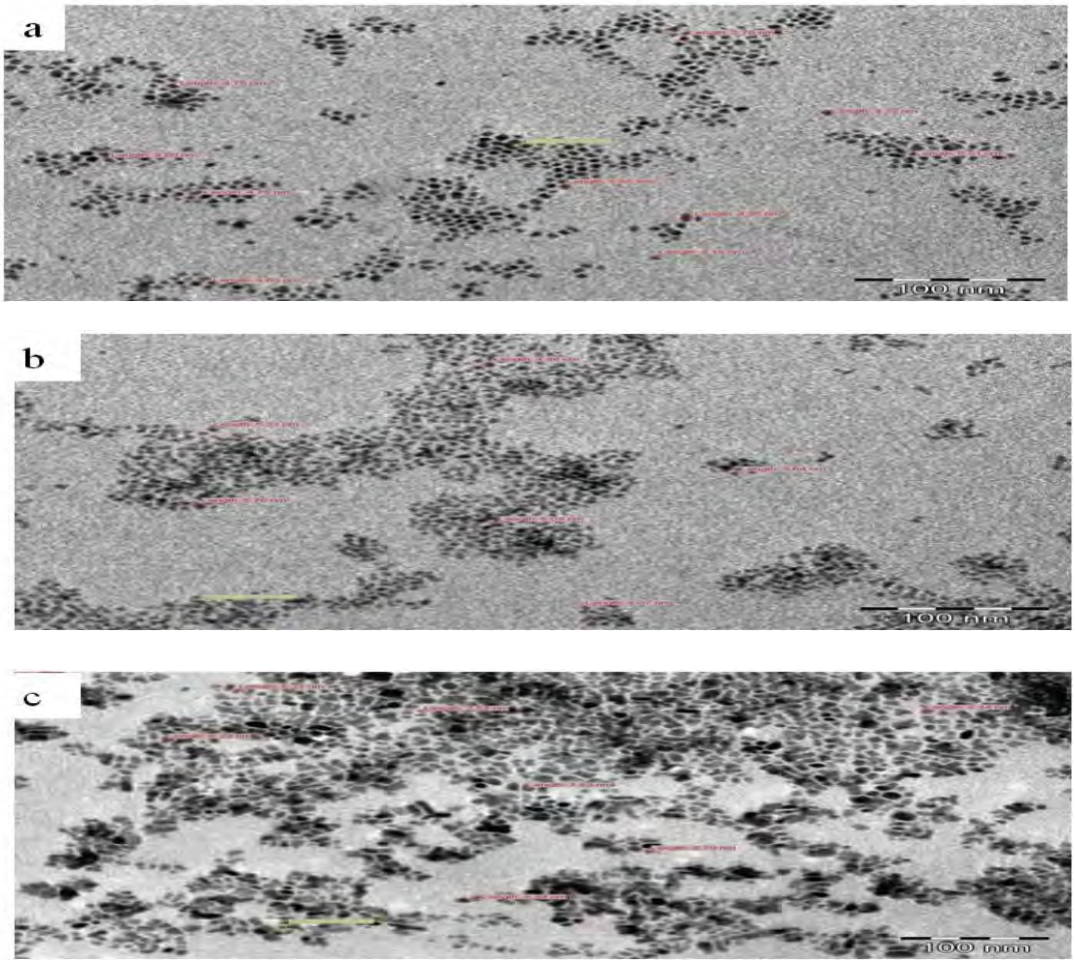

Figure 5.7: TEM micrograph of (a) CdS1, (b) CdS2 and (c) CdS3

The nanoparticles show a close to spherical morphology with a slight rod-like elongation observed in CdS3. Precursor molecules obtained from N-donor adducts has been reported to give rise to anisotropic nanoparticles [40, 41], and this has been attributed to the phenomenon of oriented attachment or self-assembly [42]. The particle sizes were estimated to be in the range 4.15 - 6.16 nm, 3.64 -7.37 nm and 5.27- 8.79 nm respectively for CdS1, CdS2 and CdS3. Nanocrystals from the CdS1 are the most monodispersed and the TEM micrograph reveals that the nanoparticle size increased in the order CdS1 < CdS2 < CdS3. The obtained TEM results indicate that the HDA-capped CdS nanoparticles were of small sizes, homogenously distributed and the particle sizes are in agreement with the size estimation obtained from the XRD analysis. There is no large dense flocs observed in the TEM images and this indicates that the prepared CdS nanoparticles were well-dispersed in the solution [43].

5. 3.4 Scanning electron microscopy (SEM) of HDA-capped CdS nanoparticles.

The surface morphology of the nanocrystals was investigated by scanning electron microscopy (SEM). SEM micrographs were taken at both lower and higher magnifications as shown in Figures 5.8 a, b and c for the CdS1, CdS2 and CdS3 respectively. The inset contains the EDX spectra. All the SEM micrograph showed smooth, spherical and regular nanoparticles shapes at lower magnification with the most pronounced aggregation obtained from CdS3 at higher magnification. The uniformity and similar dimension of the sphere reveals a good growth environment of CdS crystals, which indicate good crystallinity of the sphere [44]. The elemental compositions of the nanoparticles formed were confirmed by energy dispersive X-ray (EDX) analysis. All the 3 EDX spectra showed Cd and S peaks.

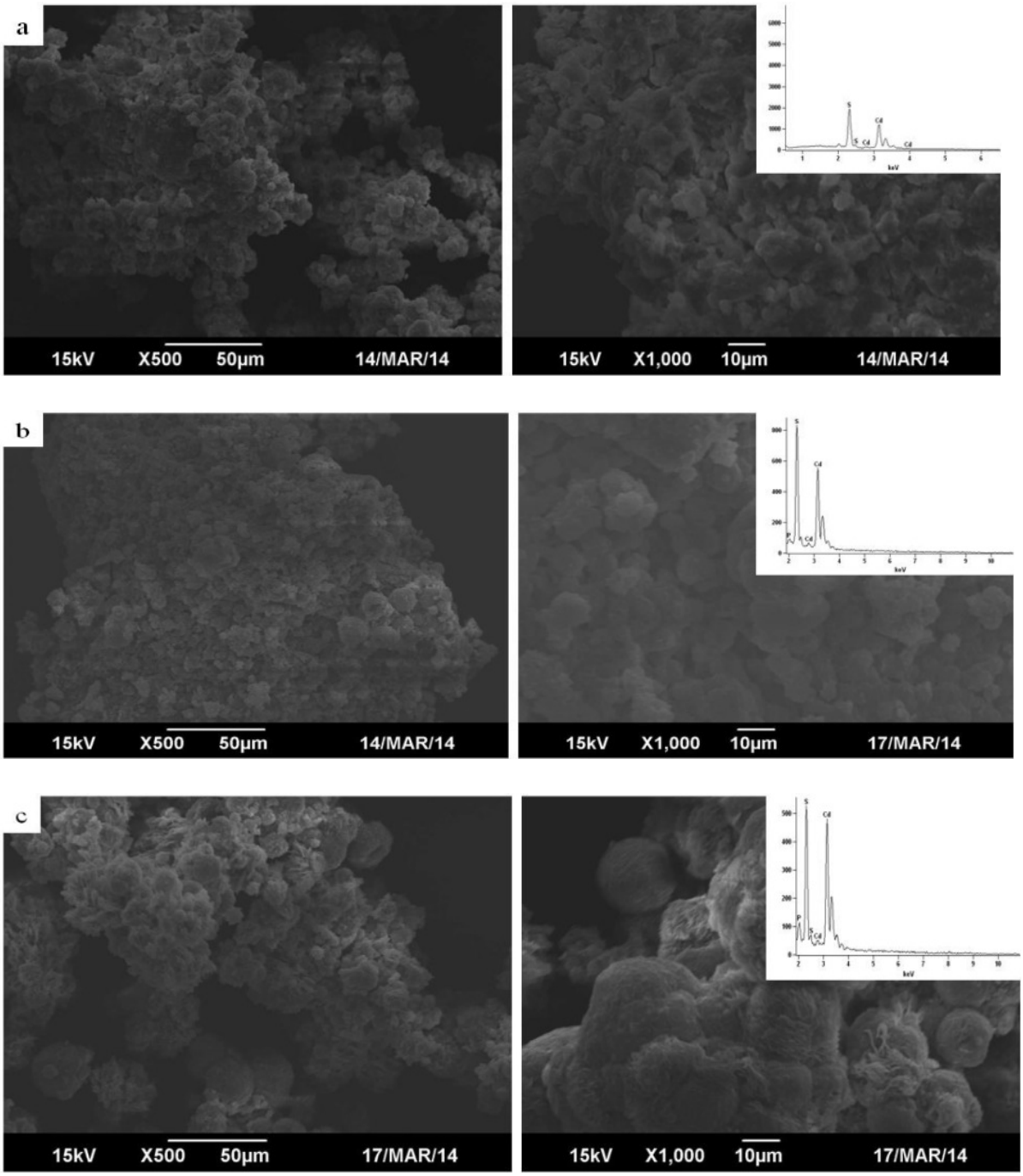

Figure 5.8: SEM and EDX inset micrograph of (a) CdS1, (b) CdS2 and (c) CdS3

5.4 Optical properties of HDA capped CdS nanopaticles

5.4.1 UV-Visible absorbance spectroscopy

The band gap of group II-VI nanoparticles lies within the UV - Visible region, and therefore, the minimum energy required to excite electron from the valence state lies in the UV-Visible region. The UV spectra of CdS1, CdS2 and CdS3 shown in Figure 5.9 and measured in toluene showed typical blue shift in the band gap energy associated with semiconductor nanoparticles. The nanoparticles showed band gap energy around 3.27 eV (379 nm); 3.26 eV (380 nm); 2.94 eV (421 nm) for CdS1, CdS2 and CdS3 respectively. The band gap of CdS bulk is 2.40 eV (515 nm) [45, 46]. The nanoparticles, CdS1, CdS2 and CdS3, showed a blue shift of 0.74, 0.73 and 0.82 eV relative to the CdS bulk which is indicative of quantum confinement in the prepared nanoparticles. The most direct way of extracting the optical band gap is to determine the photon energy at which there is a sudden increase in the absorption [47].

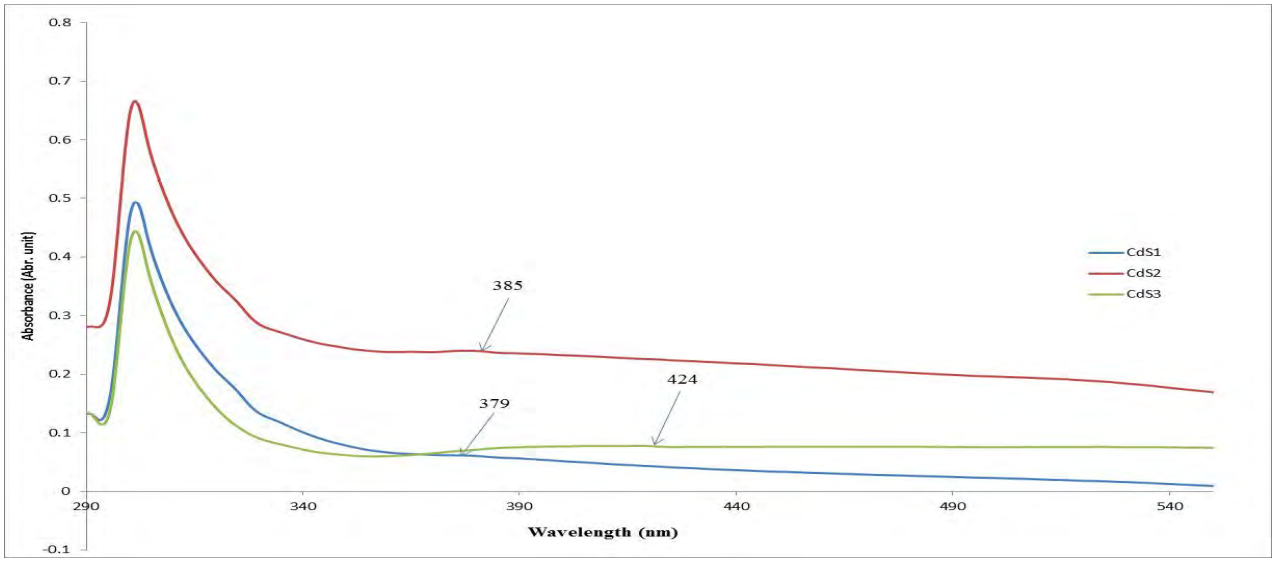

Figure 5.9: UV-Vis spectra of CdS1, CdS2 and CdS3

The optical band gap energy of nanocrystalline samples are determined from the absorption maxima and it can be calculated from the absorption peak using the simple wave equation;

$$Eg = hc/\lambda \quad \ldots\ldots (1)$$

Where Eg is band gap energy, h is the planks constant, c is the velocity of light, λ is the wavelength at which the absorption peak is obtained. From the absorption spectra of the nanoparticle samples, it could be deduced that CdS1 has the smallest size, and this is in agreement with both the TEM and XRD results. The particle size and band gap of the CdS1, CdS2 and CdS3 nanoparticles at 180 ºC are shown in table 5.2.

Table 5.2: Particle sizes and band gap values of HDA-capped CdS nanoparticles

Nanoparticles	Particle size from XRD (nm)	Particle size from TEM (nm)	Absorption peaks (nm)	Band gap - Eg (eV)
CdS1	5.1	4.15 - 6.16	379	3.27
CdS2	4.58	3.64 - 7.37	385	3.22
CdS3	7.72	5.27 - 8.79	424	2.92

5.4.2. Photoluminescence spectra of the CdS nanoparticles

The photoluminescence spectra of the three CdS nanoparticles were measured at room temperature, and at an excitation wavelength of 370 nm. The obtained spectra are shown in Figure 5.10. The peak emission maxima were observed at 380 nm for CdS1, 388 nm for CdS2 and 409 nm for CdS3. In all the as-prepared nanoparticles significant blue shifts relative to the bulk CdS, 515 nm [48], which might be due to quantum confinements are

observed. The extent of the blue shift of the HDA-capped CdS nanoparticles relative to the bulk is similar but it is worthy to note that the degree of the blue shift is in the order of ; CdS3< CdS2< CdS1. The emission peak is also broader in CdS3 than in CdS1 and CdS2 and this is indicative of particles with larger size distributions.

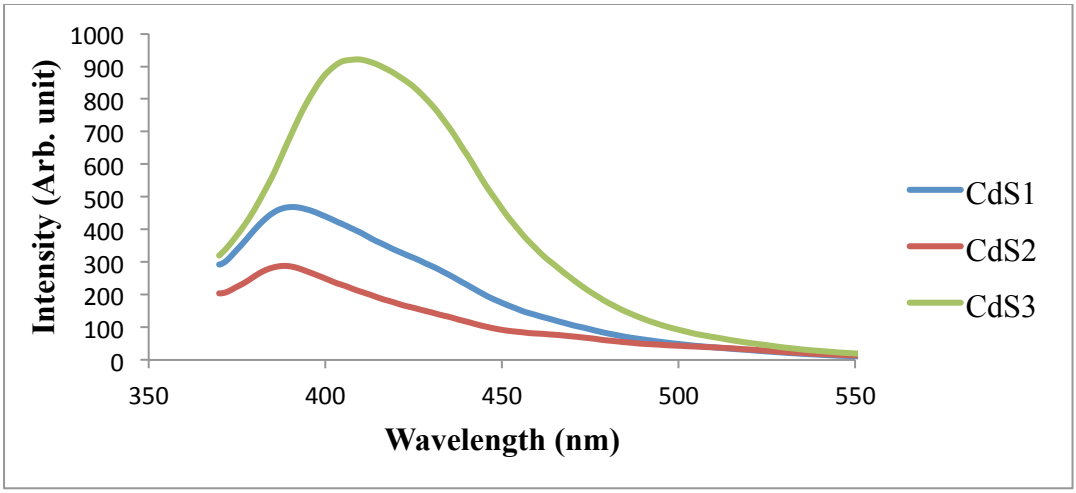

Figure 5.10: PL spectra of HDA-capped CdS1, CdS2 and CdS3.

5.4.3 Infra-red spectroscopy analysis.

To further investigate and confirm the interaction between the HDA and the CdS nanoparticles, the FTIR measurement was taken. The comparison of the spectra reveals similar features in the wave number range from 300 to 4000 cm^{-1}. Figure 5.11 shows overlapped spectra of pure HDA, the nanoparticles CdS1, CdS2, and CdS3; and the important peaks are shown in the IR spectra. In the higher wave number region, three peaks of HDA are found at 3334 cm^{-1}, 2851 cm^{-1} and 2922 cm^{-1} which correspond to ν(N-H) , νas(-CH_2-), and νs(-CH_2-). In the spectra of the nanoparticles, these peaks were found, respectively, around 3336 cm^{-1} 2851 cm^{-1}, 2933 cm^{-1} in CdS1; 3336 cm^{-1}, 2864 cm^{-1}, 2922 cm^{-1} in CdS2,

and 3338 cm^{-1}, 2852 cm^{-1}, 2922 cm^{-1} in CdS3. This examination points to the fact that HDA is indeed an essential component of CdS nanoparticles.

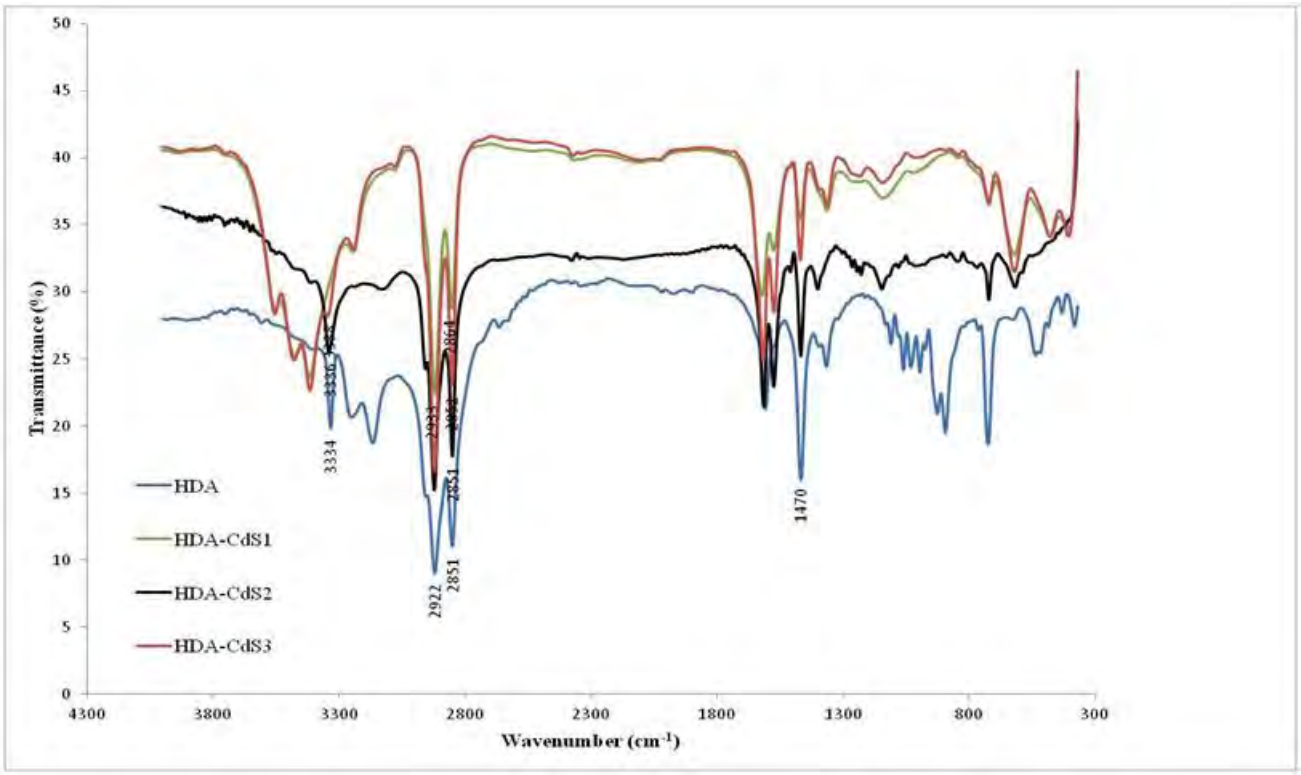

Figure 5.11: Infra-red spectra of pure HDA and HDA-capped CdS nanoparticles.

5.5 Conclusion

Two complexes and 5 pyridine and polypyridine (2, 2' bipyridine and 1,10 phenanthroline) adducts of (1-cyano-1-carboethoxyethylene-2,2-dithiolato–κS,S')–bis(N,N'-methylthiourea–κS)M(II) (where M = Zn and Cd) were prepared and all were used as single source precursors for the synthesis of HDA capped ZnS and CdS nanoparticles. The Zn(II) parent complexes, pyridine, 2,2 bipyridine and 1,10 phenanthroline adducts were thermolysed at 180 ºC. Nanorod shaped nanoparticles of ZnS were obtained from the pyridine adducts while bipyridine and 1, 10 phenanthroline adducts gave anisotropic particles. CdS1, CdS2 and

CdS3 nanoparticles prepared from the parent complex, 2,2'bipyridine and 1,10 phenanthroline respectively have different sizes which increase in the following order CdS1 < CdS2 < CdS3 (4.15 - 6.16, 3.64 - 7.37, and 5.27 - 8.79 nm). In addition, the CdS nanoparticles obtained from adducts complexes are observed to be anisotropic. All the metal sulfide nanoparticles are blue shifted in the absorption and confirms quantum confinement. Fourier transform infra-red was used to investigate the interaction between the CdS nanoparticles and the capping agent and it was confirmed the presence of HDA on the surfaces of the nanoparticle. The degree of blue shift of nanoparticles relative to the bulk material is a measure of quantum confinement of the particle. Based on this, ZnS1 and CdS1 both from the thermolyses of the parent complexes display most quantum confined metal sulfide nanoparticles.

5.6 References

1. Singh, M. K.; Das, A.; Paul, B. Synthesis and structural characterization of mixed ligand complexes of nickel(II) with 1,1-dicyanoethylene-2,2-dithiolate and some nitrogen donors. *Trans. Met. Chem*. **2005**, *30*, 655-660.
2. Ramalingam, K.; Uma, S.; Rizzoli, C.; Marimuthu. G., Supramolecular interactions in high molecular weight bisdithiocarbamate adducts of divalent Zn(II), Cd(II),and Hg(II): Spectral, VBS, and single crystal X-ray structural studies on MS_4N_2 chromophores. *J. Coord. Chem*. **2010**, *63*, 4123-4135.
3. Memon, A. A.; M. Afzaal, M.; Malik, M. A.; Nguyen, C. Q.; O'Brien P.; Raftery, J. The ***N***-alkyldithiocarbamato complexes $[M(S_2CNHR)_2]$ (M = Cd(II) Zn(II); R = C_2H_5, C_4H_9, C_6H_{13}, $C_{12}H_{25}$); their synthesis, thermal decomposition and use to prepare of nanoparticles and nanorods of CdS. *J. Dalton Trans*. **2006**, 4499-4505.
4. Abdelhady, L.; M. Afzaal, M.; Malik, MA.; O'Brien, P. Flow reactor synthesis of CdSe, CdS, CdSe/CdS and CdSeS nanoparticles from single molecular precursor(s). *J. Mater. Chem*. **2011**, *21*, 18768-18775.
5. Pradhan, N.; Katz B.; Efrima S. Synthesis of high-quality metal sulfide nanoparticles from alkyl xanthate single precursors in alkylamine solvents. *J. Phys. Chem. B*, **2003**, *107*, 13843-13854.
6. Dar, S. H.; Thirumaran, S.; Selvanayagam, S. Synthesis, spectral and X-ray structural studies on Hg(II) dithiocarbamate complexes: A new precursor for HgS nanoparticles. *Polyhedron*. **2015**, *96*, 16-24.
7. Hollingsworth, N.; Roffey, A.; Islam, H. U.; Mercy, M.; Roldan, A.; Bras, W.; Wolthers, M.; Richard, C.; Catlow, A.; Sankar, G.; Hogarth, G.; Leeuw, H. N. Active nature of primary amines during thermal decomposition of nikel dithiolates to nickel sulfide nanoparticles. *Chem. Mater*. **2014**, *26*, 6281-6292.

8. Srinivasan, N.; Thirumaran, S.; Ciattini, S. Preparation of ZnS nanosheets from (2,2'-bipyridine)bis(1,2,3,4-tetrahydroquinolinecarbodithioato-S,S')zinc(II) Spectrochim. Acta Part A Mol. Biomol. Spectrosc. **2013**, *102*, 263-268
9. Srinivasan, N.; Thirumaran S. Synthesis of ZnS nanoparticles from pyridine adducts of zinc(II) dithiocarbamates. C. R. Chimie. **2014**, *17*, 964-970.
10. Prakasam, B. A.; Ramalingam, K; Bocelli, G.; Cantoni, A. Spectral, BVS, and thermal studies on bisdithiocarbamates of divalent Zn, Cd, and their adducts: Single crystal X-Ray structure redetermination of (diiodo) (tetraethylthiuramdisulfide)mercury(II), [Hg(tetds)I_2]. *Phosphorus*, *Sulfur Silicon Relat*. *Elem*. **2009**, *184*, 2020-2033.
11. Hogarth, G; **(2005)** Transition Metal Dithiocarbamates: 1978-2003. *Prog Inorg Chem* , 53, 71-561.
12. Tiekink, E. T. R.; Haiduc, I. Stereochemical aspects of metal xanthates complexes: Molecular structures and supramolecular self-assembly. *Prog. Inorg. Chem*. **2005**, 5*4*, 127-319.
13. Onwudiwe, D. C.; Ajibade, P. A. ZnS, CdS and HgS nanoparticles via alkyl-phenyl dithiocarbamate complexes as single source precursors. *Int. J Mol. Sci.* **2011**, *12*, 5538-5551.
14. Nyamen, L. D.; Pullabhotla, V. S. R.; Nejo, A. A.; Ndifon, P.; Revaprasadu, N. Heterocyclic dithiocarbamates: Precursors for shape controlled growth of CdS nanoparticles. *New J. Chem*. **2011**, *35*, 1133-1139.
15. Onwudiwe, D. C.; Ajibade, P. A. Thermal Studies of Zn(II), Cd(II) and Hg(II) complexes of some *N*-alkyl-*N*-phenyl-dithiocarbamates. *Int. J. Mol. Sci.* **2012**, *13*, 9502-9513.
16. Subha, P. V.; Valarmathi, P.; Srinivasan, N.; Thirumaran, S.; Saminathan, K. Effect of size of metal ion on MS_4N_2 chromophore: Synthesis, spectral and single crystal X-ray structural studies on (2,2′-bipyridine)bis(*N*-cyclohexyl-*N*-methyldithiocarbamato)M(II) (M = zinc, cadmium). *Polyhedron*. **2010**, *29*, 1078-1082.

17. Chunggaze, M.; Malik, M.A.; O'Brien, P. Deposition of cadmium sulphide thin films from the single-source precursor bis(diethylmonothiocarbamato)cadmium(II) by low-pressure metalorganic chemical vapour deposition. *Adv. Mater. Opt. Electron*. **1997**, *7*, 311-316.
18. Carp, O. The influence of the ligands on the thermal behavior of solid coordination compounds. *Rev. Roum. Chim*. **2006**, *51*, 479-489.
19. Chunggaze, M.; Malik, M. A.; O'Brien, P. Deposition of cadmium sulphide thin films from the single-source precursor bis(diethylmonothiocarbamato)cadmium(II) by low-pressure metalorganic chemical vapour deposition. *Adv. Mater. Opt. Electron*, **1998**, *7*, 311-316.
20. O'Brien, P.; Otway, D. J.; Walsh, J. R. Novel precursors for the growth of α-In_2S_3: trisdialkylthiocarbamates of indium. *Thin Solid Films*. **1998**, *315*, 57- 61.
21. Kole, K. K.; Kumbhakar, P. Cubic-to-hexagonal phase transition and optical properties of chemically synthesized ZnS nanocrystals. *Results Phys*. **2012**, *2*, 150-15
22. Moloto, N.; Revaprasadua, N; Moloto, M. J.; O'Brien, P.; Raftery, J. N, N'-diisopropylthiourea and N, N'-dicyclohexylthiourea zinc(II) complexes as precursors for the synthesis of ZnS nanoparticles. *S. Afr. J. Sci.* **2009**, *105*, 1-7.
23. Srinivasan, N.; Thirumaran, S. Effect of pyridine as a ligand in precursor on morphology of CdS nanoparticles. *Superlattices Microst*. **2012**, *51*, 912-920
24. Srinivasan, N.; Thirumaran, S. Synthesis of ZnS nanoparticles from pyridine adducts of zinc(II) dithiocarbamates. *C. R. Chim*. **2014**, *17*, 964-970
25. Yan, P. Xie, Y.; Qian Y.; Liu, X. A cluster growth route to quantum-confined CdS nanowires *Chem*. *Commun*. **1999**, 1293-1294.
26. Balantseva, E.; Berlier, G.; Camino, B.; Lessio, M.; Ferrari, M. A. Surface properties of ZnS nanoparticles: A combined DFT and experimental study. *J. Phys. Chem*. C, **2014**, *118*, 23853-23862.

27. Yang, P.; Lu, M.; Xu, D.; Yuan, D.; Zhou, G. Photoluminescence properties of ZnS nanoparticles co-doped with Pb^{2+} and Cu^{2+}. *Chem*. *Phys*. *Lett*. **2001**, *336*, 768-80.

28. Ding, J. X.; Zapien J. A.; Chen, W. W.; Liftshitz, Y.; Lee, T. Lasing in ZnS nanowires grown on anodic aluminium oxide templates. *Appl. Phys. Lett*. **2004**, *85*, 2361-2363.

29. Tiwary, C. S.; Kumbhakar, P. A.; Mondal, K.; Mitra, A. K. Synthesis and enhanced green photoluminescence emission from BCT ZnS nanocrystals. *Phys. Status Solidi A*. **2010**, *207*, 1874-1879.

30. Zhang, Y.; Li, Y. Synthesis and characterization of monodisperse doped ZnS nanospheres with enhanced thermal stability. *J*. *Phys*. *Chem*. *B*. **2004**, *108*, 17805-17811.

31. Nandakumar, P.; Vijayan, C.; Dhanalakshmi, K.; Sundararajan, G.; Nair, P. K.; Murti, Y. V. G. S. Synthesis and characterization of CdS nanocrystals in a perfluorinated ionomer (Nafion). *Mater*. *Sci. Eng*. *B*, **2001**, *83*, 61-65.

32. Dhanam, M.; Devasia, P. D.; Kavitha, B Maheswari, B. Structural and optical analysis of CdS nanocrystals prepared by low temperature thermolysis. *Dig J. Nanomater. Bios*. **2010**, *5*, 587-592.

33. Lee, H. L.; Issam, A. M.; Belmahi, M.; Assouar, M. B.; Rinnert, H.; Alnot, M. Synthesis and characterizations of bare CdS nanocrystals using chemical precipitation method for photoluminescence application. *J*. *Nanomater*. **2009**, *914501*, 1-10.

34. Biswas, K.; Rao, C. N. R. Use of ionic liquids in the synthesis of nanocrystals and nanorods of Semiconducting metal chalcogenides. *Chem. Eur. J.* **2007,** *13*, 6123-6129.

35. Zhang, W. M.; Sun, Z. X.; Hao, W.; Su, D.W.; David, J.; Vaughan, D. J. Synthesis of size tuneable cadmium sulfide nanoparticles from a single source precursor using ammonia as the solvent. *Mater*. *Res*. *Bull*. **2011**, *46*, 2266-2270.

36. Sharma, K.; Kumar, S.; Pandey, O. P. Studies of 2 - mercaptoethanol passivated ZnS core-shell nanoparticles. *Optoelectron*. *Adv*. *Mat*.*-Rapid Commun*. **2008**, *2*, 881-885.

37. Dhanam, M.; Devasia, D. P.; Kavitha, B.; Maheswari B. Structural and optical analysis of CdS nanocrystals prepared by low temperature thermolysis. *Dig. J. Nanomater. Biostruct.* **2010**, *5*, 587-592.

38. Rodriquez, P.; Munoz-Aguirre, P.; San-Martin, M. E.; Cruz, G. G.; Tomas, S. A.; Angel, O. Z. Synthesis and spectral properties of starch capped nanoparticles in aqueous solution. *J. Cryst. Growth.***2008**, *310*, 160-164.

39. Murugadoss, G.; Synthesis and optical characterization of PVP and SHMP-encapsulated Mn^{2+}-doped ZnS nanocrystals. *J. Lumin.* **2010**,*130*, 2207-2214.

40. Srinivasan, N.; Thirumaran, S. Effect of pyridine as a ligand in precursor on morphology of CdS nanoparticles. *Superlattice and Microst*. **2012**, *51*, 912-920

41. Onwudiwe, D. C.; Strydom, C A.; Oluwafemi, O. S. Effect of some nitrogen donor ligands on the optical and structural properties of CdS nanoparticles: *New J. Chem*. **2013**, *37*, 834-842.

42. Onwudiwe, D. C.; Strydom, C. A.; Oluwafemi, O. S.; Hosten, E.; Jordaan, A. Synthesis, spectral and thermal studies of pyridyl adducts of Zn(II) and Cd(II) dithiocarbamates, and their use as single source precursors for ZnS and CdS nanoparticles. *Dalton Trans*. **2014**, *43*, 8703-8712.

43. Qi, L.; Colfen, H.; Antonietti, M. Synthesis and characterization of CdS nanoparticles stabilized by double-hydrophilic block copolymers. *Nano. Lett.* **2001**, *1*, 61-65.

44. Gajanan, P., Sharma, H. K. A new approach of synthesis of micro/nanoscale HgS spheres. *Synth. React. Inorg. Met.-Org. Nano-Met. Chem*. **2010**, *40*, 312-318.

45. Bera, P.; Kim, C-H.; Seok, S.I. High-yield synthesis of quantum-confined CdS nanorods using a dimeric cadmium(II) complex of S-benzyldithiocarbazate as single-source molecular precursor. *Solid State Sci.* **2010**, *12*, 435-532.

46. Brus, L. E. A simple model for the ionization potential, electron affinity, and aqueous redox potentials of small semiconductor crystallites. *J. Chem. Phys*. **1983**, *79*, 5566-5571.

47. Gupta, P.; Ramrakhiani, M. Influence of the particle size on the optical properties of CdSe nanoparticles. TONANOJ. **2009**, *3*, 15-19.

48. Xu, W.; Wang, Y.; Xu, R.; Liang, S.; Zhang, G.; Yin, D. Synthesis and fluorescence spectrum analysis of CdS nanocrystals. *J. Mater. Sci*. **2007**, *16*, 6942-6945.

CHAPTER 6

6. Synthesis and structural studies of ZnS and CdS polymer nanocomposites

6.1 Introduction

A nanocomposite is the fusion of two or more different materials in which at least one of the components has dimensions less than 100 nm [1]. In polymer nanocomposites, the blends consist of organic polymer matrix and inorganic components (semiconductors). The lack of satisfactory mechanical, thermal and electronic properties of the conventional polymer materials gave rise to the need to functionalize them in an attempt to improve their properties and extend their potential applications [2, 3]. Polymethyl methacrylate (PMMA), poly(vinyl alcohol) (PVA), and polyvinyl pyrrolidone (PVP) are among the most widely used polymers in the synthesis of nanocomposites because of their availability and low cost [4 - 7]. Among group II-VI compound semiconductor nanoparticles, ZnS and CdS are the most promising materials [8]. A lot of studies have been expanded on ZnS and CdS polymer nanocomposites with trendy focus on electrical conductivity but contrarily, little investigation is conducted about the thermal stability of these composites [9-13]. Despite the essential electrical conductivity of these materials, thermal stability of the polymer nanocomposites is uncompromisable; it is important as it modify the polymer properties to be tapped for advance applications.

The two common routes for the synthesis of polymer nanocomposites are the ex-situ and in-situ methods [14-16]. The two methods are liquid based, and the end products are solids which are obtained by either co-precipitation or solvent evaporation [17]. The synthesis of

MS/PMMA or PVA or PVP where (M = Zn or Cd) via different chemical and physical routes have been reported by many authors [18 - 22]. However, there is no report on comparative studies of the structural properties and thermal stability of the nanocomposites of ZnS/CdS nanoparticles in PMMA, PVA and PVP. In this chapter, the synthesis, structural and thermal properties of different polymer nanocomposites prepared by the incorporation of ZnS and CdS into the matrices of theses polymers; poly(methyl methacrylate) (PMMA), poly(vinyl alcohol) (PVA) and polyvinypyrrolidone (PVP) are reported. The structural studies of the metal sulfides/polymer nanocomposites was carried out by X-ray diffraction (XRD), Fourier transform infrared spectroscopy, Ultraviolet–visible spectroscopy (UV-vis), transmission electron microscopy (TEM) and thermogravimetric analysis (TGA).

6.2 Experimental

6.2.1 Synthesis of nanocomposites

The ZnS and CdS nanoparticles were synthesized as reported in the literature [23]. The ZnS and CdS nanoparticles in PMMA, PVA and PVP were prepared by a solution casting method [24]. Laboratory grade PMMA, PVA and PVP were respectively dissolved in toluene and stirred for 2 h, followed by the addition of 8 weight % of ZnS or CdS nanoparticles dissolved in the same solvent and added to the polymers solution. The choice of 8 weight % is the concentration of modifiers that exhibits appreciable properties to justify the purpose of the study. The mixture was stirred at 60 ºC for 24 h, to allow the reaction of the nanoparticles with the polymers and poured into petri dishes to give the various nanocomposites. The toluene was allowed to evaporate slowly over a period of 48 h in dry atmosphere. The film was then removed and dried in the vacuum at 70 ºC [25, 26].

6.3 Results and discussion

6.3.1 FTIR spectra studies

Figure 6:1(a) shows the overlapped FTIR spectra of pure PMMA and the respective nanocomposites incorporating ZnS and CdS nanoparticles. The graphs are rescaled to allow overlapping. Pure PMMA and the corresponding ZnS and CdS nanocomposites show a weak band in the range of 3448 - 3455 cm^{-1} that is due to stretching vibration of O-H. PMMA exhibits bands around 2952 and 2823 cm^{-1} that are assigned to C-H asymmetric and symmetric stretching vibrations respectively. The bending vibrational bands of the methyl group appear around 1490 cm^{-1} and 1457 cm^{-1} [27]. Furthermore, there is a sharp and intense band at 1769 cm^{-1} which is attributed to the stretching vibration of the carbonyl, C=O. The ZnS/PMMA and CdS/PMMA nanocomposites showed stretching vibrations with no significant difference from the pure PMMA and this is indicative of weak chemical interactions between the host polymer and the nanoparticles. Similar studies about the interaction of PMMA and nanoparticles have been reported by other researchers [28]. HDA was used as a passivating agent for the metal sulfide nanoparticles and peaks in the region of 3181-3336 cm^{-1} can be ascribed to the N-H stretching of primary amine. These peaks are observable in the infra-red absorption spectra of the nanocomposites and it's indicative of the presence of HDA [29, 30].

Figure 6.1(b) presents the overlapped FTIR spectra of pure PVA, and the respective composites with ZnS and CdS nanoparticles. PVA exhibits a broad band at 3429 cm^{-1} which is assigned to O-H stretching frequency of the hydroxyl group. This band has been shifted to 3425 and 3424 cm^{-1} in ZnS/PVA and CdS/PVA respectively.

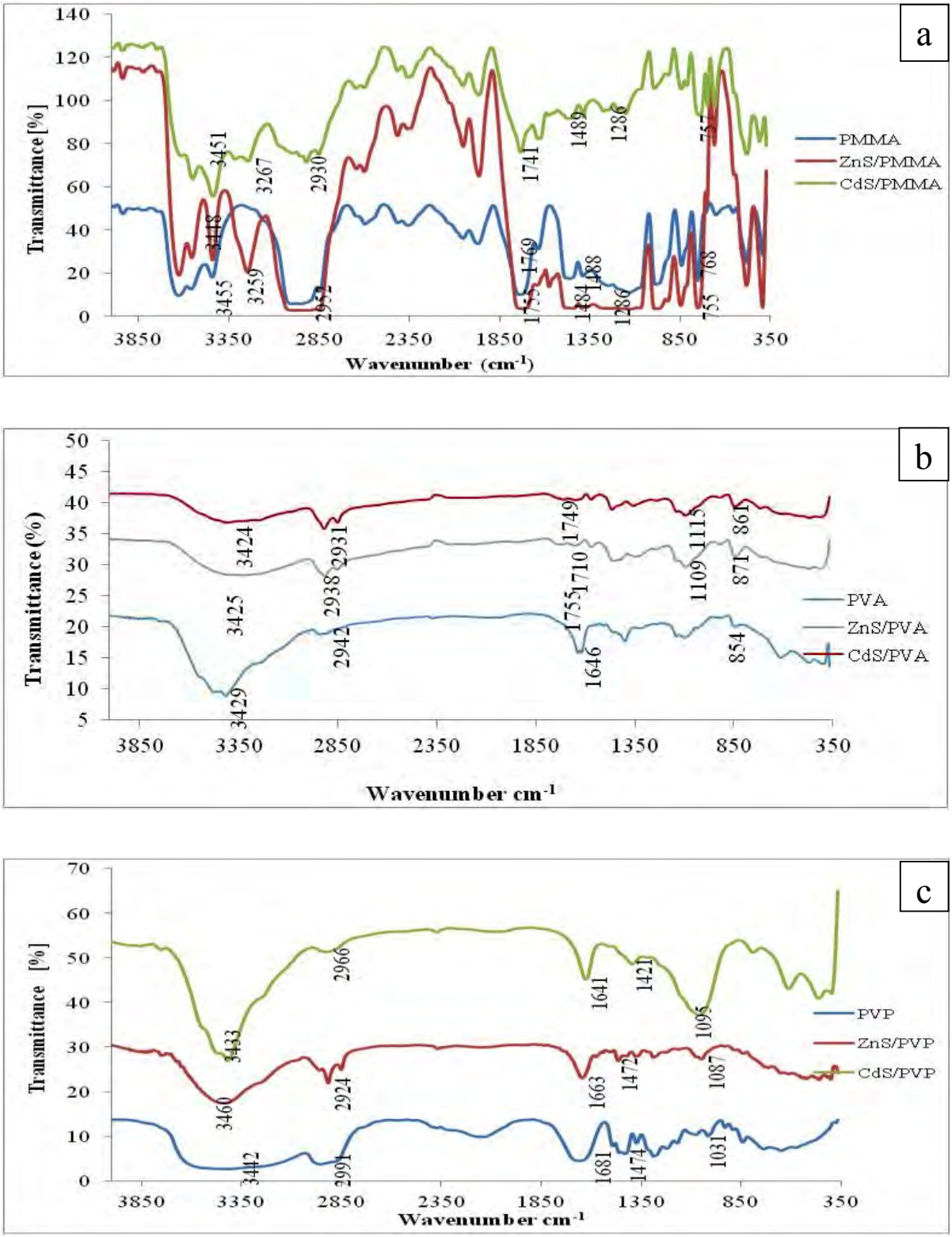

Figure 6.1: FTIR spectra of (a) pure PMMA, ZnS/PMMA, CdS/PMMA, (b) pure PVA, ZnS/PVA, CdS/PVA, (c) pure PVP, ZnS/PVP, CdS/PVP.

Two bands observed in the pure PVA at 2942, 1755 cm^{-1} which correspond to C-H and C=O stretching vibrations respectively are found at 2938, 1710 cm^{-1} and 2931, 1749 cm^{-1} in ZnS/PVA and CdS/PVA polymer nanocomposites. The vibration band at 1646 cm^{-1} due to C=C stretching in the PVA appears at 1659 and 1653 cm^{-1} in the ZnS/PVA and CdS/PVA nanocomposites respectively. The observation of characteristic bands of PVA in ZnS/PVA and CdS/PVA confirm the interaction between these semiconductor inorganic nanoparticles and PVA. Similar results have also been reported for ZnS/PVA [31] and CdS/PVA [32].

The interactions between the nanoparticles and the PVP, host polymer, were also investigated. Figure 6.1(c) shows the overlapped spectra of PVP and their respective nanocomposites. In the FTIR spectrum of PVP, the band at 1681 cm^{-1} is due to the C=O stretching mode and after the formation of ZnS/PVP and CdS/PVP nanocomposites the C=O stretching band appear at 1663 and 1641 cm^{-1}. The 17 and 40 cm^{-1} shift observed indicates a strong interaction between the nanoparticles and the PVP host. The band in the region of 1500 - 1300 cm^{-1} is fairly strong and this is because of the contribution from the in-plane C-H bending of different -CH_2 and -CH moieties. Most likely the C-H bending modes are coupled with C-N stretching modes. The existences of strong interactions between ZnS or CdS with PVP have also been reported before [33, 34].

6.3.2 Thermal analysis of PMMA and nanocomposites

The thermogravimetric analysis (TGA) of the pure PMMA, the ZnS/PMMA and CdS/PMMA nanocomposites are presented in Figures 6.2(a-c) respectively. The thermal degradation of PMMA occurs in three stages, as inferred from the DTG graph. The degradation of PMMA

usually begins with the initiation at the weak head- to- head linkage at 171.56 ºC [35], and this has been observed in Figure 6.2(a).

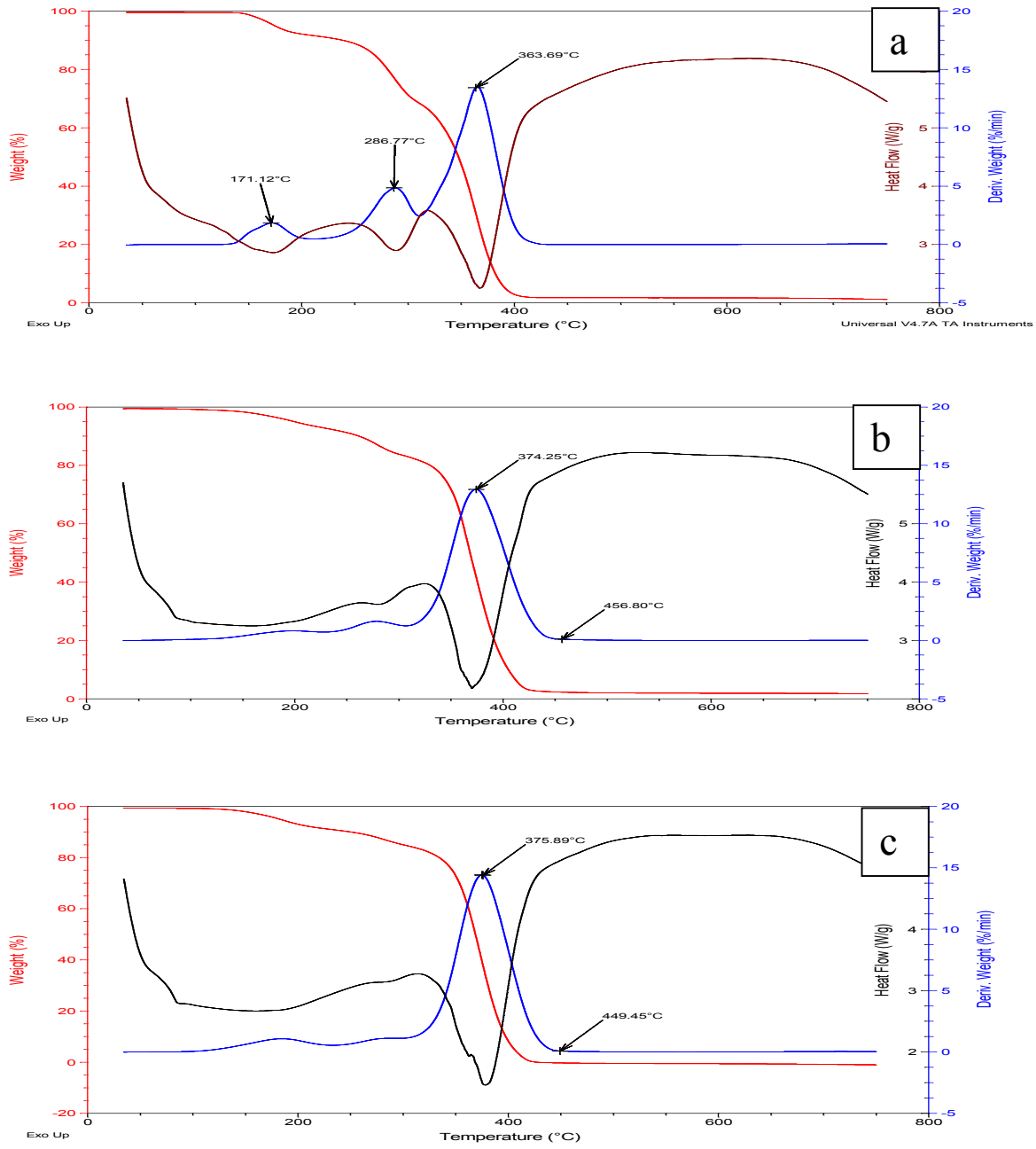

Figure 6.2: Overlapped TGA, DTG and DSC of (a) pure PMMA, (b) ZnS/PMMA and (c) CdS/PMMA.

Hence the first stage of weight loss is due to the head-to-head scission of the unsaturated end group [36]. The last two degradations occurred at 286.94 ºC and 363.32 ºC which can be ascribed to the initiation at the unsaturated end and at the polymer backbone respectively [37]. The nanocomposites, ZnS/PMMA and CdS/PMMA displayed different degradation temperatures as shown in the maximum decomposition temperature of the last stage which appeared in pure PMMA at 363.32 ºC, occurred at 374.25 and 375.89 ºC in ZnS/PMMA and CdS/PMMA respectively. The major weight loss in PMMA occurred within the range of 180 - 380 ºC which is in agreement with the structural decomposition of the polymer [36]. On the other hand, the decomposition of ZnS/PMMA nanocomposites occurred over the range of 180 - 420 ºC and 180 - 425 ºC for the CdS/PMMA nanocomposites. The DSC shows three endothermic peaks in pure PMMA which correspond to three degradation stages while three endothermic peaks are observed in ZnS/PMMA and only one in CdS/PMMA. Thus, the thermal stability of both polymer nanocomposites is greater than that of the pure polymer matrix. The thermal stability of the PMMA has been improved by the incorporation of ZnS and CdS separately into the polymer matrix.

6.3.3 Thermal analysis of PVA and nanocomposites

Figure 6.3(a-c) presents the overlapped TGA and DTG curves of the pure PVA, ZnS/PVA and CdS/PVA nanocomposites. There are three stages of weight loss in the degradation pattern of the pure PVA. The earliest one which is between 80 to 220 ºC is attributed to the release of chemically bound water [38]. The maximum rate of decomposition of this first stage is at 210 ºC, under the experimental conditions. It corresponds to a 28% weight loss. The second decomposition step is in the temperature range of 230 to 430 ºC, causing a total weight loss of about 80% and the maximum rate of decomposition is 271 ºC.

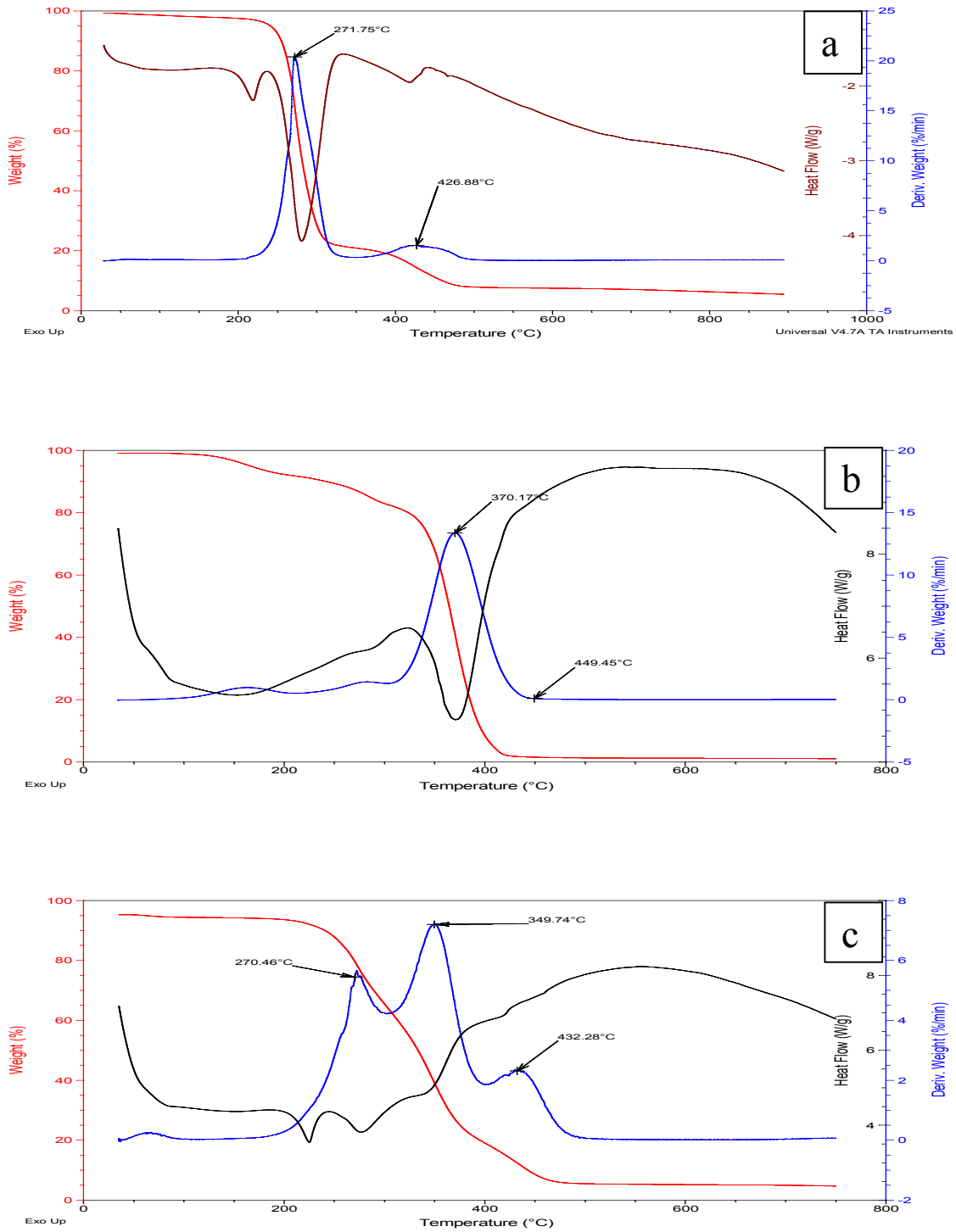

Figure 6.3: Overlapped TGA, DTG and DSC of (a) pure PVA, (b) ZnS/PVA and (c) CdS/PVA

The final decomposition temperature occurred in the range 410 to 500 ºC with peak at 426 ºC, and this is assigned to the cleavage of the C-C pillar of the PVA [39]. The ZnS/PVA degradation pattern is different from that of the pure PVA; only three major decomposition stages occurred. The temperature of the highest rate of decomposition observed at 271 ºC in the pure polymer occurred at around 370 ºC in the nanocomposites. This indicates an enhanced thermal stability with about 100 ºC. A plateau occurred at 449 ºC indicating the end of the decomposition, which is about 26 ºC higher when compared with the temperature recorded for pure PVA. In the TGA curve of CdS/PVA, there are four stages of decomposition. The first decomposition occurred in the range 40 to 80 ºC, and this can be attributed to the expulsion of weakly bound water [40]. This was followed with three decomposition steps with peaks at 270, 349 and 432 ºC respectively. After the last decomposition, approximately 60% weight loss occurred in the nanocomposites with enhanced thermal stability.

6.3.4 Thermal analysis of PVP and nanocomposites

Figure 6.4(a-c) shows the overlapped TGA-DTG graph of pure PVP and the corresponding nanocomposites. There are two stages of decomposition in the pure PVP as can be inferred from the differential thermal gravimetric (DTG) curve. The first decomposition step which occurred between 50 - 100 ºC with a slight weight loss can be attributed to the evaporation of physically trapped moisture [41]. The decomposition of the PVP commenced at 350 ºC and ended at 480 ºC, accompanied by about 95% weight loss [42]. There appeared complete decomposition of the pure PVP at 429 ºC and it is accompanied by single DSC endothermic peak whose maximum is at 282 ºC [43]. The TG and DTG curves of ZnS/PVP are similar to that of pure PVP, with two stages of decomposition but with enhanced thermal decomposition temperature observed at 433 ºC.

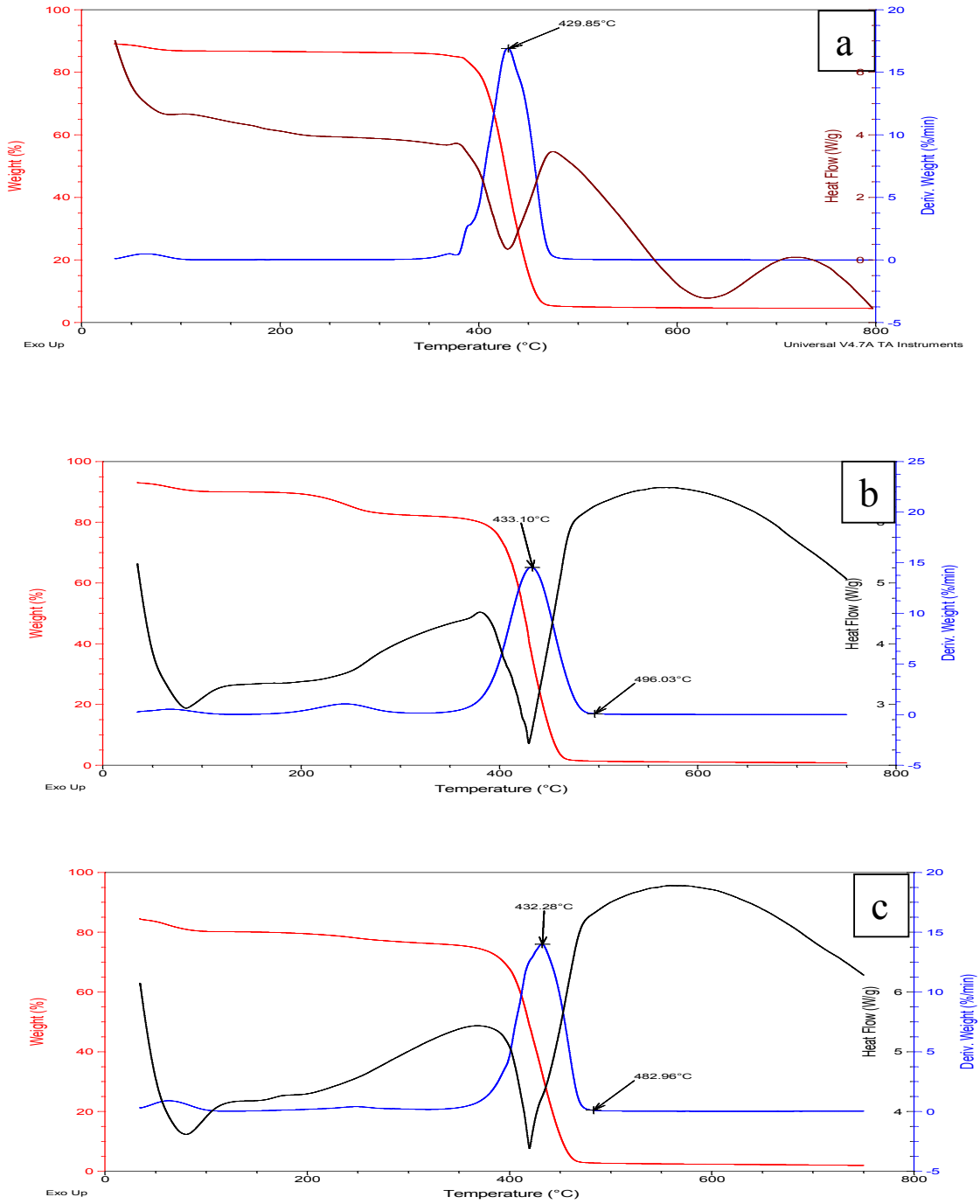

Figure 6.4: Overlapped TGA, DTG and DSC of (a) pure PVP, (b) ZnS/PVP and (c) CdS/PVP.

This could be ascribed to the effect of the incorporation of ZnS in the matrices of the PVP and good interactions between PVP and the ZnS nanoparticles. The composite shows a major weight loss of about 74% between 410-470 ºC. The TG and DTG of CdS/PVP show a slight variation from that of pure PVP with a decomposition peak at 433 ºC. It also displayed a significant weight loss of about 72% in the temperature range of 390 - 467 ºC. The DTG peak maximum for the ZnS/PVP and CdS/PVP are 433 ºC and 432 ºC compared to 429 ºC of the pure PVP. The TGA curves of the ZnS/PVP and CdS/PVP maintains a plateau from 496 ºC and 483 ºC respectively due to the complete decomposition of the volatile part of PVP leaving the metal sulfide and negligible weight of the stable substrate as the final residue.

Table 6.1: Summary of decomposition temperatures of nanocomposites relative to variations in the decomposition of their respective pure polymers

Nanocomposites	DTG decomposition peak max. (ºC)	Decomposition temperature range (ºC)	Extent of enhanced thermal stability of nanocomposites (ºC)
ZnS/PMMA	374	320 - 457	9
CdS/PMMA	376	340 - 449	12
ZnS/PVA	370	330 - 449	98
CdS/PVA	350	270 - 432	78
ZnS/PVP	433	360 - 496	3
CdS/PVP	432	370 - 482	7

The results obtained from the TGA and DTG show that the interactions of the ZnS and CdS nanoparticles with the polymers enhance thermal stability of the resulting polymer nanocomposites. This is deduced from the data obtained when the decomposition

temperatures of the nanocomposites is relatively compared with the variation in the decomposition temperature of their respective pure polymers. The summary of this is presented in Table 6-1. The sequence of thermal stabilities as a result of the incorporation of the nanoparticles in the polymer matrices is in the following order: ZnS/PVA > CdS/PVA > CdS/PMMA > ZnS/PMMA > CdS/PVP > ZnS/PVP.

6.4 X-ray diffraction studies of nanocomposites

6.4.1 XRD of pure PMMA and its composites: MS/PMMA (Where M =Zn or Cd)

The XRD pattern of pure PMMA, ZnS/PMMA and CdS/PMMA nanocomposites measured in the scan range of 10 to 80º are shown in Figure 6-5(a). The amorphous nature of PMMA is indicated by the presence of the first broad peak at lower diffraction angle around (10 - 20º). From the pattern, the characteristic peak for pure PMMA is observed at 2θ value = 12.85º [44]. ZnS/PMMA exhibits two broadened diffraction peaks (from 25º - 43º) which may be due to overlapping of (100), (002), (101) miller indices. These peaks correlate well with hexagonal ZnS wurtzite (structure standard pattern of JCPDS card No. 80 - 0007). The diffraction peaks are in agreement with earlier reported studies [45, 46]. For the CdS/PMMA the diffraction peaks appeared at; 13.32º, 28.24º, 43.13º and 52.88º. The diffraction peaks at 2θ = 13.32º is typical of PMMA. The peaks at 28.24 º, 43.13 º and 52.88º are indexed to scattering from the (1 1 1), (2 2 0) and (3 1 1) cubic phase of CdS planes [47]. The mean crystallite sizes of the ZnS/PMMA and CdS/PMMA could not be calculated using the Debye-Scherer equation due to the overlap of the nanoparticles and polymer peaks. The broadening of the XRD peaks is indicative of the small particle sizes of the as-prepared nanocomposites [48].

6.4.2 XRD of pure PVA and its composites: MS/PVA (Where M =Zn or Cd)

XRD pattern of pure PVA, PVA/ZnS and PVA/CdS are shown in Figure 6.5(b). The diffraction peaks of the pure PVA exhibits four peaks at 2θ = 10.81º, 19.37º, 22.52º and 40.19º which correspond to the crystalline phase of PVA [49]. The crystalline nature of PVA stems from the strong intermolecular interaction between PVA chains through the intermolecular hydrogen bonding [50]. In the diffraction pattern of the ZnS/PVA, the peaks that are attributable to ZnS nanoparticles of the composite are observed at 2θ = 26.94º, 47.01º and their miller indices; (100) and (110), which suggests the presence of hexagonal phase of ZnS (wurtzite). Similar results have been reported in literature [51]. The 2θ = 19.37º, 22.52º and 40.19º and 22.15º being characteristic peak of PVA component. Nevertheless, another peak is expected around 2θ = 52º (103) and this is not distinguishable. This observation has been reported in previous research by other authors [52].

The low intensity of ZnS/PVA peaks can be attributed to interaction of metal sulfides with PVA; metal sulfides decrease the degree of PVA crystallinity when incorporated in PVA polymer [53]. In the XRD pattern of the PVA/CdS composite, the characteristic peak of the PVA is noticeable with other peaks at 2θ = 10.96º, 19.73º, 22.50º, 31.74º and 40.72º and their miller indices are; (100), (101), (200), (002) (111) respectively. The peaks from the CdS nanoparticles of the composites are observed at 2θ = 26.57º, 36.63º, 46.26º and 52.42º. These peaks could be indexed to the scattering from (1 1 1), (1 0 2), (1 0 3), (3 1 1) hexagonal and cubic phase of CdS respectively. The peaks correlate both with diffraction peaks associated with hexagonal phase of CdS; (2θ = 36.84 and 46.82º) [54] and cubic phase of CdS; (26.85 and 52.24º) [55], and indicates the mixture of both phases. The particles sizes could not be calculated from using Debye-Scherer equation because the peaks overlap with the polymer peaks.

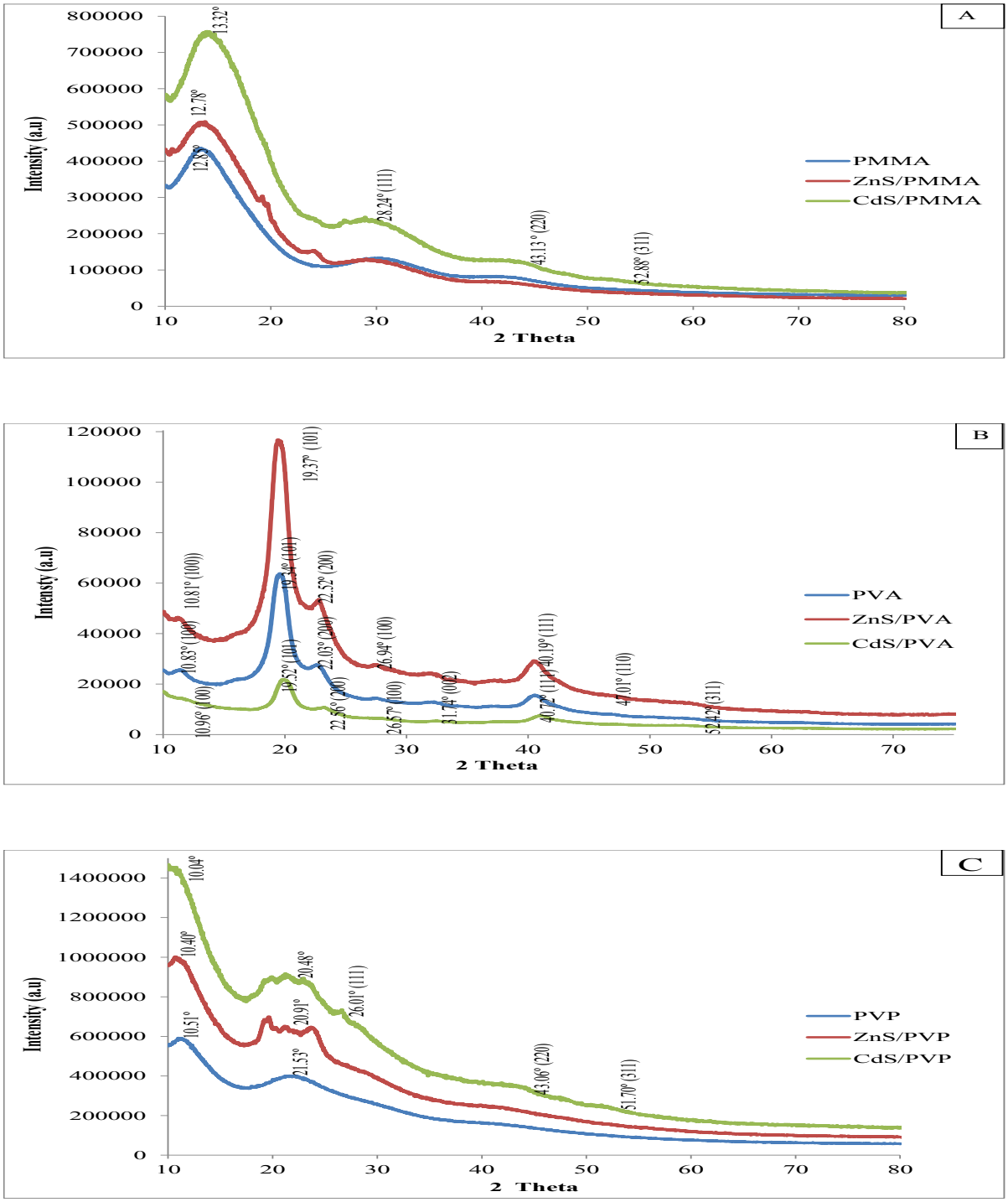

Figure 6.5: XRD diffractions (a) pure PMMA and its respective nanocomposites) (b) pure PVA and its respective nanocomposites, and (c) pure PVP and its respective nanocomposites

6.4.3 XRD of pure PVP and its composites: MS/PVP(Where M =Zn or Cd)

Figure 6.5(c) shows the XRD patterns of the pure PVP, and its respective nanocomposites: ZnS/PVP and CdS/PVP. The peaks around 2θ = 10.5º and 21.53º are typical characteristic peaks of PVP [56 - 59]. ZnS/PVP shows two peaks at 2θ = 10.5º and 21.53º, which corresponds to the characteristic peak of pure PVP, and another two broadened peaks which may be ascribed to the wurtzite phase of ZnS. This diffraction pattern is in agreement with earlier observation [46]. The XRD pattern of the PVP/CdS exhibited 4 peaks at 2θ = 25.39º, 43.06º, 46.82º and 51.70º which correspond to the (1 1 1), (2 2 0), (3 1 1) miller indices. These peaks match with the cubic CdS of JCPDS file (JCPDS no 10 - 454) [60]. The absence of peaks at 2θ values of 24.8º, 36.2º and 47.84º ruled out the possibility of hexagonal phase CdS presence in CdS/PVP [61].

6.5 Transmission electron microscopy (TEM) studies

Figure 6.6(a) shows the TEM images of the ZnS/PMMA, which appeared as slightly spherical shape, which are loosely distributed with an average particle size in the range of 1.51 - 3.35 nm. Figure 6.6(b) shows the CdS/PMMA nanocomposites with CdS also embedded in the matrices of PMMA. The nanoparticles have rod shape, and with an average size in the range of 4.07 - 6.92 nm. These particles are homogenous and almost equally distributed in the PMMA matrices. It could be noted that there occurs a slight difference in the particle size estimation using the XRD and the TEM and this can be ascribed to the intrinsic twining and dislocation present in the lattice of the sample [62]. Figure 6.6(c) and (d) represents the TEM micrograph of ZnS/PVA and CdS/PVA respectively. Figure 6.6(c) shows the incorporated ZnS nanoparticles in PVA matrices. The nanoparticles are rod-shaped with sizes in the range of 2.44 - 5.87 nm. TEM micrograph in Figure 6.6(d) reveals cocoon-

like shaped materials with size in the region of 2.57 - 4.90 nm. The nanoparticles appear polydispersed and aggregated.

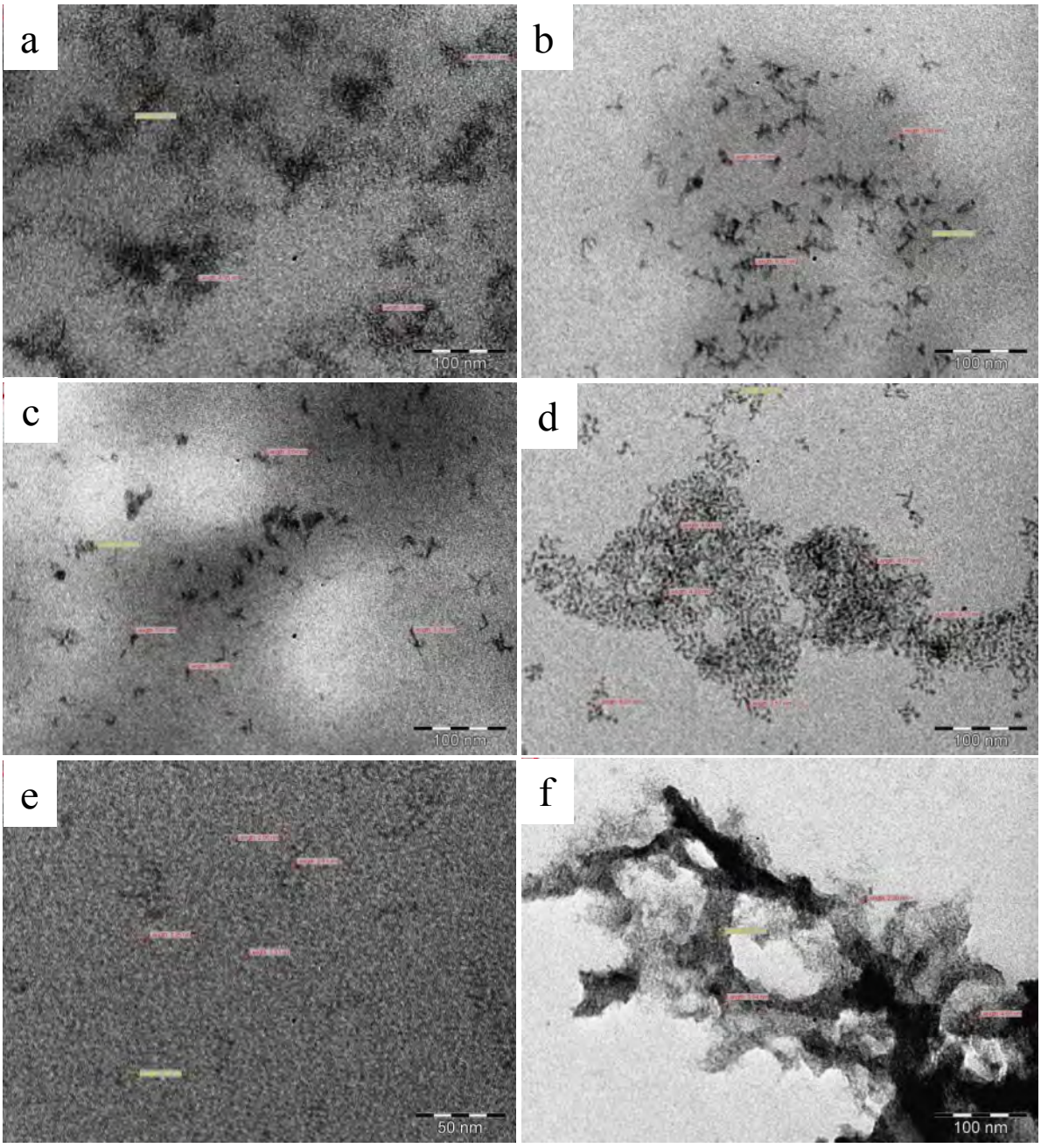

Figure 6.6: TEM micrographs of (a) ZnS/PMMA (b) CdS/PMMA (c) ZnS/PVA(d) CdS/PVA (e) ZnS/PVP (f) CdS/PVP.

The TEM micrograph of ZnS/PVP presented in Figure 6.6(e) reveals uniform distribution of spherical ZnS embedded in the polymer matrices of the PVP. The sizes of the ZnS nanoparticles are in the range of 1.5-3.25 nm. It is apparent from the TEM micrograph of CdS/PVP, Figure 6.6(f), that CdS nanoparticles embedded in the polymer matrix of PVP are distinguishable, although they are in contact with one another. They are a bit agglomerated into a massive structure although they reveal an average particle size whose ranges are in the region of 1.75 - 4.55 nm.

6.6 Scanning electron microscopy (SEM) studies

The micrographs shown in Figure 6-7(a-e) is a representative SEM images of the pure PMMA, the PMMA/ZnS and PMMA/CdS at low and high magnifications and it was observed that the ZnS nano fillers cause remarkable change in the morphology of pure PMMA (as observed in Figure 6.7(b). Higher magnification images show the presence of slight agglomeration, and this might be due to the existence of a larger interaction between nanoparticles as compared with polymer-particle interaction [63]. The SEM image of the PMMA/CdS presented in Figure 6.7(d) exhibited homogenous dispersion of CdS in the PMMA unlike the agglomeration observed at higher magnification, Figure 6.7(e).

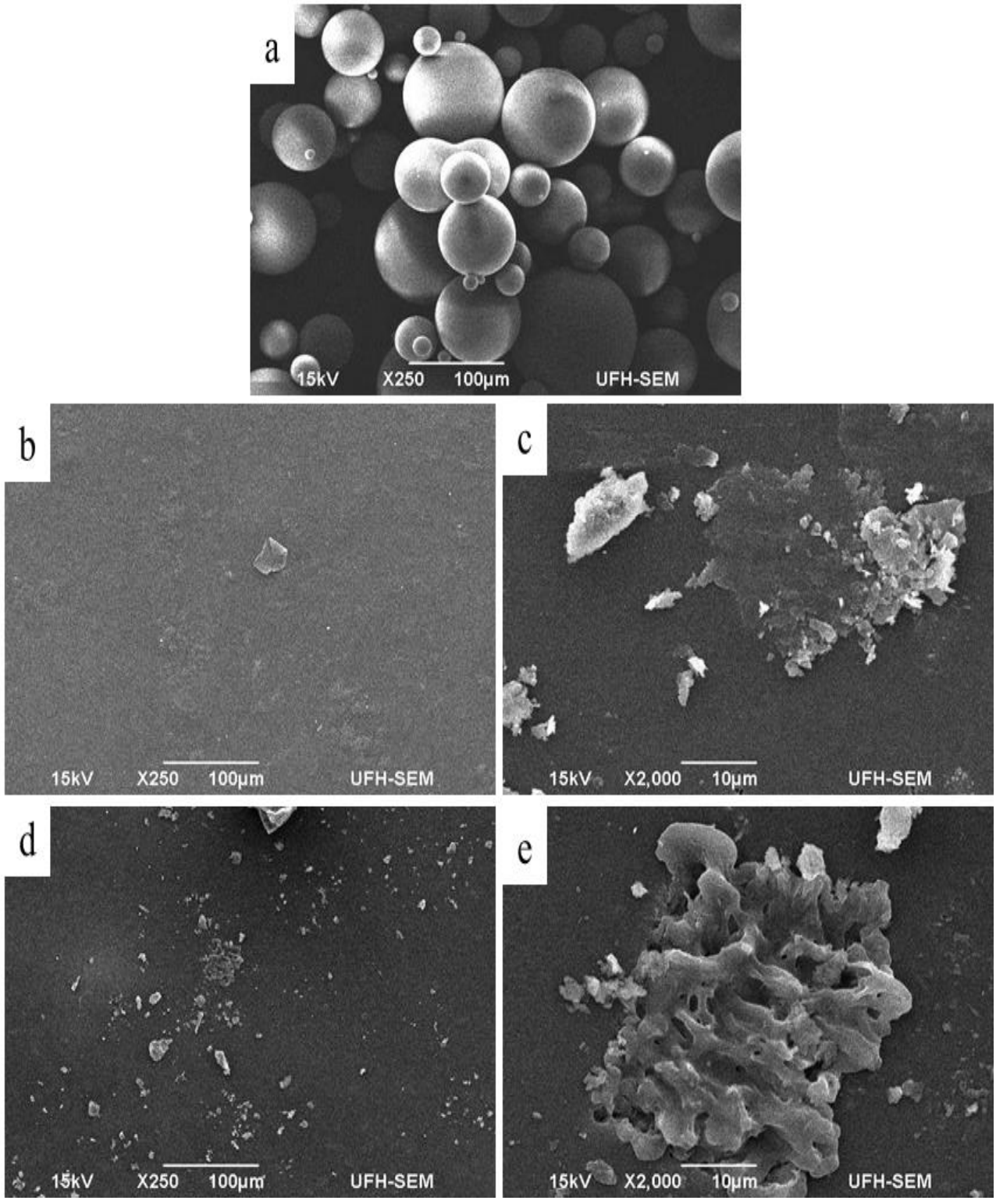

Figure 6.7: SEM micrographs of (a) Pure PMMA (b) ZnS/PMMA-low mag (c) ZnS/PMMA-high mag. (d) CdS/PMMA-low mag. (e) CdS/PMMA-high mag

.

The micrograph in Figure 6.8(a-e) shows the pure PVA, ZnS/PVA and CdS/PVA nanocomposites. The pure PVA is made up of fine spherical material.

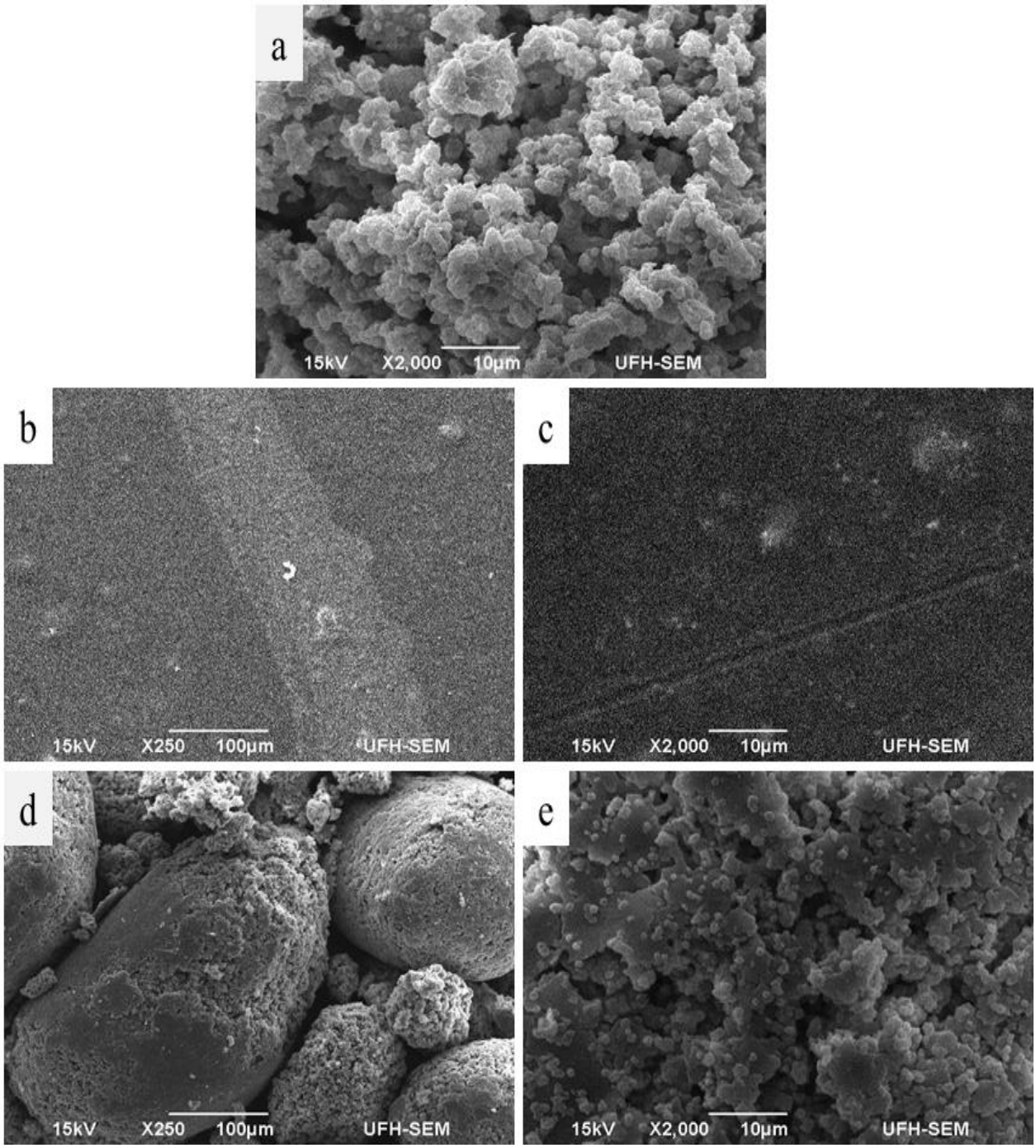

Figure 6. 8: SEM micrographs of (a) Pure PVA (b) ZnS/PVA-low mag. (c) ZnS/PVA-high mag (d) CdS/PVA-low mag. (e) CdS/PVA-high mag.

There is a significant change in the morphology of PVA/ZnS and CdS/PVA with the former exhibiting a uniform dispersion of the ZnS nanofillers in the PVA polymer matrices, Figure 6.8(b). The SEM micrograph of PVA/CdS at higher magnification displays an almost splitting image of the pure PVA with CdS embedded in the polymeric matrix. The image shows rounded spheres of uniformly dispersed CdS nanoparticles in the PVA polymer matrix.

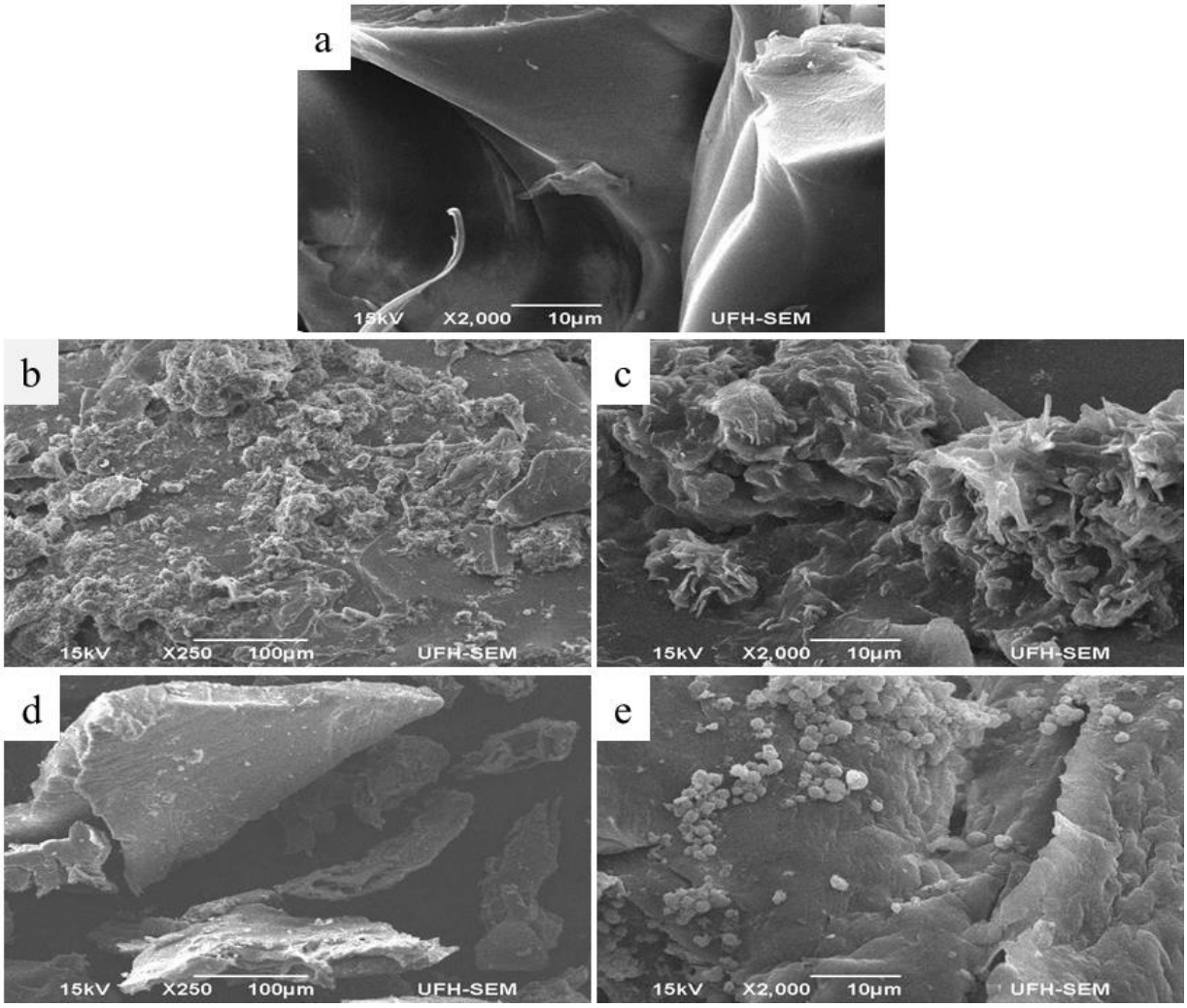

Figure 6.9: SEM micrographs of (a) Pure PVP (b) ZnS/PVP-low mag (c) ZnS/PVP-high mag. (d) CdS/PVP-low mag. (e) CdS/PVP-high mag

The SEM micrograph of pure PVP is presented in Figure 6.9(a) and it exhibits a smooth flower-like material. Part of the ZnS/PVP layers appeared to be exfoliated with the ZnS embedded in the PVP polymer matrix, Figure 6.9 (b-c). The micrograph of CdS/PVP at lower magnification, Figure 6.9(d), did not show an appreciable result unlike the image at higher magnification which shows the CdS that appeared to be incorporated in the matrix of the PVP as spherical uniformly dispersed particles, Figure 6.9 (e).

6.7 Optical property of the nanocomposites

The absorptions spectra of the pure polymers with the respective nanocomposites are presented in Fig 6.10 (a-c). All the polymers do not absorb within the measured range as evident in the absence of absorption peak in the spectrum. The onset absorption for CdS/PMMA, CdS/PVA and CdS/PVP were found as a shoulder at approximately 457 nm (2.72 eV), 441 nm (2.82 eV) and 438 nm (3.21 eV) respectively. The absorption peak of these nanocomposites show that they are 58 nm, 74 nm and 77 nm blue shifted from the bulk CdS, 515 nm (2.40 eV) [64]. The spectra of the ZnS/PMMA, ZnS/PVA and ZnS/PVP show absorption on set at approximately 316 nm (3.92 eV) 314 nm (2.25eV) and 327 nm (3.42 eV) respectively. When compared with the bulk ZnS 340 nm (3.66 eV) [65], they are 24 nm, 26 nm and 13 nm blue shifted The blue shifts of the polymer nanocomposites are indicative of quantum confinements of the embedded nanoparticles. It is important to note that all the nanocomposites exhibit enhanced quantum confinement except CdS/PMMA and CdS/PVA when compared with the HDA-capped ZnS and CdS that were earlier reported [23]. The optical band gap energy of nanocrystalline samples is determined from the absorption on-set of the various UV-Vis spectra and it can be calculated from the absorption peak [66].

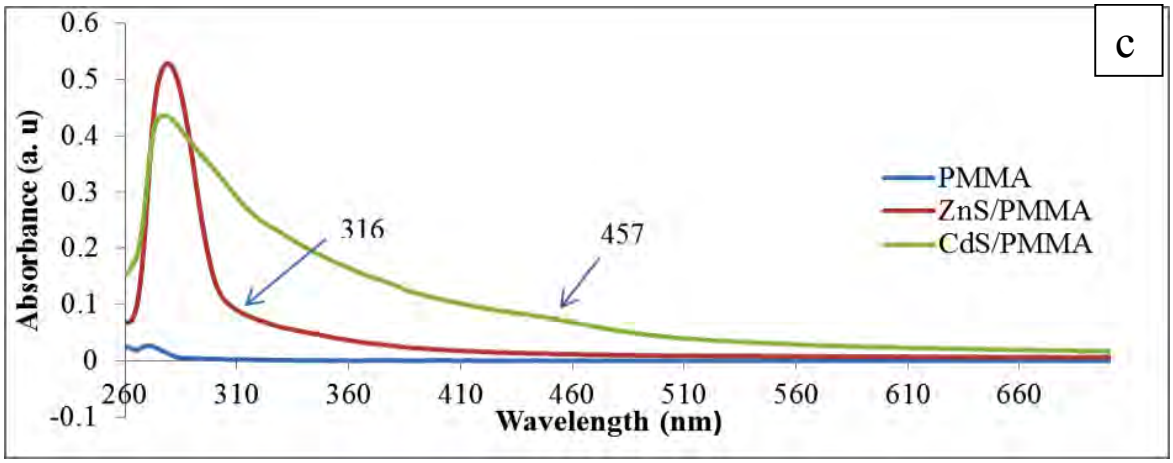

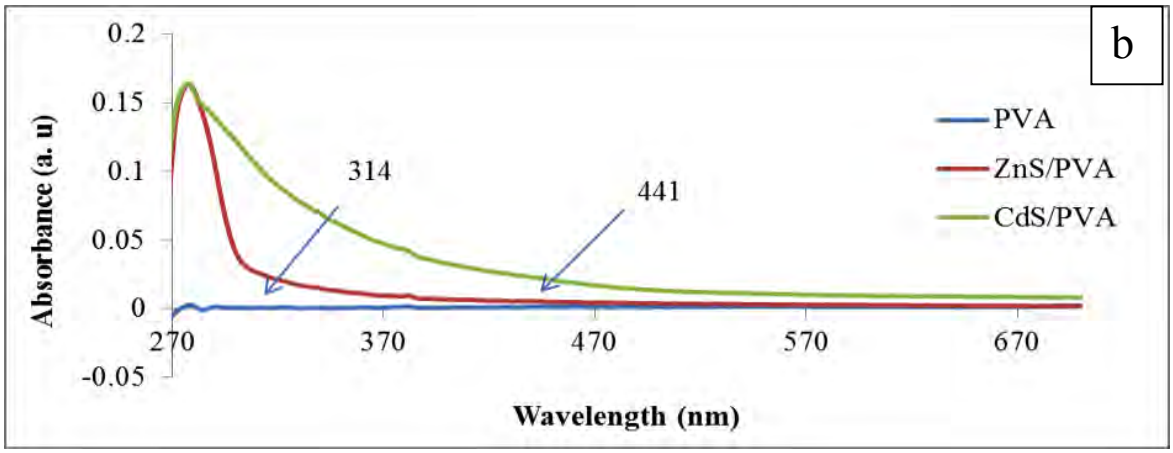

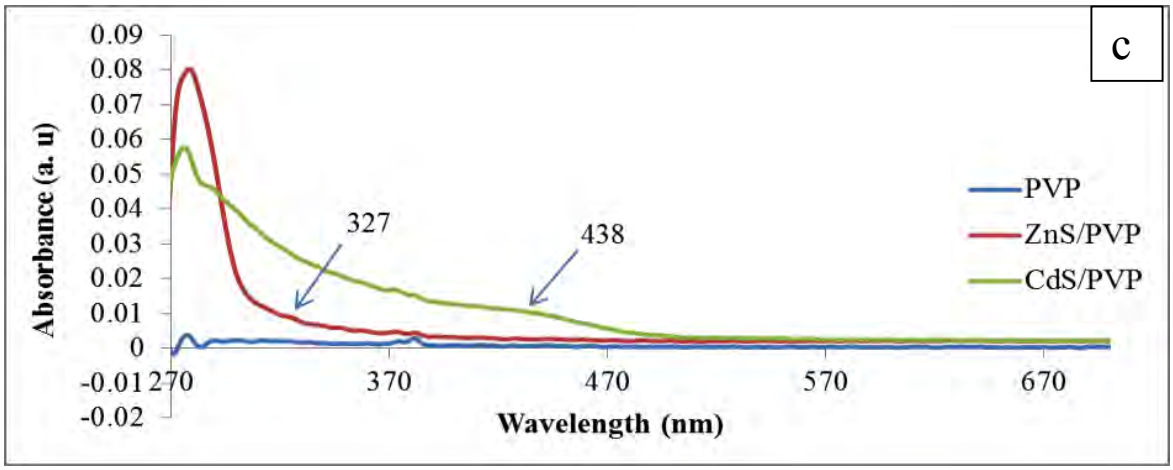

Figure 6.10: Absorption spectra of (a) PMMA, ZnS/PMMA, CdS/PMMA, (b) PVA ZnS/PVA, CdS/PVA, (c) PVP, ZnS/PVP, PVP/CdS

UV-vis spectrum is used to calculate the particle size of nanocrystals using the effective mass approximation formula, (EMA) [67]. Table 6.2 below shows the summary of the optical properties of the various polymer nanocomposites.

Table 6.2: Optical band gaps and blue shifts of absorption band of the metal sulfides/polymer nanocomposites

Sample	Wavelength (nm)	Band gap (eV)	Blue shift (eV)
ZnS/PMMA	316	3.92	0.26
CdS/PMMA	457	2.71	0.31
ZnS/PVA	314	3.95	0.29
CdS/PVA	441	2.82	0.42
ZnS/PVP	327	3.79	0.13
CdS/PVP	438	2.83	0.43

6.8 Conclusion

In this work, ZnS and CdS were incorporated into PMMA, PVA, and PVP matrices to form corresponding metal sulfides/polymer nanocomposites. The structural and thermal properties of the composites were studied with XRD, TEM, SEM and TGA. Wurtzite crystalline phase of ZnS were obtained from the XRD analysis for all the ZnS polymer nanocomposites. Cubic phase of CdS were also displayed by the CdS/PMMA and CdS/PVP but the CdS/PVA showed the combination of both cubic and hexagonal phase of CdS in PVA composite. TEM micrographs show that the sizes of the metal sulfides in the composites are in the range of 1.59 - 6.9 nm and these values are in close agreement with the ones obtained from the XRD.

SEM micrographs show almost uniform dispersion of the ZnS and CdS nanoparticles in the respective polymers. The TGA reveals that the ZnS/PVA and CdS/PVA thermal stability are the most enhanced by the incorporation of the metal sulfide in the matrices of the polymers. All except CdS/PMMA and CdS/PVA show greater degree of quantum confinement when metal sulfide were incorporated into the various polymer matrices as compared with the HDA-capped ZnS and CdS nanoparticles previously reported.

6.9 Reference

1. Twardowski, T. E. Introduction to nanocomposites material properties, processing, characterization, Lancaster, Pa Dastech Publications, Inc 2007.
2. Tamborra, M.; Striccoli, M.; Comparelli, R.; Curri, M. L.; Petrella, A.; Agostian A. Optical properties of hybrid composites based on highly luminescent CdS nanocrystals in polymer. *Nanotechnology*. **2004**, S240-S244.
3. Hussain, F.; Hojjati, M.; Okamoto, M.; Gorga, R. E. Polymer-Matrix Nanocomposites, Processing, Manufacturing, and application: An Overview. *J. Composite Mater*. **2006**, *40*, 1511-1575.
4. Resta, V.; Laera, A. M.; Camposeo, A.; Piscopiello, E., Persano, L.; Pisignano, D.; Tapfer, L. Spatially Confined CdS NCs in Situ Synthesis through Laser Irradiation of Suitable Unimolecular Precursor-Doped Polymer. *J. Phys. Chem. C*, **2012**, *116*, 25119-25125.
5. Althues, H.; Palkovits, R.; Rumplecker, A.; Simon, P.; Sigle, W.; Bredol, M.; Kynast, U.; Kaskel, S. Synthesis and characterization of transparent luminescent ZnS:Mn/PMMA nanocomposites. *Chem. Mater.* **2006**, *18*, 1068-1072.
6. Wang, C.; Guan, L.; Mao, Y.; Gu, Y.; Liu, J.; Fu, S.; Xu, Q. Optical nonlinearity of ZnS-polyvinyl pyrrolidone nanocomposites suspension. *J. Phys. D: Appl. Phys.* **2009,** *42*, 1-5.
7. Borah, J. P.; Sarma, K. C. Photo-physical properties of ZnS/PVA nanocrystals. Optoelectron. *Adv. Mater. Rapid Commun*. **2009**, *3*, 891- 898.
8. Soltani, N.; Saion, E.; Yunus, W. M. M.; Navasery, M.; Bahmanrokh, G.; Erfani, M.; Zare, M. R.; Gharibshahi. Photocatalytic degradation of methylene blue under visible light using PVP-capped ZnS and CdS nanoparticles E. *Sol. Energy*. **2013**, *97*, 147-154.

9. Seung-Wook, S.; Kang, S. R.; Yun, J. H.; Moholkar, A. V.; Moon, J. H.; Lee, J. Y.; Kim, J. H. Effect of different annealing conditions on the properties of chemically deposited ZnS thin films on ITO coated glass substrates. *Solar Energy Mater. Sol. Cells*. **2011**, *95*, 856-863.
10. Goharshadi, E. K.; Mehrkhah, R.; Nancarrow, P. Synthesis, characterization, and measurement of structural, optical, and phtotoluminescent properties of zinc sulfide quantum dots. *Mater. Sci. Semicond. Process.* **2013**, *16*, 356-362.
11. Su, B.; Choy, K. L. Microstructure and properties of the CdS thin films prepared by electrostatic spray assisted vapour deposition (ESAVD) method. *Thin Solid Films*. **2000**, *359*, 160-164.
12. Kashiwaba, Y.; Sato, J.; Abe, T. Emission of lights of various colors from p-CdS: Cu/n-CdS thin-film diodes. *Appl*. *Surf. Sci*. **2003**, 212-213, 162-165.
13. Liu, B. T.; Li, P. S.; Chen, W. C.; Yang-Yen, D. Macromolecular nanotechnology ex - situ synthesis of high-refractive-index polyimide hybrid films containing TiO2 chelated by 4-aminobenzoic acid. *Eur*. *Polym*. *J*., **2014**, *50*, 54-60.
14. Montazer, M.; Amiri, M. M. ZnO nano reactor on textiles and polymers: ex situ and in situ synthesis, application and characterization. *J*. *Phys*. *Chem*. *B*, **2014**, 118, 1453-1470.
15. Pentimalli, M.; Antolini, F.; Bauer, E. M.; Capitani, D.; Di Luccio, T.; Viel, S.; A solid state nuclear magnetic resonance study on the thermolytic synthesis of CdS nanoparticles in a polystyrene matrix. Mater. Lett. 2006, 60, 2657-2661.
16. Di Luccio, T.; Laera, A. M.; Tapfer, L. Controlled nucleation and growth of CdS nanoparticles in a polymer matrix. *J. Phys. Chem. B*. **2006**, *110*, 12603-12609.
17. Danaher, W. I.; Lyons, L. E.; Morris, G. C. Some properties of thin films of chemically deposited cadmium sulfide. *Sol*. *Energy Mater*. **1985**, *12*,137-148.

18. Ding, L. Y.; Li, T.; Zhong, Y. M.; Fan, C.; Huang, J. Synthesis and characterization of a novel nitric oxide fluorescent probe CdS-PMMA nanocomposite via in-situ bulk polymerization. *Mater. Sci. Eng.* C. **2014**, *35*, 29-35.

19. Pedone, L.; Caponetti, E.; Leone, M.; Militello, V.; Pantò, V.; Polizzi, S.; Saladino M. L. Synthesis and characterization of CdS nanoparticles embedded in a poly(methyl methacrylate) matrix. *J. Colloid Interf. Sci*. **2005**, *284*, 495-500.

20. Khannaa, P. K.; Gokhale, R. R.; Subbarao, V. V. V. S.; Singh, N.; Jun, K-W.; Dasa B. K. Synthesis and optical properties of CdS/PVA nanocomposites *Mater*. *Chem*. *Phys*. **2005**, *94*, 454-459.

21. Pattabi, M.; Amma, B. S.; Manzoor, K. Photoluminescence study of PVP capped CdS nanoparticles embedded in PVA matrix. *Mater*. *Res*. *Bull*. **2007**, *42*, 828-835.

22. Shanmugam, N.; Cholan, S.; Kannadasan, N.; Sathishkumar, K.; Viruthagiri, G. Effect of polyvinylpyrrolidone as capping agent on Ce^{3+} doped flowerlike ZnS nanostructure. *Solid State Sci*. **2014**, *28*, 55-60.

23. Ajibade, P. A.; Osuntokun J. Synthesis and characterization of hexadecylamine capped ZnS, CdS, and HgS nanoparticles using heteroleptic single molecular precursors. *J. Nanomater*. **2014**, *782526*, 1-7.

24. Abdelghany, A.M.; Mekhail, M .S.; Abdelrazek, E. M.; Aboud, M. M. Combined DFT/FTIR structural studies of monodispersed PVP/Gold and silver nano particles *J. Alloys Compd*. **2015**, *646*, 326-332.

25. Mathur, V.; Sharma, K.; Evaluation of morphological effect on thermal and mechanical performance of PS/PMMA/CdS nanocomposite systems. *Adv*. *Nanopart*. **2013**, *2*, 205-216**.**

26. Thottoli, A. K.; Chuthanunni A. K. Effect of polyvinyl alcohol concentration on the ZnS nanoparticles and wet chemical synthesis of wurtzite ZnS nanoparticles, *J. Nanostruct. Chem*. **2013**, *3*, 1-9.
27. Shehap, A. M. Thermal and spectroscopic studies of polyvinyl alcohol/sodium carboxymethyl cellulose blends. *Egypt. J. Solids*. **2008**, *31*, 75-91.
28. Raju, C. H. L.; Rao, J. L.; Reddy, B. C. V.; Brahmam, K. V. Thermal and IR studies on copper doped poly(vinyl alcohol). *Bull. Mater. Sci*. **2007**, *30*, 215-218.
29. Khoza, P. B.; Moloto, M. J.; Sikhwivhilu, L. M. The effect of solvents, acetone, water, and ethanol, on the morphological and optical properties of ZnO nanoparticles prepared by microwave. *J. Nanotech*. **2012**, *195106*, 1-6.
30. Osuntokun, J.; Ajibade, P. Synthesis and structural characterization of CdS nanoparticles using nitrogen adducts of mixed diisopropylthiourea and dithiolate derivatives of Cd(II) complexes. *Superlattices Microstruct*. **2015**, *83*, 89-100.
31. Strawhecker, K. E.; Manias, E. AFM of poly(vinyl alcohol) crystals next to an inorganic surface. *Macromolecules*. **2001**, *34*, 8475-8482.
32. Strawhecker, K. E.; Manias, E. Structure and properties of poly(vinyl alcohol)/ Na+ montmorillonite nanocomposites. *Chem. Mater*. **2002**, *12*, 2943-2949.
33. Ummartyotin, S.; Bunnak, N.; Juntaro, J.; Sain M.; Manuspiya, H. Hybrid organic-inorganic of ZnS embedded PVP nanocomposite film for photoluminescent application. *C. R. Phys*. **2012**, *13*, 994-1000.
34. Abdelghany, A. M.; Abdelrazek, E. M.; Rashad D. S. Impact of in situ preparation of CdS filled PVP nano-composite. *Spectrochim. Acta Part A*, **2014**, *130*, 302-308.
35. Gianotti, V.; Antonioli, D.; Sparnacci, K.; Laus, M.; Giammaria T. J. On the Thermal Stability of PS-b-PMMA Block and P(S-r-MMA) random copolymers for nanopatterning applications. *Macromolecules*. **2013**, *46*, 8224-8234.

36. Kole, A. K.; Gupta, S.; Kumbhakar, P.; Ramamurthy, P.C. Nonlinear optical second harmonic generation in ZnS quantum dots and observation on optical properties of ZnS/PMMA nanocomposites. *Optics Commun.* **2014**, *313*, 231-237.

37. Liu, Y. L.; Hsu, C. Y.; Hsu, K. Y. Poly(methyl methacrylate)-silica nanocomposites films from surface-functionalized silica nanoparticles. *Polymer*. **2005**, *46*, 1851-1856.

38. Gong, X. Tang, C. Pan, Y. L.; Hao, Z.; Tsui, C. P. Characterization of poly(vinyl alcohol) (PVA)/ZnO nanocomposites prepared by a one-pot method. *Compos. Part B: Eng*. **2014**, *60*, 144-149.

39. Wang, J.; Gao, C.; Zhang, Y.; Wan, Y. Preparation and in vitro characterization of BC/PVA hydrogel composite for its potential use as artificial cornea biomaterial, *Mater. Sci. and Eng: C*. **2010**, *30*, 214-218.

40. George, J.; Ramana, K.V.; Bawa, A. S.; Siddaramaiah, S. Bacterial cellulose nanocrystals exhibiting high thermal stability and their polymer nanocomposite*s*. *Int*. *J. Biol*. *Macromol*. **2011**, *48*, 50-57.

41. Kumar, M. R.; Murugadoss, G. Synthesis and study of optical and thermal properties of Mn doped CdS nanoparticles using polyvinylpyrrolidone, *J. Lumin.* **2014**, *146*, 325-332.

42. Du, Y. K.; Yang, P.; Mou, Z. G.; Hua, N. P.; Jiang, L. Thermal decomposition behaviors of PVP coated on platinum nanoparticles. *J. Appl. Polym. Sci*. **2006**, *99*, 23-26.

43. Al-Hada, N. M., Saion, E. B.; Shaari, A. H.; Kamarudin, M.A.; Flaifel, M. H., Ahmad, S. H.; Gene, A. A facile thermal-treatment route to synthesize the semiconductor CdO nanoparticles and effect of calcinations. *Mater. Sci. Semicond. Process*. **2014**, *26*, 460-466.

44. Agrawal, S.; Patidar, D.; Saxena, N. S. Glass transition temperature and thermal stability of ZnS/PMMA nanocomposites. *Phase Transit*. **2011**, *84*, 888-900.
45. Zhang, H.; Qi, L. Low-temperature, template-free synthesis of wurtzite ZnS nanostructures with hierarchical architectures. *Nanotechnol*. **2006**, *17*, 3984-3988.
46. Kumar, S.; Sharma, S. K. Growth and characterization of large-scale uniform Zinc Sulfide nanowires by a simple chemical reaction technique. *Superlattices Microstruct.* **2009**, *46*, 687-692.
47. Ding, L.; Li, T.; Zhong, Y.; Fan, C.; Huang, J. Synthesis and characterization of a novel nitric oxide fluorescent probe CdS-PMMA nanocomposite via in-situ bulk polymerization. *Mater. Sci. Eng. C*. **2014**, *35*, 29-35.
48. Seoudi, R.; Shabaka, A. A.; Kamal, M.; Abdelrazek, E. M.; Eisa W. Dependence of spectroscopic and electrical properties on the size of cadmium sulfide nanoparticles. *Physica E*. **2012**, *45*, 47-55.
49. Shahi, A. K.; Pandey, B. K; Singh, S. C.; Gopal, R. Observation of negative persistent photoconductivity in ZnS/PVA nanocomposite materials. *J. Alloys Compd*. **2014**, *588*, 440-448.
50. Saikia, D.; Saikia, P. K.; Gogoi, M. R.; Sengupta, P.; Shelke, M. V. Synthesis and characterization of CdS/PVA nanocomposite thin films from a complexing agent free system. *Mater. Chem. Phys*. **2011**, *131*, 223-229.
51. Prakasam, B. A.; Lahtinen, M.; Peuronen, A.; Muruganandham, M.; Kolehmainen, E.; Haapaniemi, E.; Sillanpää, M. Phase selective synthesis of ZnS nanoparticles from structurally new dithiocarbamate precursor. *Mater. Lett.* **2015**, *144*, 19-21.
52. Liu, S.; Zhang, H.; Swihart, M. T. Spray pyrolysis synthesis of ZnS nanoparticles from a single-source precursor. *Nanotechnol*. **2009**, *20*, 1-8.

53. Qian, X. F.; Yin, J.; Guo, X. X.; Yang, X. F.; Zhu, Z. K.; Liu, J. Polymer-inorganic nanocomposites prepared by hydrothermal method: PVA/ZnS,PVA/CdS, preparation and characterization. *J. Mater. Sci. Lett.* **2000**, *19*, 2235-2237.

54. N. Soltani, E. Saion, W.M.M. Yunus, M. Erfani M. Navasery G. Bahmank, K. Rezaee, Enhancement of visible light photocatalytic activity of ZnS and CdS nanoparticles based on organic and inorganic coating. *Appl. Surf. Sci*. **2014**, *290*, 440-447.

55. Rodrı´guez-Fragoso, P.; de la Cruz, G. G.; Toma, S. A.; Mendoza-Alvarez, J. G.; Angel Z. O. Photoluminescence of CdS nanoparticles embedded in a starch matrix. *J. Lumin*. **2010**, *130*, 1128-1133.

56. Li, X. G.; Kresse, I.; Springer, J.; Nissen, J.; Yang, Y. L. Morphology and gas perm selectivity of blend membranes of polyvinylpyridine with ethylcellulose. *Polymer*. **2001**, *42*, 6859-6869.

57. Liu, C.; Xiao, C.; Liang, H. Properties and structure of PVP-lignin "Blend Films" *J. Appl*. *Polym*. *Sci*. **2005**, *95*, 1405-1411.

58. Bai, J.; Li, Y.; Li, M.; Gao, J.; Zhang, X.; Wang, S.; Zhang, C.; Yang, Q. A novel approach to prepare AgCl/PVP nanocomposites microspheres via electrospinning with sol-gel method. *Colloid Surf*. *A*. **2008**, *318*, 259-262.

59. Qian, X. F.; Yin, J.; Feng, S.; Liu, S. H.; Zhu. Z. Preparation and characterization of polyvinylpyrrolidone films containing silver sulfide nanoparticles. *J. Mater. Chem.* **2001**, *11*, 2504-2506.

60. Muruganandam, S.; Anbalagan, G.; Murugadoss, G. Synthesis and structural, optical and thermal properties of CdS: $Zn2^{+}$ nanoparticles. *Appl. Nanosci*. **2013**, *11*, 4-8.

61. Rodriguez, P.; Munoz-Aguirre, N.; San-Martin, E.; Martinez, G. E., Gonza´ lez de la Cruz G.; Tomas, S. A.; Angel, Z. O. Synthesis and spectral properties of starch capped CdS nanoparticles in aqueous solution. *J. Cryst. Growth.* **2008**, *310*, 160-164.
62. Nanda, J.; Sapra, S.; Sarma, D. D. Size-selected zinc sulfide nanocrystallites: Synthesis, structure, and optical studies. *Chem. Mater*. **2000**, *12*, 1018-1024.
63. Agarwal, S.; Patidar, D.; Saxena, N. S. Effect of ZnS nanofiller and temperature on mechanical properties of poly(methyl methylacrylate). *J. Appl. Poly. Sci.* **2011**, *123*, 2431-2438.
64. Wang, H.; Z. Chen, Z.; Fang, P.; Wang S. Synthesis, characterization and optical properties of hybridized CdS-PVA nanocomposites *Mater. Chem. Phys*. **2007**, *106*, 443-446.
65. Guo, L.; Chen, S.; Chen, L.Controllable synthesis of ZnS/PMMA nanocomposites hybrids generated from functionalized ZnS quantum dots nanocrystals. *Colloid Polym. Sci*. **2007**, *285*, 1593-1600.
66. Chowdhury, S.; Ahmed, G. A.; Mohanta, D.; Dolui, S. K.; Avasthi, D. K.; Choudhury, A. Luminescence study of bare and coated CdS quantum dots: Effect of SHI irradiation and ageing. *Nucl. Instr. Meth. Phys. Res. B*. **2005**, *240*, 690-696.
67. Brus. L. E. Electronic wave functions in semiconductor clusters: Experiment and theory. *J. Phys. Chem*. **1986**, *90*, 2555-2560.

CHAPTER 7

7. Summary of Results, Conclusion and Future Work

7.1 Summary of Results

Nineteen complexes were reported in this work and out of which 5 were adducts, (one pyridine, two adducts of 2, 2' bipridine and two adducts of 1, 10 phenanthroline). The complexes are of mixed ligand of thiourea or tetramethyl thiuram disulfide and 1-cyano-1-carboehoxy-2, 2 ethylene dithiolate. All the complexes were thermolysed in HDA to synthesize their respective metal sulfide nanoparticles. The work is divided into six sections. Chapter one contains the introduction and literature review. The introduction included the classification of semiconductors, the different ligands that have been used as a chalcogenide source in the synthesis of metal sulfide nanoparticles and the different routes of metal sulfide synthesis. Chapter two contains the experimental part of this work and it includes detailed experimental procedures for the synthesis of all the mixed substituted thiourea or tetramethyl thiuram disulfide and 1- cyano-1-carboethoxy-2, 2 ethylene dithiolate and its mixed Zn(II), Cd(II) and Hg(II) complexes with methylthiourea, dimethylthiourea, diethylthiourea, diisopropyl thiourea or tettramethyl thiuram disulfide. The chapter also containes detailed physical and characterization techniques.

Chapter 3 is the result and discussion part of the coordination chemistry of all ligands to the central metal in the complexes and adducts. The details of the coordination between the various ligands and the metals were elucidated with spectroscopic techniques. Additionally, the TGA and the DTG spectra were also reported in the chapter and proof of the suitability of the precursor complexes for the synthesis of ZnS, CdS and HgS were also established from the decomposition of the complexes into their respective metal sulfides.

Chapter 4 gives detailed results and discussions of the twelve HDA capped ZnS, CdS and HgS nanoparticles from 12 precursor complexes. The metal sulfide nanoparticles were characterized with X-ray diffractions (XRD), transmission electron microscopy (TEM), scanning electron microscopy (SEM) and energy dispersive X-ray spectroscopy for their structural and morphological properties. Rod, spherical, cube shaped morphology were observed as the alkly substituent of the thiourea changed. It was revealed that precursor complexes with asymmetrical substituted thiourea gave spherical shaped morphology while the nanoparticles obtained from symmetrical thiourea were a rod shaped or a combinatation of rod and other shapes (anisotropic) and irregular shaped nanoparticles were obtained with sizes in the range of 1-11 nm. The crystalline phases of the ZnS nanoparticles were majorly cubic, that of CdS are cubic while the HgS exhibit metacinnabar phase.

Chapter 5 describes the synthesis, result and discussion of the thermolysis of seven HDA capped ZnS and CdS nanoparticles four of which are ZnS from; a parent complex and three adducts (pyridine, 2, 2'- bipyridine and 1, 10-phenanthroline). The XRD results revealed that the ZnS nanoparticles obtained from the pyridine adduct precursor complex is mixture of hexagonal and cubic crystalline phases. Three HDA capped CdS nanoparticles were synthesized from the thermolysis of parent complex and 2 adducts of 2, 2' bipyridine and 1, 10-phenanthroline respectively. The CdS sulfide nanoparticles from 2, 2'- bipyridine and 1, 10-phenanthroline adducts gave anisotropic shapes and the sizes of nanoparticles obtained from the 1,10-phenanthroline precursor are bigger than others.

Chapter 6 comprises all detailed incorporation of ZnS and CdS into different polymer matrices to give polymer encapsulated ZnS and CdS nanoparticles. The structural and thermal studies of the nanocomposites prepared, were investigated and compared with the

pure polymers polymethyl methacrylate, (PMMA), Polyvinyl alcohol (PVA) and Polyvinyl pyrolindonne (PVP)]. The study revealed that ZnS/PVA and CdS/PVA are the most thermally stable relative to the thermal stability of the pure polymers.

7.2 Conclusion

This work entails the synthesis of Zn(II), Cd(II) and Hg(II) complexes using respective metal halides, mixed ligands of substituted thiourea (methy, dimethyl, diethyl and diisopropyl) or tetramethyl thiuram disulfide and 1-cyano-1-carboethoxyl-2,2-ethylene dithiolate. Pyridine, 2, 2'-bipyridine and 1, 10-phenanthroline adducts of the parent diisopropyl thiourea complex of Zn(II) and Cd(II) were further synthesized. The metal complexes were characterized infrared, ^{1}H and ^{13}C-NMR spectroscopy and bonding between the ligands and the central metal ions were confirmed. All the complexes were gave respective metal sulfide on decomposition hence they were thermolyed in HDA to give ZnS, CdS and HgS nanoparticles. The nanoparticles were characterized for their structural and optical properties. From the results it was observed that for the precursor complexes of thiourea the ZnS and CdS nannoparticles have morphology that tend to follow a trend that is related to the symmetry of the alkyl substituent of the thiourea ligand in the precursor complexes. This was revealed by the rod shaped morphology from the dimethyl and diethyl thiourea and the spherical shaped that was obtained from the methyl thiourea. Adducts precursor complexes of 2, 2.- bipyridine and 1,10 phenanthroline gave anisotropics particles. Polymer nanocomposites of ZnS and CdS were also prepared using a solution casting method to investigate the structural and thermal stability of nanoparticle encapsulated composites. The polymer sused are polymethyl metharcrylate, polyvinyl alcohol and poly vinyl pyrrolidone. Infrared spectrosocopy was used to establish interaction between the nanoparticles and the pure polymer. ZnS and CdS polyvinyl alcohol nanocomposited were found to be thermally most stable when their

stabilities were compared relative to the pure polymers. This was done with thermgravimetry technique.

7.3 Future work

Future work on this project will involve the use of other chalcogenide such as a transition metal like metal selenide or tellurides for synthesis of semiconductor nanoparticles. Novel metal complexes using other 1, 1 dithiolate derivatives can also be considered as single source precursors. There are a few 1, 1 dithiolate derivatives that can come to mind as ligands for the synthesis of complexes with the ultimate use as single source precursors. The complexes used in the work are rich in sulfur and they have antimicrobial, antibacterial antifungus activities. If they are screened against these microbes the results are most likely to be impressive and effective.

Capping agents with longer carbon chain can also be considered for further synthesis of nanoparticles. The synthesis of nanoparticles for photocatalytic purification of water should also be explored. Environmentally benign metal complexes like Fe and Cu can also be synthesized as an alternative to the reported metal complexes.